The effect of cholinergic loss on the structure and function of the neurovascular unit: implications for cerebral amyloid angiopathy

Thesis

The effect of cholinergic loss on the structure and function of the neurovascular unit: implications for cerebral amyloid angiopathy

Shereen Nizari, BSc

A Thesis submission to the Open University for the degree of Doctor of Philosophy

November 2018

Declaration

I declare that the work presented in this thesis is my own and contributions made by other researchers are acknowledged in relevant parts of the text. This work does not contain any material submitted for any award or other degree.

Abstract

Innervation of cerebral blood vessels is important for the regulation of vascular tone and adequate cerebral perfusion. Alzheimer's disease (AD) is characterised by a loss of cholinergic innervation of the neurovascular unit (NVU). This loss may contribute not only to inefficient cerebrovascular perfusion, but also to the failure of removal of amyloid-β (Aβ), leading to its accumulation as cerebral amyloid angiopathy (CAA). This hypothesis was tested by mimicking loss of cholinergic innervation of the cortex and hippocampus in adult male C57BL/6 mice using the immunospecific toxin mu-p75-saporin. Using quadruple labelling immunohistochemistry and 3D reconstructions of the NVU, loss of perivascular cholinergic innervation was observed at the smooth muscle cells and basement membrane in the cortex and hippocampus, with additional perivascular loss at the astrocyte endfeet in the cortex. Arterial spin labelling fMRI revealed no differences in resting cerebral blood flow between control and saporin-treated mice in either the cortex or hippocampus. However, denervated vessels in the cortex, but not the hippocampus, failed to respond to pharmacological stimulation of endothelial nitric oxide synthase (eNOS). Further studies revealed a decrease in eNOS expression in the cortex, but an increase in eNOS expression and activity in the hippocampus following loss of cholinergic input. No differences were noted between control and saporin-treated mice in the efficiency of removal of Aβ along perivascular basement membranes in either the cortex or hippocampus. Treatment of TetO-APPSweInd mice with saporin resulted in a trend towards higher CAA load. These data suggest that there are innate differences between NVUs of the cortex and the hippocampus and a difference in their functional response to loss of cholinergic input. Loss of cholinergic input at the NVU may contribute to accumulation of Aβ; however, this likely requires additional pathological factors for CAA to develop.

Acknowledgments and dedications

I would like to dedicate this thesis firstly to the memory of my Dad, who gave me so much support and who I will never stop missing and pray that he is in eternal peace and comfort. I would also like to dedicate this thesis to my beautiful wonderful Mum and my incredible brother Maher, who have been tirelessly and unwaveringly supportive and patient with me – I am so very lucky to have them. I also wish to dedicate this thesis to my amazing supervisor Cheryl, who is a true hero of mine and an absolutely inspiring scientist who I will always look up to and I am so incredibly fortunate to have been able to call my supervisor.

I would like to acknowledge and thank Dr Jack Wells for the work carrying out the fMRI study, and for being so kind and accommodating and providing stimulating conversation and greatly improving my knowledge during my work at CABI UCL.

I would like to thank The Carare Lab at the University of Southampton; Roxana, Matt, Maureen, Nazira and all the staff at the BRF (especially Les and Lorraine) for their kind help, time and patience.

I would like to thank the BRU staff at the OU, Karen, Agata, Iwona and Gareth, for putting up with me and checking on my mice for me, as well as the OU lab support staff, Julia, Brett, Suzanne, George, Igor, Eduardo, Heather and Radka for all their support and knowledge.

I would thank Laura in particular, for all the thought-provoking conversations, and always being there for me, even when I didn't realise I needed her support. I would like to thank Nacho for all the advice he has passed onto me and his help with my project. I would like to thank the BBB group, (David, Jane, Francesco, Joyce, Zerin, Mo, Conor, Edu, David RC, Ester, Perla, Rebecca, Nayab) and other students, especially Tala for being there for me and being a great office mate, Sonia, Emily, Celia, Juan, Marcelle, Lea, Maurine, Said, Gaurav, Sophie, Sarah and Amy.

I would also like to thank my amazing friends Ellie, Chloe, Mon, Hannah, Lauren, Annabel and Charlotte, who have been so utterly supportive and have always tirelessly been there for me and I am so lucky to have.

I would like to thank past and present members at UCL IOO who have taught me so much and greatly encouraged and supported my application to do a PhD, especially Joana, Ben, Li, Will, Meng, Annalie, Anne, Francesca, Tom, Lisa, Mark, Guilia, Shannon, Eddie, Matt, Nick, Dave, Heidi, Ros, Vy, James and Katy.

I would like to acknowledge Sci-hub and all who contribute to it for creating such an essential resource. I would like to thank ARUK for travel grants and support and lastly the OU for funding this PhD project and giving me this incredible opportunity to make a contribution towards the understanding and future treatment of dementia.

Chapter 1 Contents

List of Figures

List of Tables

List of Equations

Conference items and publications

Publication

Nizari, S., Romero, I.A. & Hawkes, C.A., 2017. The role of perivascular innervation and neurally mediated vasoreactivity in the pathophysiology of Alzheimer's disease. *Clinical science (London, England : 1979)*, 131(12), pp.1207–1214. doi:10.1042/CS20160769 (Review)

Conference proceedings

Oral presentations

Nizari S, Wells JA, Carare RO, Romero IA, Hawkes CA 'The effect of loss of cholinergic perivascular innervation on cerebral blood flow' November 2016, BBB early careers symposium, Dublin, Ireland

Nizari S, Romero IA, Hawkes CA 'Effect of cholinergic loss at the neurovascular unit using 3D modelling' March 2017, ARUK, Aberdeen

Nizari S, Wells JA, Carare RO, Romero IA, Hawkes CA 'Effect of cholinergic loss at the neurovascular unit using 3D modelling' May 2017, Glio-vascular coupling symposium, London

Nizari S, Wells JA, Carare RO, Romero IA, Hawkes CA 'How does loss of cholinergic innervation affect the structure and function of the neurovascular unit?' November 2018, BBB early careers symposium, Oxford

Poster presentations

Nizari S, Romero IA, Hawkes CA 'The effect of cholinergic loss on perivascular drainage and other neurotransmitters in a model of cerebral amyloid angiopathy' BBB early careers symposium 2015

Nizari S, Romero IA, Hawkes CA 'The effect of cholinergic denervation on perivascular drainage and other neurotransmitters in a model of cerebral amyloid angiopathy' ARUK 2016

'Nizari S, Wells JA, Carare RO, Romero IA, Hawkes CA Loss of perivascular cholinergic innervation differentially affects cerebral blood flow in the cortex and hippocampus' ARUK 2018

Nizari S, Wells JA, Carare RO, Romero IA, Hawkes CA 'How does loss of cholinergic innervation affect the structure and function of the neurovascular unit?' ICAA 2018

Abbreviations

3D three dimensional

5-HT serotonin

5-HTT serotonin transporter

Aβ amyloid beta

ABC ATP binding cassette transporter proteins

ACE angiostensin-converting enzyme

ACh acetylcholine

AChE acetylcholine esterase

AChEI acetylcholine esterase inhibitor

AChR acetylcholine receptor

AD Alzheimer's disease

AICD APP intracellular domain

Akt protein kinase B

AMPA a-amino-3-hydroxy-5-methyl-4-isoxazole propionic acid

AP anterior posterior

APP amyloid precursor protein

APPTet TetO-APPSweInd

AQP4 Aquaporin 4

ATP adenosine triphosphate

BBB blood brain barrier

BM basement membrane

Bp base pairs

CAA cerebral amyloid angiopathy

CBF cerebral blood flow

cGMP cyclic guanosine monophosphate

ChAT acetylcholine transferase

COX2 cyclooxygenase-2

CSF cerebral spinal fluid

CTF c-terminal fragment

CVBM cerebrovascular basement membrane

DAB 3,3'-diaminobenzidine tetrahydrochloride

DV dorsal ventral

ECE endothelin-converting enzyme

EET epoxyeicosatrienoic acid

e.g. For example

EM electron microscopy

eNOS endothelial nitric oxide synthase

fMRI functional magnetic resonance imaging

GAPDH Glyceraldehyde 3-phosphate dehydrogenase

GFAP glial fibrillary acidic protein

h Hour

HSPG heparan sulphate proteoglycan

ICV intracerebroventricular

ISF interstitial fluid

LC locus coeruleus

LDL low density lipoprotein

LRP-1 LDL receptor-related protein-1

mAChR muscarinic acetylcholine receptor

MAPT normal human tau

MCI Mild cognitive impairment

min minutes

ML medial lateral

MLCK myosin light chain kinase

MMSE mini mental state examination

MRI magnetic resonance imaging

MS medial septum

NA noradrenaline

NGF nerve growth factor

NO nitric oxide

NOS nitric oxide synthase

nNOS neuronal nitric oxide synthase

NVC neurovascular coupling

NVU Neurovascular Unit

OCT optimal cutting temperature compound

OD optical density

PB phosphate buffer

PBS phosphate buffered saline

pCO_2 partial pressure of carbon dioxide

p-gp p-glycoprotein

PI3K phosphoinositide-3-kinase

P-Tau hyperphophorylated tau

PVD perivascular drainage

RAGE receptor for advanced glycation end-products

ROCK Rho-associated kinase protein

RN raphe nuclei

RT room temperature

s seconds

SMA smooth muscle actin

SMA-FITC smooth muscle actin-Fluorescein Isothiocyanate

SMC smooth muscle cell

SNRI serotonin/noradrenaline re-uptake inhibitor

SSRI selective serotonin re-uptake inhibitor

TBI traumatic brain injury**TET** Tetracycline

Tg transgenic

TGFβ transforming growth factor beta

Tryp H Tryptophan hydroxylase

VAChT vesicular acetylcholine transporter

VRS Virchow-robin space

v/v volume/volume

w/v weight/volume

Chapter 1 Main introduction

General Overview

The brain has a unique vasculature compared to the peripheral system in that it contains a blood brain barrier (BBB), a physical barrier created by tight junctions of endothelial cells that allows for controlled maintenance of substance entry. While the BBB confers the brain with a high degree of selectivity, it does so at the expense of waste removal, which is made more difficult by the absence of a traditional lymphatic system for extracellular drainage. The cerebrovasculature is increasingly recognised as a contributor towards the pathology of Alzheimer's disease (AD) (Iturria-Medina et al. 2016), and is known to participate in the removal of toxic proteins such as β-amyloid (Aβ). Failure of this removal is thought to underlie the accumulation of Aβ in the parenchyma and blood vessels as cerebral amyloid angiopathy (CAA) in the AD brain. However, the mechanisms that lead to the development of CAA are currently unknown. Proper functioning of the cerebral vessels is mediated via communication with neurons at the neurovascular unit (NVU). Among these neuronal populations, the loss of cholinergic neurons is an early and well-characterised feature of AD. The purpose of this thesis is to investigate the effect of loss of cholinergic innervation at the NVU on the structure and function of the cerebrovasculature in the aetiology of CAA.

The Neurovascular unit (NVU)

The NVU is the collective term for the cells that form the interface between the brain parenchyma and the peripheral blood that make up the cerebral blood vessels where regional control of cerebral blood flow (CBF) is regulated. It is composed of endothelial cells, pericytes, smooth muscle cells (SMCs), astrocytes, and neuronal fibres and is supported by continuous basement membranes formed of extracellular matrices. The composition and morphology of the NVU differs between capillaries, arteries and veins (McConnell et al. 2017; Lecrux & Hamel 2011; Iadecola 2004).

Capillaries

At the capillary level, the NVU contains a single layer of endothelial cells surrounding the vessel lumen. The endothelial cells are irregularly surrounded by pericytes that are separated from endothelial cells by a thin cerebrovascular basement membrane (CVBM), and the entire structure is surrounded by a layer of astrocyte endfeet (Morris et al. 2014). Neurons synapse onto astrocytes and may additionally innervate pericytes and the CVBM surrounding endothelial cells (Attwell et al. 2010; Hamilton et al. 2010; Vaucher & Hamel 1995) (Fig. 1.1 a).

Arteries

The leptomeningeal and pial arteries are found at the surface of the brain and enter into the brain surrounded by a Virchow-Robin space (Weller, Boche, et al. 2009). The leptomeningeal arteries consist of a multilayer of SMCs, which surround a layer of endothelial cells, and the whole structure is covered by a layer of astrocyte endfeet known as the glia limitans (Filosa et al. 2016). Each layer of cells is surrounded by a CVBM and collectively form the internal elastic media, tunica media and the fibrous adventitia (Weller, Boche, et al. 2009). These arteries receive extrinsic innervation (see section 'Extrinsic innervation' under 'Vascular function') (Hamel 2006). Within the parenchyma, penetrating arteries give rise to parenchymal arterioles that are comprised of an endothelial cell layer surrounded by a single layer of SMCs separated by a CVBM and carpeted by astrocyte endfeet (Fig. 1.1 b). These vessels are intrinsically innervated (see section 'Intrinsic innervation' under 'Vascular function') by nerve fibres that synapse onto astrocytes, or penetrate the adventitia to synapse directly onto SMCs and endothelial cells, although the degree of this innervation is low (Vaucher & Hamel 1995).

Veins

Parenchymal veins and venules have a large lumen with a thin collagenous CVBM and contain a single layer of endothelial cells and have occasional pericytes (Rhodin 1968) but lack smooth muscle cells (Zhang et al. 1990). Veins have been shown to receive some intrinsic innervation (Vaucher & Hamel 1995) and are surrounded by astrocytic endfeet (Fig. 1.1 c).

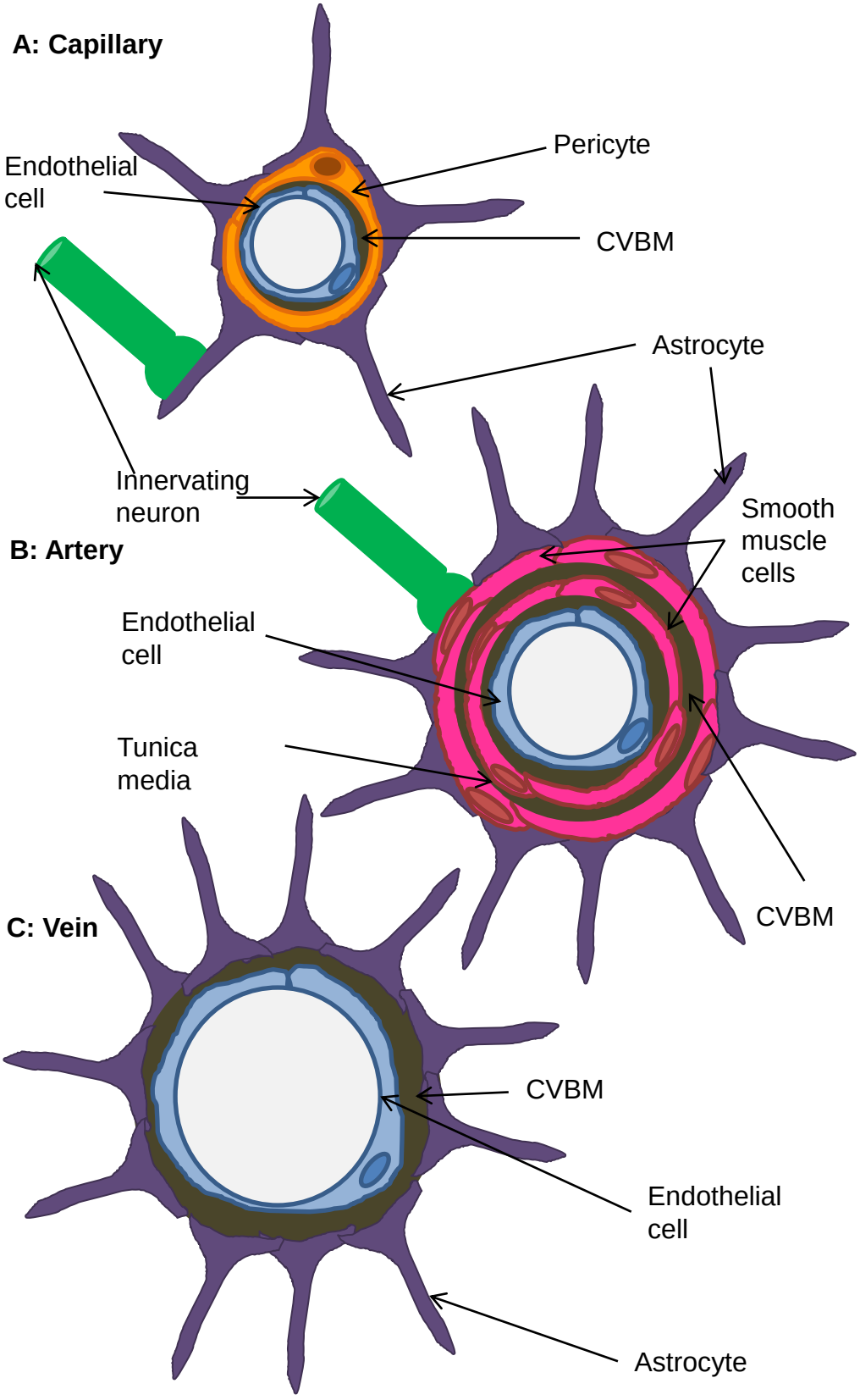

Figure 1.1 The NVU
The composition of the NVU at (a) capillaries, (b) arteries and (c) veins in the brain parenchyma. Adapted from (Nizari et al. 2017).

Endothelial cells

Endothelial cells express receptors for vasoactive mediators (Hamel 2006) and form the interface of the BBB that restricts movement of substances into and out of the brain

(Zlokovic 2005). The BBB is the boundary between the parenchyma and the blood, where solute exchange is highly regulated by tight junctions and mediated via paracellular, transcellular, transport protein- and receptor-mediated endocytosis and adsorptive transcytosis (Abbott 2004; Erickson & Banks 2013).

Pericytes

Pericytes are found at capillaries and post-capillary venules (Rhodin 1968) and are suggested to have contractile properties, although this is still controversial (Fernandez-Klett et al. 2010; Hamilton et al. 2010). Pericytes have been demonstrated to display spontaneous calcium transients, indicating baseline activity but with an additional ability to respond to stimuli (Rungta et al. 2018), which suggests they may be involved in the maintenance of vascular tone (Attwell et al. 2016).

Smooth muscle cells

Smooth muscle cells are found at the arteries (Hannocks et al. 2018) and contain smooth muscle actin allowing them to have contractile properties which enable the distortion of the vasculature to change vessel lumen shape, dictating vasodilation or vasoconstriction to maintain basal CBF and in response to neuronal activity.

Astrocytes

Astrocytes form a carpet of endfeet surrounding the NVU (Kacem et al. 1998) outside of the outer CVBM (Zarow et al. 1997). Perivascular astrocytes have been demonstrated to be involved in glucose transport from the blood to the parenchyma as part of their ability to meet the metabolic demands of the NVU and surrounding tissue (Rouach et al. 2008). Astrocytes also modulate CBF following neuronal stimulation (Mulligan & MacVicar 2004) and as a response to hypercapnia (Howarth et al. 2017). Astrocytes have also been demonstrated to regulate vascular tone based on pressure flow feedback from the vasculature, leading to bidirectional feedback with pyramidal neurons in the cortex (Kim et al. 2015; Kim et al. 2016; Filosa et al. 2016).

Microglia

Microglia are the second largest glial cell population in the brain that in addition to being expressed throughout the parenchyma, also contact the CVBM of cerebral vessels as ‘juxtavascular’ microglia. Although the exact function of this microglial population is not known, juxtavascular microglia have been reported to play a role in immune surveillance and maintenance of the BBB (Lou et al. 2016). They have also been suggested to secrete matrix metalloproteases and contribute to vascular remodelling after injury (Könnecke & Bechmann 2013). Parenchymal microglia can become reactive and ramified in pathogenic circumstances (Filosa et al. 2016) and have been demonstrated to have motile processes

which can change from a resting state to respond to sites of injury through immune surveillance and phagocytic activity (Nimmerjahn et al. 2005).

Innervating neurons

Neuronal innervation is essential for the maintenance of vascular tone and neurovascular coupling (Hamel 2006). Contact from nerve fibres has been described as 'abutting' from electron microscopy studies (Vaucher et al. 1997) and signalling at the NVU can occur within the vascular walls by means of 'intramural vascular signalling' (Iadecola 2004) and are described further below in section 'Intrinsic innervation' under 'Vascular function'.

Vascular function

Even though it only makes up 2% of body mass, the brain requires 20% of the body's energy produced when in resting state (Mishra 2016; Attwell et al. 2010). As such, it is one of the most highly perfused organs in the body and is therefore in need of constant and stable CBF (Ainslie & Brassard 2014). Moreover, the brain needs to be able to ensure an adequate supply of oxygen and glucose in response to fluctuating neuronal activity, a term referred to as functional hyperaemia, flow-metabolism or neurovascular coupling (NVC).

Cerebral autoregulation

Cerebral autoregulation is the process by which a consistent CBF is maintained over a wide range of changes in peripheral arterial pressures (60-150 mmHg) (Van Lieshout et al. 2003). This is mediated by innervation from the sympathetic nervous system, whereby ganglia of nerves from outside of the parenchyma release vasodilators or vasoconstrictors to maintain the upper limit of blood pressure (Hamel 2006) (see section 'extrinsic innervation' below, Fig. 1.2). This allows a vascular tone, the degree to which a blood vessel is constricted relative to its maximal dilation, to be maintained. This is essential in ensuring a constant and global perfusion for the brain, which in a healthy adult is about 71.8±12.0 ml/100g/min in the grey matter at rest (Bertsch et al. 2009).

Neurovascular coupling

Once sufficient resting perfusion is achieved, CBF needs to be distributed within the brain to the areas that are most active. NVC is achieved via intrinsic innervation (See section 'intrinsic innervation') (Hamel 2006; Duchemin et al. 2012; Filosa 2010). Focal increases in CBF are induced via depletion of metabolic factors including glucose, oxygen and ATP, leading to increased energy demand (Attwell et al. 2010).

Extrinsic innervation

As suggested above, cerebral autoregulation is maintained largely through extrinsic innervation. Extrinsic innervation is further divided into the sympathetic, parasympathetic and sensory systems, which are comprised of nerve fibres which have peripheral ganglia originating in the superior cervical ganglion, trigeminal ganglion, the otic ganglion and the sphenopalatine ganglion (Fig. 1.2) (Itakura et al. 1977; Baeres et al. 2004). These neurons control the degree of vasodilation and constriction by releasing a variety of peptides and neurotransmitters including neuropeptide Y, acetylcholine (ACh), vasoactive intestinal peptide, serotonin (5-hydroxytryptamine, 5-HT) and noradrenaline (NA) (Lincoln 1995; Hamel 2006; Baeres et al. 2004; Bleys et al. 1996). The control of neurotransmission has been shown to be determined by CO_2 as demonstrated by hypercapnia experiments (Toda et al. 1996) or by pH (Liu et al. 2012). As extracerebral vessels pass through the Virchow-Robin space into the parenchyma and become parenchymal arteries and arterioles, they lose innervation from these nerve fibres (Itakura et al. 1977; Filosa et al. 2016; Hamel 2006).

Intrinsic innervation

In the parenchyma, NVC is regulated by intrinsic innervation, that is, nerve fibres that originate from intracerebral nuclei (Fig. 1.2). These neuronal cell bodies are mostly located in the nucleus basalis (cholinergic system), the locus coeruleus (noradrenergic system) and the raphe nucleus (serotoninergic system) (Hamel 2006). Acetylcholine (ACh), serotonin (5-HT) and noradrenaline (NA) are the principal neurotransmitters involved in the regulation of vascular tone in the hippocampus and cortex (Hamel 2006). At the NVU, nerve fibre terminals have been shown to be <1.0 µm from vessel walls (Tong & Hamel 1999) and can regulate vascular tone by either synapsing directly on smooth muscle and endothelial cells or via pericytes and astrocytes as well as interneurons (Mulligan & MacVicar 2004; Chen et al. 2014; Toribatake et al. 1997; Hamilton et al. 2010; Hamel 2006).

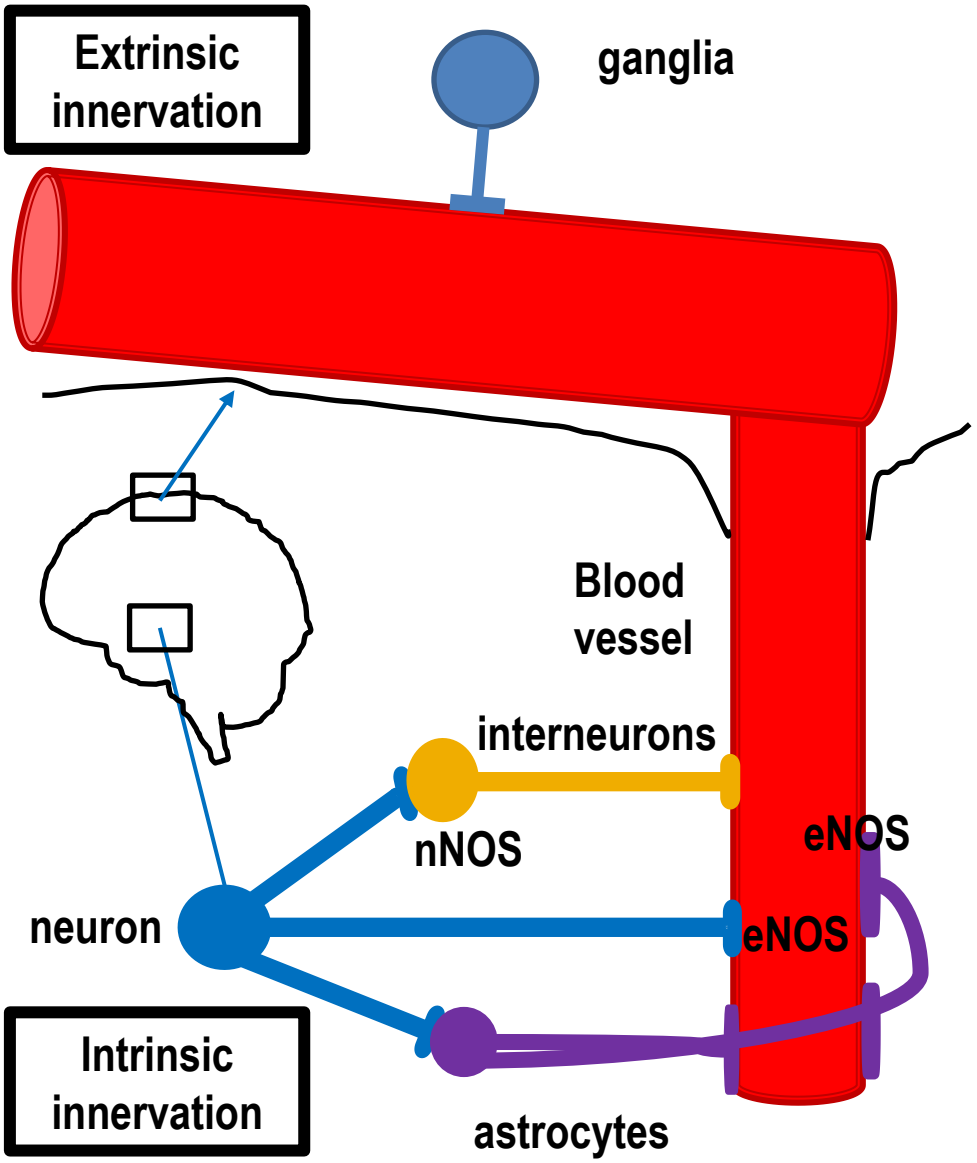

Figure 1.2 Intrinsic and extrinsic innervation
Pial and leptomeningeal vessels are extrinsically innervated by the sympathetic nervous system that regulates cerebral autoregulation. Parenchymal vessels receive intrinsic innervation from neurons within the parenchyma which act with astrocytes to mediate NVC.

Cholinergic innervation

Cholinergic neurons in the basal forebrain form the 'Ch4' complex, which includes the nucleus basalis, diagonal and horizontal bands of Broca and medial septum (Mesulam & Geula 1988; Mesulam 2013; Mesulam, E. J. Mufson, et al. 1983). The nerve fibre projections from this population of cholinergic neurons have been demonstrated to innervate the cortex and hippocampus (Selden et al. 1998) which in rodents, have been shown to have a small population (Consonni et al. 2009), and in humans there is evidence for some ACh-positive pyramidal cells in the cortex (Mesulam & Geula 1988). The main source of innervation to the hippocampus is from the horizontal and vertical bands of Broca and the medial septum (Mesulam 2013). Cholinergic innervation of the cortex arises

mostly from the nucleus basilis (Mesulam, Elliott J. Mufson, et al. 1983; Rye et al. 1984; Sato et al. 2002) but it is also innervated via thalamo-cortical projections (Hallanger et al. 1987) and from the brainstem (Mesulam, E. J. Mufson, et al. 1983; Mesulam 2013) (Fig. 1.3).

Other major cholinergic nuclei include those found in the striatum and the pedunculopontine and laterodorsal tegmental nuclei of brain stem, which tracer studies have shown to provide projections to the thalamus (Metherate & Ashe 1993). The cholinergic neurons of the striatum have also been found to receive a small amount of innervation from the Ch4 region in addition to its own cholinergic neuronal population (Mesulam & Geula 1988).

Cholinergic neurons of the basal forebrain express the p75 receptor for neurotrophic growth factor (NGF), a growth factor that is transported via retrograde transport and is essential for basal forebrain maintenance (Boskovic et al. 2014). This receptor is not found in other cholinergic neuronal populations (Sobreviela et al. 1994) (Fig. 1.3). However, the p75 receptor has been found on a small subpopulation of astrocytes in the dendrite gyrus (Dougherty & Milner 1999) and to be expressed on glial cells following injury (Cragnolini & Friedman 2008).

ACh, the neurotransmitter released by cholinergic neurons, is synthesised from choline and acetyl coenzyme A, in a reaction that is catalysed by the enzyme choline acetyltransferase (ChAT). ACh is transported to the nerve terminal via vesicular acetylcholine transporter - (VAChT) for release and is then broken down in the synapse by acetylcholine esterase for reuptake and recycling (Perry 1980). Therefore, ChAT and VAChT are widely used as markers of cholinergic neurons (Kuznetsova & Schliebs 2013; Berger-Sweeney et al. 2001).

As discussed above, release of ACh at the NVU usually induces vasodilation and increased CBF, although *in vitro* studies have shown that ACh can have vasoconstrictive properties at high concentrations (Furchgott & Zawadzki 1980). ACh actions at the NVU are mediated principally via binding to the muscarinic acetylcholine receptors (mAChR) that are located on perivascular astrocytes (subtypes $m_{1\text{-}5}$AChR), smooth muscle cells (subtypes $m_{1,2,3}$ and $_5$AChR), and endothelial cells (subtypes $m_{1,2}$ and $_5$AChR), (Badaut et al. 1997; Luiten et al. 1996; Edvinsson et al. 1977; Elhusseiny et al. 1999). Stimulation of cholinergic neurons in the basal forebrain has been demonstrated to increase cortical CBF without affecting peripheral blood pressure, highlighting the influence of neuronal control of this pathway (Sato et al. 2004; Biesold et al. 1989; Iadecola & Zhang 1996). Moreover,

Adachi et al found that while hypercapnia increased blood flow in both pial and cortical arteries, stimulation of the basal forebrain increased CBF only in the cortex (Adachi et al. 1992).

ACh is known to cause increased CBF through vasodilation via the nitric oxide (NO) pathway (Vaucher et al. 1997). At the astrocyte endfeet, direct activation of AChRs or indirect activation of mAChRs on interneurons by ACh leading to glutamate release and activation of metobotropic glutamate receptors (mGLUR) on astrocyte endfeet (Cauli et al. 2004), can lead to increased levels of intracellular calcium (Ca^{2+}). This stimulates activation of calmodulin, a co-factor of endothelial and neuronal nitric oxide synthase (eNOS and nNOS, respectively) activity (Shu et al. 2015). Activation of eNOS via Ca^{2+}/calmodulin or phosphorylation by the Akt/PI3K pathway (Dimmeler et al. 1999) leads to the conversion of L-Arginine into L-citrulline, releasing NO as a by-product which can diffuse across into SMC and induce relaxation, leading to vasodilaton (Fig. 1.3) (Duchemin et al. 2012).

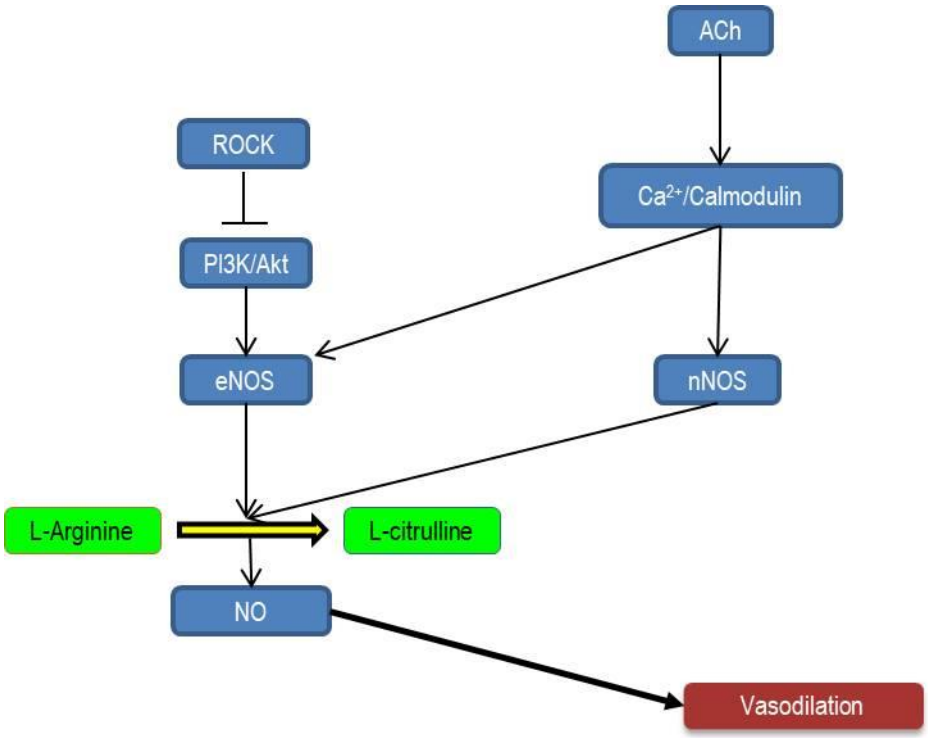

Figure 1.3 The NO pathway
eNOS and nNOS are activated following Ca^{2+}/calmodulin phosphorylation initiated by ACh signalling. eNOS can be additionally activated through the PI3K/Akt pathway.

Increasing intracellular calcium can also lead to vasodilation by inducing hyperpolarisation of SMCs via increased production of arachidonic acid and activation of cyclooxygenase-2 (COX2) and release of epoxyeicosatrienoic acid (EET) (Fig. 1.4). However, increased arachidonic acid levels can also counter excessive vasodilation by eliciting

vasoconstriction via 20-HETE activation (Stella et al. 1994; Stobart et al. 2013; Gebremedhin et al. 1992; Liu et al. 2012).

In the endothelial cell, increases in levels of intracellular Ca^{2+} can be induced by activation of AChR or shear stress (Raignault et al. 2017) which can also lead to vasodilation via eNOS activation or production of arachidonic acid and prostacyclin (Fig. 1.4) (Duchemin et al. 2012). However, prostacyclin can be inhibited by peroxynitrite, a product caused by the combination of reactive oxidative species (ROS) and excessive NO under pathological conditions (Zou & Ullrich 1996) (Fig. 1.4).

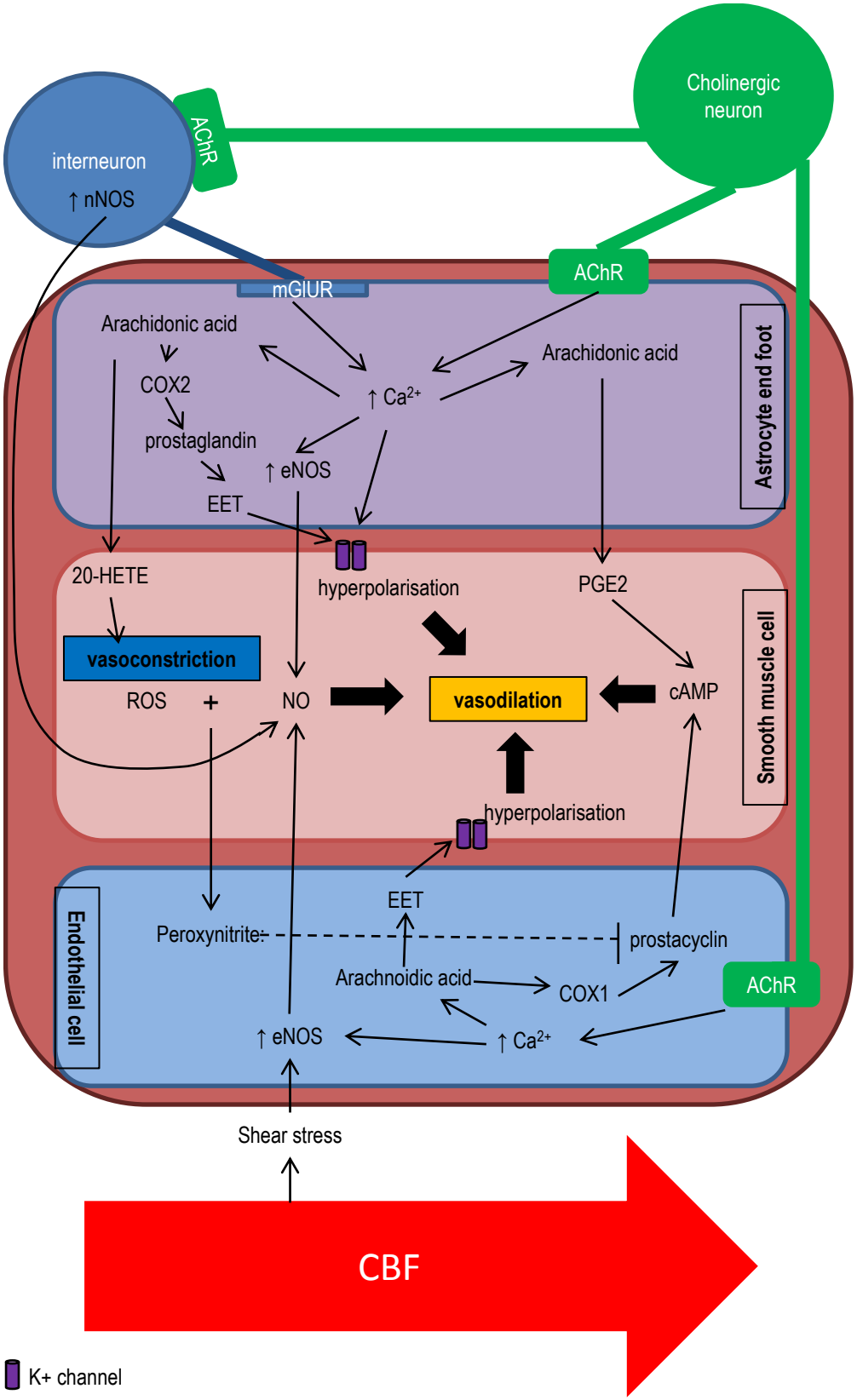

Figure 1.4 ACh induced CBF signalling pathways at the NVU
Vasodilatory and vasoconstrictive signalling pathways through cholinergic perivascular innervation at the NVU. AChR activation at the astrocyte endfeet or endothelial cell lead to intracellular Ca^{2+} elevation, leading to arachidonic acid or eNOS mediated vasodilation at the SMC. ROS production in combination with excess NO can lead to peroxynitrite inhibition of vasodilation. nNOS from ACh innervated interneurons can also lead to vasodilation at the SMC. Shear stress caused by CBF can also lead to endothelial cell-led vasodilation (COX1/2, cyclooxygenase 1/2, EET, epoxyeicosatrienoic acid, cAMP, cyclic adenosine monophosphate, PGE-2, prostaglandinE2, 20-HETE, 20-hydroxyeicosatetranoic acid).

Other intrinsic neurotransmitter pathways that regulate CBF in the cortex and hippocampus

Noradrenergic nerve fibres originate from nuclei in the locus coeruleus (Sato & Sato 1995; Edvinsson et al. 1977) in the brainstem (Fig. 1.5). These fibre projections innervate the hippocampus and cortex, hypothalamus, amygdala and thalamus (Wainer et al. 1993) and contain the enzyme tyrosine hydroxylase that is involved in the synthesis of NA from dopamine (Hardebo et al. 1980). NA leads to vasoconstriction by binding to α2 adrenergic receptors (Högestätt et al. 1989) in response to hyperaemia (Bekar et al. 2012). NA can also stimulate NO-mediated vasodilation (Thorin 2001) via noradrenergic β2 receptors (Court & Perry 2003; Lincoln 1995). NA has been suggested to have vasoconstrictive and vasodilatory effects depending on vessel type (Sercombe et al. 1990; Lincoln 1995).

Serotoninergic nerve fibre projections originate from the raphe nucleus in the brainstem (Court & Perry 2003) to innervate parenchymal and pial arteries and arterioles in the cortex and hippocampus (Bonvento et al. 1990; Itakura et al. 1985). The pattern of serotoninergic innervation has been demonstrated to be similar to NA fibres (Jackowski et al. 1988). 5-HT is synthesised from the conversion of L-tryptophan in a series of reactions that are catalysed by tryptophan hydroxylase and aromatic L-amino acid decarboxylase (Cohen et al. 1992; Lincoln 1995). Serotonergic neurons can also be identified by the expression of the 5-HT transporter, which participates in the reuptake of 5-HT from the synapse into presynaptic neurons. Binding of 5-HT_1 and 5-HT_2 receptors leads to vasoconstriction (Hamel et al. 1988; Lincoln 1995) while binding to 5-HT_{1B} causes vasodilation (Elhusseiny & Hamel 2001). This effect is dose-dependent, causing vasodilation at lower concentrations, and vasoconstriction at higher concentrations (Elhusseiny & Hamel 2001; Harper & MacKenzie 1977).

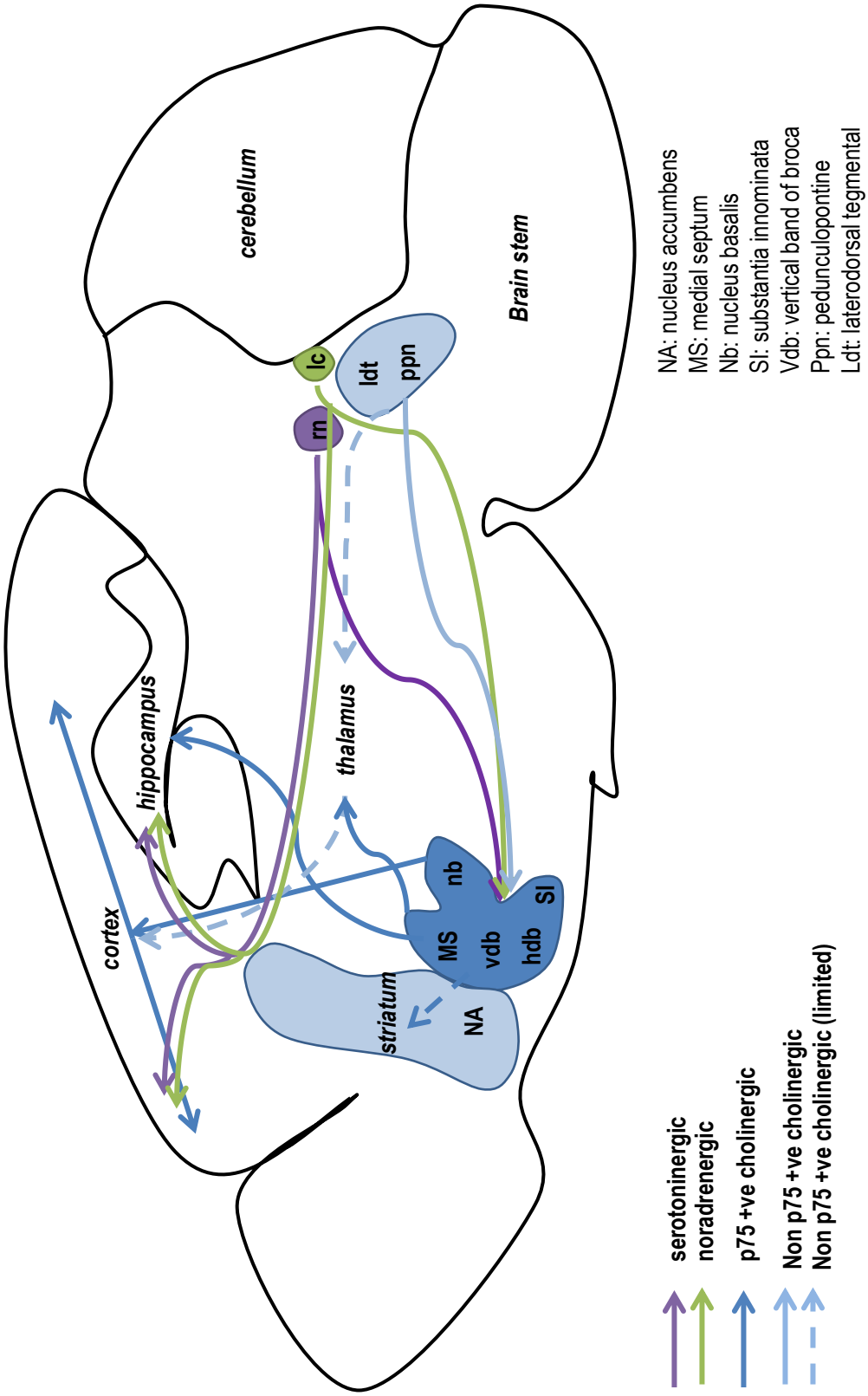

Figure 1.5 Cholinergic, noradrenergic and serotonergic fibre pathways in the mouse brain
Schematic representation of ascending cholinergic, noradrenergic and serotonergic pathways from the brainstem and basal forebrain to the cortex and hippocampus and thalamus. Adapted from (Woolf & Butcher 2011; Mesulam, E. J. Mufson, et al. 1983; Wainer et al. 1993).

Other vasoactive modulators

In addition to ACh, NA and 5-HT, vasodilation and vasoconstriction of cerebral blood vessels is also regulated through a variety of compounds, including glutamate, GABA, lactate, derivatives of arachidonic acid, potassium and hydrogen ions, carbon dioxide, oxygen, adenosine and NO (Vaucher et al. 1997; Frahm et al. 1996; Iadecola 1993).

As discussed above, activation of NOS and release of NO plays a crucial role in maintaining a baseline vascular tone. Iadecola and Xu have shown that pharmacological inhibition of NOS decreases CBF without affecting glucose consumption (Iadecola & Xu 1994). In addition to the expression of eNOS in endothelial cells and astrocytes, two other NOS isoforms are present in the brain, neuronal (nNOS) and inducible (iNOS) NOS. nNOS is constitutively expressed in neurons and astrocytes (Yuan et al. 2004) while iNOS is expressed in the endothelium (Jeynes & Provias 2009) during pathological events such as ischaemia (Jiang et al. 2014).

Although much of the role of NO at the NVU is mediated by the activity of eNOS, the importance of nNOS in regulating CBF has been highlighted by Lovick et al who have suggested that nNOS from a subpopulation of interneurons in the hippocampus is responsible for moderating NVC in response to metabolic demand (Lovick et al. 1999). nNOS has also been shown to contribute to increased CBF elicited by hypercapnia, as inhibition of nNOS activity resulted in decreased CBF responses to CO_2 in the rat (Harada et al. 1997). Glutamate-stimulated increases in CBF *in vivo* have also been shown to be dependent on activation of nNOS (Lourenço et al. 2014). Cholinergic neurons originating from the basal forebrain also synapse on nNOS-containing GABAergic interneurons in the cortex (Cauli et al. 2004; Vaucher et al. 1997), which adds an additional layer of complexity to the regulation of NVC.

CBF

As suggested above, individual cells of the NVU, including endothelial cells, pericytes, SMCs and astrocytes, contribute to the regulation of CBF under basal and stimulated conditions (Hamel 2006).

Endothelial cells and pericytes

As outlined above, activation of endothelial cells by binding of ACh or via shear stress can induce relaxation of SMCs through production of NO, cAMP or the activity of potassium channels (Hannah et al. 2011). Pericytes contain smooth muscle actin that confers contractile properties (Hamilton et al. 2010; Attwell et al. 2016) and have been shown to respond to cholinergic signalling in retinal capillaries (Wu et al. 2003) and cerebral

microvessels (Oishi et al. 2007). Pericytes have also been shown to display spontaneous calcium transients, indicating baseline activity but with an additional ability to respond to stimuli (Rungta et al. 2018), which suggests they are involved in vasomotion and maintenance of vascular tone. However, using optogenetics to induce vasoconstriction, Hill et al. have shown that only vessels with smooth muscle cells and not pericytes were able to respond to light stimulus, suggesting that capillaries do not contribute to the regulation of CBF (Hill et al. 2015).

Smooth muscle cells

There is little evidence to suggest that SMCs in parenchymal vessels express ACh receptors unlike those which are extrinsically innervated (Edvinsson et al. 1977; Luff 1996), and ACh-mediated dilation of SMCs is thought to be mediated predominately by endothelial cells (Manicam et al. 2016). However, studies have identified the presence of nAChRs and mAChRs on SMCs in the cortex and the hippocampus (Clifford et al. 2008; Elhusseiny et al. 1999; Ferreira-Vieira et al. 2016) and it has been suggested that nNOS upregulation in SMCs is able to compensate for decreases in eNOS to maintain vascular tone (Ward et al. 2005). Contraction of SMCs is also believed to underlie vasomotion, the spontaneous contraction of arteries that is thought to be independent of neuronal activity, although this independence has been questioned (Rivadulla et al. 2011; Pradhan & Chakravarthy 2011).

Astrocytes

In addition to neurons, astrocytes also contribute to the regulation of the vascular tone of parenchymal arterioles (Kim et al. 2015). Astrocytes can mediate NVC (Gordon et al. 2008) and have been suggested to respond to perfusion-induced changes in blood pressure (Blanco et al. 2008; Kim et al. 2015) in order to redirect CBF. However, it has been argued that astrocytes are unable to mediate signalling to arterioles and only do so via pericytes in the capillaries (Mishra et al. 2016). Xu et al. have suggested that astrocytes also contribute to hypercapnia-induced vasodilation of pial arterioles (Xu et al. 2004),

Assessment of CBF

Invasive imaging techniques

In order to measure CBF, invasive techniques such as the intravenous injection of radiotracers such as [15O]H_2O or [18F]fluoxyglucose can be used to estimate CBF and/or metabolic activity either *in vivo* or post-mortem (Cholet et al. 1997). Animal models used to carry out real-time imaging also include thinning the skull in order to create a surface

through which imaging of cortical vessels can be carried out using laser speckle or laser Doppler imaging which measures CBF based on detection of red-blood-cell induced shifts in light waves (Huang et al. 1994; Duncombe et al. 2017; Anenberg et al. 2015). Recently, Lourenço et al have combined laser Doppler probes with oxygen and NO detecting microsensors, allowing CBF measurements of the hippocampus to be made (Lourenço et al. 2017; Lourenço et al. 2014; Lourenço et al. 2018). Another technique of exposing the cerebrovasculature is by creating a cranial window through which fluorescent labelling of the cerebrovasculature and genetically fluorescently-tagged components can be observed using laser microscopy (Tajima et al. 2014; Klohs et al. 2014). Recently, this has been combined with using optical coherence tomography, which allows label-free imaging of CBF using light scattering in deep brain tissue (Park et al. 2018). Deep tissue imaging has also been achieved by inserting an objective as a probe and using an Argon laser for light scattering in order to measure CBF (Kuga et al. 2009; Devor et al. 2012).

Non-invasive imaging techniques

To visualise NVC non-invasively, changes in blood flow and oxygenation can be imaged using functional magnetic resonance imaging (fMRI). Mapping of neuronal activity is routinely assessed using blood oxygen level dependent (BOLD) contrast signalling, which is generated from the change in the magnetic field surrounding oxygenated and de-oxygenated red blood cells. BOLD-weighted MRI sequences can therefore be used as a proxy for oxygen utilisation based on the metabolic activity of the neurons and provide a high signal-to-noise ratio and good temporal resolution signal (Ogawa et al. 1990; Attwell & Iadecola 2002). However, the interpretation of changes in the BOLD signal can be complicated by variations in the rate of oxygen metabolism, blood volume and magnetic field strength which can be affected by age and disease (Liu & Brown 2007).

Perfusion fMRI based on arterial spin labelling (ASL) offers a useful complement to BOLD fMRI. This technique magnetically ‘tags’ water within the blood in peripheral blood vessels, such as the carotid arteries, and detects changes in the magnetisation as the blood passes into the brain tissue. By calculating changes against a baseline image, a measurement of CBF in millilitres of blood per 100g of tissue per minute can be estimated (Wierenga et al. 2014).

Alzheimer’s disease

Dementia is a chronic and progressive neurodegenerative disease which leads to the loss of numerous higher cognitive functions (World Health Organisation 2011). Alzheimer’s disease (AD) is the most common form of dementia, with more than 850,000 individuals affected in the UK alone (Prince et al. 2014). The World Alzheimer Report 2015 estimates

that 46.8 million people are currently living with dementia globally, and predict this figure to increase to 74.7 million by 2030 (Alzheimer's Disease International 2015).

Clinical symptoms of AD

AD presents as progressively worsening memory loss with cognitive impairment and psychotic symptoms (López & DeKosky 2008). AD has been characterised as occurring in three stages; the first being asymptomatic with subclinical pathology, the second being prodromal, which is associated with mild cognitive impairment (MCI) and includes early cognitive abnormalities such as episodic memory impairment before being lastly defined as AD dementia (Jack et al. 2010), where patients have severe cognitive impairments and require help with daily activities (López & DeKosky 2008).

Pathological changes in AD

AD is characterised pathologically by the extracellular deposition of amyloid-β (Aβ)-containing plaques, the intracellular accumulation of tau-positive tangles and neuronal loss (Braak & Braak 1991). The development of both plaques and tangles occurs in stages, wherein Aβ deposits are first deposited in the isocortex and the basal areas of the frontal, temporal and occipital cortex, eventually becoming established in the hippocampus (Braak & Braak 1991). Neurofibrillary changes in AD occur in six stages, beginning with the accumulation of intracellular neurofibrillary tangles and neuropil threads in the entorhinal cortex (EC), which spread throughout the hippocampus and isocortex in the later stages (Braak & Braak 1991). Neuronal cytoskeletal dysfunction is associated with hyperphosphorylated tau (P-Tau) (Grundke-Iqbal et al. 1986) and leads to neuronal and synaptic loss (Serrano-Pozo et al. 2011; Weller et al. 2008; Tarasoff-Conway et al. 2015). However, the cortical beginnings of this disease have recently been challenged by a longitudinal MRI study which suggests that significant changes in grey matter volume of individuals who went on to develop AD occurred firstly in the basal forebrain before affecting the EC. This study suggested that $A\beta_{1\text{-}42}$ was detected in the CSF of asymptomatic individuals after damage to the basal forebrain, and that clinical impairments developed when there was degeneration of the basal forebrain and EC (Schmitz et al. 2016).

The variation of the spread of tangle pathology within the brain was first suggested to represent three subtypes of AD (Murray et al. 2011) which was associated with different amounts of grey matter atrophy (Whitwell et al. 2012). This was more recently developed in a cluster analyses study by Poulakis et al, who identified 5 different subtypes of spatially differing pathology including minimal atrophy, limbic predominant, hippocampus sparing

and two diffuse subtypes, each of which had different cognitive and symptomatic variations with hippocampal sparing being the most severe (Poulakis et al. 2018).

Cerebrovascular changes in AD

In addition to pathological changes in the parenchyma in AD, increasing evidence suggests that alterations of the cerebrovasculature contribute to the aetiology and /or progression of AD. In fact, vascular pathology has been suggested to be the earliest indicator of the development of AD (Jack et al. 2010; Iturria-Medina et al. 2016). One-third of AD cases present with vascular pathologies (Kalaria 1999). Examples of these include the presence of 'string vessels', indicating collapsed capillaries (Hunter et al. 2012), and thickening of the CVBM (Attems et al. 2004) possibly due to increased amounts of collagen I, III and IV (Kalaria & Pax 1995). Other changes in the biochemical composition of the CVBM in AD include increased levels of laminin and heparan sulphate proteoglycans (HSPG) compared to age matched controls (Christov et al. 2008; Kalaria 1999). Pericyte degeneration and BBB breakdown associated with leakage have also been found to be significantly increased in AD tissue (Halliday et al. 2016).

CAA

The most common form of cerebrovascular pathology associated with AD is CAA. CAA is defined as the presence of Aβ deposits in the walls of cerebral blood vessels (Vinters 1987). It is present in up to 98% of AD cases (Jellinger 2002) and also in the non-demented elderly, where it has been shown to be present in 10-38% of individuals over the age of 70 (Jellinger 2002). Although the majority of cases of CAA occur sporadically with age being a significant risk factor (Tanzi & Bertram 2005), an autosomal dominant form of CAA, called hereditary cerebral haemorrhage with amyloidosis-Dutch type (HCHWA-D), has been identified in the Dutch population (Kamp et al. 2014). Other forms of hereditary CAA include the HCH-WA Italian type, Iowa mutation, Flemmish, Piedmont and Arctic mutations which are characterised by specific fibrillar formations and specific APP mutation sites (Miravalle et al. 2000; Grabowski et al. 2001; Brooks et al. 2004; Obici et al. 2005), and the Icelandic form where the non-amyloid beta cystatin-c protein leads to CAA (Pezzini et al. 2009).

CAA topography

CAA is diagnosed post mortem, but individuals may also be classified as having 'probable CAA' from MRI imaging using the Boston criteria for diagnosis of CAA (Knudsen et al. 2001). In CAA, Aβ deposits predominantly in leptomeningeal arteries and cortical arterioles, less frequently in capillaries and is rarely observed in veins (Attems et al. 2011).

Within the arteries, Aβ is proposed to deposit in the basement membrane of the tunica media, eventually killing and replacing the underlying multicellular layer of SMCs (Preston et al. 2003; Keable et al. 2015). CAA presents initially in the occipital lobe, followed by the temporal, frontal and parietal lobes, then in the hippocampus and EC and is observed in thalamus and cerebellum only in the late stages of the disease (Tian et al. 2003; Pfeifer et al. 2002; Attems et al. 2011).

Allen et al recently set out a classification system for 4 types of CAA as shown in Table 1.1 (Allen et al. 2014). CAA severity has been found to be more correlated with missense mutations and duplication of the gene that encodes for the amyloid precursor protein (APP) and ApoEε4 homozygosity than with sporadic AD (Mann et al. 2018), suggesting it to be associated with failure of Aβ waste management. Interestingly, Buss et al recently found that although the presence of additional copies of the APP gene increased the risk of CAA-associated intracerebral haemorrhage, the presence of 3 copies of the APP gene as found with Down's syndrome decreased this risk, suggesting some protection through an unknown mechanism (Buss et al. 2016).

Table 1.1 CAA types 1-4 as classified by Allen et al (Allen et al. 2014)

Type	**1**	**2**	**3**	**4**
Gender prevalence	Female	Male	No difference	No difference
Presence of senile plaques	Present	Present	Present	Very few, sparse
CAA location	Mainly leptomeningeal	Deeper penetrating, intracortical arteries	Mainly capillary CAA	Leptomeningeal & cortical arteries and capillaries

Clinical characteristics of CAA

CAA is most frequently associated with intracerebral haemorrhages (ICH). A study by Meretoja and colleagues found that 20% of ICH treated patients at the Helsinki University Central hospital were found to have CAA, which was the second highest cause of stroke in the study (Meretoja et al. 2012). Also, the Rotterdam study has recently demonstrated that during a follow-up of patients identified with microbleeds, the risk of having new strokes was highest for patients who had had microbleeds in areas associated with CAA (Akoudad et al. 2015). In individuals with HCHWA-D, ICH in patients is the main symptom and

CAA load is associated with reduced vascular function (Kalaria 2001; van Opstal et al. 2016; Kamp et al. 2014; Fotiadis et al. 2016).

An independent effect of CAA on cognitive decline, separate from other AD pathologies, has also been demonstrated by regression analysis of data from the Religious Orders study (Arvanitakis et al. 2011). Recently, white matter hyperintensities, including enlarged perivascular spaces, have also been found to occur in younger age groups, and may be a predicting factor for the development of CAA (Ishikawa et al. 2018). The cognitive deficits associated with severe CAA are also associated with neocortical CAA but not with hippocampal CAA (Arvanitakis et al. 2011).

In animal models of CAA, a loss of contact of astrocytic endfeet and decreased expression of potassium channels and dystrophin-1 (Wilcock et al. 2009), along with a loss of SMCs has been associated with CAA-affected vessels (Haglund et al. 2006). Vasoreactivity in the Tg2576 mouse model of CAA has been demonstrated to be reduced due to elevated reactive oxidative species (Han et al. 2015), and additionally in the TgSwDI mouse model, where oxidative stress contributed to reduced CBF responses to functional hyperaemia prior to CAA pathology (Park et al. 2014).

There is also evidence that CAA affects CBF in humans with AD. Vasoreactivity has been measured in humans in different ways, including hypercapnia (Maggio et al. 2013) and by blood oxygen level dependent time to peak (BOLD-TTP) MRI, where visual cues are used to measure NVC. Interestingly, it has been demonstrated that resting CBF, does not differ between CAA and non-CAA patients (Dumas et al. 2012). However, a recent study found that patients both with sporadic CAA or HCHWA-D showed poor vascular reactivity in response to BOLD-TTP MRI (Fotiadis et al. 2016), indicative of impaired NVC. Hypo-perfusion has been noted in the temporal and also the hippocampal regions of individuals diagnosed with early AD (Alsop et al. 2008). Interestingly, the hippocampus, striatum and amygdala, have been found to be hyper-perfused in MCI affected patients in comparison to control patients (Dai et al. 2009). MCI patients have also been found to have hypo-perfusion in the precuneus and cuneus regions of the brain (Xu et al. 2007; Dai et al. 2009), consistent with regions affected during symptomatic AD (Miners et al. 2015). MCI patients who went on to develop dementia were shown to have significantly poorer perfusion in the parietal and frontal cortices in relation to decreased hippocampal volume as detected by MRI (Chao et al. 2010).

The precuneus and parietal regions have also been noted to be hypo-perfused in AD in addition to the posterior, temporal, orbitofrontal lobes, hippocampus, striatum and amygdala, and as the disease progresses, the frontal cortex (Brown et al. 1996; Hu et al. 2010; Dai et al. 2009). Hu et al also found areas of significant hyper-perfusion in AD patients in the frontal and lateral temporal lobes, where AD pathology is known to occur in the severe stages of the disease (Hu et al. 2010), suggestive of a possible compensatory mechanism. Changes in perfusion in vulnerable areas has led to the 'Critically Attained Threshold of Hypoperfusion'(CATCH) hypothesis proposed by de la Torre (de la Torre 2000) who suggest that once innate age-related decreases in cerebral perfusion and pathology arising from risk factors associated with vascular dementia reaches a threshold, this leads to pathological hypo-perfusion.

Aetiology of CAA

The mechanisms that underlie the aetiology of CAA remain unknown. The presence of Aβ in the walls of the cerebrovasculature is thought to principally result from impaired clearance of neuronally-produced Aβ (Goedert 1987), although *in vitro* cultures of smooth muscle cells also produce Aβ (Davis-Salinas et al. 1995). It has also been suggested to accumulate through age-related failure of removal of Aβ either across the BBB into the bloodstream (Mackic et al. 1998) and/or along the walls of the blood vessels.

Aβ production

Aβ is naturally produced in the brain by the processing of amyloid precursor protein (APP), a transmembrane glycoprotein that is highly expressed in neuronal membranes. APP can be processed through two different pathways; in the non-amyloidogenic pathway, APP is cleaved by α secretase into a soluble sAPPα fragment and a CTF83 carboxy terminal fragment (Fig. 1.6). CTF83 is then cleaved by the γ secretase enzyme into CTF59 and P3 fragments which do not contain the full-length Aβ sequence. In the amyloidogenic pathway, APP is cleaved first by β secretase, generating the sAPPβ fragment and a remaining CTF99 fragment (Fig. 1.6). It is the cleavage of the latter fragment by γ secretase which generates the neurotoxic species of Aβ (Puzzo et al. 2015) (Fig. 1.6).

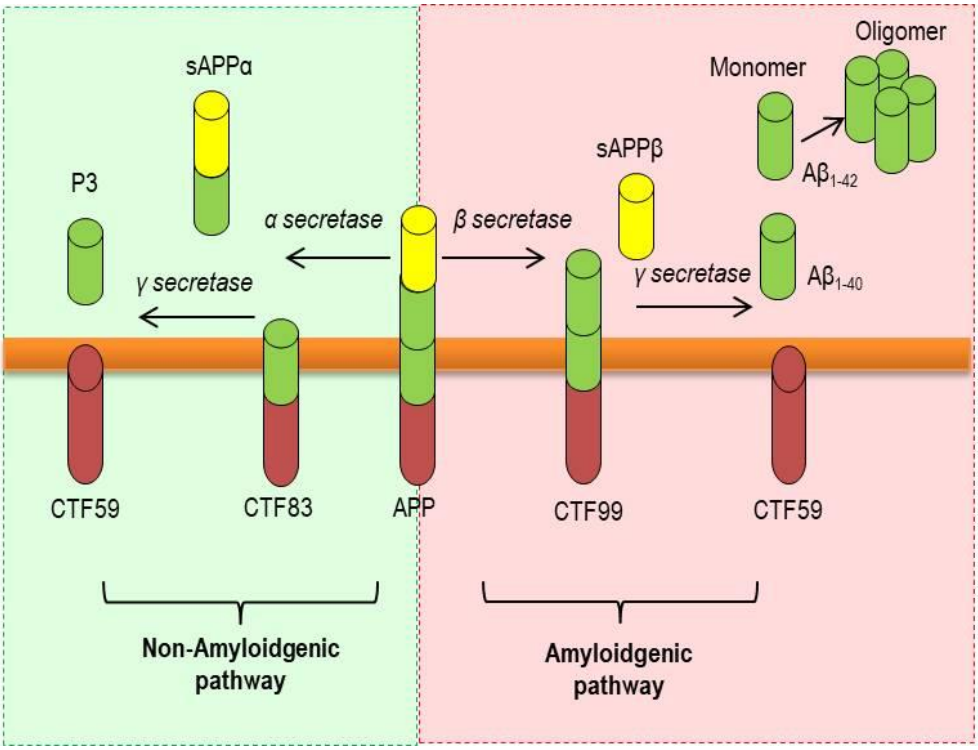

Figure 1.6 APP processing
Schematic of APP processing via the non-amyloidgenic pathway, leading to the production of sAPPα, or the amyloidogenic pathway, leading to Aβ production.

The Aβ peptide can be of varying lengths, predominantly 39-42 amino acids long. $A\beta_{1-42}$ is more prone to aggregation and aggregates more quickly than the $A\beta_{1-40}$ fragment (Jarrett et al. 1993; Sinha & Lieberburg 1999). Parenchymal plaques in AD are composed predominantly of $A\beta_{1-42,}$ while $A\beta_{1-40}$ deposits primarily in CAA (Suzuki et al. 1994). This is supported by analysis of cerebrospinal fluid (CSF), where there is a significant decrease in both $A\beta_{1-40}$ and $A\beta_{1-42}$ CSF levels in CAA, compared to AD, where only a decrease in $A\beta_{1-42}$ CSF levels is detected with disease progression (Verbeek et al. 2009).

Aβ clearance

In healthy individuals, Aβ production is balanced by its removal. Isotype labelling experiments have estimated that Aβ synthesis occurs at a rate of 7.6%/hour and exogenous Aβ is removed from the brain parenchyma and vasculature at a rate of 8.3%/hour as calculated from the ratio of labelled Aβ produced compared to unlabelled Aβ in CSF over time (Bateman et al. 2006). Four main clearance mechanisms by which Aβ is removed from the brain have been identified including i) degradation by enzymes, ii) uptake by perivascular macrophages and microglia, iii) transcytosis across the BBB, and iv) drainage along blood vessels (Fig. 1.7).

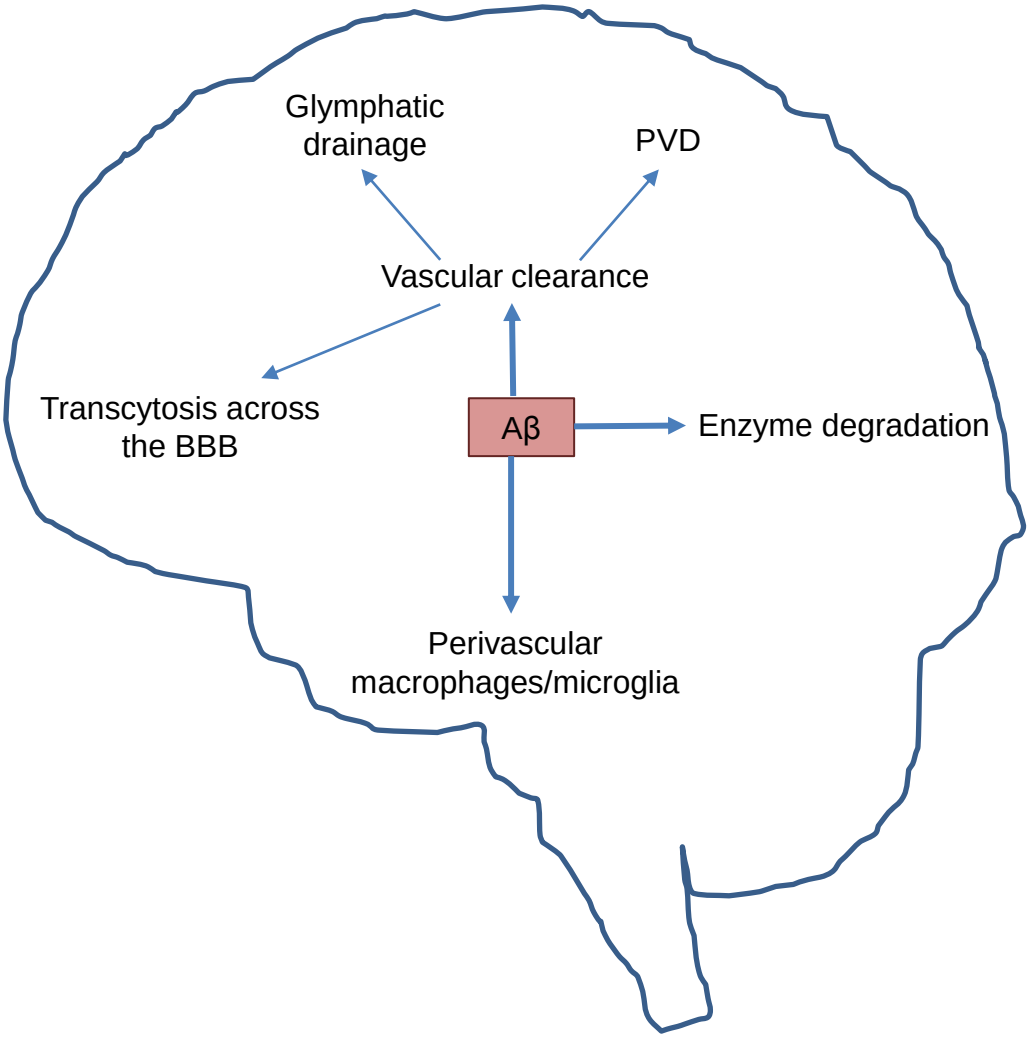

Figure 1.7 Aβ clearance routes
Schematic representing the main routes of Aβ removal from the parenchyma

Enzymatic degradation

Aβ is cleared from the brain following degradation by enzymes including neprilysin (Iwata et al. 2001; Hafez et al. 2011), insulin-degrading enzyme (Farris et al. 2003), angiostensin-converting enzyme (ACE) (Miners et al. 2008) and endothelin-converting enzyme (ECE) (Palmer et al. 2010). Knockout of the neprilysin gene in a transgenic mouse model has been shown to increase Aβ levels in the plasma and hippocampus, as well as increase CAA pathology (Farris et al. 2007). ACE and ECE-1 are expressed in cerebrovascular vessels and astrocytes (Palmer et al. 2010; Miners et al. 2014) and ACE has been shown to be increased in AD, possibly to compensate for increased Aβ deposition (Miners et al. 2008).

Perivascular macrophages and microglia

Microglia, the primary inflammatory cells of the brain, have been shown to position themselves around sites of brain injury such as following damage to the BBB (Nimmerjahn et al. 2005). Microglia have been implicated in Aβ clearance following immunization with anti-Aβ antibodies, potentially through a phagocytotic mechanism (Wilcock et al. 2004). It

has also been suggested that microglia become activated by dystrophic neurons (Streit 2004). A recent publication by Bachstetter and colleagues on human brains suggested that there are five different morphologies of microglia which are specific to age-related diseases, such as AD and hippocampal sclerosis (Bachstetter et al. 2015). However, it has been noted that increased dystrophic microglia also correlates with age, suggesting a possible effect on age-related changes in the inflammatory profile of the normal brain (Streit et al. 2004).

Perivascular macrophages, which are peripherally-derived macrophages that reside within the perivascular spaces surrounding leptomeningeal and large penetrating arteries, have been shown to be localised to CAA-affected vessels (Klohs et al. 2014; Pey et al. 2014). Activation of perivascular macrophages has been shown to decrease in vascular $A\beta_{1-42}$ in the transgenic TgCRND8 mouse model of CAA (Hawkes & McLaurin 2009).

Transcytosis across the BBB

Receptors that have been shown to transport Aβ across the BBB include the receptor for advanced glycation end-products (RAGE) (Mackic et al. 1998), LDL receptor-related protein-1 (LRP-1) (Shibata et al. 2000), p-glycoprotein (p-gp) (Qosa et al. 2014), and ATP binding cassette transporter proteins (ABC) ABCG2 and ABCG4 (Do et al. 2012). LRP-1 has been shown to transport $A\beta_{1-40}$ and $A\beta_{1-42}$ from the parenchyma into the vessel lumen with $A\beta_{1-40}$ cleared at a faster rate than $A\beta_{1-42}$ (Bell et al. 2007). Shibata et al showed that LRP-1 expression decreases with age in mice and that levels of LRP-1 are decreased in AD brains (Shibata et al. 2000). Inhibiting the transporter protein p-gp on the abluminal side has also been shown to inhibit transcytosis of Aβ across the BBB. Hartz et al found p-gp to be downregulated in Tg2576 mice, and the restoration of p-gp levels lead to a reduction in $A\beta_{1-40}$ and $A\beta_{1-42}$ in cerebral capillaries (Hartz et al. 2010). Conversely, RAGE acts to transport Aβ from the blood into the brain (Mackic et al. 1998).

Clearance along blood vessels

In addition to clearance across the BBB, evidence suggests that blood vessels can also act as conduits along which Aβ is removed from the brain. Two pathways have been identified, the glymphatic and perivascular pathways.

Glymphatic pathway

The glymphatic clearance hypothesis proposes a principal role for CSF in the clearance of Aβ (Iliff et al. 2012). Experimental evidence from mice suggests that that CSF enters the

brain from the subarachnoid space along the periarterial space surrounding penetrating arteries (Iliff et al. 2013). Following exchange of solutes between the CSF and the parenchymal ISF, Aβ contained within the CSF is removed from the brain along paravenous spaces and is returned to the blood. This is dependent upon glial water influx mediated through the astrocyte aquaporin 4 (AQP4) water channel. This water exchange is believed to drive ISF and solutes from the parenchyma through exchange with paravenous CSF or CSF in the subarachnoid space and is driven by convective flow. Deletion of AQP4 in transgenic mice led to poor removal of intracerebrally injected Aβ, suggesting an obstruction of glymphatic drainage (Iliff et al. 2012; Jessen et al. 2015). Nedergaard and colleagues have also suggested that sleep and anaesthesia play an important role in clearance, and found that the rate of clearance was increased in animals during sleep (Xie et al. 2013).

However, findings from recent *in silico* and *in vivo* experiments have challenged several aspects of this hypothesis. Calculations based on known concentrations of ions in the ISF and CSF have shown that unidirectional water movement is not possible under physiological conditions. Moreover, clearance of solutes by convective or bulk flow does not match the rates of solute clearance that are observed in experimental conditions (Smith et al. 2017; Abbott et al. 2018; Smith & Verkman 2018; Hladky & Barrand 2014). It has also been demonstrated that tracers injected into the CSF move out of the brain along per-arterial pathways and not the venous paravascular routes suggested by the glymphatics hypothesis (Albargothy et al. 2018). Smith et al have reported that AQP4 deletion did not hinder clearance of tracer from the parenchyma and Gakuba et al have found that solute clearance is higher during states of wakefulness (Gakuba et al. 2018; Smith et al. 2017). A recent report has also suggested that there is minimal entry of CSF into the brain under normal conditions and that entry along peri-arterial spaces may be a post-mortem artefact (Ma et al. 2018).

Perivascular drainage

Perivascular drainage (PVD) aka intramural perivascular arterial drainage has been proposed as another pathway of clearance of Aβ from the brain (Fig. 1.8). In this model, Aβ secreted into the ISF moves through the parenchyma and enters the CVBM of capillaries which invaginate the extracellular space (Morris et al. 2014). Aβ eventually moves into the CVBMs of the tunica media of cortical and leptomeningeal arteries, and is ultimately cleared into the cervical lymph (Hawkes et al. 2014; Weller, Djuanda, et al.

2009; Abbott 2004). Disruption in the efficiency of perivascular drainage is proposed to lead to the disruption in parenchymal homeostasis, causing a rise in soluble Aβ, which triggers tau pathology and initiates neuronal death (Weller, Preston, et al. 2009).

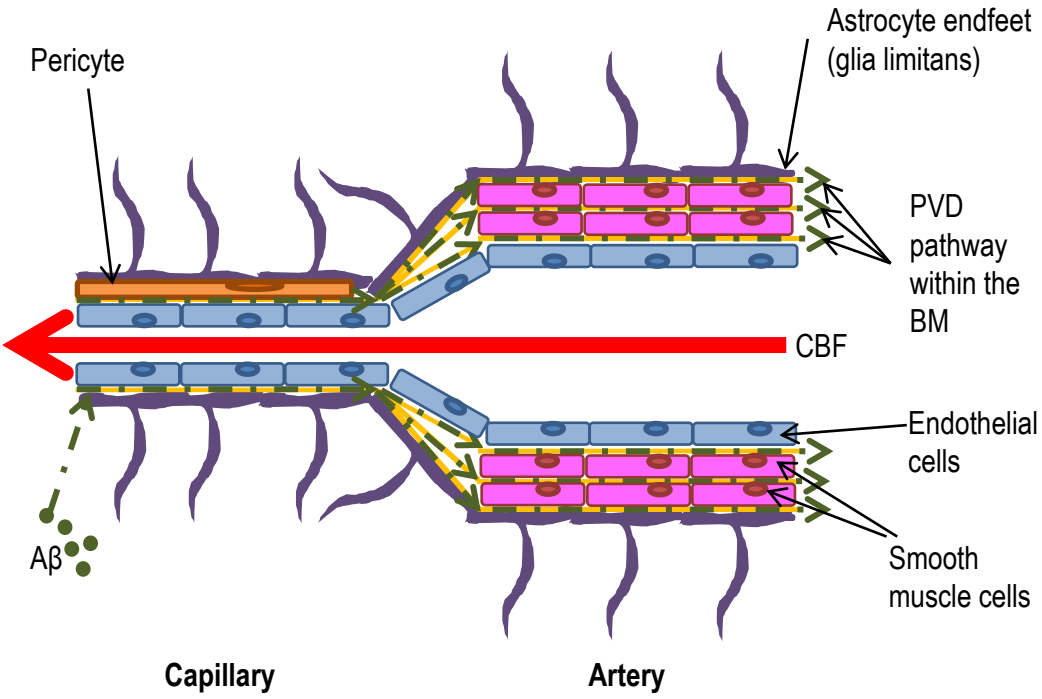

Figure 1.8 Perivascular drainage
Diagram depicting perivascular drainage of Aβ through the cerebrovascular basement membrane of the capillary into the basement membranes of the artery.

Evidence to support this hypothesis comes from the observation that tracers injected in the deep grey matter of the brain were found in capillaries and arteries and minimally in veins, which matches the pattern of CAA observed in humans (Preston et al. 2003; Keable et al. 2015). Furthermore, injected Aβ and dextran have been shown to co-localise with the CVBM (Carare et al. 2008; Dorr et al. 2012; Hawkes et al. 2011) in the same pattern as that observed in human brains (Keable et al. 2015; Attems et al. 2011). These data suggest that the CVBM may play a role in PVD, and that changes to the CVBM may contribute to impaired removal of Aβ from the brain (Morris et al. 2014).

Although experimental evidence suggests movement of ISF in the direction opposite to blood flow (e.g. from capillaries to arteries), the mechanisms by which this movement is generated are currently unknown. The flow of ISF has been suggested to be pulse-dependent, as this movement has been seen to be decreased following middle cerebral artery occlusion in mice (Arbel-Ornath et al. 2013) and ceases following cardiac arrest (Carare et al. 2008) and stroke (Garcia-Alloza et al. 2011). Using labelled dextran injected into the deep grey matter and monitoring its progress at varying timepoints, Carare et al

observed tracers in the CVBM of leptomeningeal cortical arteries by 5 min post injection. Dextran was no longer detectable in vessel walls after 3 h (Carare et al. 2008). Such findings have also been replicated using fluorescently-labelled human $A\beta_{1-40}$ (Hawkes et al. 2012; Hawkes et al. 2011; Hawkes et al. 2013). Ball et al. reported that $A\beta_{1-40}$ could be detected in the olfactory bulb of rats within 10 min of injection into the inferior colliculus, suggesting a very rapid movement of ISF (Ball et al. 2010). ISF clearance via PVD was also shown in real time using multi-photon microscopy (Arbel-Ornath et al. 2013). This study demonstrated ISF drainage within the CVBM around smooth muscle cells in a 'bi-exponential mode', suggesting that there is a driving force behind PVD, and it is unlikely to occur by diffusion alone.

Mathematical modelling by Schley et al hypothesised that the force for ISF movement could be generated during cardiac pulse cycles, where vasoconstriction is followed by vasorelaxation and could propel the movement of ISF in the direction opposite to blood flow (Schley et al. 2006). However, recent modelling of ISF drainage by Diem et al suggest that the arterial pulsatility is not strong enough to match the rapid flow rate of experimental data (Diem et al. 2017; Carare et al. 2008).

Vasomotion, the spontaneous contraction of arteries, has been linked to ultraslow oscillations of neuronal activity and is thought to ensure maintenance of oxygen levels, under resting state and during stimulation (Mateo et al. 2017). A recent study using diffusion tensor imaging suggested that vasomotion drives 'perivascular fluid movement' that was linked to heart rate (Harrison et al. 2018). However, the data from that study was derived from the circle of Willis, which is extrinsically innervated (Bleys & Cowen 2001), and may therefore not be reflective of vasomotion control from the intrinsically innervated parenchyma. Recent computational analyses by Aldea et al have suggested that the forces driving PVD may be generated from neuronally-induced relaxation and dilation of the cerebrovasculature, most likely propagated by contractions of SMCs (Aldea et al. 2018).

Does loss of intrinsic innervation play a role in the aetiology of CAA?

As discussed in section 'Intrinsic innervation' under 'Vascular function', innervation of the NVU by cholinergic neurons contributes to the regulation of CBF and NVC. A large body of evidence has demonstrated that there is significant death of cholinergic neurons in AD. Loss of cholinergic innervation, including nerve fibres, decreased ChAT activity and lower expression of muscarinic and nicotinic ACh receptors are observed in individuals with

MCI and at the earliest stages of AD (Kuznetsova & Schliebs 2013; Mann et al. 1984; Svensson et al. 1992; Geula et al. 2008; McNeely et al. 2015).

The loss of cholinergic neurons as one of the earliest features of AD gave rise to the cholinergic hypothesis of AD, which suggests that cholinergic denervation plays a significant role in the aetiology of AD and underlying dementia (Francis et al. 1999; Bartus et al. 1982; Van Beek & Claassen 2011; Schliebs & Arendt 2011; Terry & Buccafusco 2003; Perry et al. 1995) This hypothesis is supported by the correlation between loss of cholinergic neurons and increased Aβ plaque deposition and CAA severity (Tong & Hamel 1999; Roher et al. 2000; Perry 1980; Ramos-Rodriguez et al. 2013; Perez et al. 2007; Laursen et al. 2013).

Relationships between basal forebrain degeneration and Aβ load in the cortex have been documented in non-demented elderly brains (Grothe et al. 2014) and basal forebrain atrophy has been suggested to predict cortical Aβ burden (Teipel et al. 2014). More recently, a longitudinal study reported a significant loss of volume in the basal forebrain preceding pathological changes in the entorhinal cortex of individuals who went on to develop AD (Schmitz et al. 2016). Administration of donepezil, a cholinesterase inhibitor approved for the treatment of AD, has been shown to increase CBF in the middle and posterior cingulate cortices, part of the medial cholinergic pathway of the brain, and is linked to an improvement in cognitive function (Li et al. 2012). A recent study where donepezil was given to prodromal AD patients showed a reduction in the rate of atrophy of the basal forebrain (Cavedo et al. 2017).

NOS expression has been found to be stably expressed across a wide range of ages (Sobreviela & Mufson 1995) but has been shown to be affected in AD and CAA. A loss of nNOS-positive cells has been found to correlate with plaque pathology in the EC in AD brains (Thorns et al. 1998). Levels of eNOS have also been found to be decreased in AD (Jeynes & Provias 2009), although in other studies eNOS and iNOS expression has been found to be elevated in AD (Dorheim et al. 1994).

Given the contribution of ACh in the regulation of CBF via NOS signalling, early loss of cholinergic input at the NVU may disrupt the structure and/or function of the cerebrovasculature. This may induce a consequent reduction in the force of ISF clearance from the brain and thereby contribute to the accumulation of Aβ as CAA.

Hypothesis

This PhD project has investigated the hypothesis that loss of cholinergic innervation at the NVU contributes to the development of CAA by decreasing the clearance of Aβ along perivascular pathways. To do so, the following aims were carried out:

1. To replicate the death of cholinergic neurons in the basal forebrain and fibre projections to the cortex and hippocampus of adult male wildtype mice using the immunotoxin mu-p75-saporin.
2. To evaluate the loss of perivascular innervation at the NVU in the cortex and hippocampus using quadruple labelling immunohistochemistry and 3D reconstruction.
3. To determine how loss of cholinergic innervation affects CBF in the cortex and hippocampus using fMRI and investigate the effects on NOS expression and activity.
4. To analyse the effect of cholinergic degeneration on PVD of Aβ from the cortex and hippocampus of wildtype mice.
5. To examine the consequences of the death of cholinergic neurons on CAA severity in the TetO-APPSweInd mouse model of AD.

Chapter 2 : Main Materials and Methods

Materials

mu-p75-saporin was purchased from Advanced Targeting Systems (San Deigo, USA), the human $A\beta_{1-40}$ HiLyte Fluor™ 555 and $A\beta_{1-40}$ HiLyte Fluor™ 488 labelled was obtained from AnaSpec (Fremont, USA) and optimal cutting temperature compound (OCT) was from Fisher Scientific (Loughborough, UK). Vectastain™ ABC kit was obtained from Vector Laboratories Ltd (Peterborough, UK) and all other chemicals were purchased from Sigma-Aldrich (Dorset, UK) or Fisher Scientific (New Hampshire, US). A list of antibody sources is provided in Table 2.1.

Table 2.1 List of Antibodies used, their properties and source

Antigen	Antibody host	Working dilution	Antigen retrieval	Source
Primary Antibodies				
Anti-$A\beta_{1-40}$	Rabbit (IgG)	1:100	70% Formic acid (v/v) (45 s at RT)	Merck Millipore (Temecula, USA)
Anti-$A\beta_{1-42}$	Rabbit (IgG)	1:100	70% Formic acid (v/v) (45 s at RT)	Merck Millipore (Temecula, USA)
Anti-CD31	Rat (IgG2a, κ)	1:50	1 mg/ml Pepsin in 0.2 M HCl (30 s at 37^0 C)	BD Pharmingen (San Jose, USA)
Anti-ChAT	goat IgG	1:75 (IHC) 1:500 (WB)	-	Millipore (Temecula, USA)
Anti-Collagen IV	Rabbit (IgG)	1:100	1 mg/ml Pepsin (sigma) in 0.2 M HCl (30 s at 37^0 C)	Abcam (Cambridge, USA)
Anti-Collagen IV	mouse IgM	1:250	1 mg/ml Pepsin in 0.2 M HCl (30 s at 37^0 C)	Sigma-Aldrich (Dorset, United Kingdom)
Anti-eNOS	Rabbit (IgG)	1:5000 (WB)	-	Cell Signalling (Danvers, USA)
Anti-GAPDH	Rabbit (IgG)	1:5000 (WB)	-	Sigma-Aldrich (Dorset, UK)
Anti-GFAP	Chicken IgG	1:500	-	Abcam (Cambridge, USA)
Anti-Iba1	Rabbit (IgG)	1:500	0.01 M Sodium Citrate 0.01% tween pH 6 (15 min at ~90^0 C)	Abcam (Cambridge, USA)

Anti-Laminin	Rabbit (IgG)	1:350	1 mg/ml Pepsin in 0.2 M HCl (30 s at 37^0 C)	Sigma-Aldrich (Dorset, United Kingdom)
Anti-nNOS	Rabbit (IgG)	1:250 (WB)	-	Cell Signalling (Danvers, USA)
Anti-p75NTR	Rabbit (IgG)	1:400	-	Merck Millipore (Temecula, USA)
Anti-Serotonin transporter (5-HTT)	Rabbit (IgG)	1:250,000	Tris-EDTA 0.01% tween pH 9 (0.01 M) Tris, 0.0013 M EDTA) (15 min at ~90^0 C)	Immunostar (Hudson, USA)
Anti-SMA-FITC conjugated	mouse IgG2a	1:350	-	Sigma-Aldrich (Dorset, United Kingdom)
Anti-Tyrosine hydroxylase (TH)	Rabbit (IgG)	1:100	-	Millipore (Temecula, USA)
Anti-Total NOS	Mouse (IgM)	1:200	-	Novus Biologicals (Abingdon, UK)
Anti-Tryptophan Hydroxylase	Goat IgG	1:100	-	Abcam (Cambridge, USA)
Secondary antibodies				
Anti-chicken AlexaFluor®633	Goat-anti-Chicken IgY	1:200	-	AlexaFluor®, Molecular Probes (Rockford, USA)
Anti-goat AlexaFluor®488	Donkey-anti-goat IgG	1:200	-	AlexaFluor®, Molecular Probes (Rockford, USA)
Anti-mouse AlexaFluor®633	Goat-anti-mouse IgG	1:200	-	AlexaFluor®, Molecular Probes (Rockford, USA)
Anti-rabbit AlexaFluor®488	Goat-anti-rabbit IgG	1:200	-	AlexaFluor®, Molecular Probes (Rockford, USA)
Anti-rabbit AlexaFluor®633	Goat-anti-rabbit IgG	1:200	-	AlexaFluor®, Molecular Probes (Rockford, USA)

Animals

C57BL/6 mice were obtained from The Open University (OU, Milton Keynes, UK) or C57BL/6 mice were obtained from the University of Southampton (Southampton, UK). TetO-APPSweInd mice carrying the Swedish (KM670/671NL) and Indiana (V717F) mutations in the human amyloid precursor protein (APP) (Jankowsky et al. 2005) were obtained as a generous gift from Dr JoAnne McLaurin (Sunnybrook Research Centre, Toronto, Canada) and bred at the OU. All animal work was approved by and carried out in accordance to guidelines set up by the Animal Welfare and Ethics Research Boards (AWERB) at the OU, University of Southampton and UCL in accordance with Home Office regulations and approved project licences (PPL 70/8507 and PPL 30/3095) under the Animals Scientific Procedures Act (1986). All animals were housed on a 12 hour light/dark cycle. Food and water were provided *ad libitum.*

Cholinergic denervation

Mice were anesthetised under isoflurane gas (induction at 5% in medical air, maintenance at 1.5 - 2% in medical air) and placed into a stereotaxic frame (Kopf instruments, CA, USA). Topical anaesthetic (Cryogesic (ethyl chloride), Acorus Therapeutics Ltd, Chester, UK) was applied to the scalp before the head was shaved. A midline incision was made and the skull cleaned. A small burr hole was drilled over the left and right lateral ventricles and 0.5 µL of mu-saporin (0.596 µg/µl) or 0.9% saline was injected into each ventricle (coordinates from Bregma: AP=-0.4 mm, ML=-/+1.0 mm, DV=-2.3 mm) at a rate of 0.2 µl/min using a 32 G Hamilton syringe (Esslab, Hadleigh, England). The needle was left in situ for 2 minutes after the injection to allow for diffusion. The skin incision was sutured and mice returned to their home cages after recovery from anaesthesia. Analgesia was administered intraperitoneally at the time of surgery (Carprieve, 5% w/v, 0.32 ml/kg, Norbrook, Northamptonshire, UK) and mice were able to self-administer sugar free jelly (Hartley, Histon sweet spreads Ltd, Leeds, UK) containing Carprofen (250 µg in 500 µl jelly per mouse, Zoetis, London, UK) for 1 week post-surgery.

Immunohistochemistry

Mice were deeply anesthetised with an overdose of sodium pentobarbitone (20% w/v IP, Animalcare, York, UK) and perfused intracardially with 0.01 M phosphate buffered saline (PBS) followed by 4% paraformaldehyde (PFA) at a rate of 5 ml/min. The brains were post-fixed in 4% PFA overnight and left in 30% sucrose for one week before being embedded in OCT for cryosectioning. Brains were sectioned at 20 µm thickness using a cryostat and collected onto slides or as free-floating coronal sections that were stored in

anti-freeze storage solution (30% glycerol, 30% ethylene glycol, 40% 0.01 M PBS) at -20°C.

For all immunohistochemistry experiments, a general procedure was carried as detailed below. Sections were washed three times in 0.01 M PBS, before being blocked for endogenous peroxidase activity by incubation with 3% hydrogen peroxide (H_2O_2) (Sigma-Aldrich, Dorest, UK) diluted in methanol for slide mounted sections or in 0.01 M PBS for free floating sections for 15 min at room temperature (RT). If necessary, antigen retrieval was carried out (see Table 1), followed by 3 x 5 min washes in PBS, after which sections were then blocked in 15% normal donkey serum (NDS) (Sigma-Aldrich, Dorset, UK), diluted in 0.01M PBS for 15 min to prevent background staining, followed by primary antibody incubation overnight at 4°C (see Table 1 for antibody concentrations used). Antibodies were diluted in 0.01 M PBS + 0.1 – 0.5% Triton-x100 for free-floating sections, or 0.01 M PBS + 0.01% Tween-20 for slide mounted sections.

Enzyme-linked immunohistochemistry

Following incubation with primary antibody, sections were washed 3 x 5 min in 0.01 M PBS before incubation for 1 h in a biotinylated secondary antibody raised against the host of the primary antibody, diluted in 0.01 M PBS+0.01% v/v Triton-x100 at 1:400. Sections were then washed 3 x 5 min in PBS before being incubated in Vectastain™ ABC kit (Vector Laboratories Ltd, Peterborough, UK) (1:200) diluted in 0.01M PBS+0.01% v/v Triton-x100 for 1 h. Staining was developed using DAB chromagen (Sigma-Aldrich, Dorset, UK) with glucose oxidase enhancement, which was followed by slide mounting and dehydration through a series of alcohols and xylenes. Slides were then coverslipped using DPX (Fisher Scientific, Loughborough, UK).

Immunofluorescence

For single labelling immunofluorescence, after incubation with the primary antibody, sections were washed 3 x 5 min in 0.01 M PBS before being incubated in the appropriate secondary antibody (AlexaFluor®, Molecular Probes Rockford, USA) at 1:200 for 2 h at RT (Table 1). Following 3 x 5 minute washes in 0.01 M PBS, sections were coverslipped using Mowiol® (Sigma, Dorset, UK) containing 0.1% v/v Citifluor (Citifluor ltd, London, UK) mounting media. For multiple labelling immunohistochemistry, primary antibodies raised in different hosts were applied either sequentially or simultaneously incubated depending on the conditions that ensured non-specific staining (see individual chapters for details).

Thioflavin S (Sigma-Aldrich, Dorset, UK) staining to identify fibrillar Aβ (Kelényi 1967) was carried out by incubating tissue in 1% Thioflavin S in dH_2O (w/v) for 5 min, before differentiating in 70% ethanol (v/v) for 5 min and then washing 3 x 5 min with 0.01 M PBS before mounting in Mowiol® (Sigma, Dorset, UK) containing 0.1% v/v Citifluor (Citifluor Ltd, London, UK).

Photomicrographs from DAB-stained tissue were obtained using a Nikon Eclipse 80i light microscope and Picture Frame Software. Images were analysed using Image J.

Photomicrographs from fluorescently-labelled tissue were obtained using a Leica SP5 confocal microscope and LAS software. Imaging was carried out at either x10 or x20 magnification (air) or at x100 (oil immersion) for images to be used for Imaris software processing. Images were captured using multiple sequential z-stacks and then reconstructed using maximum projection.

Functional Magnetic Resonance Imaging (fMRI)

Surgeries to induce cholinergic loss were carried out in male C57BL/6 mice as described above at the University of Southampton and 0.9% saline or mu-saporin-treated mice were shipped to UCL 1 week before imaging to allow for acclimatisation (Home office license PPL 30/3095). 45 days post-surgery, mice were assessed for CBF using fMRI at the UCL Centre for Advanced Imaging. A 9.4 T VNMRS horizontal bore scanner (Agilent Inc., Santa Clara, CA, USA) with a 72 mm inner diameter volume coil and 2 channel array head coil (Rapid Biomedical, Columbus, OH, USA) was used for radio frequency transmission and signal detection. Mice were initially anaesthetised under 2% isoflurane in medical air and were maintained under 1.5% during imaging. A rectal probe and a pressure pad (SA Instruments, Stony Brook, NY, USA) were used to measure core temperature and monitor respiration throughout the procedure. Heated water tubing and a warm air blower using a feedback system (SA Instruments, Stony Brook, NY, USA) was used to regulate the temperature of the mice to 37^0 C. Arterial spin labelling fMRI was carried out using 5% CO_2 to induce hypercapnia in 5 min periods to increase CBF. Increased CBF via eNOS-mediated mechanisms were induced using the Rho-kinase inhibitor Fasudil hydrochloride (Tokyo Chemical Industries, Tokyo, Japan). 15 brain image slices were acquired with a thickness of 1 mm and an 'in-plane' resolution of 0.28 mm per mouse per experiment. Analyses of acquired images were processed as described in Chapter 4.

Assessment of Perivascular drainage of Aß

45 days after treatment with mu-saporin or saline, male C57BL/6 mice were injected with human $A\beta_{1\text{-}40}$ HiLyte Fluor™ 555 labelled (AnaSpec, USA) (50 µM) into the left

hippocampus (0.5 µL; co-ordinates from Bregma: AP=-1.9 mm, ML=1.5 mm, DV=-1.7 mm) or was injected into the right cortex (0.25 µL; co-ordinates from Bregma AP=-2 mm, ML=-1.5 mm , DV=-0.5 mm) at a rate of 0.2 µL/min. using a Hamilton precision syringe with a 32 G needle (Esslab, Hadleigh, England). For injections into the hippocampus, the needle was left in situ for 2 min after the injection to prevent reflux and mice were overdosed with sodium pentobarbitone (20% w/v IP, Animalcare, York, UK) five minutes post-injection and then perfused intracardially with 0.01 M PBS followed by 4% w/v PFA. For mice that received cortical injections, the needle was also left in situ for a total of 2 min 30 s before being overdosed and perfused in the same way. The brains were post-fixed in 4% PFA overnight and dehydrated in 30% w/v sucrose before being embedded in OCT for cryosectioning.

Tissue collection for Western blotting and the NOS activity assay

45 days post-surgery with either mu-p75-saporin or saline, C57BL/6 mice were intracardially perfused with 0.01 M PBS at a rate of 5 ml/min following an overdose using 20% sodium pentobarbitone (Animalcare, York, UK). Brains were removed and regionally dissected for septum, striatum, hippocampus, and cortex before being snap frozen on dry ice and stored at -80^0 C until use.

Western blotting

Brain tissues were homogenised in RIPA lysis buffer (20 mM Tris pH 8.0, 0.15 M NaCl, 1.27 mM EDTA, 1 ml Igepal, 0.1% SDS, 50 mM NaF, 1.48 mM $NaVO_3$ containing 1:100 Protease inhibitor cocktail Set III, EDTA free (Merck Millipore, Darmstadt, Germany)) using ultrasound sonication (Fisher Scientific™ Model 120 Sonic Dismembrator, Fisher Scientific, Loughborough, UK). Cortices were homogenised on ice for 20 s at 25 amps and immediately briefly afterwards for 7 s at 20 amps, and the hippocampal and striatal tissue were homogenised for 15 s at 25 amps. The homogenate was then centrifuged at 8000 rpm at 4^0 C for 10 min and the supernatant was collected. Protein concentration of the supernatant was assessed using the Thermo Scientific™ Pierce™ BCA™ Protein assay kit (ThermoFisher Scientific, MA, United States). Tissue supernatent was loaded at 30 µg or 40 µg, diluted in 2 x or 4 x Tris-glycine sample buffer (250 µM Tris, 40% glycerol, 4% SDS, 2% bromophenol blue) under non-reducing conditions. Samples were run on 4-12% tris-glycine gels (Novex™ WedgeWell™ Tris-Glycine Mini Gel, Invitrogen MA, USA) and transferred onto 0.2 µm nitrocellulose membranes (GE Healthcare, Little Chalfont, UK). Membranes were then blocked in 8% milk diluted in 1x Tris buffered saline (TBS) containing 2% Tween (TBST) for one hour before being incubated with the primary antibody (Table 1) diluted in 8% milk overnight at 4^0 C. Membranes were then washed in

TBST before being incubated in their respective HRP-conjugated secondary antibody (Table 1) for 1 h at room temperature. Membranes were washed in TBST, developed using an enhanced chemiluminescence kit (GE Healthcare, Little Chalfont, UK) and visualised using the Geldoc system (G:box, Syngene, Cambridge, UK). Membranes were then stripped and re-probed with anti-GAPDH (Table 1) to ensure equal protein loading.

NOS activity assay

Brain tissues were homogenised in ice cold homogenisation buffer (25 mM Tris-HCl pH 7.4, 1 mM EDTA, 1 mM EGTA containing 1:100 Protease inhibitor cocktail Set III, EDTA free (Merck Millipore)). Homogenates were centrifuged (13000 rpm, 25 min, 4^0 C), supernatant was collected as the nNOS-enriched fraction and the pellet was resuspended in 150 µl homogenisation buffer including protease inhibitor cocktail and collected as the eNOS-enriched fraction.

The NOS assay was carried out as per manufacturer's instruction (Cayman Chemical, Ann Arbor, MI, USA). Briefly, the homogenate was added to a reaction mixture (see Table 2 for composition) containing radiolabelled [^{3}H] L-Arginine monohydrochloride (50.5 Ci/mmol, 1µCi/µl, Perkin Elmer, Llantristant, UK). The reaction was incubated at room temperature (22^0 C) for 30 min allowing the active endogenous NOS in the tissue homogenate to convert the [^{3}H] L-Arginine into [^{3}H] L-citrulline, following which stop buffer (50 mM HEPES and 5 mM EDTA, pH 5.5) was added. The reaction was then pipetted onto resin which bound any unconverted [^{3}H] L-Arginine, which was then separated from the rest of the mixture using a glass pipette under gravity filtration. Scintillation fluid (Emulsifier-safe, Packard Instrument Company, CT, USA) was then added to this mixture and radioactivity was measured using a liquid scintillation and luminescence counter (1450 microbeta Wallac Trilux, Perkin Elmer). Background counts (reaction mixture, stop buffer and resin without homogenate) and total counts (reaction mixture and stop buffer only) were also obtained.

Table 2.2 Reaction mixture components for NOS assay

Component	Concentration	Source
2 x reaction buffer	50 mM Tris-HCl pH 7.4, 6 µM tetrahydrobiopterin (BH_4), 2 µM Flavin adenine dinucleotide, 2 µM Riboflavin 5′-monophosphate sodium salt hydrate	Sigma (Dorset, UK)
NADPH	10 mM prepared in 10 mM	Sigma (Dorset, UK)

	Tris-HCl pH 7.4	
[^{3}H] L-Arginine monohydrochloride	50.5 Ci/mmol, 1 µCi/µl	Perkin Elmer (Waltham, MA, US).
Calcium Chloride	6 mM	Sigma (Dorset, UK)

Statistics

Data were analysed using GraphPad Software (La Jolla, US). Following the Kolmogorov-Smirov normality test for normal distribution, data was analysed using Student's t-test or ANOVA if normally distributed, and Mann-Whitney U-test or the Kruskal-Wallis test if not non-parametric (see individual chapter methods for exact test used).

Chapter 3 : Cholinergic denervation and the effect on the structure of the NVU

Introduction

The loss of cholinergic neurons in the basal forebrain and the areas innervated by their fibre projections is a hallmark of AD (Whitehouse et al. 1982; Francis et al. 1999). Decreased cholinergic innervation in the hippocampus and cortex is associated with memory impairment, decreased MMSE scores and behavioural changes (Damasio et al. 1985; Perry 1980; Tong & Hamel 1999; Garcia-Alloza et al. 2005), suggesting that loss of cholinergic neurotransmission contributes significantly to AD dementia (Francis et al. 1999; Bartus et al. 1982; Van Beek & Claassen 2011; Terry & Buccafusco 2003; Schliebs & Arendt 2011). Recently, a longitudinal study demonstrated that volume loss in the basal forebrain as detected by MRI imaging was an early event in the onset of sporadic AD (Schmitz et al. 2016), further supporting this hypothesis.

Numerous experimental models have been used to ablate cholinergic neurons in the basal forebrain, including injection of ibotenic acid into the substantia innominate (Vaucher & Hamel 1995), lesioning of the fimbria fornix (van der Staay et al. 1989) and electric pulse ablation of the medial septum (Scheiderer et al. 2006; Nelson et al. 2014). However, these models caused widespread degeneration and did not specifically target cholinergic cell populations. The discovery that cholinergic neurons in the basal forebrain express the p75NTR receptor, while other populations of cholinergic neurons (e.g. in the striatum and brainstem) do not (Steininger et al. 1993), allowed for the development of the targeted immunotoxins such as 192IgG-saporin. 192IgG-saporin's mouse analogue, mu-p75-saporin, is a ribosome inhibitor that is conjugated to an antibody against the p75NTR receptor. *In vivo* administration of mu-p75-saporin has been shown to selectively kill cholinergic neurons in the medial septum, horizontal and diagonal band of Broca and nucleus basalis of Meynert and cause withdrawal of cholinergic projections in the cortex and hippocampus (Berger-Sweeney et al. 2001; Hunter et al. 2004; Ramos-Rodriguez et al. 2013; Hamlin et al. 2013; Kerbler et al. 2013; Laursen et al. 2013). Although recent genetically-driven technologies such as optogenetics and designer receptor exclusively activated by designer drug (DREDD) have led to more targeted approaches to silence specific cholinergic populations (Zhang et al. 2017; Hangya et al. 2015), it is not clear if those techniques replicate the loss of cholinergic innervation that is seen in AD.

The NVU is also a target of cholinergic innervation, which can occur at multiple sites, including astrocytes, smooth muscle and endothelial cells (Vaucher & Hamel 1995). Loss of cholinergic contact with blood vessels has been reported in the cortex of AD brains (Tong & Hamel 1999) and in transgenic mouse models of AD (Kuznetsova & Schliebs 2013; Michalski et al. 2017). However, those studies were done on 2D sections, and without investigating cholinergic contact with specific components of the NVU, thereby limiting the information that can be gained about the impact of cholinergic loss at blood vessels.

In these first set of experiments, the saporin model was used to mimic the loss of cholinergic neurons that is observed in AD. Quadruple labelling immunohistochemistry and 3D reconstruction were carried out to characterise specific points of contact between cholinergic fibres and various components of the NVU and to compare this pattern between the cortex and the hippocampus.

Materials and methods

Mouse model of cholinergic denervation

8-10 week old C57BL/6 mice received a stereotaxic injection of saline (n=25) or mu-saporin (n=25) as outlined in Chapter 2 section 'Cholinergic denervation' page 45. Mice were fix-perfused with 4% PFA and their brains processed for immunohistochemistry at 15 days (n=9), 30 days (n=8) and 45 days post-surgery (n=33). Experiments were carried out in compliance with guidelines of the AWERB at the OU and the University of Southampton and with approval from the Home Office (PPL 70/8507; PPL 30/3095).

Immunohistochemistry

Brain tissue was sectioned and collected in a free-floating manner as described in Chapter 2 section 'Immunohistochemistry' page 45. Sections were stained with anti-ChAT, anti-tyrosine hydroxylase, anti-5HTT and anti-tryptophan hydroxylase antibodies as outlined in Chapter 2 (Table 2.1, page 43). In the case of double labelling with anti-p75 NTR and anti-ChAT, sections underwent antigen retrieval using pepsin (1 mg/ml, 30 s) before sequential staining using anti-p75NTR overnight followed by anti-ChAT the following day. For quadruple labelling, sections were incubated with anti-ChAT, followed by simultaneous staining with anti-collagen IV and anti-SMA-FITC, and incubation with anti-GFAP to visualise the cholinergic nerve endings, basement membrane, smooth muscle cells and astrocytes, respectively.

Photomicrographs of coronal brain sections containing the medial septum, striatum, raphe nucleus, and locus coeruleus were captured using the x10 objective, while sections of the

hippocampus and cortex were imaged at x20 on an SP5 Leica scanning laser confocal microscope (Milton Keynes, Buckinghamshire). Blood vessels in the hippocampus and cortex were imaged on the Leica SP5 confocal using the x100 oil immersion objective. Z stacks with ≤ 2 μm spacing between slices were acquired sequentially. Vessels in the hippocampus were pseudo-randomly selected due to bias from the dominant location of large vessels along the centre of the region. Vessels in the cortex were randomly acquired from the same regions analysed for cholinergic nerve fibre density, primarily the somatosensory cortex. Maximum projection images were deconvolved and converted into Imaris-compatible files using AutoQuant X3 version X3.0.4 (MediaCybernetics Inc, Rockville MD) software.

Western blotting

8-10 week old C57BL/6 male mice received intraventricular injections of either 0.9% saline (n=8) or 0.596 μg mu-saporin (n=6) as described in chapter 2, section 'Cholinergic denervation' page 45. 45 days following surgery, mice were overdosed with sodium pentobarbitone and perfused intracardially with 0.01M PBS. Brains were immediately dissected and snap frozen on dry ice and stored at -80°C. Tissue was then homogenised and protein content was quantified and gels were run. Blots were incubated in anti-ChAT (1:500) and visualised using HRP-conjugated anti-goat secondary and an enhanced chemiluminescence kit, as described in chapter 2, section 'Western blotting' page 48. Membranes were then stripped and re-probed for the loading control anti-GAPDH (see chapter 2, Table 2.1, section page 43) and optical densities of bands corresponding to the estimated molecular weight of ChAT were quantified using Image J.

Analysis

Density of cell bodies and fibres

The density of neuronal cell bodies and fibres in each region of interest was quantified from low magnification images by calculating the percentage area covered by staining using Image J software (NIH. Maryland, USA). The threshold values used to detect specific staining for each antibody are listed in Table 3.1. For quantification of staining in the hippocampus, overlapping images were stitched together and the free-hand draw tool was used to select and specify the area containing the hippocampus to be analysed. For quantification of densities in the hippocampus and striatum, values of regions from both the ipsilateral and contralateral hemispheres were averaged and treated as n = 1. For quantification of images from the cortex, six random non-overlapping spanning the somatosensory cortex of the ipsilateral cortex to the somatosensory cortex of the contralateral cortex were averaged and analysed.

Table 3.1 Threshold values for analysis of percentage area covered

Label	Minimum grey value	Maximum grey value
Anti-ChAT	44	255
Anti-p75NTR	94	255
Anti-TH	77	255
Anti-5HTT	33	255
Anti-TrypH	100	255

Parameters of the NVU and cell-cell contacts

To quantify the parameters of each component of the NVU, deconvolved images were processed using Imaris software (Bitplane ®) and surfaces were created for each component of the NVU (Table 3.2). Examples of individual surfaces generated from staining of collagen IV, smooth muscle actin, and astrocytes in a reconstructed artery are shown in Fig. 3.1 and Fig. 3.2. For each vessel, the following measurements were acquired: the total area of a selected surface (μm^2), the volume of a selected surface (μm^3), the length of the vessel imaged (µm) and the average diameter of the vessel (µm) in the space of the z stack. The total area of contact between two selected surfaces (e.g. ChAT nerve fibres contacting collagen IV) was calculated using the Imaris Xtension 'Surface to Surface Contact Area' (Imaris V8.31, ImarisXT Bitplane Inc. created by Matthew J Gastinger, Bitplane). Only surfaces that made direct contact with each other (i.e. 0 µm distance apart) were quantified. Vessels were classified as capillaries if they were <10 µm in diameter, arteries were identified as having a diameter of >10 µm and positive for SMA, while veins were identified as having a diameter >10 µm but lacking SMA. A total of five capillaries, five arteries and three veins were quantified for each mouse and the average values per mouse were used for statistical analysis.

Table 3.2 Surface creation values for 3D reconstruction using Imaris

Surface	Surface detail	Threshold (Absolute Intensity)	Manual threshold value B
ChAT	0.250 µm	24.9693	290.359
SMA	0.303 µm	35.0000	220.254
Collagen IV	0.35 µm	84.0000	289.379

GFAP	0.300 µm	92.7983	423.268

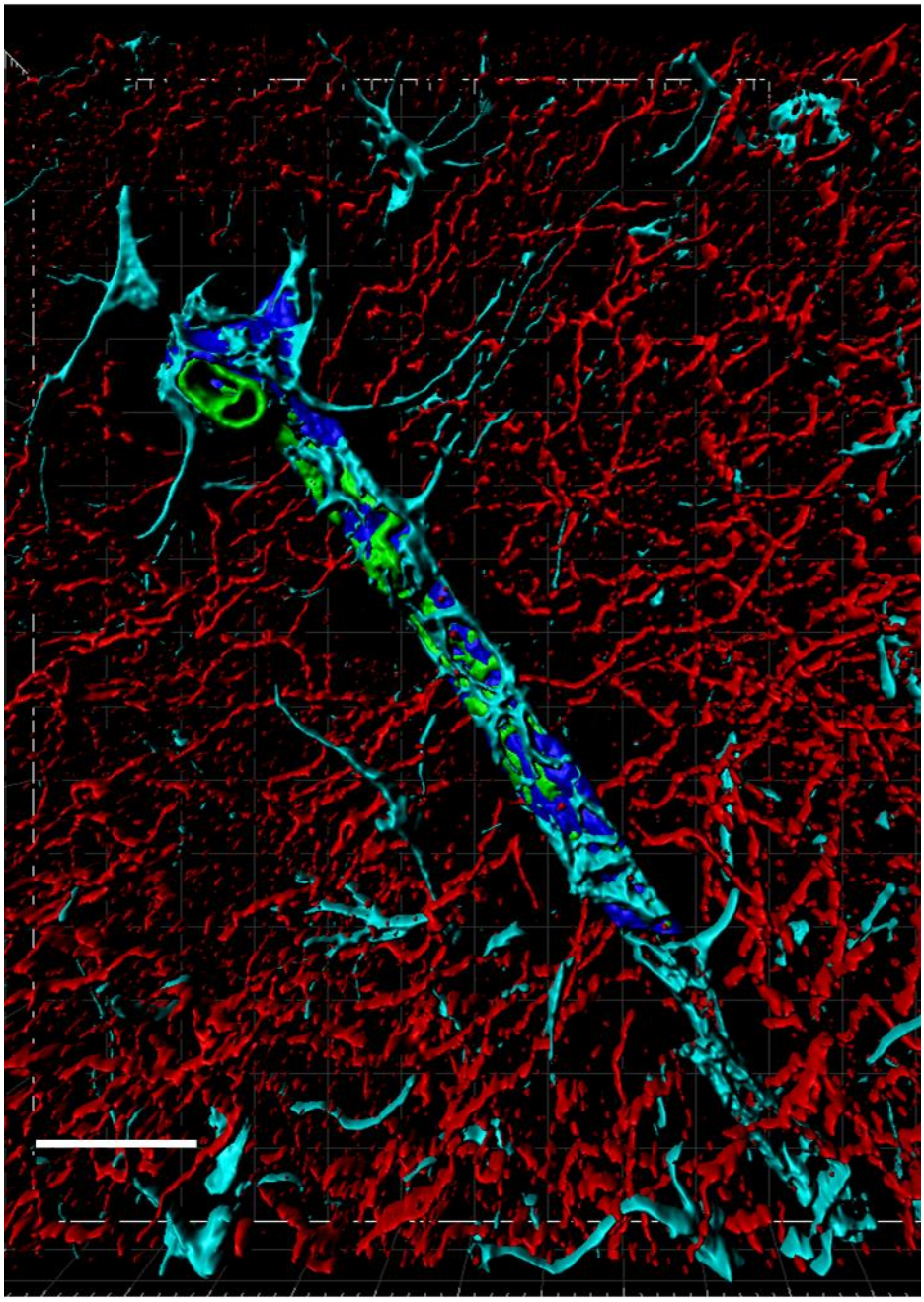

Figure 3.1 3D reconstructed artery
Representative image of a 3D reconstructed artery stained for collagen IV (dark blue), smooth muscle actin (green), astrocytes (turquoise) and cholinergic nerve fibres (red).

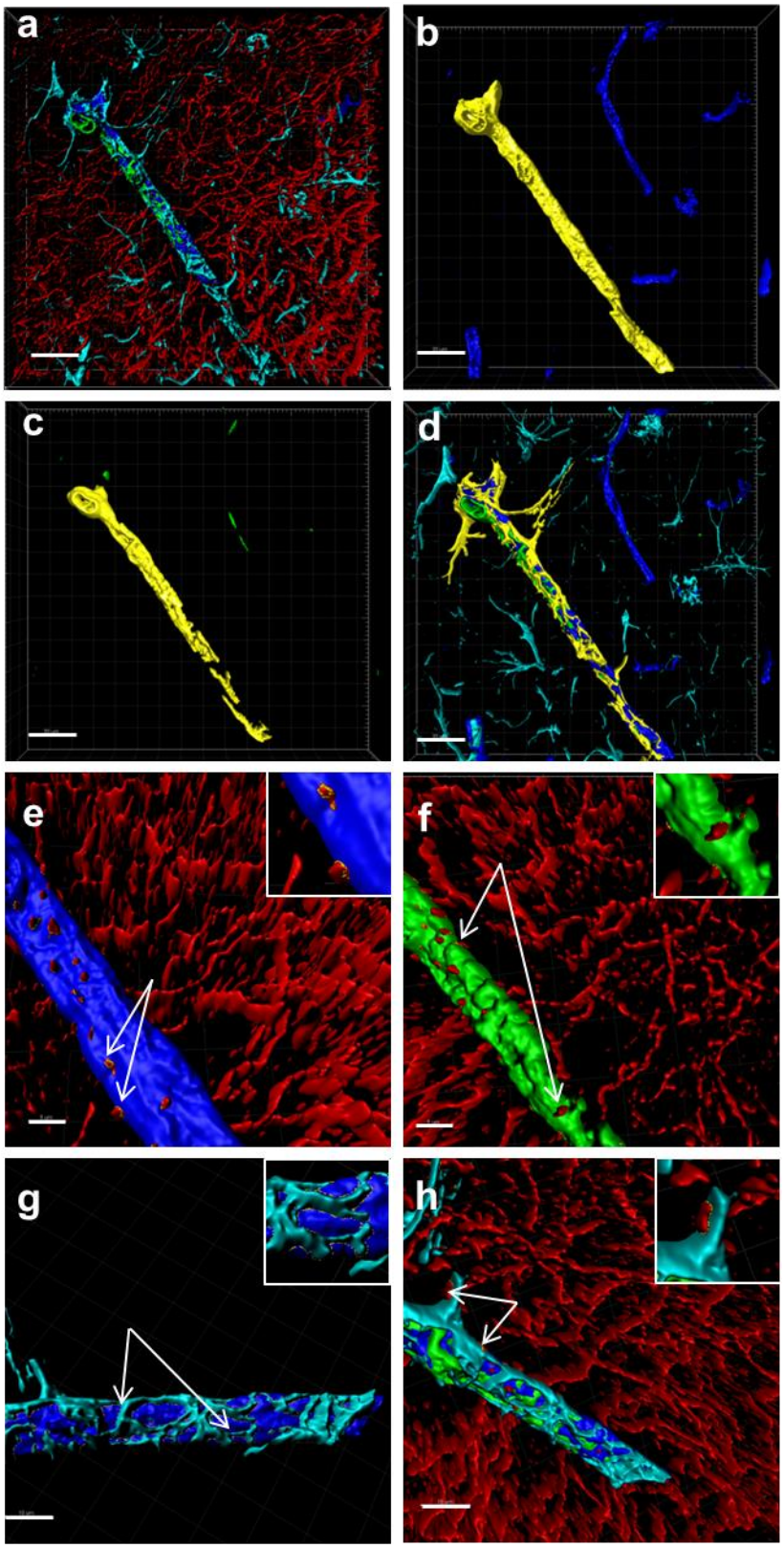

Figure 3.2 3D reconstructed artery regions of measurement
Original reconstructed vessel (a). (b and c) Yellow outlines indicate the surfaces created of collagen staining (b) and of smooth muscle actin (c) in the artery shown in (a). (d) Contacts between astrocyte endfeet and collagen along the artery are outlined in yellow. (e-h) As indicated by the white arrows and enlarged in insert, surface area contact between cholinergic nerve fibres and collagen (e) or smooth muscle (f) was calculated for each individual vessel. Similarly, the surface area contact between astrocytes and collagen IV (g) and between cholinergic fibres and perivascular astrocytes (h) was also determined for each vessel. Scale bar = (a-d) 20 µm, (e, f) 5 µm, (g, h) 10 µm.

Western blotting

The optical density (OD) of bands on Western blots were quantified using Image J (NIH, Maryland) and were normalised to the corresponding OD of GAPDH. The mean ratio of two blots per antibody was then used for statistical analysis.

Statistics

Data was tested for normality using the Kolmogorov-Smirov test. For normally distributed data, comparisons between two groups were carried out using two-tailed Student's t test. Where there were more than two groups, one-way or two-way ANOVA was used followed by Sidak's post-hoc test unless otherwise stated in the results. The ROUT test was used to identify any outliers. For data that was not normally distributed, the Mann-Whitney U test or Kruskal-Wallis test with Dunn's post-hoc test was used. Data represents mean ±SEM and $p<0.05$ was considered to be statistically significant.

Results

Cholinergic loss in the medial septum, hippocampus and cortex following saporin administration

In agreement with previous reports (Mesulam, Elliott J. Mufson, et al. 1983; Rye et al. 1984; Berger-Sweeney et al. 2001), ChAT and p75NTR-positive cholinergic neurons were observed by double labelling immunohistochemistry in the medial septum, horizontal and vertical limbs of the diagonal band of Broca and the nucleus basalis of Meynert of control mice (Fig. 3.2 a-c). Cholinergic nerve fibre density was found to be significantly higher in the hippocampus compared to the cortex in control mice (Fig.3.3). To determine the time-course of degeneration following saporin administration, the percentage area of cholinergic staining of the medial septum was quantified in control and saporin-treated mice at 15, 30 and 45 days following injection. No significant differences were detected between the two groups at 15 and 30 days post-surgery, but significantly less ChAT and p75NTR staining was detected in the medial septum of saporin-treated mice at 45 days post-surgery (Fig. 3.2 d-g). Therefore, the 45-day time point was used in all subsequent experiments and analyses. The density of ChAT-positive neurons in non-injected mice did not differ from control mice (Fig. 3.2 g), indicating that the surgery itself did not induce changes in ChAT expression. Although behaviour was not assessed in this study, it was noted that unlike control treated mice, saporin treated mice were less likely to form and maintain nests from available nesting material throughout the 45 day period.

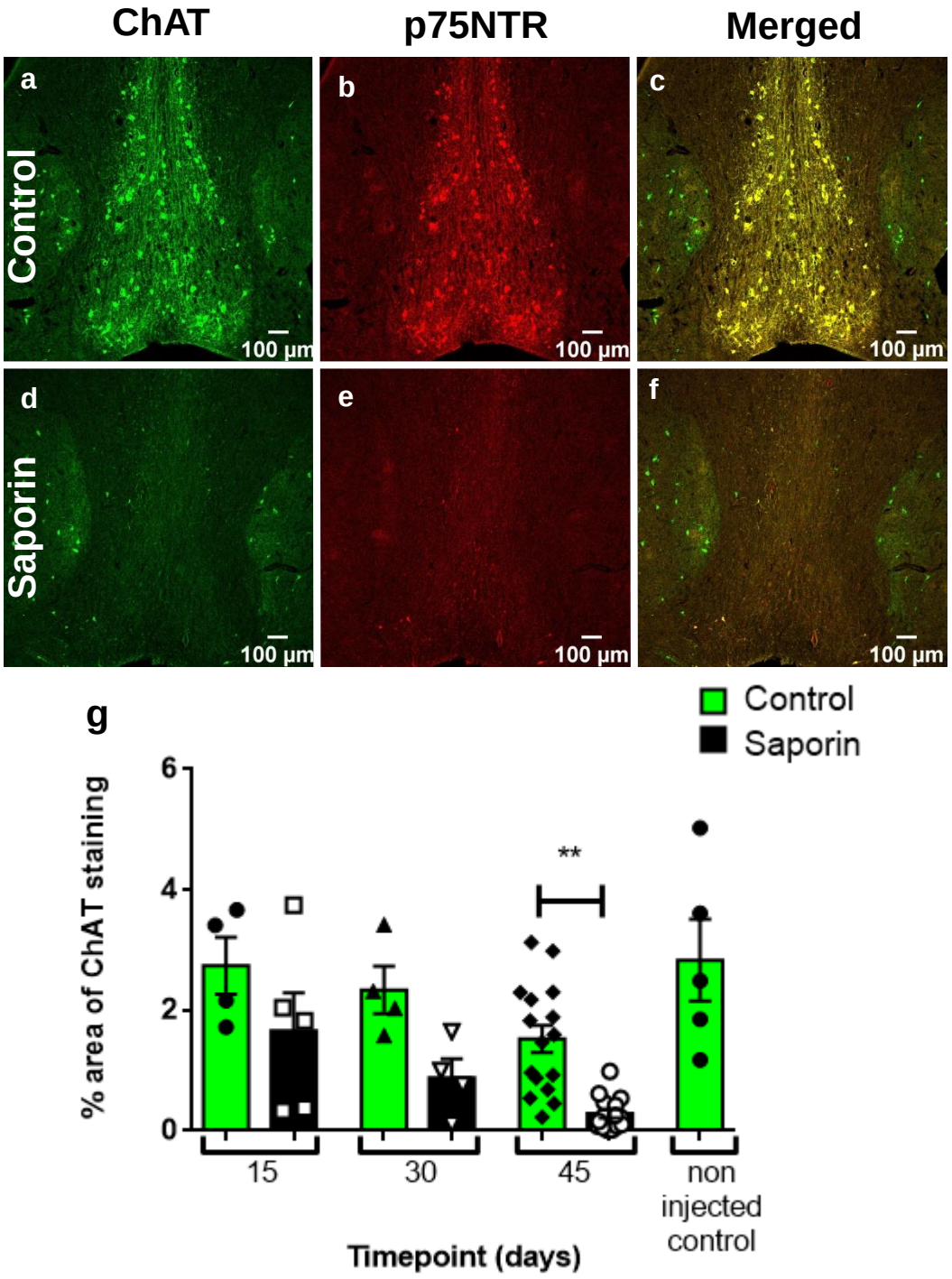

Figure 3.3 Timecourse of cholinergic cell loss in the MS following mu-p75-saporin treatment
(a-c) Neuronal cell bodies that are positive for ChAT (a, green) and p75NTR (b, red) are co-localized (c, yellow) in the medial septum and diagonal band of Broca of control mice. (d-f) Loss of ChAT (d) and p75NTR-positive (e) neurons is observed following administration of saporin. p75NTR-negative cholinergic neurons in the striatum are not affected by saporin treatment. (g) Quantification of ChAT staining in the medial septum and diagonal band of Broca at 15 (control n=4, saporin n=5), 30 (control n=4, saporin n=4) and 45 (control n=17, saporin n=16) days after saporin treatment showed a statistically significant decrease at the 45 day timepoint. $^{**}p<0.01$, Scale bar = 100 µm.

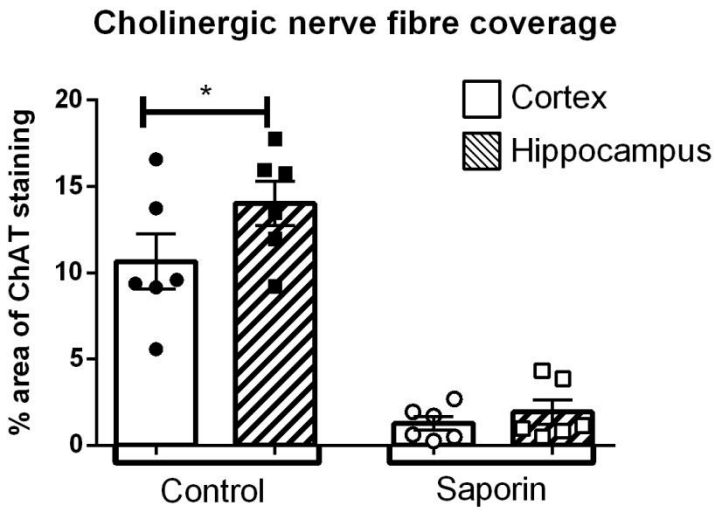

Figure 3.4 Regional comparison of cholinergic innervation and denervation with saporin treatment
Regional comparison of % area of ChAT positivity shows that the hippocampus has more nerve fibre coverage than the cortex, although this is lost with saporin treatment (control n=6, saporin n=6). *p<0.05.

The loss of cholinergic neurons in the medial septum was accompanied by a significant decrease in cholinergic nerve fibre density in the hippocampus (Fig 3.4 a-g), which was confirmed by Western blotting (Fig. 3.4h). A similar pattern was observed in the cortex (Fig 3.5 a-h). Analysis of the density of cholinergic cells bodies in the striatum confirmed that p75NTR-negative cholinergic neurons were not affected by saporin treatment (Fig. 3.6 a-h).

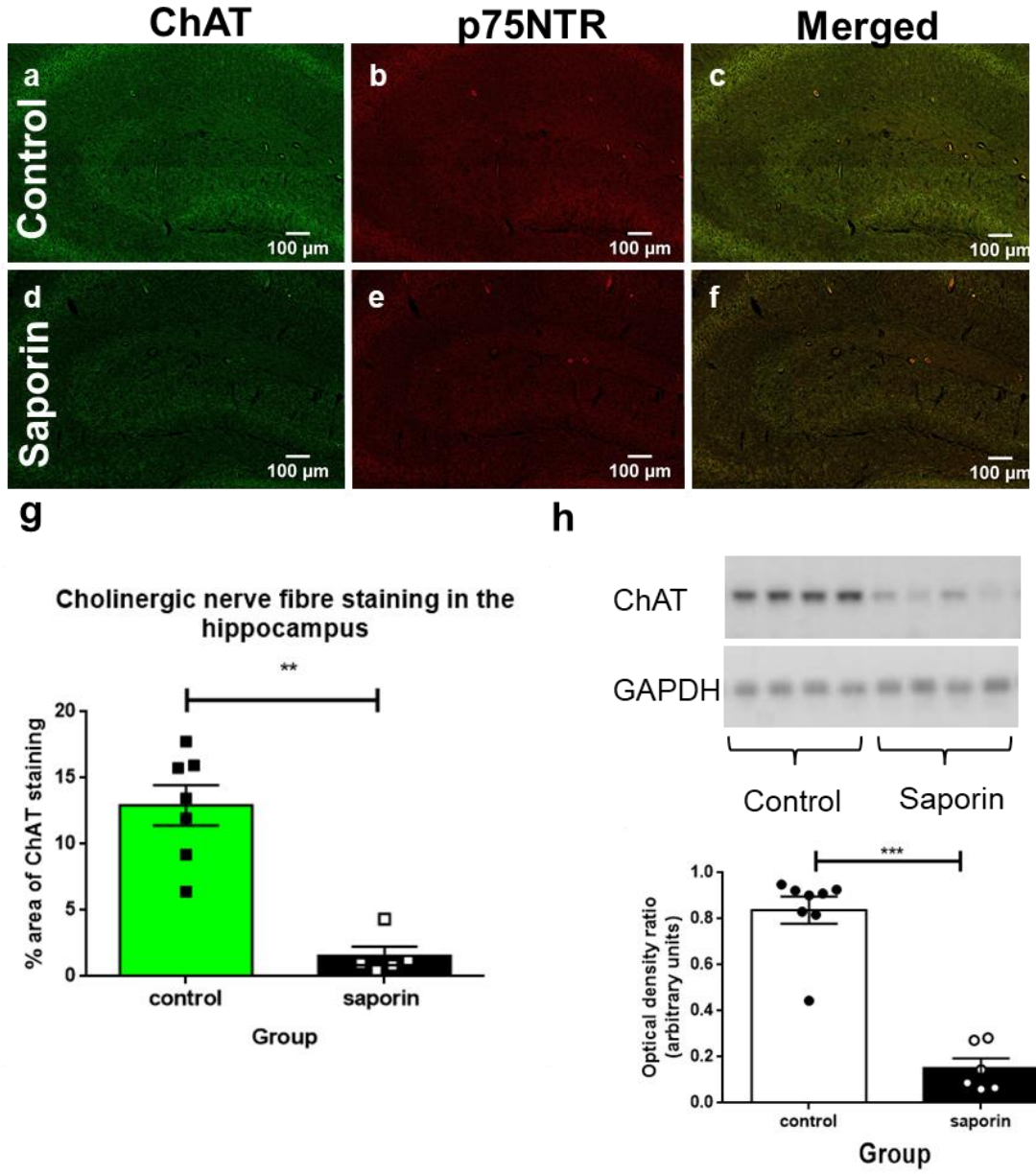

Figure 3.5 Saporin induced cholinergic denervation in the hippocampus
(a-c) Neuronal fibres that are positive for ChAT (a, green) and p75NTR (b, red) are co-localised (c, yellow) in the hippocampus of control mice. (d-f) Loss of ChAT (d, f) and p75NTR-positive (e, f) fibres is observed following administration of saporin. (g-h) Quantification of ChAT staining (control n=7, saporin n=6) (g) and levels of the ChAT protein (control n=8, saporin n=6) (h) in the hippocampus showed a statistically significant decrease in saporin-treated mice 45 days after injection. $^{**}p<0.01$, $^{***}p<0.001$. Scale bar = 100 µm.

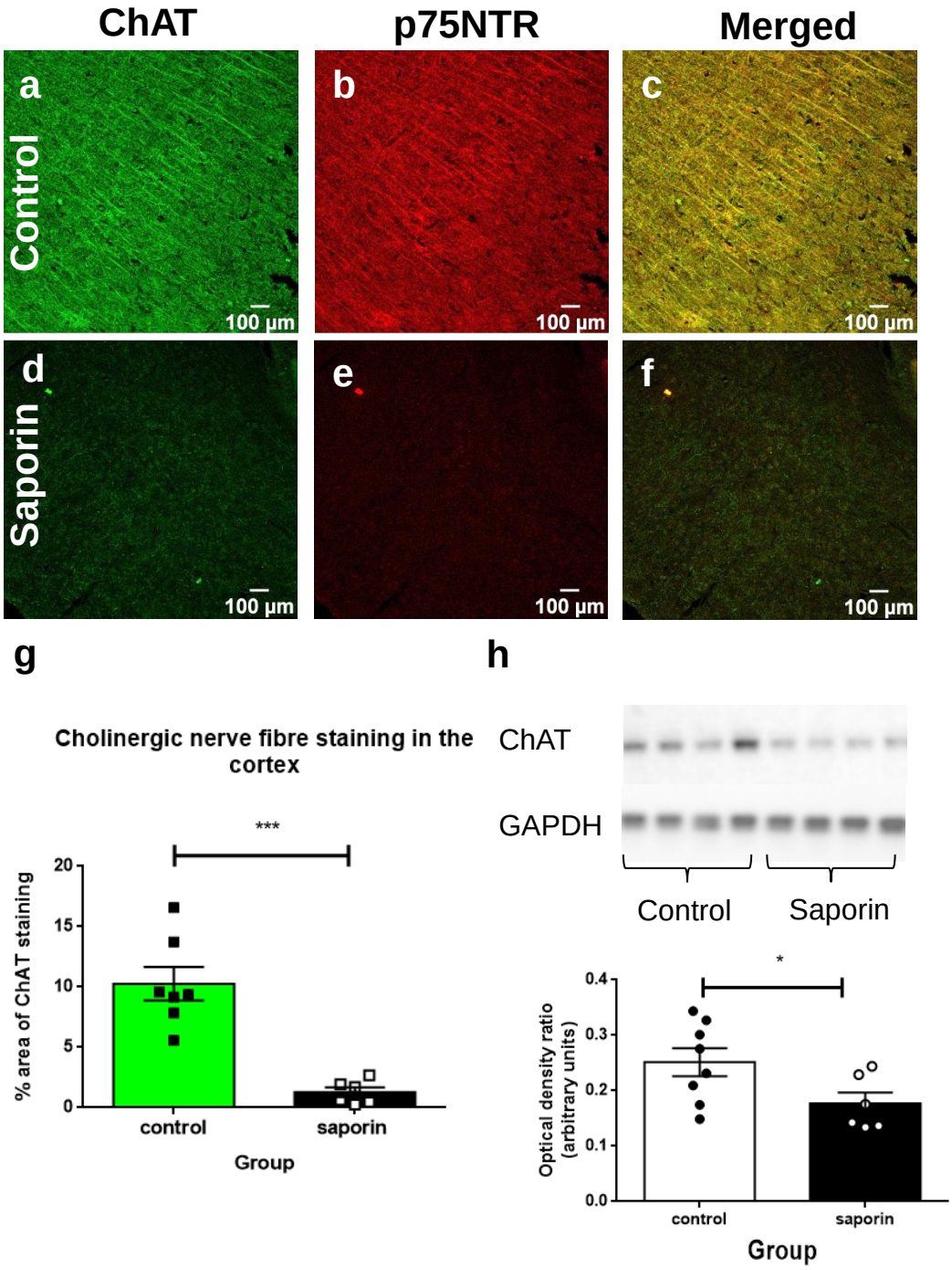

Figure 3.6 Saporin induced cholinergic denervation in the cortex
(a-c) Neuronal fibres that are positive for ChAT (a, green) and p75NTR (b, red) are co-localised (c, yellow) in the cortex of control mice. (d-f) Loss of ChAT (d, f) and p75NTR-positive (e, f) fibres is observed following administration of saporin. (g-h) Quantification of ChAT staining (control n=7, saporin n=6) (g) and levels of the ChAT protein (control n=8, saporin n=6) (h) in the cortex showed a statistically significant decrease in saporin-treated mice 45 days after injection. *p<0.05, ***p<0.001. Scale bar = 100 µm.

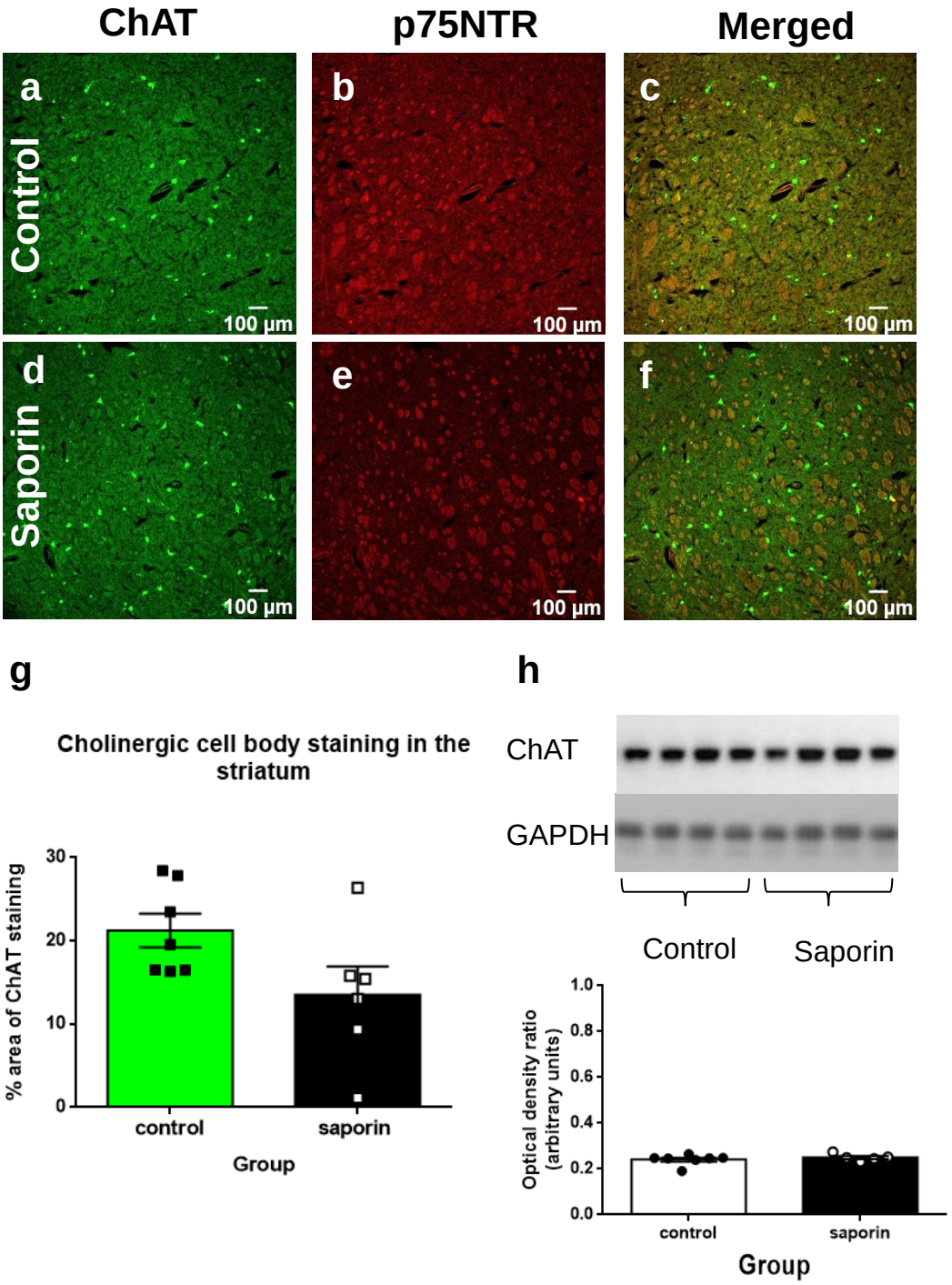

Figure 3.7 Saporin induced cholinergic denervation in the striatum
(a-c) Cell bodies in the striatum that are positive for ChAT (a, green) do not express the p75NTR (b, red) and are not co-localised (c, yellow) in control mice. (d-f) Saporin treatment does not induce loss of ChAT-positive cell bodies in the striatum. (g, h) Quantification of ChAT staining (control n=7, saporin n=6) (g) and levels of the ChAT protein (control n=8, saporin n=6) (h) in the striatum showed no loss with saporin-treated mice 45 days after injection. Scale bar = 100 µm.

The effect of cholinergic loss on other neurotransmitter pathways

Collateral growth of surviving, non-cholinergic nerve fibres has previously been reported following ablation of cholinergic neurons (Szot et al. 2006; Nelson et al. 2014; Scheiderer et al. 2006; McGinty et al. 1982). To determine if saporin treatment induced a change in the expression of serotonergic and noradrenergic neurons and their fibre projections, tissue sections from control and saporin-treated mice were stained for 5-HTT and TH as markers

of serotonin and noradrenaline respectively. No differences were noted in the density of serotoninergic nerve fibres in the hippocampus or in the cell bodies in the raphe nucleus of control versus saporin mice (Fig. 3.7 a and b). Similarly, saporin treatment did not affect the density of noradrenergic nerve fibres in the hippocampus (Fig. 3.7 c) or cell bodies at the locus coeruleus (Fig. 3.7 d).

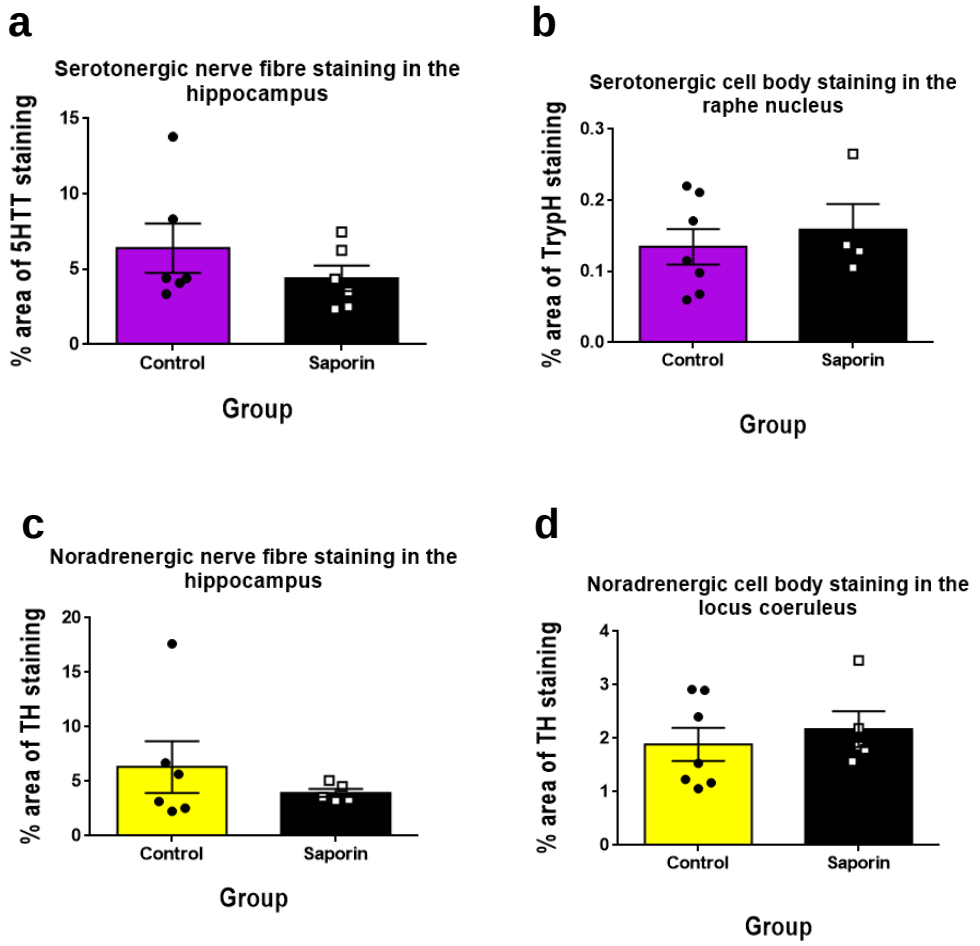

Figure 3.8 The effect of cholinergic loss on noradrenergic and serotoninergic innervation
(a-d) No significant differences were found in the density of serotonergic (control n=6, saporin n=6) (a) or noradrenergeric (control n=6, saporin n=6) (c) fibres in the hippocampus (a, c) or serotoninergic cell bodies in the Raphe nucleus (control n=7, saporin n=4) (b) and noradrenergic cell bodies in the Locus coeruleus (control n=7, saporin n=5) (d) between control and saporin-treated mice.

Characterisation of cholinergic loss at the NVU in the hippocampus and cortex

Cholinergic nerve fibres are known to innervate blood vessels in the hippocampus and cortex (Vaucher & Hamel 1995). To characterise the precise effects of saporin treatment at the NVU, vessels in the cortex and hippocampus were stained for cholinergic fibres and three components of the NVU (the basement membrane, smooth muscle cells and astrocytes), and then reconstructed using 3D modelling software. The surface area of ChAT contact with each component of the NVU (standardised to vessel length) was analysed across capillaries, arteries/arterioles and veins/venules from control and saporin-treated mice.

In blood vessels of the hippocampus, a significant decrease in the contact of cholinergic nerve fibres to the basement membrane was found in arteries of saporin-treated mice compared to controls (Fig. 3.8). A similar trend was also observed in the capillaries and veins, but this did not reach statistical significance (Fig. 3.8).

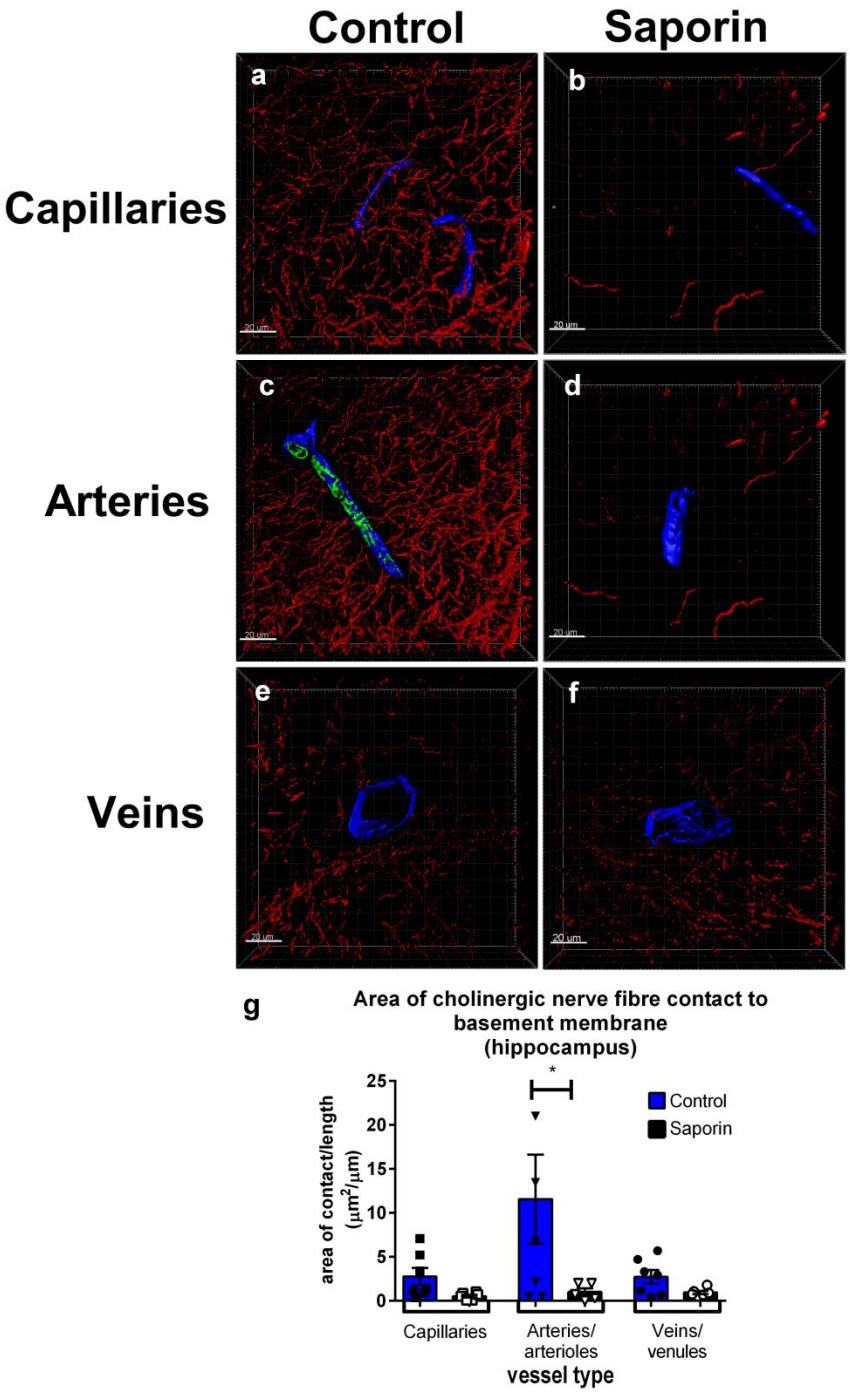

Figure 3.9 Perivascular cholinergic innervation at the basement membrane - hippocampus
(a-f) Representative images of the 3D reconstructions of capillaries (a and b), arteries (c and d) and veins (e and f) in the hippocampus of control (a, c, e) and saporin-treated mice (b, d, f). ChAT-positive fibres are shown in red, collagen IV is shown in blue and smooth muscle actin is shown in green. There is a significant reduction in the amount of contact between ChAT-positive fibres and collagen IV in the arteries of saporin-treated animals (g). A similar but non-significant trend is also observed in capillaries and veins. (Control n=7, saporin n=6), *p<0.05. Scale bar = 20 µm.

Analysis of perivascular innervation at the smooth muscle level of arteries of the hippocampus found that there was a significant decrease in the surface area contact in saporin treated animals (Fig 3.9). However, the surface area contact of cholinergic fibres and GFAP-positive astrocytes was similar between control and saporin-treated mice across all vessel types (Fig. 3.10 a-g).

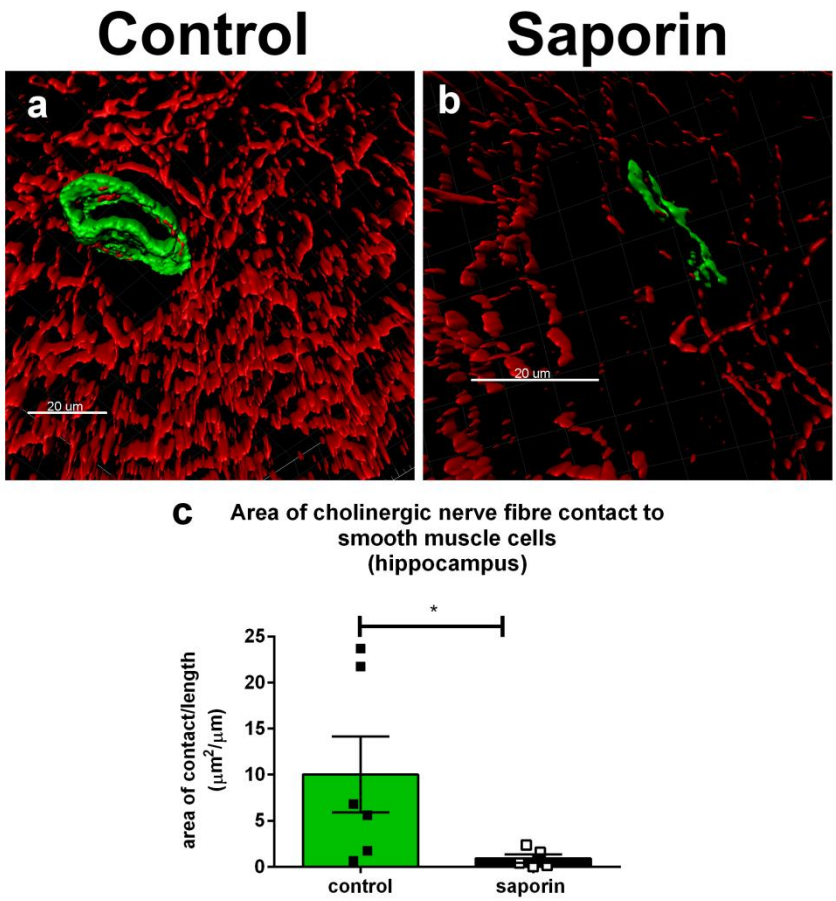

Figure 3.10 Perivascular cholinergic innervation at the SMC - hippocampus
(a-c) Representative images of a 3D reconstruction of a hippocampal artery from control (a) and saporin-treated (b) mice. ChAT-positive nerve fibres are shown in red and smooth muscle cells are shown in green. There is a significant decrease in cholinergic innervation of smooth muscle cells in the saporin-treated mice (c). (Control n=7, saporin n=6), *p<0.05 Scale bar = 20 µm.

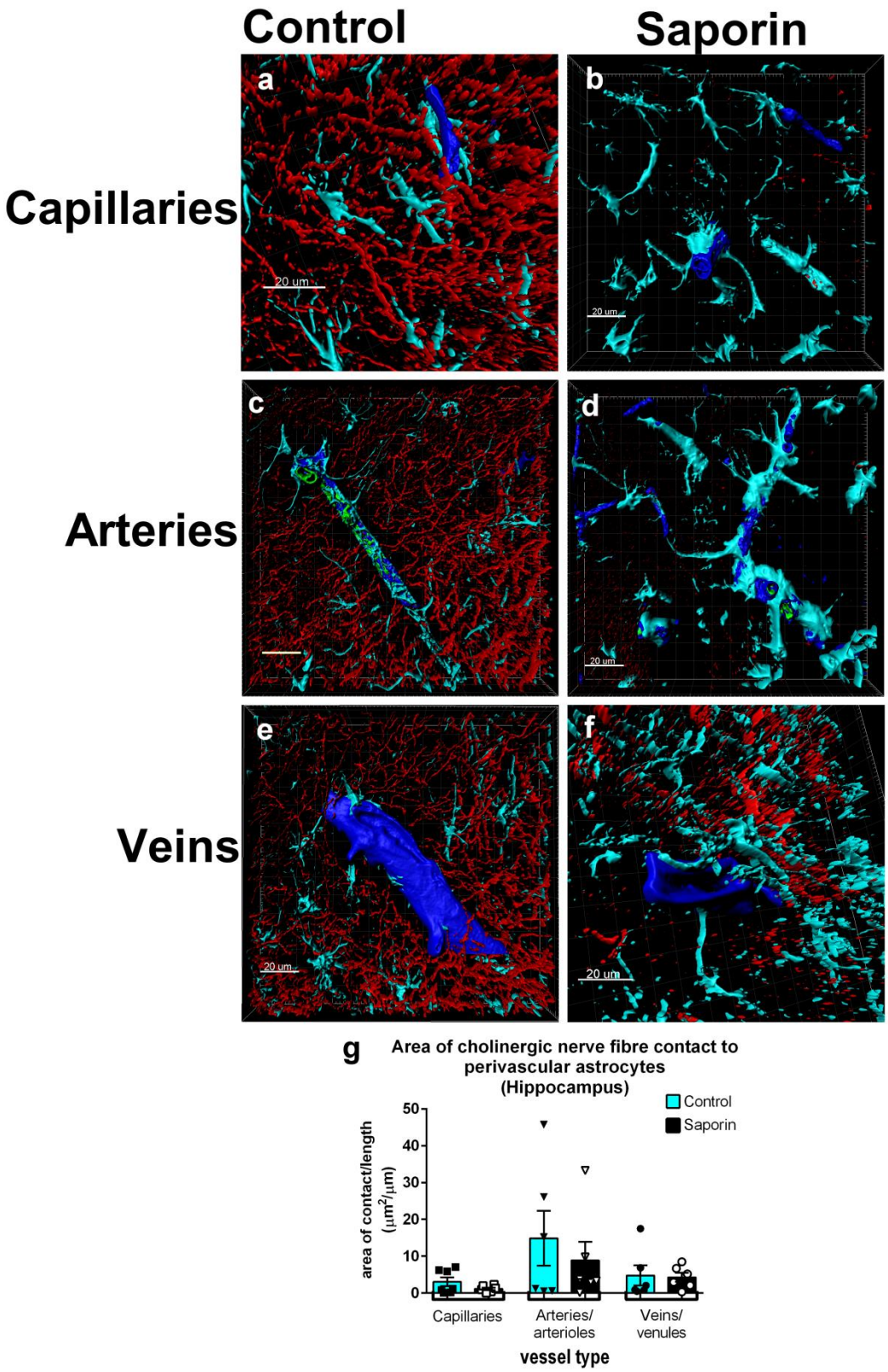

Figure 3.11 Perivascular cholinergic innervation at the astrocyte endfeet - hippocampus
(a-f) Representative images of the 3D reconstructions of capillaries (a and b), arteries (c and d) and veins (e and f) in the hippocampus of control (a, c, e) and saporin-treated mice (b, d, f). ChAT-positive fibres are shown in red, collagen IV is shown in blue and GFAP is shown in turquoise. No significant differences were found in the amount of surface area contact of cholinergic nerve fibres to GFAP-positive astrocytes between control and saporin-treated mice (g). (Control n=7, saporin n=6), scale bar = 20 µm

In the cortex, cholinergic innervation of the basement membrane was significantly decreased in arteries, but not capillaries or veins, following saporin treatment (Fig. 3.11 a-g). A significant decrease was also observed in the surface area contact between ChAT and smooth muscle cells in arteries of saporin mice compared to controls (one-tailed t-test, Fig. 3.12). A significant decrease was also found in cholinergic contact to GFAP-positive perivascular astrocytes in arteries of the cortex (Fig. 3.13).

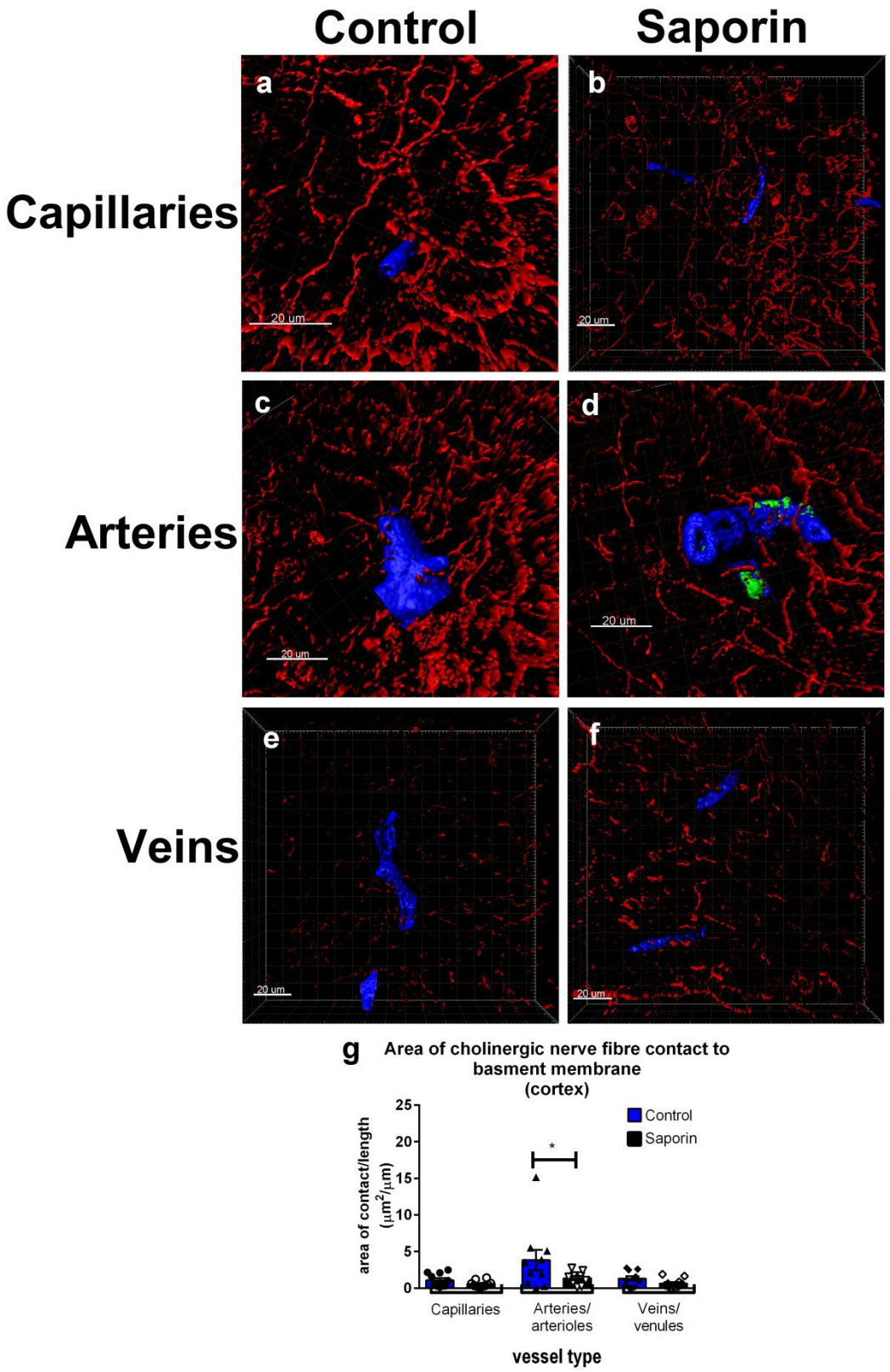

Figure 3.12 Perivascular cholinergic innervation at the basement membrane - cortex
(a-f) Representative images of the 3D reconstructions of capillaries (a and b), arteries (c and d) and veins (e and f) in the cortex of control (a, c, e) and saporin-treated mice (b, d, f). ChAT-positive fibres are shown in red, collagen IV is shown in blue and smooth muscle actin is shown in green. There is a significant reduction in the amount of contact between ChAT-positive fibres and collagen IV in the arteries of saporin-treated animals (g). (Control n=11, saporin n=10), *p<0.05. Scale bar = 20 μm.

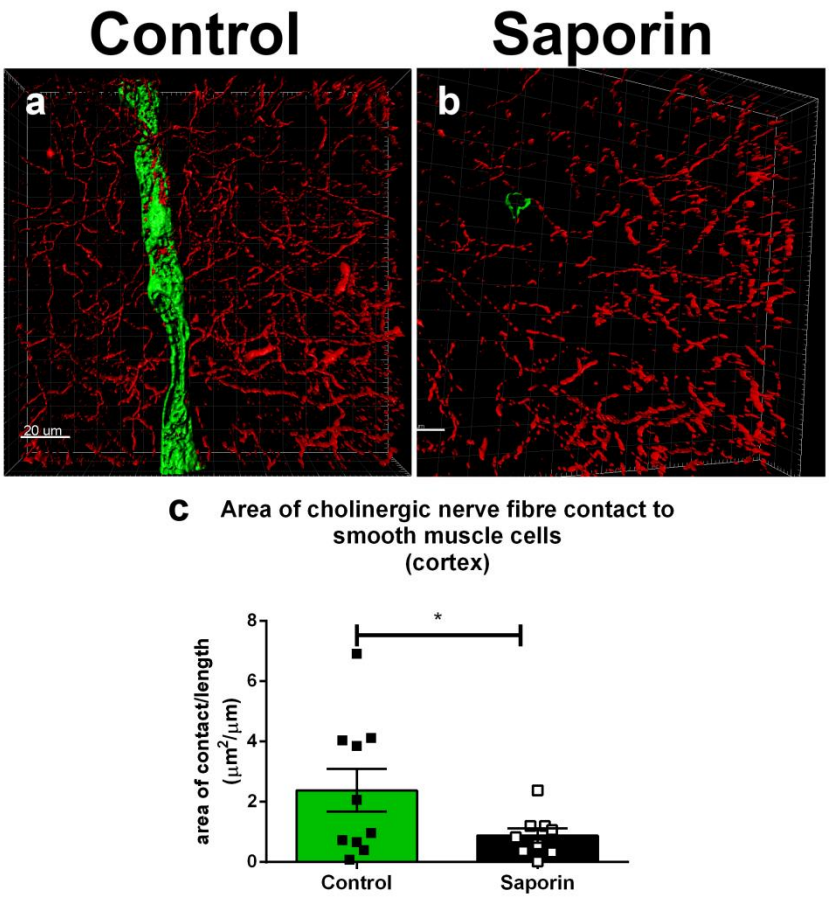

Figure 3.13 Perivascular cholinergic innervation at the SMC - cortex
(a-c) Representative images of a 3D reconstruction of a cortical artery from control (a) and saporin-treated (b) mice. ChAT-positive nerve fibres are shown in red and smooth muscle cells are shown in green. There is a significant decrease in cholinergic innervation of smooth muscle cells in the saporin-treated mice (c). (Control n=11, saporin n=10), *p<0.05. Scale bar = 20 μm.

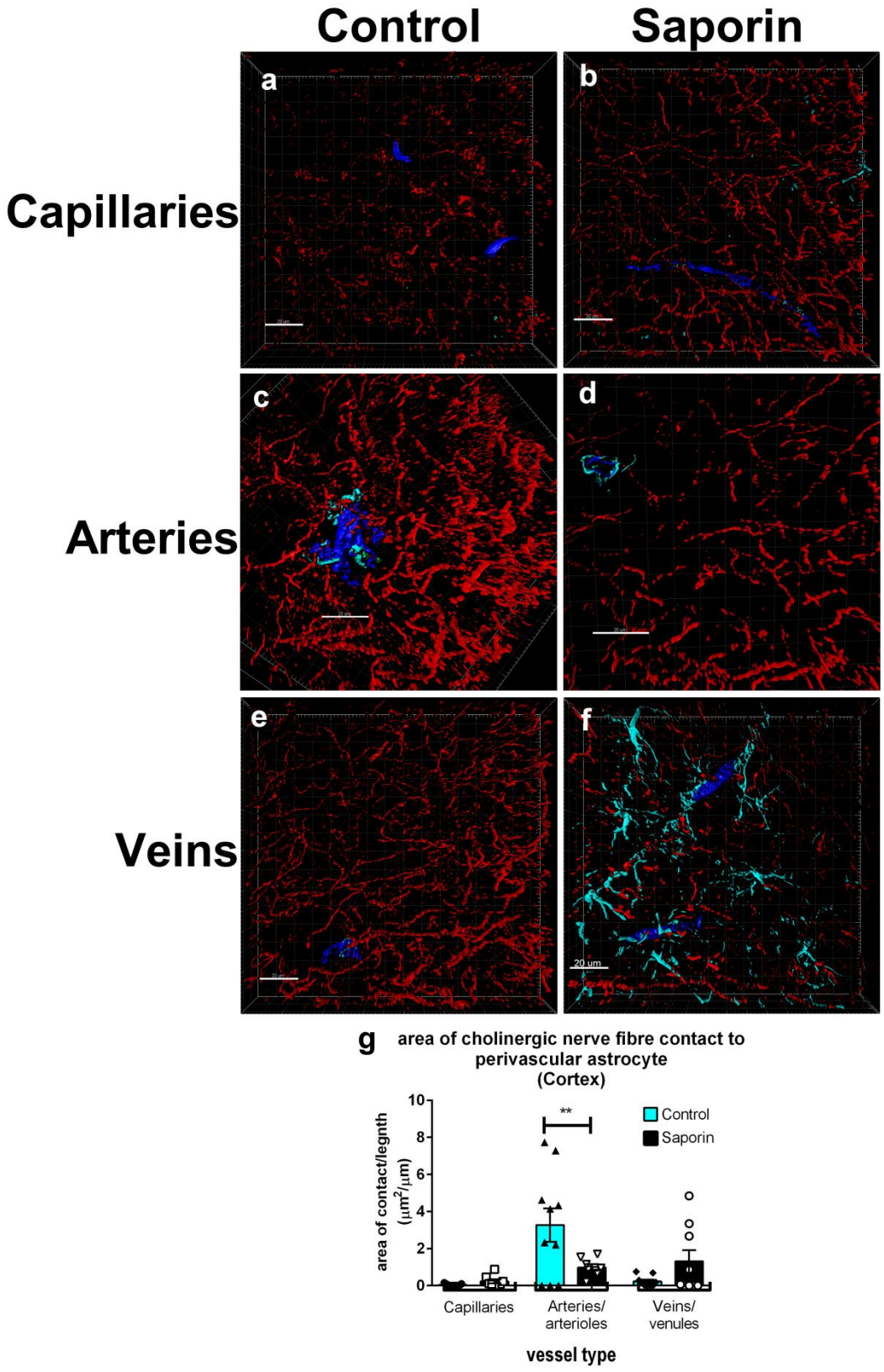

Figure 3.14 Perivascular cholinergic innervation at the astrocyte endfeet - cortex
(a-f) Representative images of the 3D reconstructions of capillaries (a and b), arteries (c and d) and veins (e and f) in the cortex of control (a, c, e) and saporin-treated mice (b, d, f). ChAT-positive fibres are shown in red, collagen IV is shown in blue and GFAP is shown in turquoise. A significant difference was found in the amount of surface area contact of cholinergic nerve fibres to GFAP-positive astrocytes between control and saporin-treated mice at the arterial level (g). (Control n=11, saporin n=10), $^{**}p<0.01$. Scale bar = 20 µm

Does loss of perivascular innervation vary between the hippocampus and cortex?

As cholinergic nerve fibre density was found to differ between the hippocampus and cortex, innervation of the NVU in control and saporin-treated mice was compared between the two regions. Cholinergic innervation at the basement membrane and smooth muscles was found to be significantly decreased with saporin in arteries in both the hippocampus and the cortex as shown in Fig. 3.8, 3.9, 3.11 and 3.12, but no regional differences in innervation were found (Tables 3.3 and 3.4). However, regional differences were noted in the amount of perivascular innervation at the astrocytic end feet, with significantly less innervation of the cortex in comparison to the hippocampus at the capillaries of the control group and at the veins of the saporin group (Table 3.5, $p<0.05$).

Table 3.3 Regional comparisons of loss of perivascular cholinergic contact at the basement membrane across vessel types

Mean area of contact/length ($\mu m^2/\mu m$) ±SEM	**Hippocampus**			**Cortex**		
	Capillaries	*Arteries*	*Veins*	*Capillaries*	*Arteries*	*Veins*
Control	2.77±1.0	11.57±5.1♦	2.71±0.8	1.10±0.3	3.83±1.4♦	1.32±0.3
Saporin	0.54±0.2	2.32±1.4♦	0.95±0.2	0.69±0.2	2.01±1.2♦	0.83±0.3

♦$p<0.05$, control vs. saporin

Table 3.4 Regional comparisons of loss of perivascular cholinergic contact at the smooth muscle cell across arteries

Mean area of contact/length ($\mu m^2/\mu m$) ±SEM	**Hippocampus**	**Cortex**
Control	10.03±4.1♦	6.08±4.0♦
Saporin	0.90±0.5♦	2.37±1.8♦

♦$p<0.05$, control vs. saporin

Table 3.5 Regional comparisons of loss of perivascular cholinergic contact at the astrocyte endfeet across vessel types

Mean area of contact/length ($\mu m^2/\mu m$) ±SEM	**Hippocampus**			**Cortex**		
	Capillaries	*Arteries*	*Veins*	*Capillaries*	*Arteries*	*Veins*
Control	3.05±1.2▲	14.9± 7.5	4.77±2.7	0.039±0.02▲	3.26±0.9♦	0.23±0.1
Saporin	1.14±0.3	8.87±5.0	4.29±1.2▲	0.23±0.1	0.98±0.2 ♦	1.31±0.6 ▲

♦$p<0.05$, control vs. saporin; ▲$p<0.05$ hippocampus vs. cortex

Does loss of perivascular innervation alter the components of the NVU?

To determine if loss of cholinergic innervation induced changes in components of the NVU, the volume of collagen IV and smooth muscle cells as well as the area of GFAP-to-collagen contact as a measure of astrocyte end feet coverage was evaluated in vessels of control and saporin-treated mice. Because cholinergic degeneration appeared to be more extensive in the cortex than in the hippocampus, regional comparisons between the cortex and hippocampus were also carried out.

As shown in Table 3.6, no significant difference in collagen volume was found between control and saporin treated regions in each vessel type, although across vessel types both control and saporin treated arteries were observed to have higher collagen volume compared to capillaries and veins in the cortex. Interestingly, the volume of collagen IV was significantly higher in veins in the hippocampus than veins in the cortex in both the control and saporin-treated mice ($p<0.05$ and $p<0.001$ respectively) (Table 3.6).

Table 3.6 Regional comparison of volume of basement membrane across vessel type

Basement membrane Mean volume/length ($\mu m^3/\mu m$) ±SEM	**Hippocampus**			**Cortex**		
	Capillaries	*Arteries*	*Veins*	*Capillaries*	*Arteries*	*Veins*
Control	33.28±6.2	124.08±29.0	179.93±34.7 ▲	20.96±2.7	111.88±28.9	70.07±25.2 ▲
Saporin	30.76±4.8	101.96±22.2	151.15±24.9 ▲	18.71±3.2	72.43±15.4	34.80±6.4 ▲

▲ $p<0.05$ hippocampus vs. cortex

Although there was a significant reduction in perivascular innervation of smooth muscle cells in both the cortex and hippocampus, the volume of smooth muscle cells was not different between the cortex and hippocampus and there was no effect with saporin treatment (Table 3.7).

Table 3.7 Regional comparison of volume of smooth muscle cells in arteries

SMA Volume/length ($\mu m^3/\mu m$) ±SEM	**Hippocampus**	**Cortex**
Control	59.72±9.5	45.76±11.9
Saporin	33.10±7.4	39.54±9.0

GFAP was used as a marker of astrocytic end feet of the neurovascular unit, and so the contact between GFAP and collagen basement membrane of 3D reconstructed NVUs was calculated. In the hippocampus, a significantly greater area of contact between the astrocytes and the basement membrane was seen in comparison to the cortex in control mice ($p<0.01$), and this difference was not affected by saporin treatment ($p<0.001$). Although the arteries of the cortex had higher values suggesting more astrocyte endfeet coverage compared to capillaries and veins, this was not significant (Table 3.8).

Table 3.8 Area of astrocyte coverage of basement membrane

Astrocyte end feet coverage of basement membrane Area of contact/length ($\mu m^2/\mu m$) ±SEM	**Hippocampus**			**Cortex**		
	Capillaries	*Arteries*	*Veins*	*Capillaries*	*Arteries*	*Veins*
Control	8.88±2.9	44.60±11.2	93.34±17.0 ▲	2.11±1.1	19.61±10.1	7.78±4.5 ▲
Saporin	15.26±3.5	52.54±12.0	84.35±14.4 ▲	4.22±1.8	21.05±6.6	8.57±5.3 ▲

▲ $p<0.05$ hippocampus vs. cortex

Discussion

- mu-p75-saporin treatment induced significant loss of cholinergic cell bodies in the MS 45 days after administration.
- Cholinergic nerve fibre projections in the cortex and hippocampus were also killed following saporin administration, while p75NTR-negative cholinergic neurons in the striatum were unaffected.
- The noradrenergic and serotonergic pathways were not affected by mu-p75-saporin treatment.
- In the hippocampus, loss of perivascular cholinergic nerve fibres was observed at the BM and SMCs of the arteries, but not at the astrocyte endfeet.
- In the cortex, loss of perivascular cholinergic nerve fibres was seen at the BM, SMC and the astrocyte endfeet of the arteries.
- Significantly less cholinergic innervation was found at the astrocytic endfeet of cortical capillaries and veins compared to the hippocampus.
- Hippocampal veins had endogenously significantly higher volume of collagen IV-labelled basement membrane and astrocytic endfeet coverage compared to veins in the cortex.

Loss of cholinergic neurons in AD has been described extensively, however the effect of this loss on the NVU is not well characterised. Moreover, previous studies that have looked at perivascular innervation by cholinergic nerve fibres have largely been carried out using 2D images obtained from double or triple labelling immunohistochemistry or immuno-EM experiments (Itakura et al. 1977; Tong & Hamel 1999; Kuznetsova & Schliebs 2013). By combining quadruple labelling immunohistochemistry with 3D reconstruction, the current study allowed not only for individual components of the NVU to be assessed under basal and pathological conditions, but also for perivascular innervation to be quantified along multiple components of the NVU around the entire surface of the blood vessel.

In the current study, administration of mu-saporin led to a significant and specific loss of p75NTR-positive cholinergic neurons in the basal forebrain at 45 days post-surgery. The fibre projections from these neurons were also lost in the hippocampus and cortex. These findings are in agreement with previous studies that have used saporin to induce death of cholinergic neurons in the basal forebrain of mice, rats and non-human primates (Lehmann et al. 2002; Hawkes et al. 2005; Birthelmer et al. 2003; Lin et al. 1999; Ramos-Rodriguez et al. 2013; Leanza 1998; Berger-Sweeney et al. 2001; Scheiderer et al. 2006; Fine et al. 1997). Other major populations of cholinergic neurons that do not express the p75NTR, including those in the striatum (Yeo et al. 1997) were not affected by saporin treatment. Although previous studies have reported decreased serotoninergic fibres and sprouting of noradrenergic fibres alongside ChAT-depleted vessels (Chen et al. 2000; Palmer et al. 1987; Arai et al. 1984; Reinikainen et al. 1990; Heider et al. 1997; Szot et al. 2006; Nelson et al. 2014; Birthelmer et al. 2003; Scheiderer et al. 2006) no differences in serotoninergic or noradrenergic cell density were found following saporin administration. However, as only one timepoint was used in the current experiments, it is possible that changes in noradrenaline or serotonin may occur at a later time, and would be a consideration for future studies.

Using 3D reconstruction of blood vessels, ChAT-positive fibres were found to innervate capillaries, arteries and veins in the hippocampus and cortex, although the majority of the innervation was observed at arteries, in agreement with previous electromicrograph studies (Vaucher & Hamel 1995; Chédotal et al. 1994; Kuznetsova & Schliebs 2013; Luiten et al. 1996). Innate regional differences were observed between the NVU of the hippocampus and cortex. This included a significantly thicker basement membrane in the veins of the hippocampus and greater coverage of the basement membrane by astrocyte endfeet of the veins in the cortex. These two observations are likely related, given that astrocytes and

endothelial cells are the main sites of basement membrane production. Expression of collagen IV has been shown to be significantly upregulated in capillaries and arteries during normal ageing as well as in AD (Kalaria & Pax 1995; Christov et al. 2008; Farkas & Luiten 2001; Magaki et al. 2018), however some studies have found no significant change with AD or CAA (Keable et al. 2015; Merlini et al. 2016). Although much less studied, age-related collagenosis in the venous wall has also been reported (Brown et al. 2002). Thickening of the basement membrane and alterations in basement membrane composition has been hypothesised to precede the development of CAA in capillaries and arteries. However, given that veins are the vessel type least likely to be affected by CAA, the significance of the current findings for CAA are currently unclear. It is possible that the increased basement thickness in veins of the hippocampus make them less likely to be deformed by pressure changes to help ensure a consistent cerebral perfusion (Zócalo et al. 2013; Thorin-Trescases et al. 2018) and to maintain a driving force for clearance of solutes in the CSF and/or ISF. This may also have implications for regional differences in CBF.

We also observed that although total cholinergic fibre density was higher in the hippocampus, the amount of direct cholinergic contact did not differ between the hippocampus and cortex at the basement membrane or the SMC at the arteries where significant loss of perivascular innervation was observed. In contrast to previous studies that have classified perivascular innervation to be within a distance of 3 µm from the BM (Vaucher & Hamel 1995), in the current study, only direct contact between ChAT fibres and BM or SMC was quantified. Thus, additional quantifications could be carried out to determine if the higher degree of cholinergic innervation in the hippocampus reflects a greater influence at the NVU compared to the cortex. This is supported by our findings that innervation of astrocyte endfeet tended to be higher in the hippocampus across all vessel types and was significantly higher at capillaries compared to the cortex.

Saporin treatment significantly reduced the amount of cholinergic contact with the basement membrane of arteries in both the cortex and hippocampus, while capillaries and veins where unaffected. This may reflect the proportional endogenous degree of cholinergic innervation between vessel types. However, perivascular loss of cholinergic fibre contact has been previously reported at microvessels including capillaries in the fronto-parietal cortex following ablation of the substantia innominate (Vaucher & Hamel 1995). Although the reason for this discrepancy is unknown, it may be due to methodological differences including the injection of ibotenic acid into the substantia inominata, which may have induced a stronger death and a more focalised loss in the cortex (Vaucher & Hamel 1995).

Regional differences were also observed in the degree of cholinergic loss at the NVU. While saporin treatment induced a loss of cholinergic contacts only at the basement membrane and SMCs of arteries in both regions, there was additional loss of cholinergic innervation astrocyte endfeet of cortical arteries. Again, this is may be related to the lower endogenous level of astrocyte innervation in the cortex, which may make cortical vessels more susceptible than those in the hippocampus to loss of cholinergic innervation. The loss of innervation seen at the smooth muscle level is important as smooth muscle cells are important in mediating vascular reactivity by responding to NVC by deforming the vessel lumen in order to modulate CBF (Hill et al. 2015). They also express the LRP-1 receptor involved in the transcyctotic removal of Aβ across the BBB (Kanekiyo et al. 2012) and localised contraction of smooth muscles has recently been proposed to generate the force that drives perivascular drainage (Aldea et al. 2018).

Similarly, astrocytes also play a key role in mediating NVC and stimulation of the nucleus basilis has been shown to drive calcium wave signalling in cortical astrocytes via binding to mAChRs (Chen et al. 2012). However, Mishra et al have recently suggested that that arteriolar dilation is achieved by a interneuron-dependent pathway independent of intracellular calcium increases (Mishra et al. 2016). A limitation of this study is that only innervation of the endfeet was quantified, but innervation could also occur at other parts of the astrocyte which may have also changed with cholinergic loss. Moreover, GFAP is known to label only ~15% of all astrocyte populations (Bushong et al. 2002) and other markers of astrocyte endfeet (e.g. AQP4) may have been differentially altered by saporin treatment that were not quantified in this study. Nevertheless, retraction of endfeet, loss of GFAP and decreased AQP4 expression has been reported in astrocytes in the presence of CAA (Wilcock et al. 2009), suggesting dysfunctional contact with the NVU.

Collectively, the current results suggest that cortical arteries are more strongly affected by cholinergic denervation than arteries in the hippocampus. This may have implications for both the relative vulnerability of the cortex and hippocampus to ACh-mediated changes in CBF and the efficiency of clearance of Aβ from the brain that map onto brain regions that are more and less likely to develop CAA.

Chapter 4 : The implication of cholinergic loss on cerebral blood flow and the role of NOS

Introduction

The brain is one of the most highly vascularised and perfused organs in the body (Farkas & Luiten 2001). Hypo-perfusion is a known characteristic of AD and impaired CBF has been suggested to be a biomarker of AD, as well as a driver of amyloidogenic pathology in AD (Ramirez et al. 2015). However, hyper-perfusion has been reported in areas known to affected in the late stages of AD, including the frontal and lateral temporal lobes (Hu et al. 2010). In MCI patients, the hippocampus and amygdala have also been found to be hyper-perfused (Dai et al. 2009), but become hypo-perfused in AD (Alsop et al. 2008). A recent study by Williams et al found a reduction in the latency and duration of the haemodynamic response in the motor cortex in cases of probable CAA compared to healthy control patients (Williams et al. 2017). Similar findings were also indicated by a study comparing pre-symptomatic and symptomatic patients with the hereditary CAA HCHWA-D (van Opstal et al. 2016).

Recent studies have suggested that loss of cholinergic innervation in AD precedes pathological changes in the cortex (Schmitz et al. 2016), and may contribute to hypo-perfusion in AD. On the other hand, changes in CBF may also affect cholinergic neuronal function (Román & Kalaria 2006) and cholinergic neurons have been shown to naturally decline with age (Perry 1980). The saporin model of cholinergic denervation has previously been used to investigate the link between loss of cholinergic input and CBF in rats. An early study found that saporin-treated animals had decreased baseline CBF in the cortex as determined by autoradiography (Waite et al. 1999). However, Sorger et al. reported no effect of cholinergic loss on CBF in either the hippocampus or cortex (Sorger et al. 1999). More recently, a study using laser Doppler flow has reported a decrease in CBF in the cortex of denervated rats only when challenged with whisker deflection (Lecrux et al. 2017). Therefore, the effect of loss of cholinergic input from the medial septum on baseline and evoked CBF remains undetermined.

As discussed in the main introduction, ACh causes vasodilation primarily by inducing the production of nitric oxide (NO) in endothelial cells via activation of eNOS (Furchgott & Zawadzki 1980). Although cholinergic neurons originating in the basal forebrain have been shown to innervate both eNOS-containing endothelial cells (Vaucher & Hamel 1995) and nNOS-containing inter-neurons in the cortex (Cauli et al. 2004; Vaucher et al. 1997),

experimental data suggests that increased cortical CBF following direct stimulation of the basal forebrain is mediated primarily through activation of eNOS (Zhang et al. 1995). Decreased expression of eNOS has been reported in the occipital cortex in AD (Jeynes & Provias 2009), a region that is most commonly affected by CAA (Attems et al. 2011) and which has been shown to be hypo-perfused in AD (Brown et al. 1996). Conversely, eNOS and iNOS activity have been shown to be significantly increased in the temporal and frontal cortices of AD patients (Dorheim et al. 1994), in association with hyper-perfusion (Hu et al. 2010). eNOS deficiency has also been implicated in AD pathology, as increased levels of APP, $A\beta_{1-40}$ and errors in performance of a radial maze arm test were found in eNOS deficient mice compared to control mice (Austin et al. 2013). In addition, a study by Tan et al reported increased CAA in a mouse model of partial eNOS deficiency (Tan et al. 2015). These data support the importance of eNOS in regulating cerebral perfusion and suggest a possible link between eNOS deficiency and vascular pathology in AD.

The aim of this study was to determine the effect of cholinergic loss on CBF in our model and to identify whether there were regional variations between the cortex and hippocampus. We also investigated whether changes in CBF were associated with underlying changes in eNOS and nNOS signalling.

Materials and methods

Functional Magnetic resonance imaging (fMRI)

8-10 week old male C57BL/6 mice that received an ICV injection of mu-saporin (n=7) or saline (n=7) as detailed in Chapter 2 (section 'Cholinergic denervation', page 45) were imaged at the UCL Centre for Advanced Biomedical Imaging (CABI, London) 45 days after surgery. Arterial spin labelling fMRI was carried out using a 9.4 T VNMRS horizontal bore scanner (Agilent Inc., Santa Clara, CA, USA). A diagram of the imaging procedure is shown in Fig. 4.1. In each 5 minute imaging block, 5 coronal slices of the mouse brain were acquired. Hypercapnia was induced using 5% CO_2 through a mask after baseline CBF was acquired and 15 minutes after administration of Fasudil hydrochloride (10 mg/kg IP, Tokyo Chemical Industries, Tokyo, Japan).

Statistical Parametric Mapping (SPM, http://www.fil.ion.ucl.ac. uk/spm/) was applied to perfusion-weighted acquired ASL images (Wells et al. 2015). Acquired images were processed using a Matlab (Mathworks, MA, USA) customised script. Regions of interest (cortex, hippocampus, striatum) were then manually traced on a single slice and quantified using a Matlab script which converted pixel intensity into CBF (ml/100g/min). The Matlab script was written and run by Dr Jack Wells (Wells et al. 2015). At the end of the imaging

experiments, mice were perfusion fixed with 4% PFA and their brains collected for immunohistochemistry.

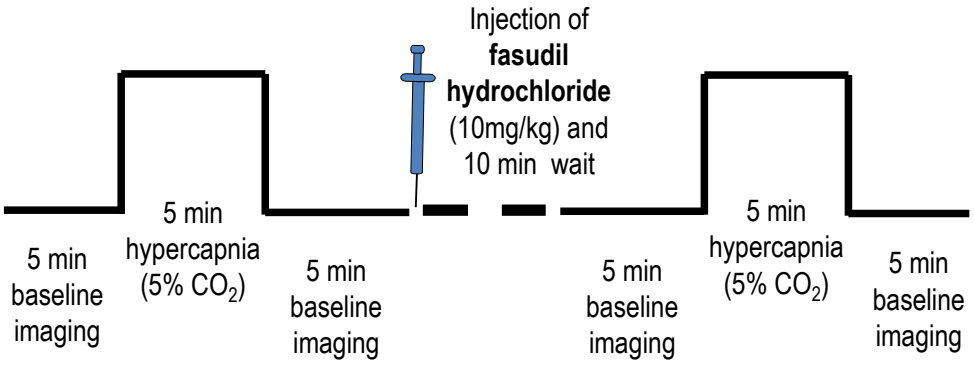

Figure 4.1 Timeline of fMRI imaging protocol
Baseline CBF was obtained for 5 mins, following which hypercapnia (5% CO_2) was induced for 5 mins after which there was a 5 min recovery period. Mice were then injected with fasudil hydrochloride and imaged 10 minutes later, followed by a repeated application of hypercapnia and recovery.

Immunohistochemistry

To assess eNOS expression in the cortex, hippocampus and striatum, brains collected from mice that underwent fMRI imaging were sliced on a cryostat and free-floating sections were collected. Sections were sequentially stained using double-labelling immunohistochemistry with antibodies against the endothelial cell maker CD31 and total-NOS (see Chapter 2, Table 2.1 for antibody concentrations). Images were captured using a Leica SP5 confocal microscope and degree of colocalisation between CD31 and NOS was determined using the Manders correlation (Bolte & Cordelieres 2006) in Image J (JaCop plug-in). For quantification of co-localisation in the hippocampus, values from both the ipsilateral and contralateral hemispheres were averaged and treated as n = 1. For quantification of images from the cortex, six random non-overlapping spanning the somatosensory cortex of the ipsilateral cortex to the somatosensory cortex of the contralateral cortex were averaged and analysed.

Western blotting

In order to ascertain protein levels of NOS enzymes, brains were collected from a separate cohort of 8-10 week old C57BL/6 mice that received an ICV injection of mu-saporin (n=6) or saline (n=7) 45 days earlier. Homogenates from the cortex, hippocampus and striatum were probed using antibodies against eNOS and nNOS (see Chapter 2, section ‘Western blotting’, page 48). Membranes were stripped and re-probed for GAPDH as a loading control. Optical density (OD) of the bands corresponding to the estimated molecular weight of the eNOS and nNOS proteins were quantified using Image J and calculated as a ratio of the OD of GAPDH per corresponding sample.

NOS activity assay

To assess levels of NOS activity in control and saporin-treated mice, brain homogenates from control and saporin-treated mice (n=5/group) were processed to isolate the membrane and soluble fractions. Brain tissues were homogenised in ice cold homogenisation buffer (25 mM Tris-HCl pH 7.4, 1 mM EDTA, 1 mM EGTA containing 1:100 Protease inhibitor cocktail Set III, EDTA free (Merck Millipore)). Homogenates were centrifuged (1300 rpm, 25 min, 4^0 C), supernatant was collected as the nNOS-enriched fraction and the pellet was resuspended in 150 µL homogenisation buffer and collected as the eNOS-enriched fraction.

The NOS assay was carried out as per manufacturer's instruction (Cayman Chemical, Ann Arbor, MI, USA). Briefly, the tissue homogenate was added to a reaction mixture (see Chapter 2, Table 2.2, page 49, for composition) containing radiolabelled [^{3}H] L-Arginine monohydrochloride (50.5 Ci/mmol, 1 µCi/µl, Perkin Elmer, Llantristant, UK). The reaction was incubated at room temperature (22^0 C) for 30 min to allow the active endogenous NOS to convert the [^{3}H] L-Arginine into [^{3}H] L-citrulline, following which stop buffer (50 mM HEPES and 5 mM EDTA, pH 5.5) was added. To determine the relative activity of specific NOS isoforms, tissue homogenates were pre-incubated with the selective nNOS inhibitor 7-Nitroindazole (7-NI, 1 µM final concentration, Tokyo Chemical Industry Co. (Tokyo, Japan)) or the pan-NOS inhibitor Nitro-L-arginine Methyl Ester Hydrochloride (L-NAME, 10 µM final concentration, Tokyo Chemical Industry Co.). Fig. 4.2 shows a diagram of the sites of action of fasudil hydrochloride, L-NAME and 7-NI on the eNOS stimulation pathway.

The reaction mixture was then pipetted onto resin which bound any unconverted [^{3}H] L-Arginine, which was then separated from the rest of the mixture using a glass pipette under gravity filtration. Scintillation fluid (Emulsifier-safe, Packard Instrument Company, CT, USA) was then added to this mixture and radioactivity was measured using a liquid scintillation and luminescence counter (1450 microbeta Wallac Trilux, Perkin Elmer). Background counts (reaction mixture, stop buffer and resin without homogenate) and total counts (reaction mixture and stop buffer only) were also obtained.

The relative proportion of eNOS and nNOS activity in the total reaction was calculated as follows:

$$1 - \left[\frac{\text{rate of citrulline production in presence of NOS inhibitor}}{\text{rate of endogenous citrulline production}} \right] \text{x } 100 = \text{\% NOS activity blocked by inhibitor}$$

Equation 4.1: % activity blocked by total NOS inhibition (L-NAME) - % activity blocked by inhibition of nNOS (7-NI) = % activity blocked by inhibition of i/eNOS.

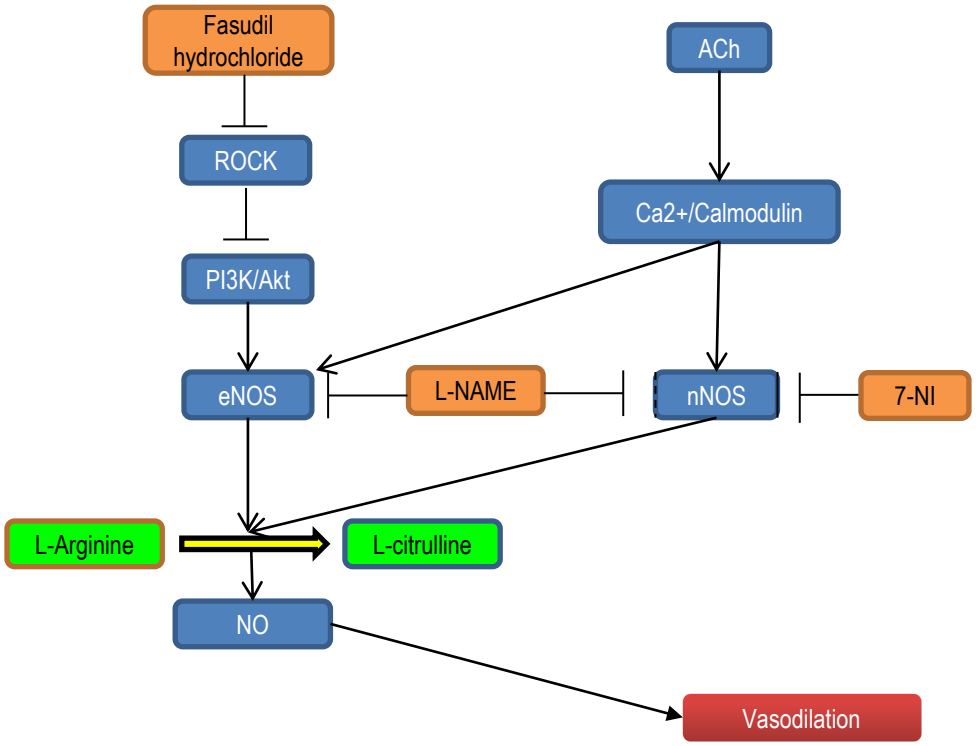

Figure 4.2 Pharmacological manipulation of eNOS/nNOS activity
Pathway of eNOS and nNOS-mediated vasodilation and sites targeted pharmacologically. Acetylcholine (ACh) stimulates eNOS and/or nNOS by inducing Ca^{2+}/calmodulin signalling. nNOS can be inhibited using the drug 7-NI. L-NAME inhibits both eNOS and nNOS (Iadecola et al. 1994). Fasudil hydrochloride is a rho-kinase (ROCK) inhibitor, which prevents ROCK from inhibiting the PI3K/Akt pathway, allowing it to activate eNOS, which can then convert L-Arginine into L-citrulline, releasing the vasodilatory by-product NO.

Statistics

Data was tested for normality using the Kolmogorov-Smirov test. Statistical analysis of CBF in saporin vs control mice at each time point was carried out using a paired two-tailed Student's t tests with Holm-Sidak correction for multiple comparisons. Comparisons between control and saporin-treated mice for Western blot and immunohistochemistry data were analysed using two-tailed Student's t-test. To analyse differences of NOS activity data, one-way ANOVA with Newman-Keuls post-hoc test was used to assess differences between brain regions and treatment groups, and two-tailed t-test was used to analyse differences between saporin and control groups. In all cases, significance was set at $p<0.05$ and data are displayed as mean ±SEM.

Results

Effect of cholinergic loss on regional cerebral blood flow

In order to assess the effect of loss of perivascular cholinergic innervation from the basal forebrain on CBF in the cortex and hippocampus, *in vivo* arterial spin labelling fMRI was used to image cerebral perfusion the brains of control and saporin-treated mice.

In the hippocampus, baseline CBF did not differ between control and saporin-treated mice (Fig. 4.3 a). To determine if denervated vessels were responsive to a general vasodilatory stimulus, control and saporin-treated mice were administered 5% CO_2 to induce hypercapnia. Administration of hypercapnia increased CBF, which was significantly higher than baseline in saporin-treated mice. To determine if loss of cholinergic input affected eNOS-mediated vasodilation, mice were then administered the Rho-kinase inhibitor Fasudil hydrochloride. No differences in CBF were noted between control and saporin mice after administration of fasudil hydrochloride, suggesting that both groups of animals responded equally to eNOS stimulation (Fig. 4.3 b). Fasudil hydrochloride administration did not affect the hypercapnia-induced increase in CBF in either control or saporin mice in the hippocampus (Fig. 4.3 b).

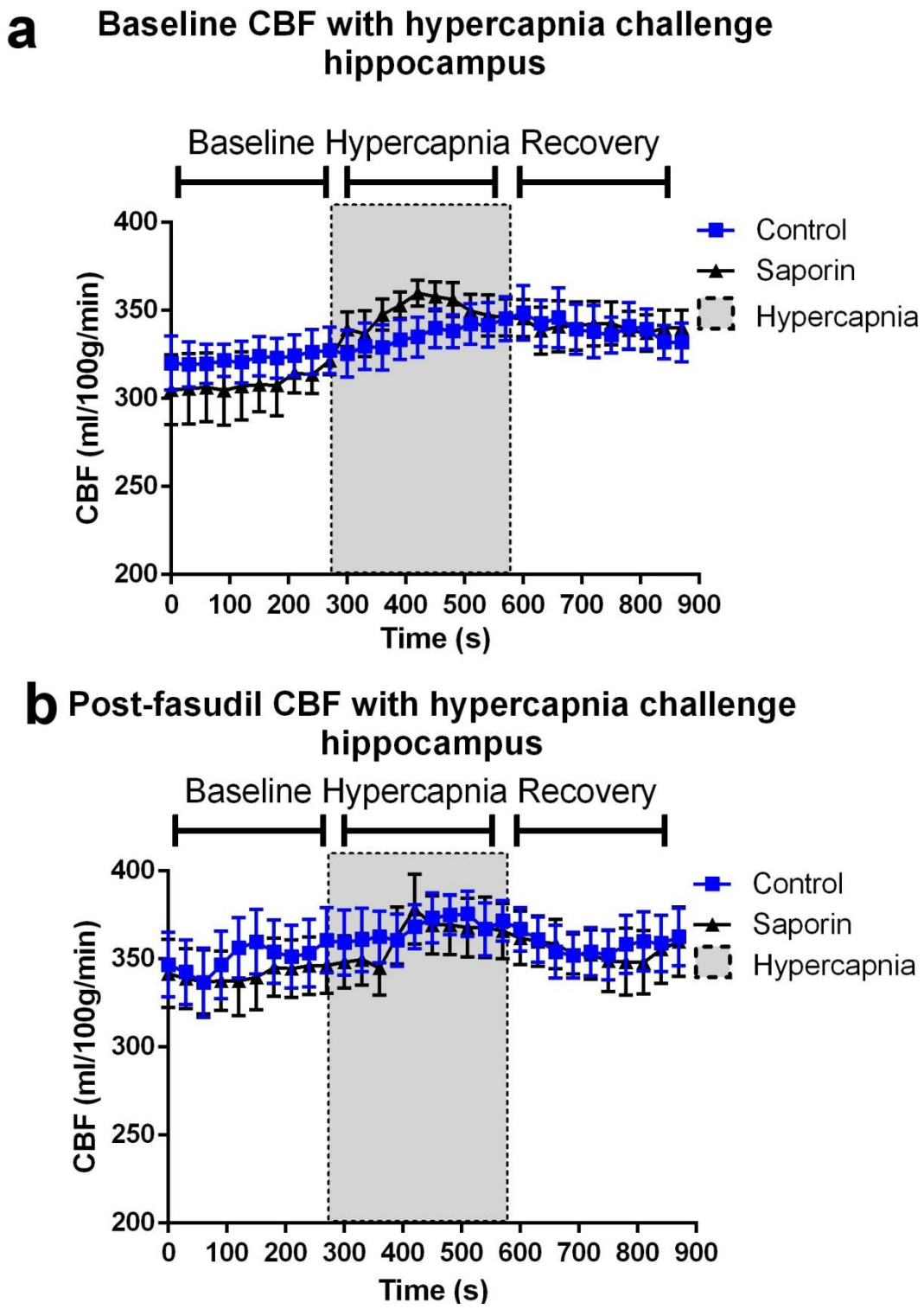

Figure 4.3 CBF fMRI data of control and saporin-treated mice from the hippocampus
(a) In the hippocampus, there was no significant difference in resting CBF or response to hypercapnia between control and saporin groups. (b) Administration of fasudil hydrochloride increased CBF equally in both groups and both groups responded to the subsequent hypercapnia challenge. Grey box between 300 s – 600 s indicates administration of 5% CO_2. (Control n=7, saporin n=5), error bars are shown as ±SEM

In the cortex, similarly to the hippocampus, no differences in CBF were noted between control and saporin-treated animals at baseline (Fig. 4.4 a). Both control and saporin-treated mice showed a significant increase in CBF in response to hypercapnia compared to baseline CBF (p<0.05), and no differences were noted between control and saporin animals. After administration of fasudil hydrochloride, CBF was significantly higher in the

control group compared to the saporin treated animals (Fig. 4.4 b) (p<0.05), suggesting that saporin-treated mice did not respond to stimulation of the eNOS pathway. Fasudil hydrochloride administration did not affect hypercapnia-induced increase in CBF in either control or saporin mice (Fig. 4.4 b).

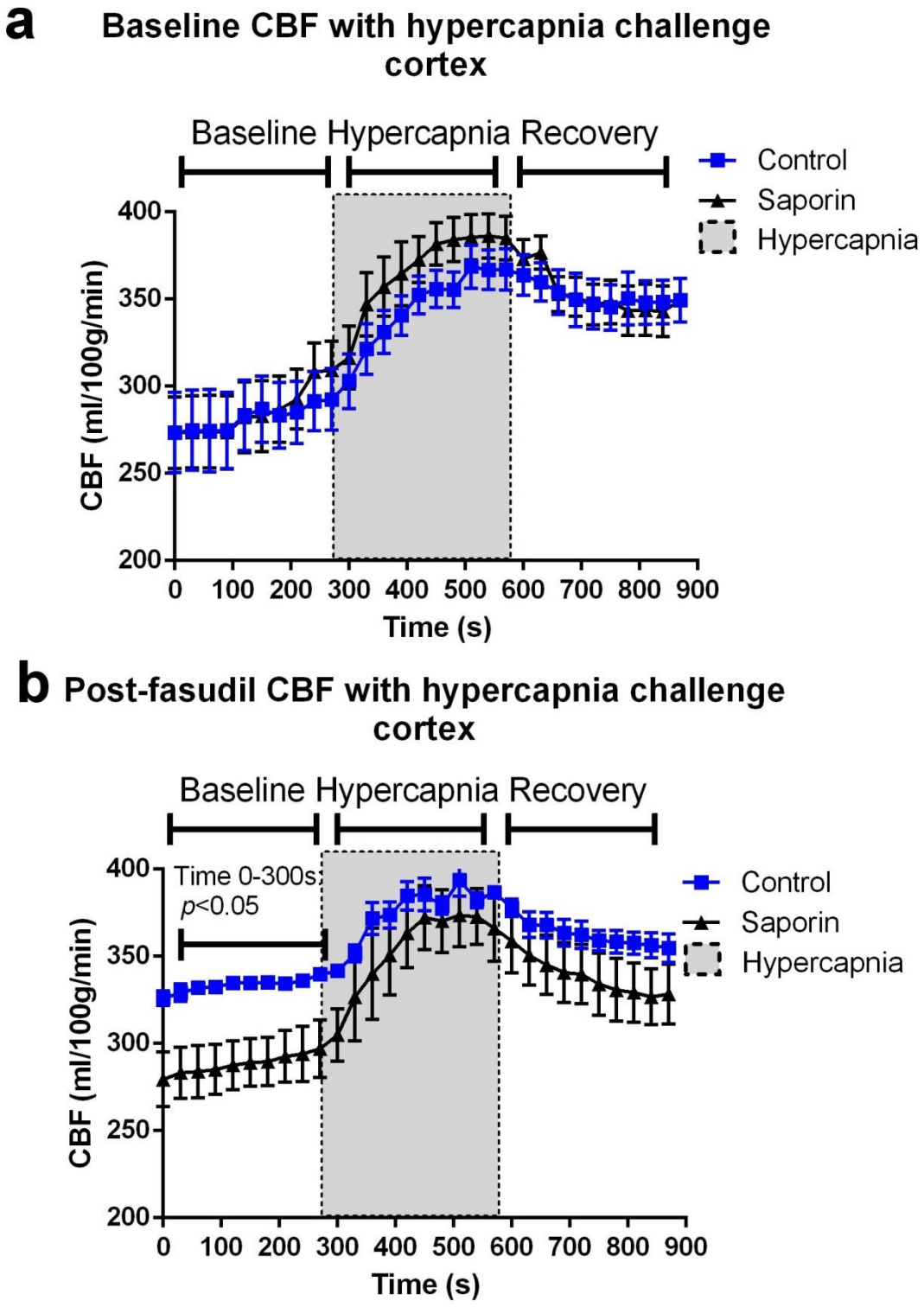

Figure 4.4 CBF fMRI data of control and saporin-treated mice from the hippocampus
(a) In the cortex, baseline CBF was similar between control and saporin-treated groups and no differences were noted in their response to hypercapnia. (b) Following administration of fasudil hydrochloride, the saporin-treated animals had significantly lower CBF compared to the control group (p<0.05). However, both groups responded to equally to subsequent hypercapnia. Grey box between 300 s – 600 s indicates administration of 5% CO_2. (Control n=7, saporin n=7), error bars are shown as ±SEM

Because saporin does not induce loss of cholinergic neurons in the striatum, resting and evoked CBF were also assessed in the striatum as a negative control. The profile of CBF was similar to that observed in the hippocampus, in that there was no difference between control and saporin-treated mice in resting CBF or response to hypercapnia (Fig. 4.5 a). However, administration of fasudil hydrochloride did not appear to significantly increase CBF in either control or saporin animals and the response to hypercapnia was muted in this area (Fig. 4.5 b).

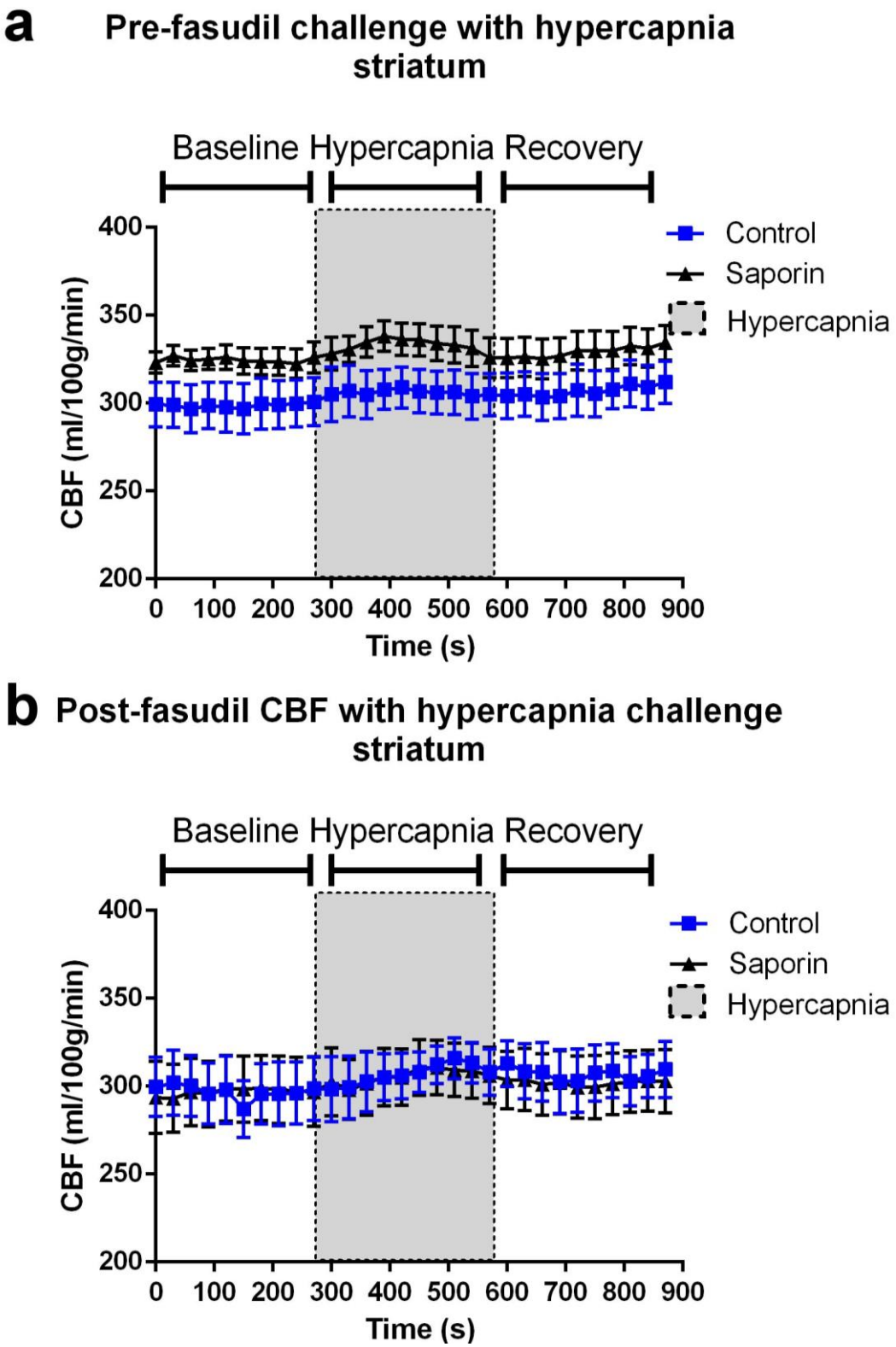

Figure 4.5 CBF fMRI data of control and saporin-treated mice from the striatum
(a) In the striatum, there was no significant difference between the groups. (b) There was no differences post fasudil hydrochloride treatment between the groups. Grey box between 300 s – 600 s indicates time during which 5% CO_2 was used as hypercapnia. (Control n=4, saporin n=7), error bars are shown as ±SEM.

Effect of cholinergic loss on regional NOS protein levels

To determine whether regional differences in eNOS-mediated increased CBF were due to differences in levels of NOS proteins, tissues from the cortex and hippocampus of control and saporin-treated mice were processed by Western blotting using antibodies against

eNOS and nNOS, and by double-labelling immunohistochemistry using a pan-NOS antibody and anti-CD31 to label endothelial cells.

As shown in Fig. 4.6 a, in the hippocampus, levels of eNOS were significantly higher in saporin-treated mice than controls as determined by Western blotting (p<0.05). However, NOS expression in CD31-positive endothelial cells was not altered by saporin treatment (Fig. 4.6 b). No differences were noted in the levels of nNOS between control and saporin mice (Fig.4.6 c).

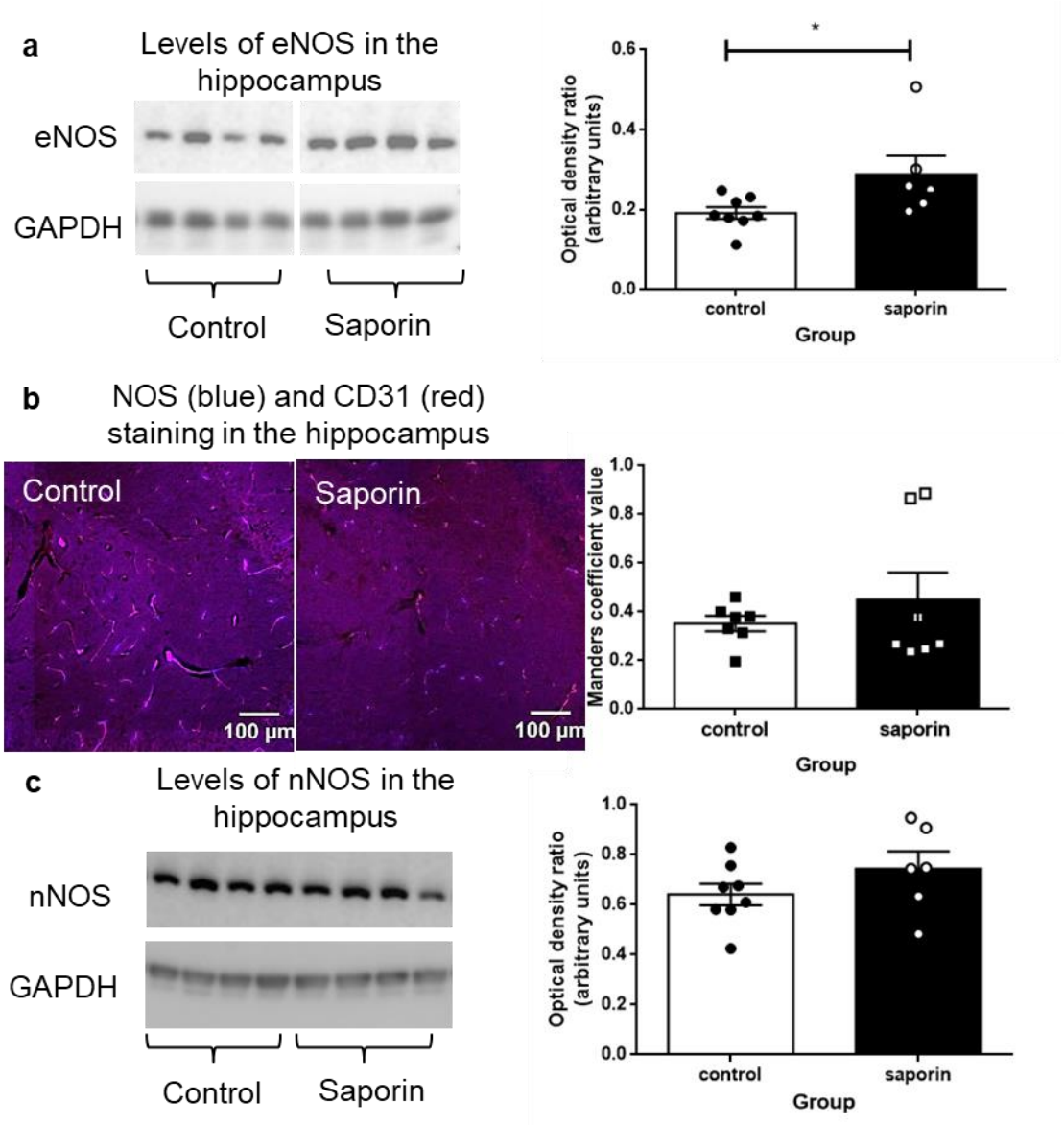

Figure 4.6 The effect of cholinergic loss on protein levels of eNOS and nNOS in the hippocampus
(a) Protein levels of eNOS as detected by Western blotting in the hippocampus were significantly increased in the saporin group compared to control (control n=8, saporin n=6). (b) Photomicrographs of NOS (blue) and CD31 (red) staining in the hippocampus (control n=7, saporin n=7). (c) Levels of nNOS did not differ between control and saporin mice (control n=8, saporin n=6). Error bars are shown as ±SEM.*p<0.05.

In the cortex, levels of total eNOS were significantly lower in saporin-treated animals compared to the control group (Fig. 4.7 a) (p<0.05). These results were confirmed by

immunohistochemistry, where NOS expression in CD31-positive cells was significantly decreased in the cortex of saporin mice (Fig. 4.7 b) (p<0.05). By contrast, levels of nNOS were not altered by saporin treatment (Fig. 4.7 c).

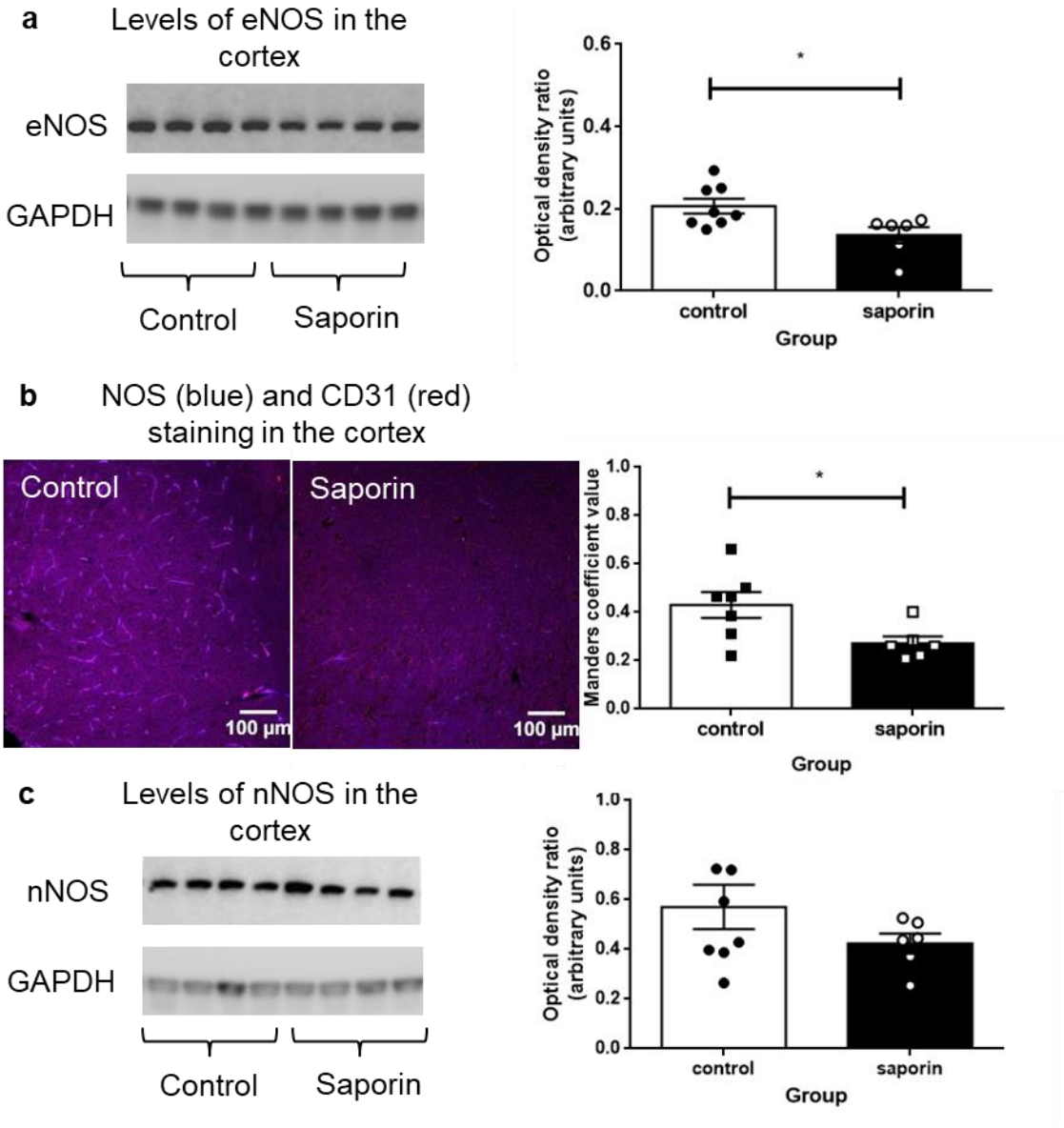

Figure 4.7 The effect of cholinergic loss on protein levels of eNOS and nNOS in the cortex
(a) Levels of eNOS in the cortex were significantly decreased compared to control mice (control n=8, saporin n=6). (b) Photomicrographs of NOS (blue) and CD31 (red) showed decreased levels of colocalisation in the saporin group compared to control (control n=7, saporin n=7). (c) Levels of nNOS were not significantly different between saporin and control groups (control n=8, saporin n=6). Error bars are shown as ±SEM. *p<0.05.

Levels of eNOS and nNOS in the striatum did not differ between control and saporin groups (Fig. 4.8 a and b).

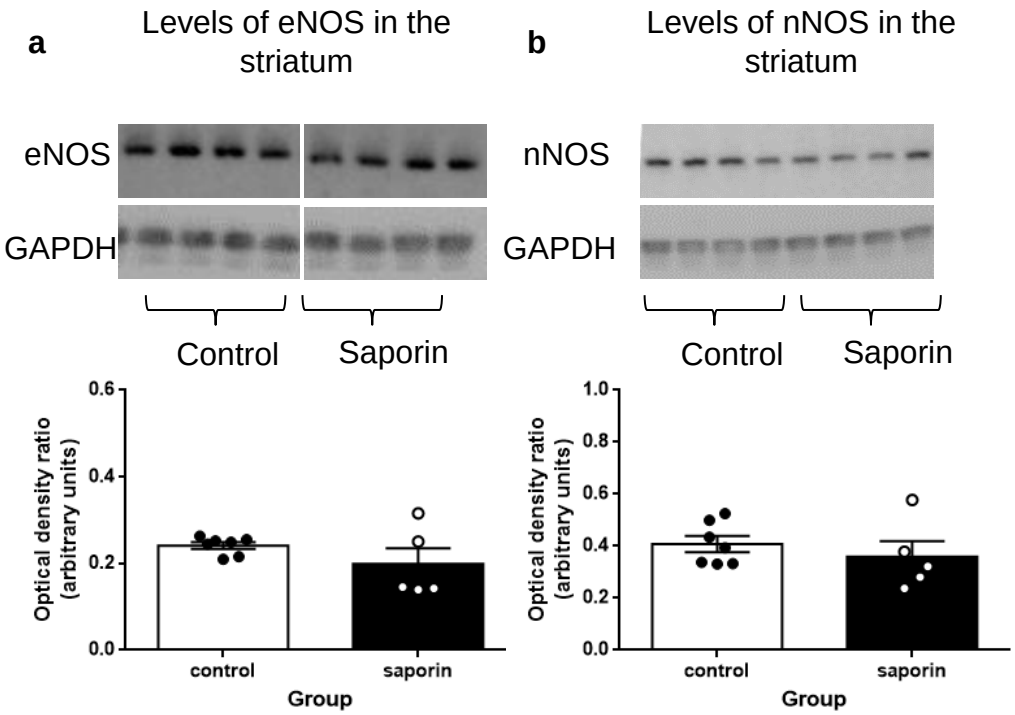

Figure 4.8 The effect of cholinergic loss on protein levels of eNOS and nNOS in the striatum
(a and b) Protein levels of eNOS (a) or nNOS (b) in the striatum were not significantly affected by saporin treatment (control n=8, saporin n=6). Error bars are shown as ±SEM.

Effect of cholinergic loss on NOS activity

To determine whether changes in levels of NOS expression were associated with alterations in enzyme activity, tissue homogenates enriched for eNOS (membrane fraction) or nNOS (soluble fraction) were processed using a radioactivity assay in which the rate of ^{3}H-L-Citrulline production is reflective of enzyme activity.

To first determine if there was regional variation in endogenous NOS activity, concentrations of ^{3}H-L-Citrulline in the cortex and hippocampus from control mice were compared. As shown in Fig. 4.9, endogenous NOS activity was significantly higher in the hippocampus compared to the cortex, with concentrations of ^{3}H-L-Citrulline approximately 4-6 times greater in the membrane fractions in the supernatent (Fig. 4.9 a) and pellet (Fig. 4.9 b) fractions of the hippocampus compared to the cortex, respectively ($p<0.01$, $p<0.001$).

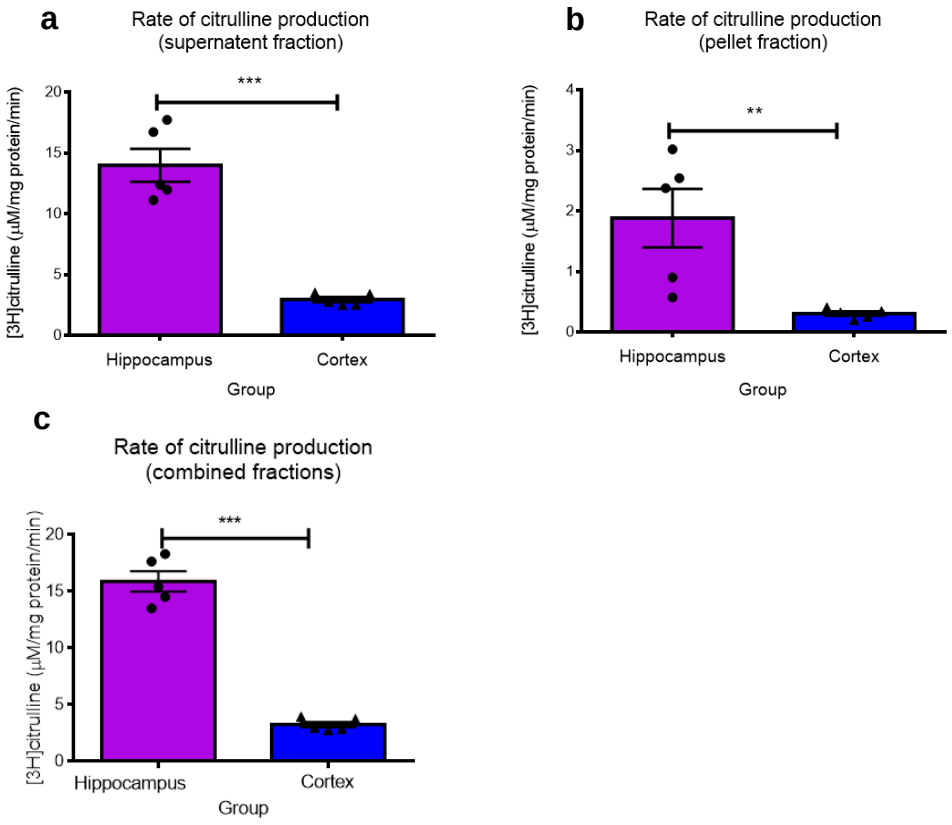

Figure 4.9 Endogenous NOS activity in the hippocampus and cortex
(a-c) Endogenous NOS activity in the hippocampus and cortex of control mice as measured by the rate of production of [^{3}H]L-Citrulline in the nNOS-enriched supernatant (a), eNOS-enriched membrane fraction (b) and in the combined fractions (c). (control n=5, saporin n=5) **p<0.01; ***p<0.001. Error bars are shown as ±SEM.

Analysis of ^{3}H-L-Citrulline concentrations in the membrane and soluble fractions of control and saporin mice in the hippocampus did not show differences between the treatment groups (Table 4.1). Similarly, no differences were noted between control and saporin mice in concentrations of ^{3}H-L-Citrulline in the cortex (Table 4.2) or in the striatum (Table 4.3).

To determine if residual expression of eNOS and nNOS in the respective soluble and membrane fractions may have masked potential differences between control and saporin treatments, the NOS activity assay was repeated in the presence of pharmacological inhibitors. Because eNOS-specific inhibitors are not available, samples were incubated with the general NOS inhibitor L-NAME (Iadecola et al. 1994; Wang et al. 2013; Antošová et al. 2015) and the nNOS specific inhibitor 7-NI (Moore et al. 1993). eNOS activity was interpolated from the difference between total NOS inhibition and inhibition of nNOS.

The rate of ^{3}H-L-Citrulline production in hippocampal samples in the presence of L-NAME and 7-NI are shown in Table 4.1. Inclusion of the pan NOS inhibitor L-NAME significantly reduced enzyme activity by approximately 52-58% and 75-79% in the membrane and soluble fractions, respectively, of both control and saporin samples. There was a trend towards greater inhibition of total NOS activity in the soluble fraction of saporin-treated mice (p=0.059). In the membrane fraction, the amount of total NOS inhibition was significantly higher in control samples (p=0.033), suggesting that there was more NOS activity in the eNOS-enriched fraction in saporin samples. Inhibition of nNOS activity also induced a decrease in ^{3}H-L-Citrulline production in the soluble fraction of control and saporin mice (53-55% reduction from baseline), but no differences were noted between treatment groups. In the membrane fraction, inhibition of nNOS caused a smaller decrease in the rate of citrulline production in the saporin samples (48.3% control vs. 25.8% saporin, p=0.0582), suggesting that there is either less nNOS or that that its activity was higher in the saporin-treated mice. In the membrane fraction, the estimated reduction in enzyme activity following inhibition of i/eNOS was greater in control vs. saporin mice (3.05 ± 6.72% control vs. 25.8 ± 12% saporin), suggesting that eNOS activity was higher in saporin treated animals, however this difference was not statistically significant (p=0.137).

Table 4.1: NOS activity in the hippocampus

Hippocampus	Control (µmol/mg protein/min)	Saporin (µmol/mg protein/min)	Control + L-NAME (µmol/mg protein/min)	Saporin + L-NAME (µmol/mg protein/min)	Control + 7-NI (µmol/mg protein/min)	Saporin + 7-NI (µmol/mg protein/min)	Control (% reduction in enzyme activity in presence of eNOS inhibition)	Saporin (% reduction in enzyme activity in presence of eNOS inhibition)
Soluble (nNOS-enriched)	14.0 ± 1.35	13.6 ± 0.82	3.4 ± 0.23 (75.0%)	2.8 ± 0.19 (79.7%)	6.6 ±0.93 (53.2%)	6.0 ± 0.36 (55.5%)	21.9 ± 3.84%	24.2 ± 2.83%
***P* value**	*p*=0.829		*p*=0.059		*p*=0.581		*p*=0.647	
Membrane (eNOS-enriched)	1.9 ± 0.48	2.5 ± 0.21	0.7 ± 0.14 (57.6%)	1.2 ± 0.14 (51.6%)	0.9 ± 0.26 (48.3%)	1.9 ± 0.42 (25.8%)	9.33 ± 5.08%	25.8 ± 11.99%
***P* value**	*p*=0.271		*p*=0.033*		*p*=0.0582		*p*=0.242	

Table 4.1: Table showing NOS activity in the hippocampus with pharmacological inhibition using the general NOS inhibitor L-NAME or the nNOS inhibitor 7-NI and estimated eNOS inhibition calculated from subtracting 7-NI counts from L-NAME counts. Values show mean count ± SEM. Figures in brackets represent % inhibition of endogenous NOS activity. P values show comparison between control and saporin groups.

In the cortex, incubation with L-NAME resulted in an almost complete reduction of ^{3}H-L-Citrulline production in samples from both control and saporin mice (91-99% reduction from baseline, Table 4.2). No significant differences in nNOS activity were observed between the saporin and control groups in either the soluble or membrane fractions, although the reduction was greater in the soluble fraction (~95%) compared to the

membrane fraction (49 – 56%) (Table 4.2). The estimated reduction in enzyme activity following inhibition of i/eNOS in the membrane fraction was smaller in saporin-treated mice compared to controls (39.3% saporin vs. 73.3% control; p=0.052), suggesting less i/eNOS activity after saporin treatment.

Table 4.2: NOS activity in the cortex

Cortex	Control (µmol/mg protein/min)	Saporin (µmol/mg protein/min)	Control + L-NAME (µmol/mg protein/min)	Saporin + L-NAME (µmol/mg protein/min)	Control + 7-NI (µmol/mg protein/min)	Saporin + 7-NI (µmol/mg protein/min)	Control (% reduction in enzyme activity in presence of eNOS inhibition)	Saporin (% reduction in enzyme activity in presence of eNOS inhibition)
Soluble (nNOS-enriched)	2.9 ± 0.22	3.1 ± 0.34	0.02 ± 0.009 (99.4%)	0.0± 0.00 (99.7%)	0.14 ± 0.009 (95.2%)	0.16 ± 0.05 (94.9%)	4.18 ± 0.30%	4.78 ± 1.22
***P* value**	*p*=0.680		*p*=0.057		*p*=0.739		*p*=0.585	
Membrane (eNOS-enriched)	0.3 ± 0.04	0.4 ± 0.06	0.00 ± 0.00 (99.9%)	0.02 ± 0.03 (91.5%)	0.16 ± 0.02 (48.7%)	0.18 ± 0.04 (56.2%)	50.44 ± 4.46%	35.68 ± 8.37%
***P* value**	*p*=0.127		*p*=0.0746		*p*=0.611		*p*=0.158	

Table 4.2: Table showing NOS activity in soluble and membrane fractions of the cortex. Values show mean count ± SEM. Figures in brackets represent % inhibition of endogenous NOS activity. P values show comparison between control and saporin groups.

In the striatum, there was marked reduction in general NOS activity in the presence of L-NAME in both the membrane and soluble fractions (75 – 80% reduction from baseline),

but no differences were noted between control and saporin groups (Table 4.3). Decreased nNOS activity was also evident with incubation with 7-NI, but again no differences were observed between the experimental groups. No differences were observed in the estimated reduction in enzyme activity following inhibition of i/eNOS.

Table 4.3: NOS activity in the striatum

Striatum	Control (µmol/mg protein/min)	Saporin (µmol/mg protein/min)	Control + L-NAME (µmol/mg protein/min)	Saporin + L-NAME (µmol/mg protein/min)	Control + 7-NI (µmol/mg protein/min)	Saporin + 7-NI (µmol/mg protein/min)	Control (% reduction in enzyme activity in presence of eNOS inhibition)	Saporin (% reduction in enzyme activity in presence of eNOS inhibition)
Soluble (nNOS-enriched)	9.2 ± 2.13	7.6±0.95	1.32±0.620 (85.7%)	2.00±0.56 (73.7%)	2.96±1.59 (67.8%)	4.10±0.41 (45.7%)	6.00±28.08%	29.07±6.81%
***P* value**	*p*=0.510		*p*=0.45		*p*=0.51		*p*=0.45	
Membrane (eNOS-enriched)	0.8±0.054	0.8±0.15	0.16±0.10 (80.0%)	0.18±0.06 (77.5%)	0.12±0.07 (85.0%)	0.30±0.04 (62.5%)	13.39±22.59%	22.58±11.14%
***P* value**	*p*=0.879		*p*=0.89		*p*=0.14		*p*=0.71	

Table 4.3: Table showing NOS activity in soluble and membrane fractions of the striatum. Values show mean count ± SEM. Figures in brackets represent % inhibition of endogenous NOS activity. P values show comparison between control and saporin groups.

Discussion

- Loss of cholinergic innervation did not affect baseline or hypercapnia-induced increase in CBF in either the cortex or the hippocampus.
- CBF in the cortex was not affected by administration of fasudil hydrochloride in saporin-treated mice, which was associated with a decrease in eNOS levels and activity.
- Mu-p75-saporin-treated mice remained responsive to fasudil hydrochloride-induced increase in CBF in the hippocampus which was associated with increased eNOS levels with a trend towards increased eNOS activity.

AD is characterised by loss of cholinergic innervation, alterations in CBF and decreased levels of NOS. However, the direct interrelationship between these factors has not been investigated. The aim of the experiments in this chapter was to investigate the effects of loss of perivascular cholinergic innervation on CBF via the NOS pathway.

Given that stimulation of the basal forebrain has been demonstrated to lead to an increase in cortical CBF (Iadecola & Zhang 1996; Hotta et al. 2011), which can be inhibited by AChR antagonists (Biesold et al. 1989), we first determined whether decreased cholinergic innervation affected resting CBF. We found that loss of cholinergic innervation of blood vessels in the cortex and hippocampus did not affect baseline CBF in either region. These findings are consistent with recent findings by Lecrux et al who demonstrated that cholinergic denervation decreased the CBF response to whisker deflection, without affecting resting CBF (Lecrux et al. 2017).

Responsiveness to hypercapnia was also unaltered between control and saporin-treated mice. Hypercapnia is known to cause a global increase in CBF by inducing relaxation of smooth muscle cells and is detected by chemoreceptors that are sensitive to the pH and pCO_2 of the blood (Yoon et al. 2012). Traditional vasoactive peptides (e.g. neuropeptide Y, vasoactive intestinal peptide and neurotransmitters) have not been directly implicated in hypercapnia-induced CBF, although the control of neurotransmission can be influenced by pCO_2 (Toda et al. 1996; Liu et al. 2012). Our findings are consistent with the idea that ACh does not play a significant role in the CBF response to hypercapnia and suggest that the degree of cholinergic death induced in this study does not impair the ability of the cerebral vessels to respond to a general vasodilatory stimulus.

At the NVU, ACh stimulates vasodilation by activating eNOS to convert L-Arginine into L-Citrulline which releases NO as a by-product (Shin et al. 2007). Phosphorylation of eNOS on serine/tyrosine activates the enzyme and leads to its translocation to the plasma

membrane, where the majority of NO production occurs (Qian et al. 2010; Fulton et al. 2004; Dimmeler et al. 1999). Release of ACh from basal forebrain neurons that synapse onto interneurons can also influence CBF through activation of nNOS, which has been suggested to induce vasodilation in vessels > 70 μm from the source in the hippocampus (Lovick et al. 1999). We observed that denervated vessels in the cortex did not respond to treatment with the ROCK inhibitor fasudil hydrochloride, suggesting that the responsiveness of the eNOS pathway was impaired in the cortex. However, vessels in the hippocampus remained responsive to eNOS stimulation. This corresponded with decreased levels of eNOS in the cortex and increased expression of eNOS in the hippocampus of saporin-treated mice, while levels of nNOS were not affected by saporin treatment in either brain region.

It has previously been reported that nNOS expression is higher in the cortex than the hippocampus of the adult mouse brain (Gotti et al. 2005). The regional distribution of eNOS has been found to be similar in both the hippocampus and cortex of the rat brain (Sessa et al. 1993). Although we did not directly compare the expression of eNOS in the cortex and hippocampus of control mice, endogenous activity of NOS in both the nNOS and eNOS-enriched fractions was significantly higher in the hippocampus compared to the cortex, as previously reported (Sehba et al. 2000). This proportional expression was maintained following saporin treatment. This suggests that the capacity to induce vasodilation and increase CBF is higher in the hippocampus than the cortex of wildtype mice. Moreover, despite a more dramatic loss of cholinergic input in the cortex (Chapter 3), levels of eNOS were significantly upregulated in the hippocampus, but not in the cortex, of saporin-treated mice. This suggests that the hippocampus may regulate eNOS expression more tightly than the cortex and may therefore be better able to maintain CBF when challenged. This hypothesis is supported by previous reports that changes in CBF in the hippocampus were more proportional to changes in nNOS activity than in the cortex (Lourenço et al. 2014) and that the cortex is more sensitive to inhibition of nNOS activity than the hippocampus (Kalisch et al. 1996).

Although these experiments were carried out in wildtype mice, they may have implications for regional variations in CBF that are also observed in AD. Several studies have reported decreased CBF in the cortex, but not hippocampus, of MCI and AD patients (Lacalle-Aurioles et al. 2014; Wirth et al. 2017; Alsop et al. 2008). Significantly less eNOS has been found in the occipital cortex of AD cases compared to age-matched controls (Jeynes & Provias 2009) and a ‘sparing’ of NOS positive neurons has been reported in the

hippocampus of AD cases (Hyman et al. 1992). However, other studies have found increased levels of levels of iNOS and eNOS and higher NOS activity in cortical microvessels isolated from the brains of individuals with AD compared to control (Dorheim et al. 1994). Taken together, these studies suggest a higher sensitivity of the cortex than the hippocampus to loss of cholinergic innervation on CBF, but that this difference may be dependent on vessel type and disease progression. While further studies are needed to understand the relationship between regional expressions of NOS, changes in CBF and disease progression, the current findings suggest that a differential response to loss of cholinergic innervation may contribute to regional differences in regional CBF observed in AD.

Chapter 5 : Effect of cholinergic loss on perivascular drainage of Aβ

Introduction

CAA is characterised by a build-up of Aβ in the walls of the cerebrovasculature. Aβ is constitutively produced in the brain and cleared away through multiple mechanisms including enzymatic cleavage, clearance by microglia and astrocytes as well as receptor-mediated clearance across the BBB (Miners et al. 2008; Iwata et al. 2001; Hafez et al. 2011; Farris et al. 2003; Palmer et al. 2010; Wilcock et al. 2004; Mackic et al. 1998). Aβ is also hypothesised to be removed from the brain along the walls of the capillaries and arteries via PVD (Carare et al. 2008) or around the walls of the veins via glymphatic drainage (Iliff et al. 2012).

The PVD hypothesis of Aβ clearance is based in part on experimental observations that nanoparticles and solutes including dextrans and Aβ injected into the ISF of deep brain structures localise to CVBMs in dorsal cortical and leptomeningeal vessels (Ichimura et al. 1991; Carare et al. 2008; Arbel-Ornath et al. 2013). This process occurs very rapidly, within 5-10 minutes of injection (Ball et al. 2010; Hladky & Barrand 2014; Hladky & Barrand 2018; Rennels et al. 1985). Anatomical studies suggest that there is continuity between the extracellular matrix of the parenchyma and the CVBMs of capillaries (Morris et al. 2016). Solutes are then hypothesised to travel to the CVBM of cortical and leptomeningeal arteries before exchanging with CSF at the VRS and subarachnoid space, ultimately draining to cervical lymph nodes (Ball et al. 2010; Ma et al. 2018; Louveau et al. 2015). Because the pattern of distribution of solutes closely mimics that of Aβ accumulation in CAA and other angiopathies (Roher et al. 2003; Jeffrey & González 2007; Tikka et al. 2009; R. O. Carare et al. 2013), failure of this process is thought to contribute to CAA pathology.

As the movement of solutes along CVBMs is counter to the direction of blood flow, the driving force that underlies PVD is still unknown. Initial calculations suggested that this force could be generated by the refractory wave that follows an arterial contraction (Schley et al. 2006). However, recent mathematical models have demonstrated that arterial pulsations are not sufficient to generate drainage velocities that match the experimental observations (Diem et al. 2017). Alternatively, oscillating pulsatile flow generated by the focal contraction and relaxation of arteries has been proposed to mediate perivascular drainage (Sharp et al. 2016) and is supported by experimental *in vitro* data (Partyka et al. 2017). Localised arterial dilatation and contraction can occur both spontaneously (e.g.

vasomotion) and in response to neuronal activity (e.g. NVC) and both mechanisms have been shown to be decreased in AD (Di Marco et al. 2015; Rivera-Rivera et al. 2016; Simic et al. 2014). Application of ACh has been used to induce localised vascular contractions (Sercombe et al. 1990; Zhang et al. 1995; Librizzi et al. 2000) and increased cholinergic tone using AChEI has been shown to increase CBF in response to NVC in the barrel cortex (Lecrux et al. 2017). This suggests that in addition to regulating blood flow, the action of ACh at the NVU may also contribute to clearance of Aβ from the brain.

In the previous chapter, loss of perivascular cholinergic innervation was found to be associated with altered CBF in the cortex, but not the hippocampus. The aim of this chapter was to determine if cholinergic denervation affects the efficiency of PVD of Aβ and if this differs between the cortex and hippocampus.

Materials and methods

PVD of human Aβ in control and saporin-treated mice

The saporin model was used to induce cholinergic denervation as described in Chapter 2 (section 'Cholinergic denervation' page 45). 45 days after ICV injection of saline or mu-saporin, male C57BL/6 mice received an injection of human $A\beta_{1-40}$ HiLyte Fluor™ 555 (50 µM, AnaSpec, USA). For experiments assessing PVD in the hippocampus, n=16 control and n=14 saporin mice were injected with 0.5 µL $A\beta_{1-40}$ into the left hippocampus (coordinates from Bregma: AP=-2mm, ML=1.5mm, DV=-1.7mm) and mice were sacrificed 5 minutes later with an overdose of sodium pentobarbitone (20% w/v; Animalcare, York, UK). For PVD in the cortex, n=8 control and n=7 saporin mice received 0.25 µL $A\beta_{1-40}$ into the right cortex (coordinates from Bregma: AP=-2mm, ML=1.5mm, DV=-0.5mm) and mice were overdosed 2.5 minutes later. All injections were carried out at a rate of 0.2 µL/min using a 32 G Hamilton syringe (Esslab, Hadleigh, England). For both hippocampal and cortical injections the needle was left in situ for 2 minutes (inclusive of drainage times) after the injection to allow for diffusion. Mice were perfused intracardially with 0.01 M PBS followed by 4% PFA, brains removed and post-fixed for 24 hours in 4% PFA before processing.

Immunohistochemistry

Brain tissue sections (20 µm) were collected onto glass slides and in a free-floating manner in alternating sections. Free-floating sections were used to confirm cholinergic loss in the medial septum, hippocampus and cortex using anti-ChAT (1:100) as described in chapter 2, section 'Immunohistochemistry', page 45. They were also used to assess microglial activation using anti-Iba1 (1:500 with sodium citrate buffer antigen retrieval) and astrocyte

reactivity using anti-GFAP (1:500) labelling as described in Chapter 2 (Table 2.1, page 43). For quantification of densities in the hippocampus, values of regions from both the ipsilateral and contralateral hemispheres were averaged and treated as n = 1. For quantification of images from the cortex, six random non-overlapping spanning the somatosensory cortex of the ipsilateral cortex to the somatosensory cortex of the contralateral cortex were averaged and analysed.

For assessment of PVD, slide mounted sections were used to confirm the site of injection and ensure that the ipsilateral hemisphere could be identified. Tissue sections were processed for double-labelling immunohistochemistry as described in Chapter 2 and were simultaneously incubated with anti-laminin (1:350) and FITC-conjugated anti-SMA (1:350) antibodies at 4°C overnight. Sections were then incubated with anti-rabbit AlexaFluor 633 (1:200) and sections were coverslipped in Mowiol with citifluor anti-fading agent. Preliminary experiments to determine optimal conditions for assessment of PVD were carried out with 50 μM human $A\beta_{1\text{-}40}$ HiLyte Fluor™ 488 (AnaSpec, USA).

Quantification of PVD

Sections containing the injection site as identified by the bolus of the injected Aβ-555 were noted and sections 400 μm from that point were imaged for assessment to avoid potential biases at the site of injection, as per previously published protocols (Hawkes et al. 2013; Hawkes et al. 2012). These sections were imaged using a Leica SP5 confocal microscope and LAS software (Milton Keynes, Buckinghamshire). Sections were imaged at x 20 magnification and then stitched together using Image J (NIH, Maryland, USA). Arteries were defined as SMA-positive vessels with a lumen diameter of >10 μm, veins were defined as vessels with a dimeter of >10 μm that are negative for SMA and capillaries were defined as vessels with a lumen <10 μm (Roxana Octavia Carare et al. 2013; Hawkes et al. 2011). Vessels containing Aβ were manually counted and the number of Aβ-positive arteries, veins and capillaries per tissue area was calculated by dividing the number of vessels by the total area analysed (mm^2).

Quantification of glia and blood vessel density

The percentage area containing microglia, astrocytes and blood vessels was calculated using Image J using the threshold values listed in Table 5.1. Additionally, for anti-laminin staining, in order to quantify density by vessel type, a mask was set to select small and large-diameter vessels on calibrated images using the 'Analyse particles' function. The mask settings for a capillary were defined by an area of 10 μm x 10 μm and were therefore set as 0-100 μm for capillaries, 100-infinity μm for arteries and veins, and 0-infinity μm for all vessels.

Table 5.1 Threshold values for analysis of percentage area covered

Label	Minimum grey value	Maximum grey value
Anti-Iba1	68	255
Anti-GFAP	86	255
Anti-laminin	98	255

Statistical analysis

Data was tested for normality using the Kolmogorov-Smirov normality test. For groups of two, a two-tailed Student's t-test was used to assess significance. Other data was analysed using two-way ANOVA with Sidak's post-hoc test. Data is shown as mean ±SEM and $p<0.05$ was considered to be significant.

Results

Loss of cholinergic innervation was confirmed in the hippocampus and cortex of saporin-treated mice as previously shown in Chapter 3 (Fig. 5.1 a-d).

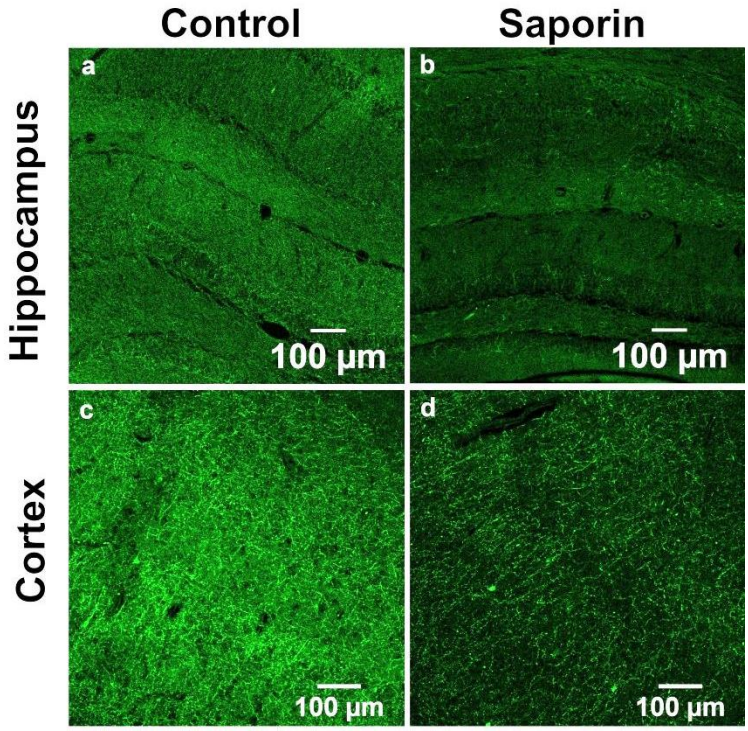

Figure 5.1 Loss of cholinergic nerve fibres using saporin in the hippocampus and cortex
a-d: Representative images of ChAT-stained nerve fibres (green) in the hippocampus of control mice (a) and saporin treated mice (b) and the cortex of control (c) and saporin (d) treated mice. Scale bar = 100 µm.

Immunohistochemistry demonstrated that hippocampal blood vessels 400 µm away from the injection site contained AlexaFluor555-conjugated Aβ within 5 min after injection (Fig. 5.2 a-d). Quantification of the number of Aβ-positive vessels revealed that similar amounts of Aβ were present in the CVBM of capillaries and arteries in control and saporin mice (Fig. 5.2 e). As per previous reports (Hawkes et al. 2011; Arbel-Ornath et al. 2013; Maki et al. 2014; Albargothy et al. 2018) significantly fewer hippocampal veins contained Aβ

compared to arteries and capillaries (p<0.05).

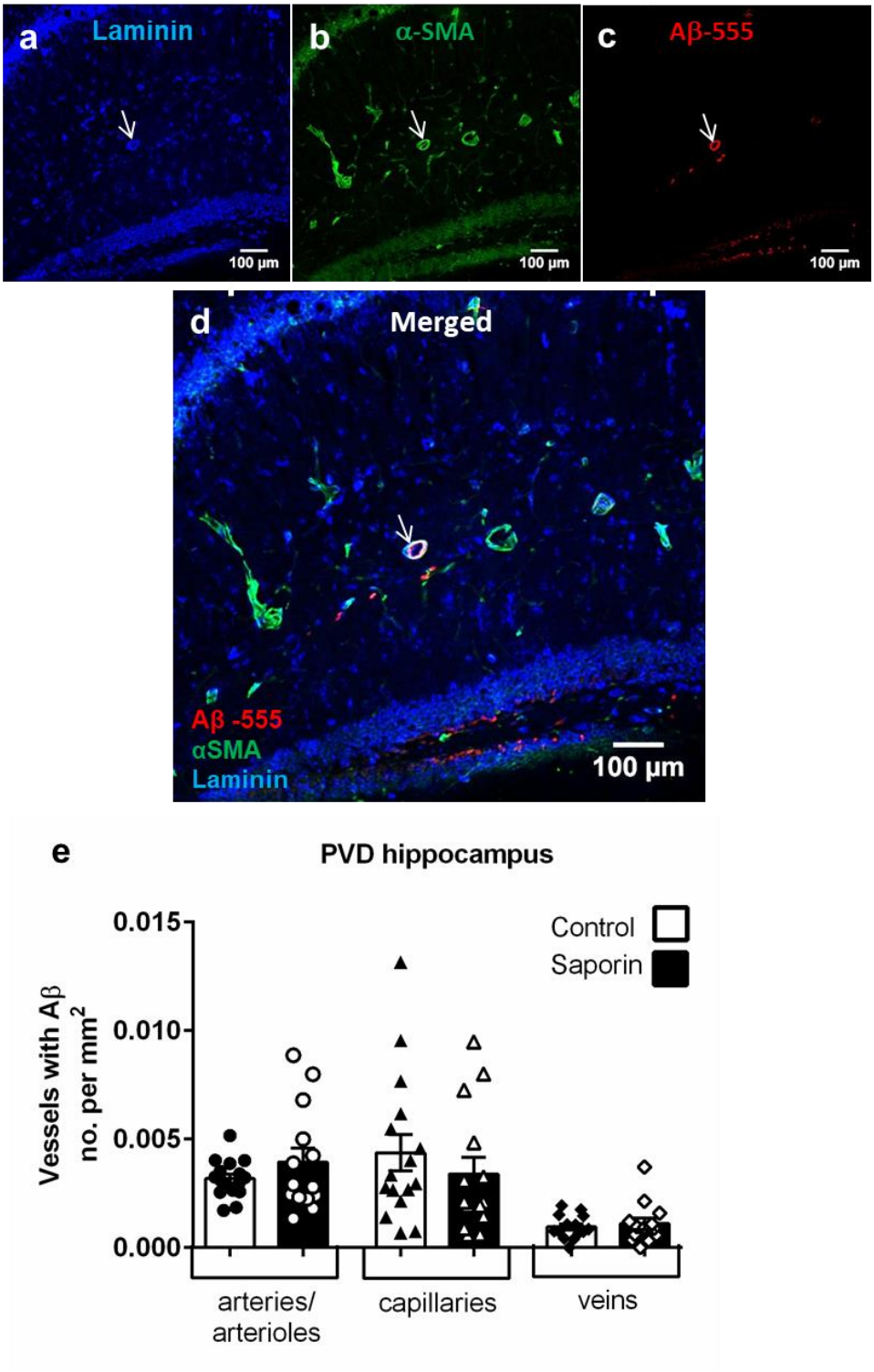

Figure 5.2 Perivascular drainage of injected Aβ in the hippocampus with saporin treatment
(a-e) Representative photomicrographs of blood vessels in the hippocampus stained with anti-laminin (blue; a, d), anti-α smooth muscle actin (green; b and d), and fluorescently labelled injected Aβ (red; c, d). An artery containing Aβ is highlighted by the white arrow (a-d). (e) Quantification of the number of vessels containing Aβ showed no difference between control and saporin-treated mice (control n=16, saporin n=14). Image is taken 400 µm away from injection site. Scale bar = 100 µm.

Preliminary assessment of PVD in the cortex using the same parameters as that in the hippocampus (0.5 µL + 5 min clearance) revealed a much smaller bolus of Aβ at the site of injection (Fig. 5.3 a and b) and very few Aβ-positive vessels were visible at 400 µm away

from the injection site compared to the hippocampus (Fig. 5.2 c and d). Because this difference may have been due to technical issues relating to the proximity of the cortex to the surface of the brain, a series of differing volumes (0.25 µL to 0.5 µL) and drainage times (2.5 to 5 mins) were trialled in the cortex (Fig. 5.3 e-g). The injection protocol of 0.25 µL with 2.5 mins drainage (Fig. 5.3 g) was found to most closely replicate the pattern of PVD observed in the hippocampus and was therefore used to assess PVD in the cortex.

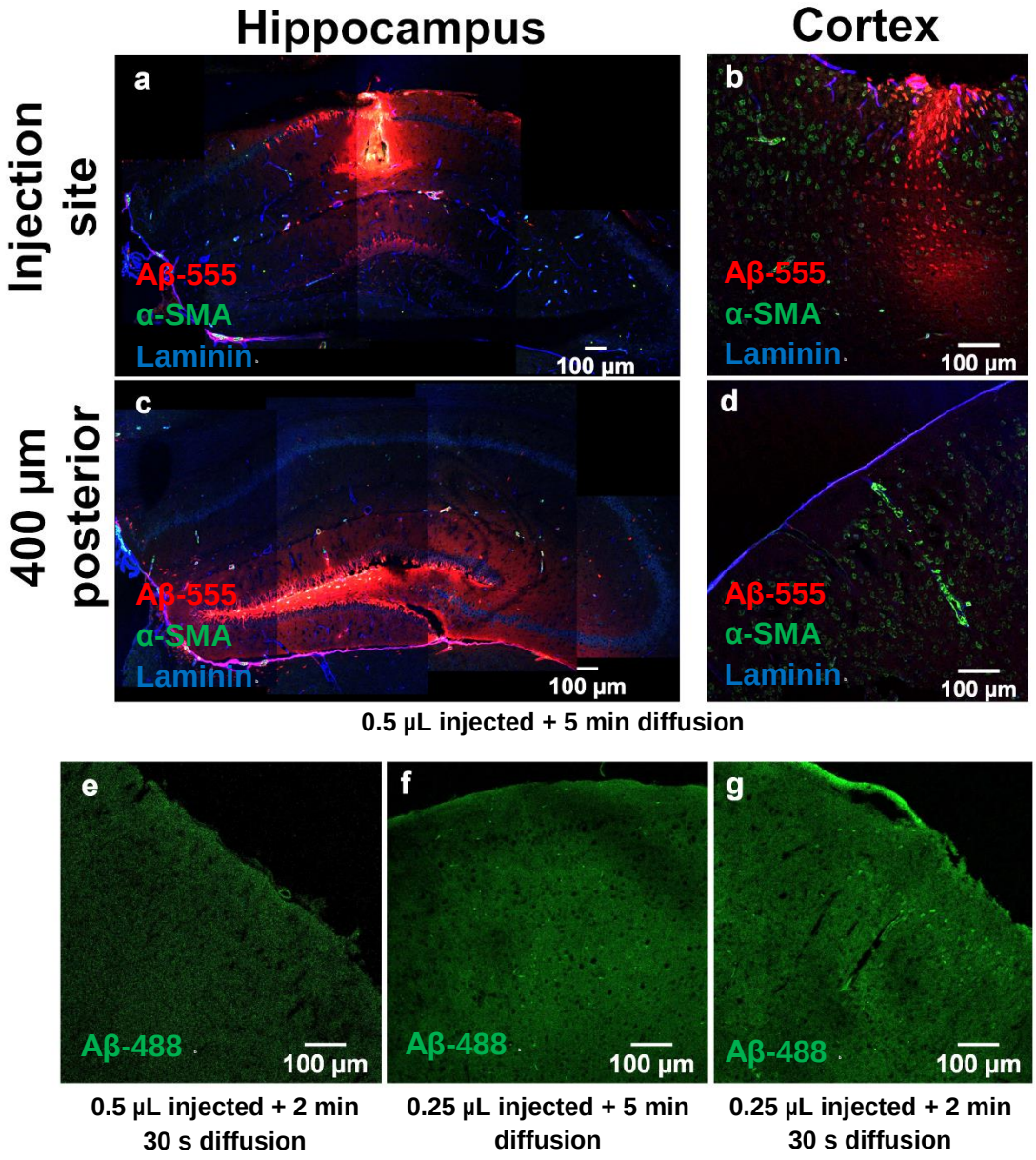

Figure 5.3 Preliminary investigation of perivascular drainage in the cortex compared to the hippocampus

a-g: Representative images showing the bolus of human $A\beta_{1\text{-}40}$ (555, red) injected into the hippocampus (a, c) and into the cortex (b, d) at the site of injection (a and b) at a volume of 0.5 µL and a diffusion time of 5 min. (c and d) show the distribution of Aβ at 400 µm away from the injection site in the hippocampus (c) and in the cortex (d). (e-g) Representative images of the distribution of $A\beta_{1\text{-}40}$ (488, green) at 400 µm away from the injection site following injection of 0.5 µL plus 2 min 30 s drainage (e), 0.25 µL plus 5 mins drainage (f), or 0.25 µL plus 2 min 30 s drainage (g). Scale bar = 100 µm.

Quantification of Aβ-containing vessels in the cortex revealed no differences in the number of capillaries, arteries or veins between control and saporin-treated mice (Fig. 5.4 a-e). Cortical capillaries contained significantly more Aβ compared to the arteries and

veins, regardless of saporin treatment (p<0.05).

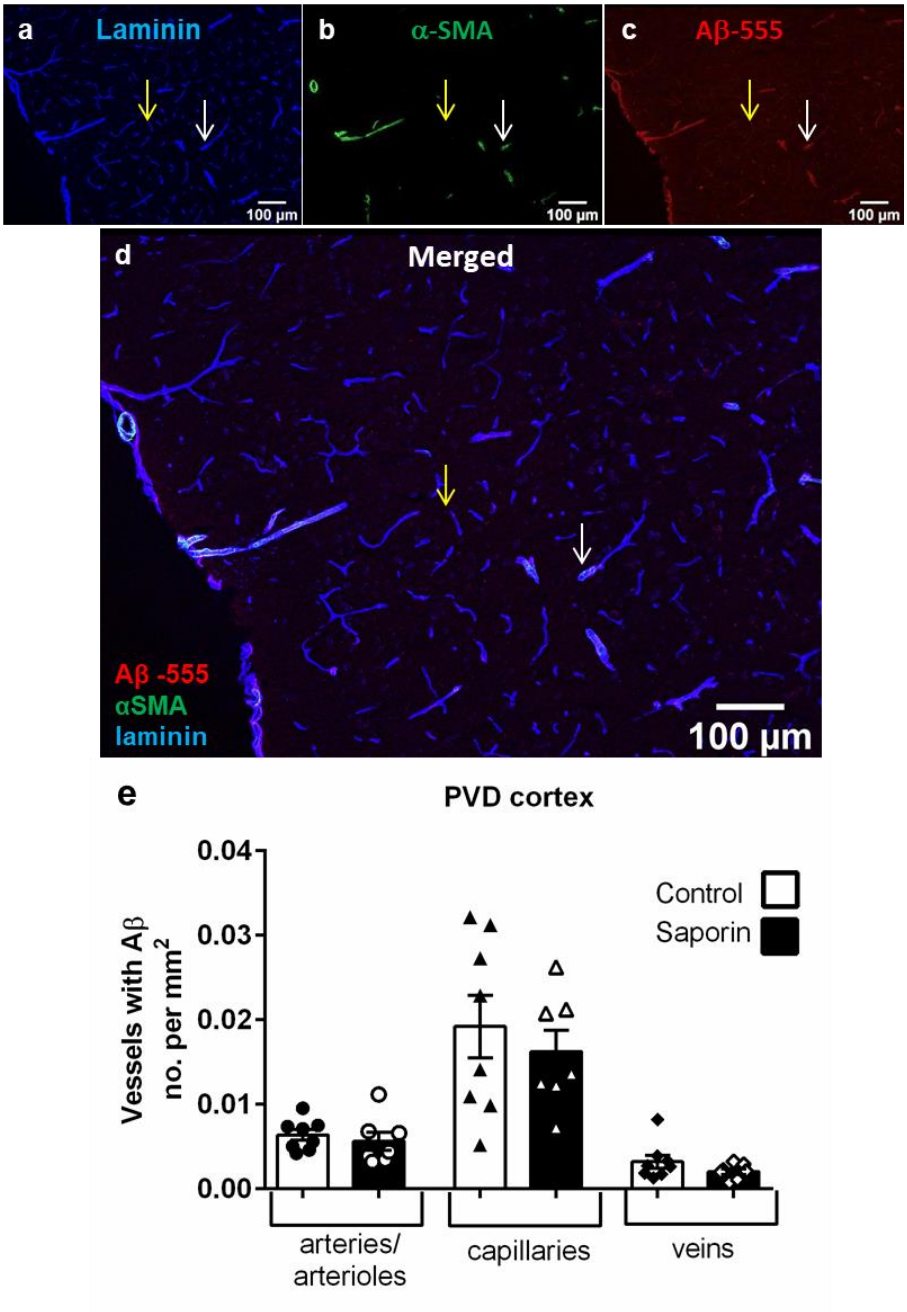

Figure 5.4 Perivascular drainage of inject Aβ in the cortex with saporin treatment
(a-d) Photomicrograph of blood vessels in the cortex stained with anti-laminin (blue; a, d), anti-α smooth muscle actin (green; b and d), and fluorescently labelled injected Aβ (red; c, d). A cortical artery containing Aβ is indicated by a white arrow, and a capillary highlighted by the yellow arrow. (e) Quantification of the number of vessels containing Aβ showed no difference between control and saporin-treated mice (control n=8, saporin n=7). Scale bar = 100 µm.

To determine if there was a difference in the density of vessels between the hippocampus and cortex, the percent area covered by small and large-diameter laminin-positive vessels was quantified in both brain areas. A significantly higher density of arteries/veins and capillaries was noted in the cortex of control mice compared to the hippocampus (Fig. 5.5 a-c, p<0.05). This difference was maintained following saporin treatment (Fig 5.5 a-c).

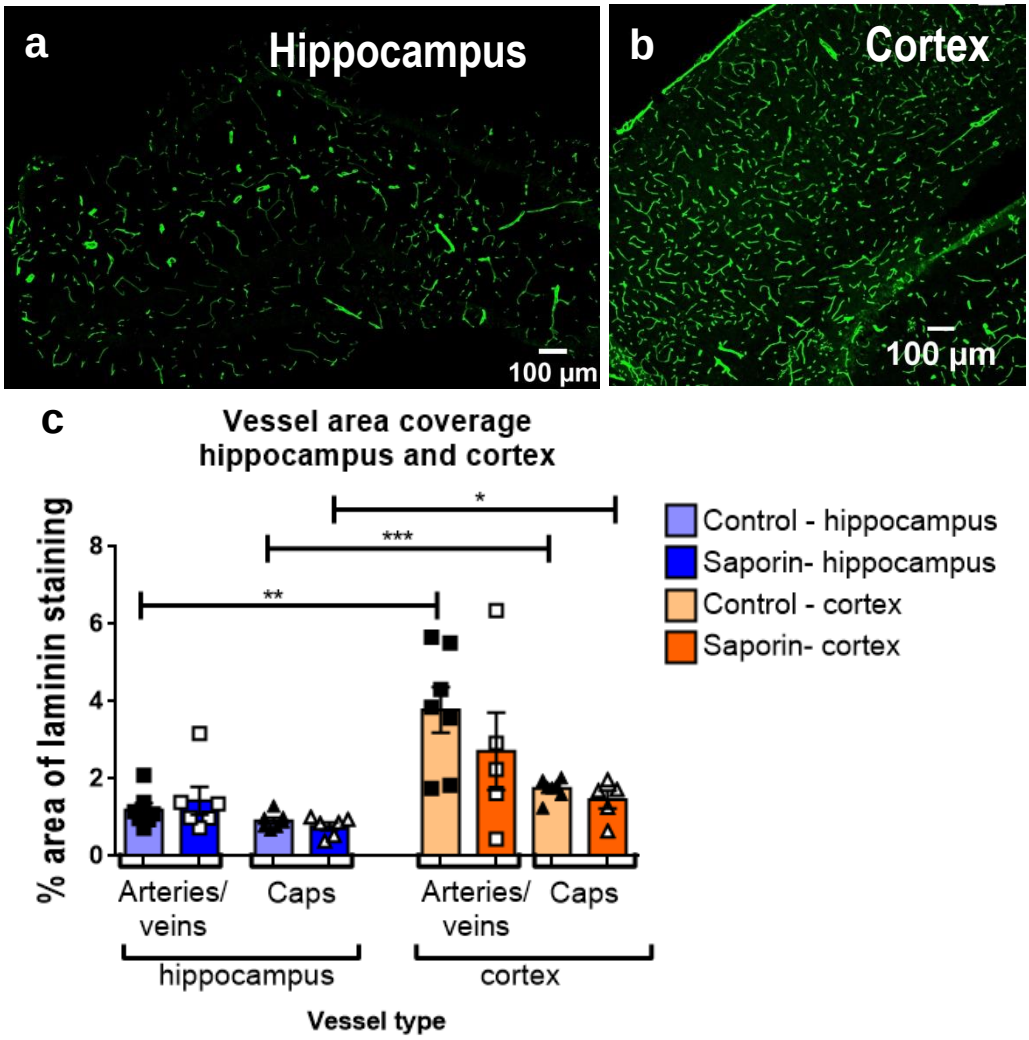

Figure 5.5 Regional variation in vascular density between the hippocampus and cortex
(a and b) Representative photomicrographs of laminin staining (green) in the hippocampus (a) and cortex (b). (c) Quantification of laminin density showed significantly higher capillary density in the cortex in both the saporin and control groups compared to the hippocampus. Arterial density was also significantly higher in the cortex then in the hippocampus of control mice. No differences were detected between the density of arteries and veins between control and saporin-treated mice (control n=7, saporin n=6) (two-tailed t-test) (c). **p*<0.05; ***p*<0.01; ****p*<0.001. Scale bars = 100 µm.

In order to assess whether microglial and/or astrocyte activation may have impacted the drainage of Aβ, sections of the hippocampus and cortex were stained for Iba1 and GFAP. Quantification of Iba1 staining revealed no effect of saporin treatment on microglial coverage of the hippocampus or cortex (Fig. 5.6 a-g). However, regional analyses showed that the hippocampus had significantly more microglial coverage than the cortex (Fig. 5.6 g).

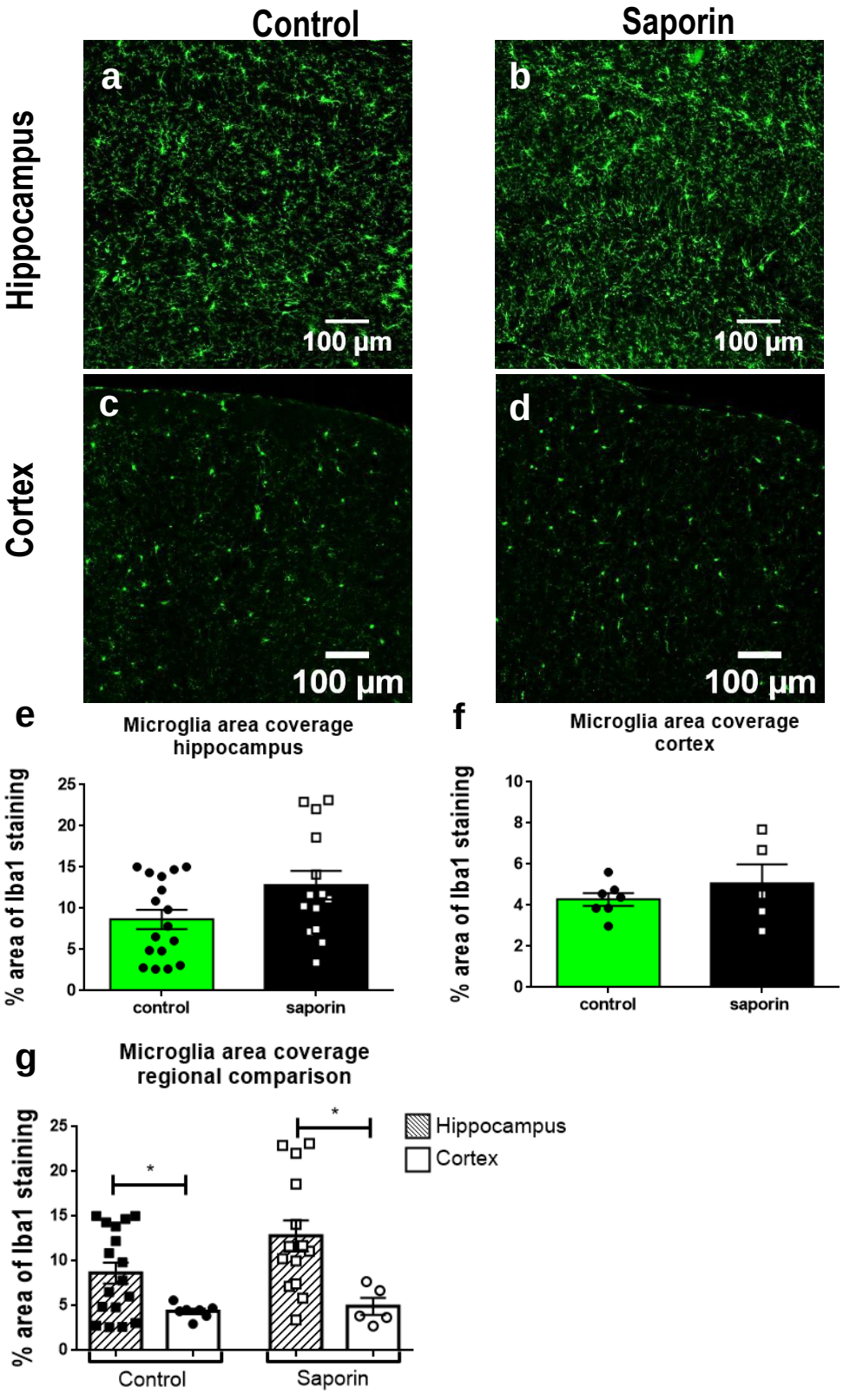

Figure 5.6 Regional variation in microglial density between the hippocampus and cortex
(a-d) Representative photomicrographs of microglial density as assessed by Iba1 staining (green) in the hippocampus (a, b) and cortex (c, d) of control (a, c) and saporin-treated mice (b, d). (e-g) Quantification of Iba1 density showed no difference between saporin and control groups in the hippocampus (control n=17, saporin n=16) (e) and the cortex (control n=7, saporin n=5) (f). Regional comparison showed significantly more Iba1 coverage in both the control and saporin groups in the hippocampus compared to the cortex (g). **p*<0.05. Scale bars =100 µm.

GFAP staining was also similar between control and saporin groups in both the hippocampus and the cortex (Fig. 5.7 a-g). As with the microglia, regional analyses showed that the hippocampus had significantly more astrocytic coverage than the cortex which was unaffected by cholinergic loss (Fig. 5.7 g).

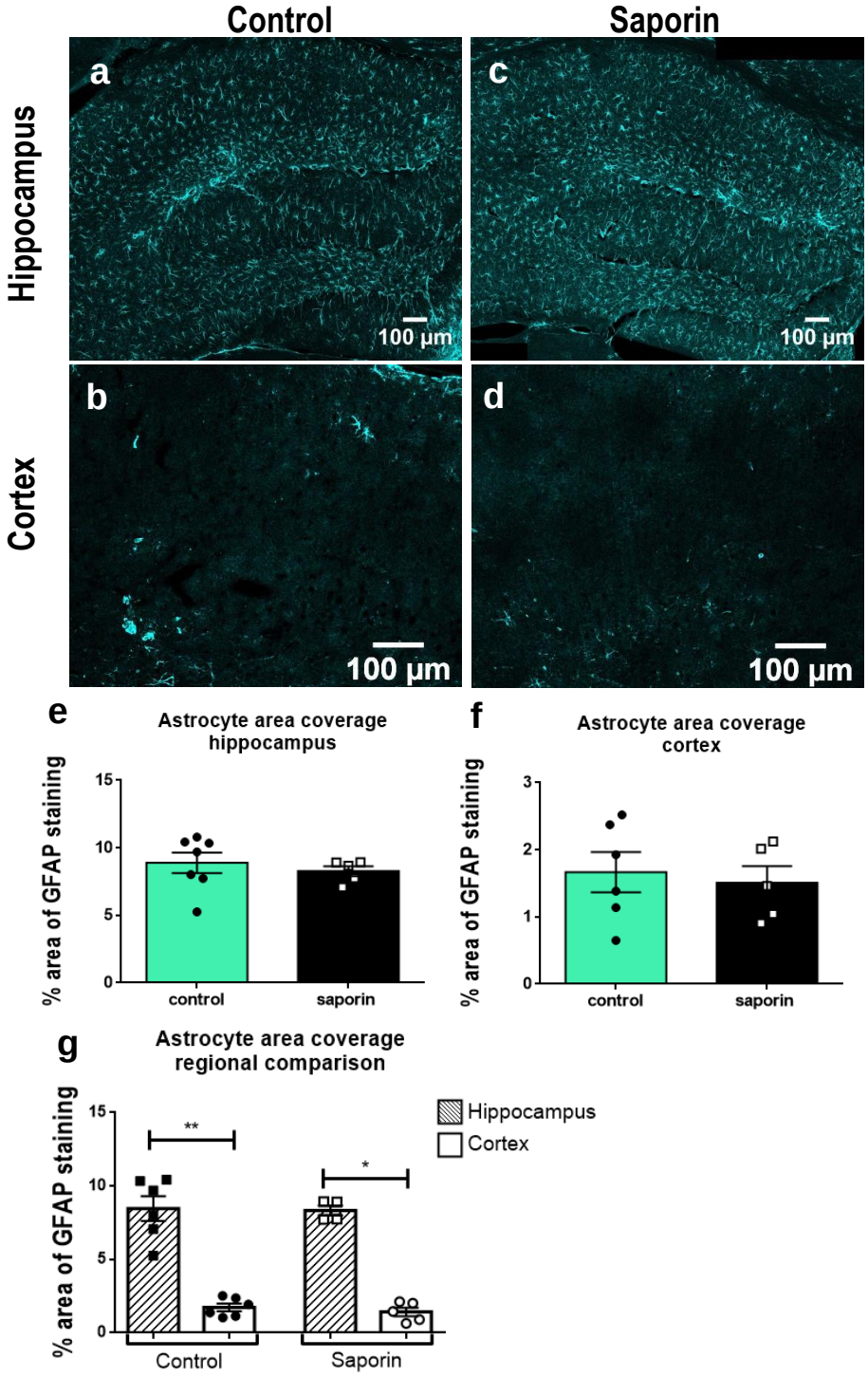

Figure 5.7 Regional variation in astrocyte density between the hippocampus and cortex
(a-d) Representative photomicrographs of astrocyte density as assessed by GFAP staining (green) in the hippocampus (control n=7, saporin n=5) (a, b) and cortex (control n=6, saporin n=5) (c, d) of control (a, c) and saporin-treated mice (b, d). (e-g) No differences in astrocyte density was noted between control and saporin-treated mice in the hippocampus (e) or the cortex (f), but regional analysis revealed significantly more GFAP coverage in the hippocampus compared to the cortex (g) as previously noted in Chapter 3. *p<0.05; **p<0.01. Scale bars = 100 µm.

Discussion

- Cholinergic loss did not affect PVD of injected human $A\beta_{1-40}$ in either the hippocampus or cortex.
- The cortex was found to have an endogenously higher vascular density than the hippocampus.
- The hippocampus was found to have an endogenously higher area coverage of microglia and astrocytes, which was not affected by mu-p75-saporin treatment.

Results from this chapter demonstrate that loss of cholinergic innervation does not have a significant impact on PVD of Aβ from either the cortex or the hippocampus. However, endogenous differences were noted in blood vessel density and glial coverage between the hippocampus and cortex, further highlighting the heterogeneity between the two brain regions.

Previous studies have suggested that arterial pulsations are required for drainage to occur along blood vessels, especially against the direction of CBF (Arbel-Ornath et al. 2013; Schley et al. 2006; Carare et al. 2008; Iliff et al. 2013), although this pulsation is unlikely to contribute to bulk flow of ISF and CSF (Bedussi et al. 2018; Hladky & Barrand 2014). It has been demonstrated that the vasoreactivity of vessels in patients with AD is improved following treatment with AChEIs (Rosengarten et al. 2006; Rosengarten et al. 2009). This suggests that cholinergic denervation may contribute to poorer reactivity of the vasculature in AD, and may therefore affect the ability of the vasculature to generate sufficient force to remove Aβ that is contained within the ISF and CSF. In Chapter 4, we observed that loss of ChAT innervation did not affect baseline CBF but lead to reduced responsiveness to eNOS-specific stimulation in the cortex but not the hippocampus. We hypothesised that PVD is related to CBF and that saporin-treated mice would show decreased PVD in the cortex, but not in the hippocampus, compared to control mice. However, the current set of experiments found no differences in PVD of Aβ between control and saporin-treated mice in either brain region.

There are several possible explanations for this observation. It is possible that there is no relationship between vasoreactivity and PVD and that other mechanisms are responsible for generating the force to remove solutes along the CVBMs. Alternatively, the extent of cholinergic denervation in our model may not have been sufficient to alter the force of arterial contractions to an extent that there could be appreciable difference in PVD. In addition, because basal CBF was not affected by saporin treatment, it may be that loss of ChAT input in itself may not be sufficient to affect drainage, and that an additional eNOS-

specific challenge or NVC may be needed to observe differences in PVD between control and saporin mice as well as between brain regions.

Age may also play a role in the current observations. PVD has been demonstrated to be negatively affected by increased age, which is associated with changes to the morphology and composition of the basement membrane (Hawkes et al. 2011). Regional differences in PVD with impairment of drainage of $A\beta_{1-40}$ have been reported in the hippocampus but not the thalamus, which correlated with age-related decrease in collagen IV in the hippocampus (Hawkes et al. 2013). Therefore, because the mice used in the current study were relatively young, they may have been able to maintain adequate PVD in the absence of cholinergic innervation that may not be possible in the aged brain.

Interestingly, regional differences were also noted in the PVD of Aβ from the hippocampus versus the cortex, as both the diffusion time as well as the volume of Aβ injected into the cortex had to be halved to be able to detect a sufficient number of vessels to assess drainage. This may have been due to technical limitations that are associated with intracerebral injections into the cortex; an injection site of -0.5 mm dorsal to ventral was chosen to ensure sufficient distance from the corpus callosum and the subarachnoid space. However, this depth may not be sufficient to avoid flooding the subarachnoid space when using the 0.5 µL bolus of Aβ. On the other hand, we observed that the cerebrovascular density was significantly higher in the cortex compared to the hippocampus, which has also been reported in other studies (Oomen et al. 2009; Dorr et al. 2007). This suggests that there may be a larger surface area for solutes contained within the ISF to be removed from the cortex either across the BBB or along peri/paravascular routes, resulting in more rapid elimination from the brain under normal conditions. Under conditions of impaired drainage, this increased density may also provide additional opportunity for accumulation of Aβ as CAA and contribute to the topography of CAA.

In addition to clearance via the vasculature, both microglia and astrocytes are also known to mediate uptake of Aβ (Wilcock et al. 2004; Bouvier et al. 2016). To determine if saporin treatment induced a difference in the expression of glial cells, expression of Iba1 and GFAP was assessed in the cortex and hippocampus of control and saporin-treated mice. Unlike previous studies which have found increased microglial activity after 7 days in the saporin model (Hunter et al. 2004), no differences in microglial or astrocyte density were noted between saporin and control mice in the cortex and the hippocampus at the 45 day timepoint. This different is likely due to the lower concentration of saporin and longer timeframe used in the present study, which may have induced an attenuated inflammatory

response to loss of cholinergic neurons. Interestingly, a higher density of Iba1 and GFAP-positive cells was noted in the hippocampus compared to the cortex in both control and saporin-treated mice. The finding of a lower density of astrocytes in the cortex compared to the hippocampus has previously been reported in mice (Emsley & Macklis 2006), and a more pronounced age-related increase in reactive astrocytes has been observed in the hippocampus than in the cortex of rats (Amenta et al. 1998). Increased expression of glial cells in the hippocampus may provide additional mechanisms to clear waste products and may compensate for the lower vascular density. However, a limitation of this study is that only GFAP was used to label astrocytes, and it has been reported that not all astrocytes express GFAP (Emsley & Macklis 2006; Kimelberg 2004), therefore the results presented in this chapter cannot be assumed for all astrocyte populations.

It would therefore be of interest to follow up this study by examining the impact of cholinergic denervation in the presence of additional factors including old age, and to determine how different astrocyte subpopulations and NVC affect the efficiency of PVD from different brain regions.

Chapter 6 : Implication of cholinergic loss on CAA severity in a transgenic AD mouse model

Introduction

Transgenic (Tg) mouse models are a useful tool for studying AD. More than a hundred Tg AD mouse models are available, expressing various pathological and behavioural characteristics of AD and CAA (Jankowsky & Zheng 2017), although none completely replicate the complexity of the disease.

The effect of cholinergic loss on Aβ pathology has been previously studied in several Tg mouse models. Using the APP/PS1 model, Ramos-Rodriguez found that saporin treatment did not alter CAA severity, but did lead to increased Aβ deposition and exacerbated memory and learning impairments (Ramos-Rodriguez et al. 2013). A similar study in the same mouse model using saporin also found significantly increased plaque load in both the hippocampus and the cortex (Laursen et al. 2013). Saporin-induced cholinergic loss in the 3xTg AD model also led to increased levels of soluble monomeric Aβ and P-Tau in the hippocampus (Härtig et al. 2014). However, neither of these latter studies evaluated the impact of saporin treatment on CAA severity. Thus, although these studies suggest that loss of cholinergic innervation increases AD pathology in the parenchyma, the impact on CAA is still unclear.

Our group and others have previously reported that perivascular drainage of dextran, inulin and Aβ is impaired in the APP/PS1 and Tg2576 mouse models (Hawkes et al. 2011; Peng et al. 2016) suggesting that impaired clearance of Aβ along perivascular pathways may contribute to Aβ pathology in TgAPP models. We originally hypothesized that loss of cholinergic input would reduce the efficiency of PVD of Aβ from the brain, but as reported in Chapter 5, found that this was not the case in wildtype mice. However, we did observe that loss of cholinergic innervation was associated with reduced eNOS activity. Decreased eNOS expression has been found to correlate with increased AD pathology in human brains (Jeynes & Provias 2009) and increased CAA load in mice (Tan et al. 2015). Furthermore, clearance of Aβ from the brain is mediated via multiple PVD-independent mechanisms that may also contribute to the development and/or progression of CAA such as perivascular macrophages, enzymatic digestion and receptor-mediated transcytosis across the BBB (Hawkes & McLaurin 2009; Farris et al. 2007; Kanekiyo et al. 2012). Therefore, the current set of experiments were conducted to determine the effect of

cholinergic loss on CAA severity using the TetO-APPSweInd mouse model of AD (Jankowsky et al. 2005).

Materials and methods

TetAPP mice

Tetracycline-responsive APP-transgenic mice (TetO-APPSweInd) (Jankowsky et al. 2005) were kindly gifted by Dr JoAnne McLaurin (Sunnybrook Research Centre, Toronto, Canada) and were bred on a C57BL/6 background at the OU in accordance with the guidelines set out by the AWREB at the OU and Home Office approval (PPL 70/8507).

This mouse model expresses the human Swedish (KM670/671NL) and Indiana (V717F) mutations APP mutations under the control of a tetracycline-responsive (TET-OFF) CaMKIIα promotor (Jankowsky & Zheng 2017; Jankowsky et al. 2005). Aβ plaques can be detected in the parenchyma by 8 weeks of age without doxycycline treatment, and parenchymal Aβ and CAA pathology is established by 6 months of age, predominantly in the cortex and hippocampus (Jankowsky et al. 2005). This model has also been demonstrated to show regional spread of pathology from the left entorhinal cortex to the parietal cortex (Khan et al. 2014) and develops cognitive impairment by 12-13 months (Melnikova et al. 2013).

Genotyping

Genotyping was carried out as described by Jankowsky et al with modifications (Jankowsky et al. 2005). Briefly, ear punches were digested in 150 µl of digestion buffer [50 mM Tris pH 7.5, 200 mM EDTA plus 5.2% 10 mg/ml Proteinase K (in 10 mM Tris pH 7.5, 20 mM $CaCl_2$, 50% glycerol v/v)] overnight at 55°C. Following heat deactivation of proteinase K for 30 min at 85°C, samples were vortexed and spun down to separate debris. The DNA in the supernatant was then measured, diluted to 30 ng/µl and amplified for genotyping by PCR. The primers used include the S36 (CCG AGA TCT CTG AAG TGA AGA TGG ATG) and the PrP-Antisense-J primer sequence (AGC CTA GAC CAC GAG AAT GC) for the APP transgene, TET forward (CGC TGT GGG GCA TTT TAC TTT AG) and reverse (CAT GTC CAG ATC GAA ATC GTC) and MAPT forward (CTC AGC ATC CCA CCT GTA AC) and reverse (CCA GTT GTG TAT GTC CAC CC) primers as in an internal control. The PCR reaction contained 30 ng DNA in a 25 µl Mastermix (containing 10 U of Taq polymerase). The PCR reaction was carried out using one cycle at 94°C for 3 min, and 35 cycles of 94°C for 30 s, 57°C for 1 min and 72°C for 1 min, followed by 72°C for 4 min. Reaction products were run on 2% Agarose gels for 25 mins,

yielding bands at 400bp for APP, 480bp for TET and 200bp for the reaction control (Fig. 6.1 a).

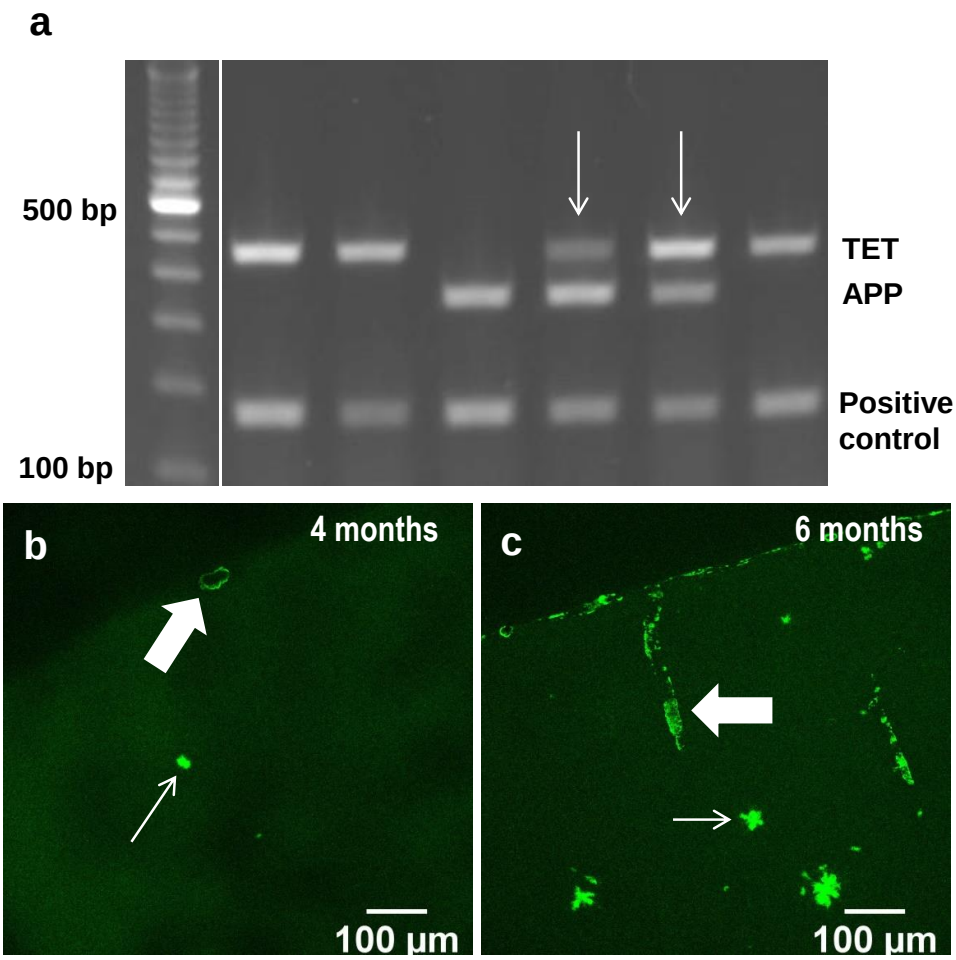

Figure 6.1 Characterisation of TetO-APPSweInd mice; genotyping and plaque/CAA pathology
(a): Example of a PCR gel from TetO-APPSweInd mice showing bands corresponding to the APP gene (400 bp), TET gene (480 bp) and double transgenics (arrows). The 200 bp positive control is also indicated. (b and c) Photomicrograph of representative Thioflavin S staining in the cortex of 4- (a) and 6-month-old (b) TetO-APPSweInd mice, showing the degree of plaque (slim arrows) and CAA pathology (thick arrows). Scale bar = 100 µm.

mu-p75-saporin treatment

4-month old male and female TetO-APPSweInd mice without doxycycline supplementation were used in the study. Cholinergic loss was induced by bilateral administration of mu-saporin into the lateral ventricles as described in Chapter 2, section 'Cholinergic denervation', page 45 (n=6 saline [3 males, 3 females] and n=7 saporin [3 males and 4 females]). 42 days post-surgery, mice were perfused fixed with 4% PFA. Brains were collected and sectioned as free-floating tissue as described in chapter 2 section 'Immunohistochemistry', page 45.

Immunohistochemistry

Sections were stained with 1% Thioflavin S for 5 min to label fibrillar Aβ as described in Chapter 2 section 'Immunohistochemistry', page 45. A separate set of sections were then incubated with antibodies against human $A\beta_{1\text{-}40}$ and $A\beta_{1\text{-}42}$ which was visualised using

DAB as described in Chapter 2, section: enzyme-linked immunohistochemistry page 46. Sections were also stained with anti-ChAT to confirm cholinergic loss, and anti-Iba1 and anti-GFAP assess glial changes. Anti-laminin staining was also carried out to assess vessel density. Tissue processing procedures and antibody concentrations were the same as those described in Chapter 2, Table 2.1, page 43.

Analysis

For staining using anti-ChAT, anti-laminin, anti-Iba1 and anti-GFAP, density of staining in the MS or cortex was quantified from x 10 magnification images. The hippocampus was assessed from stitched images taken at x 20. The percentage area of staining was quantified using the threshold parameters as detailed in Table 6.1 using Image J (NIH, Maryland, USA). As the Iba1 staining formed clear glial nets around Aβ positive plaques, these were excluded from analysis using the free-hand draw tool in Image J. The density of anti-laminin labelled capillaries and arteries/veins was carried out using the 'analyse particle' function of Image J as described in Chapter 5. For quantification of the area of staining in the hippocampus, values of regions from both the ipsilateral and contralateral hemispheres were averaged and treated as n = 1. For quantification of images from the cortex, six random non-overlapping spanning the somatosensory cortex of the ipsilateral cortex to the somatosensory cortex of the contralateral cortex were averaged and analysed.

Quantification of Thioflavin S-positive staining was performed by manually counting plaques and CAA-positive vessels and dividing the number counted by the total area quantified. For quantification of Anti-Aβ staining, x 4 magnification images of the hippocampus and cortex were stitched together using Image J software. Images were converted to 8 bit greyscale images and the % area covered by CAA and plaques were quantified separately using the threshold parameters as outlined in Table 6.1.

Table 6.1 Antibodies used and analysis parameters

Label	Minimum grey value	Maximum grey value
Anti-ChAT	107	255
Anti-laminin	98	255
Anti-Iba1	86	255
Anti-GFAP	86	255
Anti-$A\beta_{1-40}$	0	125
Anti-$A\beta_{1-42}$	0	125

Statistics

Data was tested for normality using the Kolmogorov-Smirov test. Two-tailed Student's t-test was used to analyse normally distributed data otherwise a Mann-Whitney U test was used. For data sets of more than two variables, a two-way ANOVA was used followed by Sidak's post-hoc test. Data represents mean ±SEM and $p<0.05$ was considered to be statistically significant.

Results

Cholinergic loss was induced in 4-month old TetO-APPSweInd mice using the saporin model characterised in Chapter 3. This age was chosen to ensure that there was a sufficient but submaximal degree of Aβ pathology to be able to detect potential effects of saporin on CAA severity by the time of analysis (e.g. ~ 5 ½ months old) (Fig. 6.1 b, c). Unexpectedly and in contrast to the observations made in the C57BL/6 mice (Chapter 3), no significant differences were noted in the number of ChAT-positive neurons in the medial septum between control and saporin-treated mice (Fig. 6.2 a-c). Significant loss of cholinergic fibres was observed in the hippocampus following saporin treatment ($p<0.05$) (Fig. 6.3 a-c), but similarly to the septum, significant fibre loss was not observed in the cortex after administration of saporin (Fig. 6.4 a-c). Moreover, the morphology of fibre staining in the TetO-APPSweInd appeared shorter and more punctate than that of cholinergic fibres in the C57BL/6 mice (Fig. 6.4 d-e) Comparison of endogenous ChAT fibre density between brain regions showed that the hippocampus had a significantly higher percentage area of cholinergic coverage compared to the cortex ($p<0.05$) (Fig. 6.5).

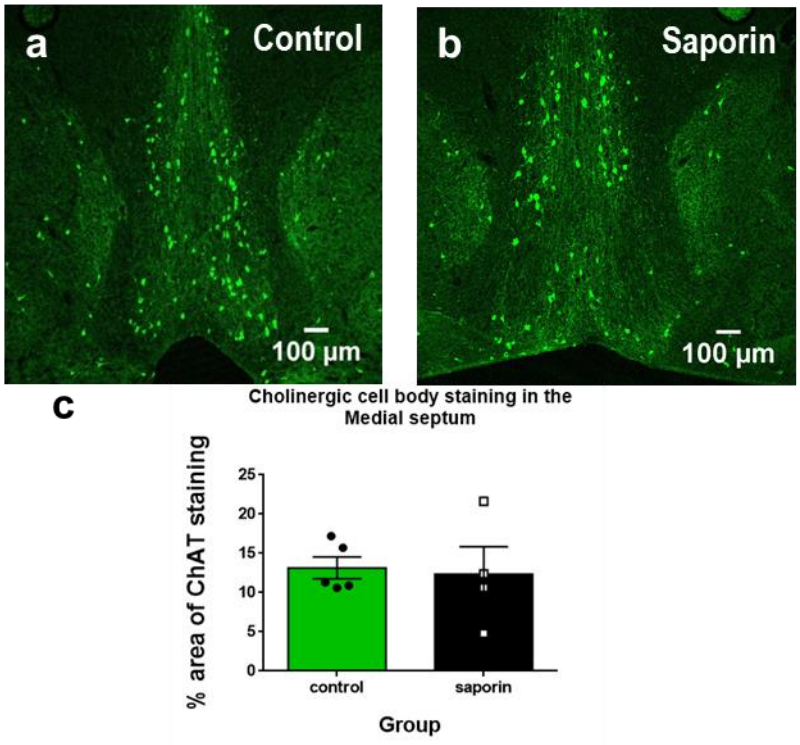

Figure 6.2 Cholinergic staining in the MS of control and saporin treated TetO-APPSweInd mice
(a and b) Photomicrographs of ChAT-positive cholinergic neurons (green) from the medial septum (MS) and diagonal band of Broca in TetO-APPSweInd mice injected with saline (a) and saporin (b). (c) Quantification showed no statistically significant difference in the percentage area of ChAT staining (control n=5, saporin n=4). Scale bar = 100 µm

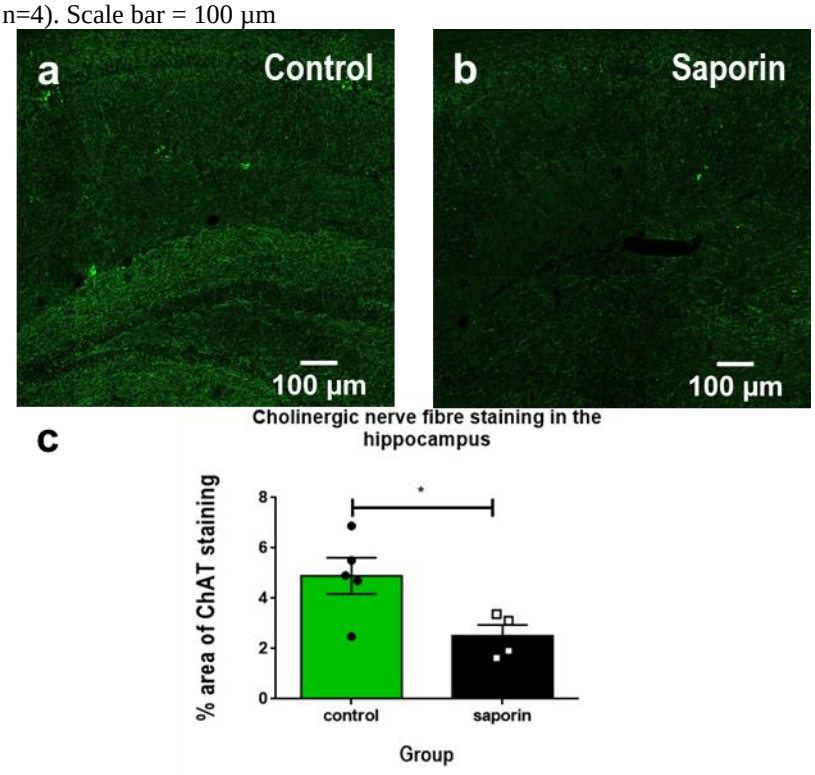

Figure 6.3 Cholinergic staining in the hippocampus of control and saporin treated TetO-APPSweInd mice
(a and b) Photomicrographs of ChAT-labelled cholinergic nerve fibres (green) in the hippocampus of TetO-APPSweInd mice treated with saline (a) or saporin (b). (c) Quantification revealed the density of nerve fibre coverage to be significantly lower in saporin-treated mice (control n=5, saporin n=4). Two-tailed t-test, *p<0.05. Scale bar = 100 µm

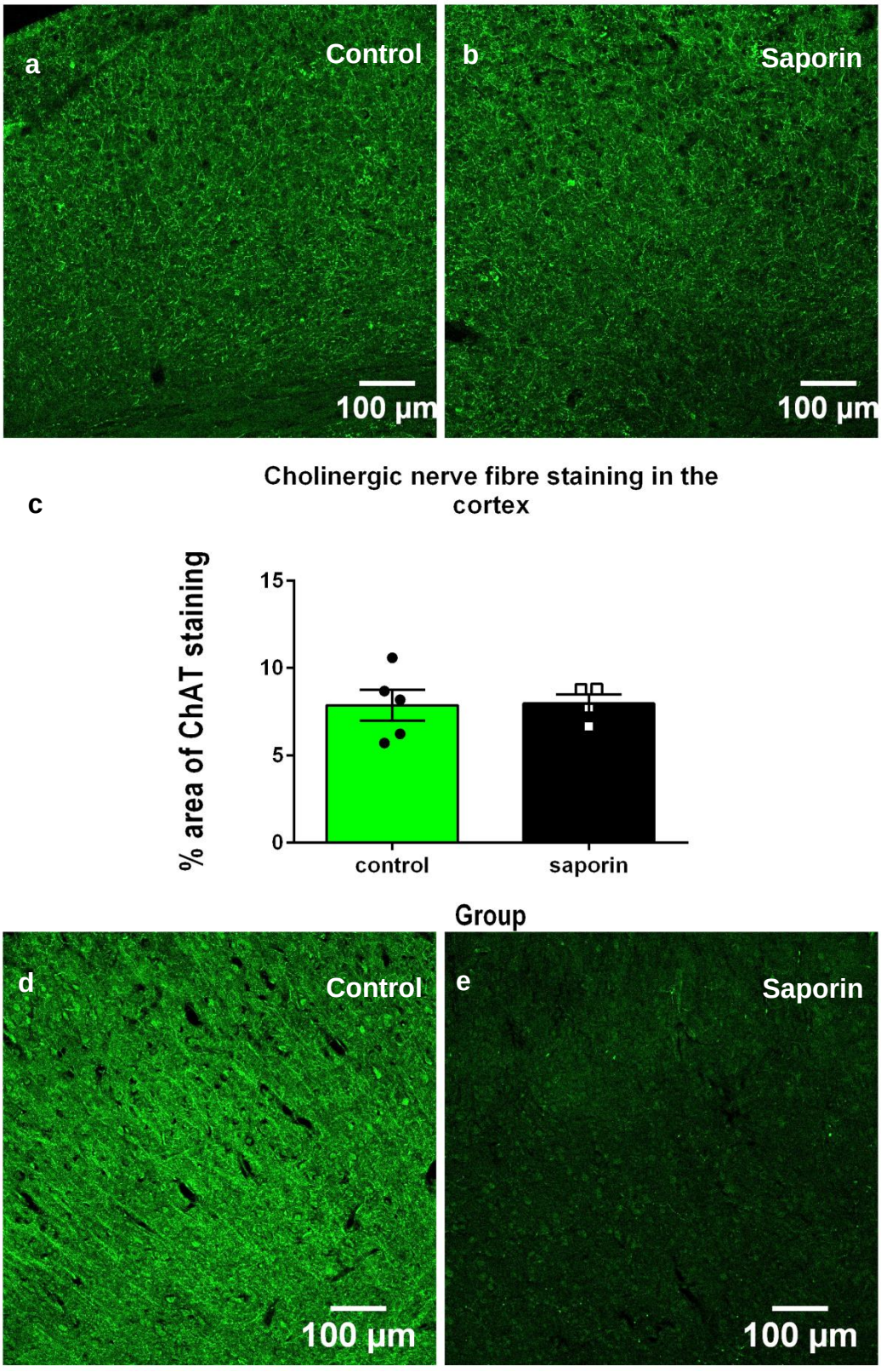

Figure 6.4 Cholinergic staining in the cortex of control and saporin treated TetO-APPSweInd mice
(a and b) Photomicrographs of ChAT-labelled cholinergic nerve fibres (green) in the cortex of TetO-APPSweInd mice treated with saline (a) or saporin (b). (c) No difference in nerve fibre density was found between saline and saporin-treated mice (control n=5, saporin n=4). (d and e) Photomicrographs of examples of C57BL/6 ChAT labelled cortex from control (d) and saporin treated (e) mice. Scale bar = 100 µm

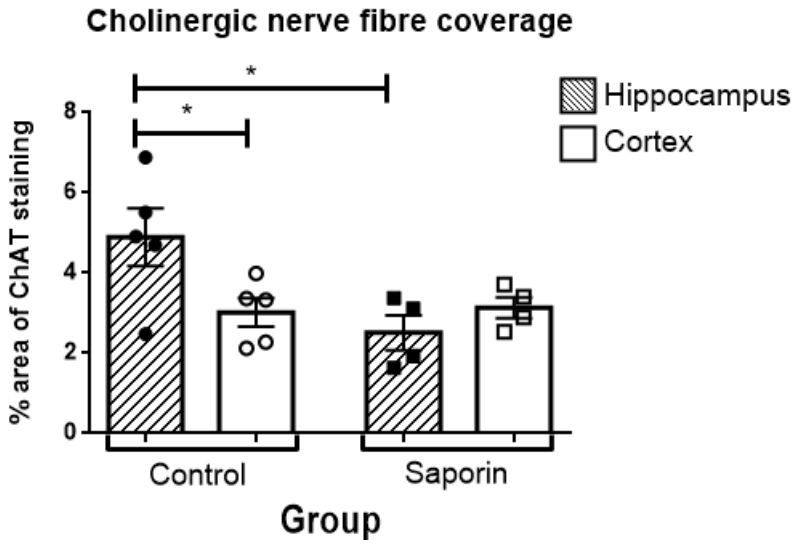

Figure 6.5 Regional variation in cholinergic nerve fibre density in TetO-APPSweInd mice
(a) Quantification of cholinergic nerve fibre density showed significantly higher coverage in the hippocampus in comparison to the cortex in the control animals ($p<0.05$) (control n=5, saporin n=4). Two-tailed t-test, *$p<0.05$.

To determine the effects of saporin treatment on fibrillar Aβ, brain tissue sections were processed for thioflavin S staining. Numerous plaques and CAA-positive blood vessels were observed in the hippocampus of control and saporin-treated mice (Fig. 6.6 a, b). No significant differences were noted in plaque density or CAA load between control and saporin animals (Fig. 6.6 c). Because thioflavin S staining does not bind to soluble Aβ and cannot differentiate between Aβ isoforms, sections were also processed by immunohistochemistry using antibodies against human $Aβ_{1-40}$ and $Aβ_{1-42}$. Quantification of $Aβ_{1-40}$ staining showed no difference in the percentage area of the hippocampus covered by plaques between control and saporin mice (Fig. 6.7 a-c). However, a significant ($p=0.0082$) increase in CAA load was observed in the saporin-treated mice. No difference in parenchymal and vascular Aβ was observed for $Aβ_{1-42}$ staining (Fig. 6.7 d-f).

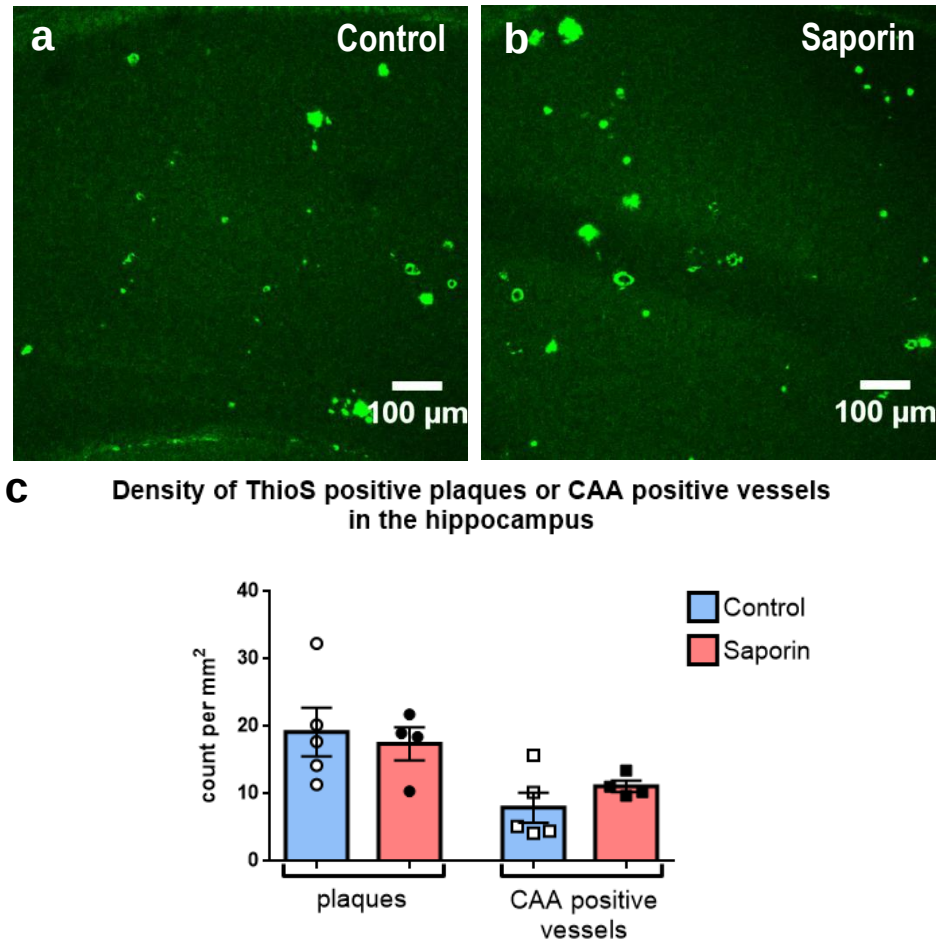

Figure 6.6 Thioflavin S positive Aβ plaque and CAA pathology in the hippocampus of TetO-APPSweInd mice
(a and b): Photomicrographs of thioflavin S staining of plaques and CAA in the hippocampus of TetO-APPSweInd mice treated with saline (a) or saporin (b). (c) No significant differences were observed between control and saporin-treated mice (control n=5, saporin n=4). Scale bar = 100 µm

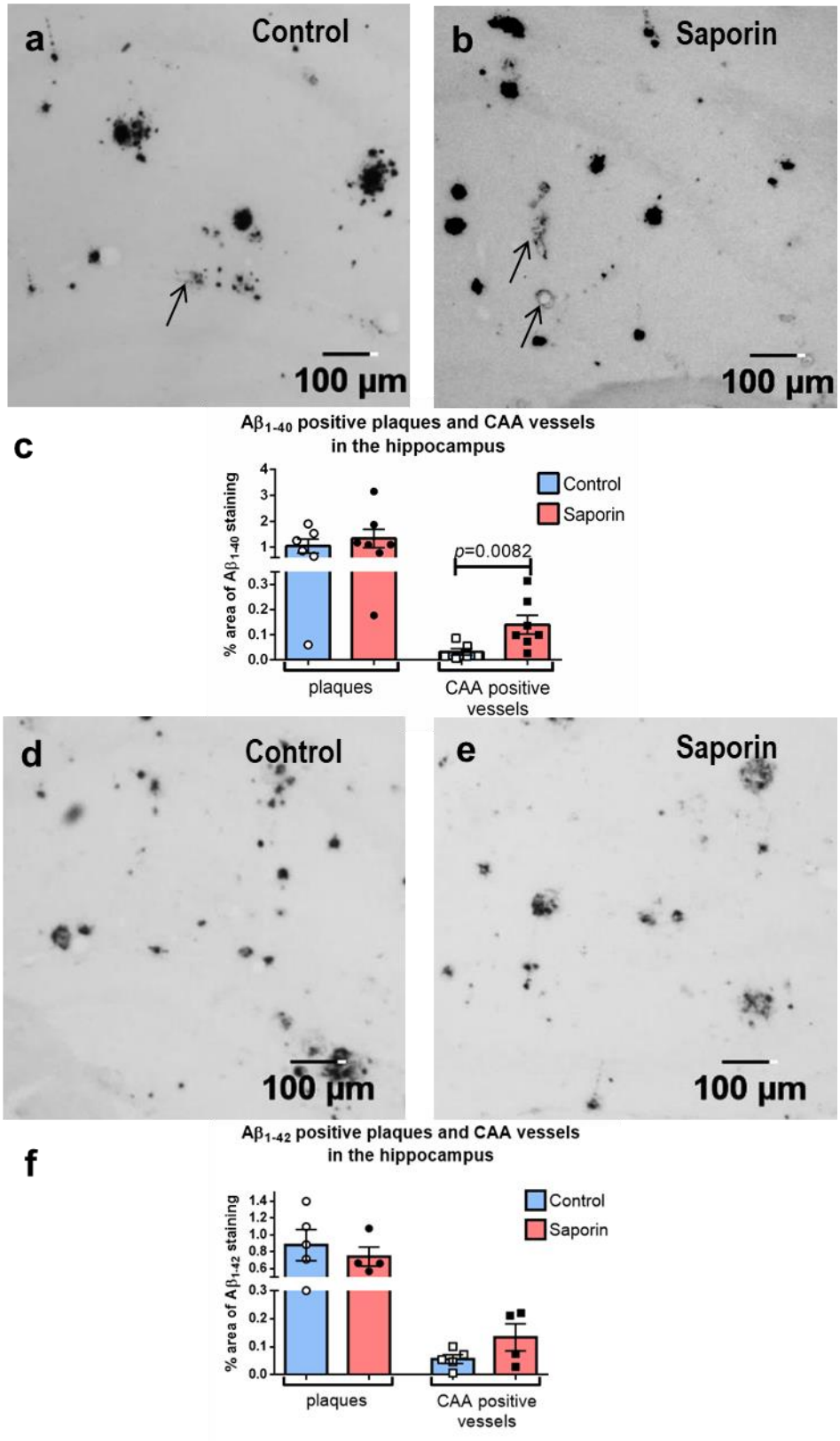

Figure 6.7 $A\beta_{1-40}$ and $A\beta_{1-42}$ staining in the hippocampus of TetO-APPSweInd mice
(a-c) Photomicrographs of $A\beta_{1-40}$ staining of parenchymal plaques and CAA (arrows) in the hippocampus of control (a) and saporin-treated mice (b). Quantification of $A\beta_{1-40}$ staining showed no difference in the percentage area of the hippocampus covered by plaques between control and saporin mice (c). Significantly increased CAA load was observed in the saporin-treated mice (p=0.0082). (d-f) Photomicrographs of $A\beta_{1-42}$ staining of parenchymal plaques and CAA in the hippocampus of control (d) and saporin-treated mice (e). Quantification of $A\beta_{1-42}$ staining showed no difference in the percentage area of the hippocampus covered by plaques between control and saporin mice. No difference in $A\beta_{1-42}$-positive CAA load was observed between control and saporin-treated mice (f). (control n=6, saporin n=7), scale bar= 100 µm.

In the cortex, no differences in either plaque density or CAA load were observed between control and saporin mice for tissues stained with thioflavin S (Fig. 6.8 a-c). Similarly, no differences were observed between control and saporin-treated mice in the density of $A\beta_{1-40}$ or $A\beta_{1-42}$-positive plaques or CAA (Fig. 6.9 a-f).

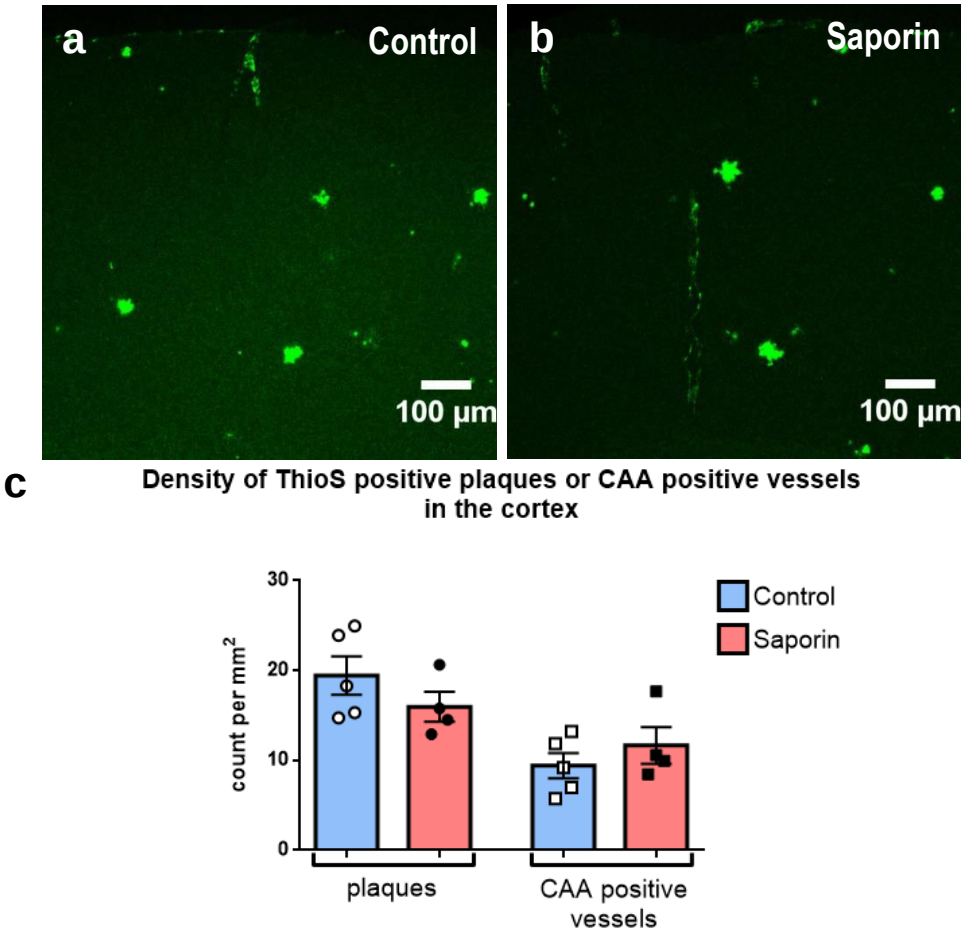

Figure 6.8 Thioflavin S positive Aβ plaque and CAA pathology in the cortex of TetO-APPSweInd mice
(a and b) Photomicrographs of thioflavin S staining of plaques and CAA in the cortex of TetO-APPSweInd mice treated with saline (a) or saporin (b). (c) No significant differences were observed between control and saporin-treated mice (control n=5, saporin n=4). Scale bar = 100 µm.

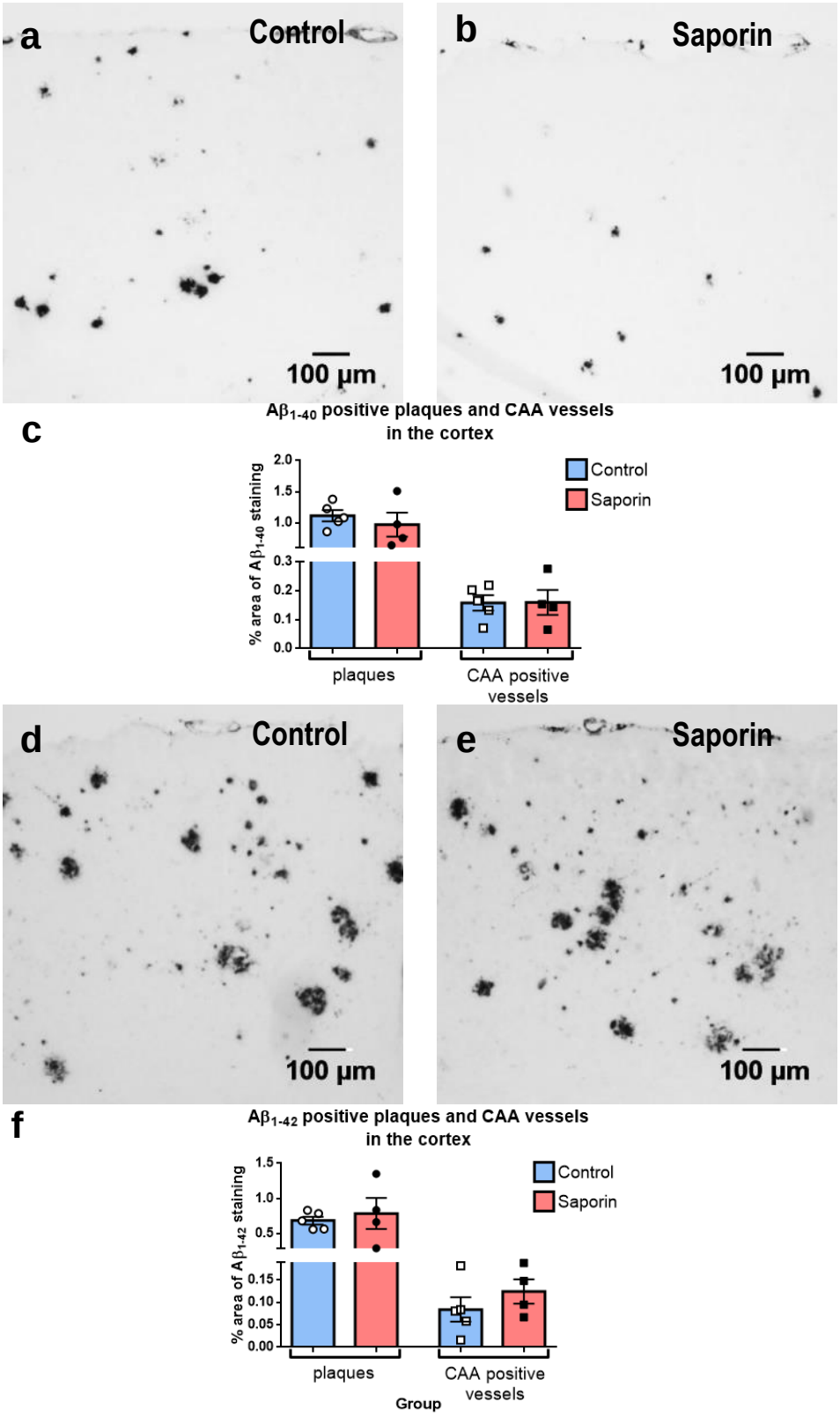

Figure 6.9 Aβ1-40 and Aβ1-42 staining in the cortex of TetO-APPSweInd mice
(a-c) Photomicrographs of $A\beta_{1-40}$ staining of parenchymal plaques and CAA in the cortex of control (a) and saporin-treated mice (b). Quantification of $A\beta_{1-40}$ staining showed no difference in the percentage area of the cortex covered by plaques or CAA between control and saporin mice (c). (d-f) Photomicrographs of $A\beta_{1-42}$ staining of parenchymal plaques and CAA in the cortex of control (d) and saporin-treated mice (e). Quantification of $A\beta_{1-42}$ staining showed no difference in the percentage area of the cortex covered by plaques or CAA between control and saporin mice (f). (control n=5, saporin n=4), scale bar = 100 µm.

Comparison of regional differences showed no significant difference in plaque or CAA density stained by thioflavin S between the hippocampus and the cortex (Fig. 6.10 a and b). The density of $A\beta_{1\text{-}40}$ and $A\beta_{1\text{-}42}$ positive plaques was similar between the cortex and hippocampus in both control and saporin treated mice (Fig. 6.10 c and e). However, significantly fewer $A\beta_{1\text{-}40}$ positive vessels were observed in the hippocampus versus the cortex of control mice (p<0.01; Fig. 6.10 d), while the density of $A\beta_{1\text{-}42}$ positive CAA did not differ between brain regions or treatment groups (Fig. 6.10 f).

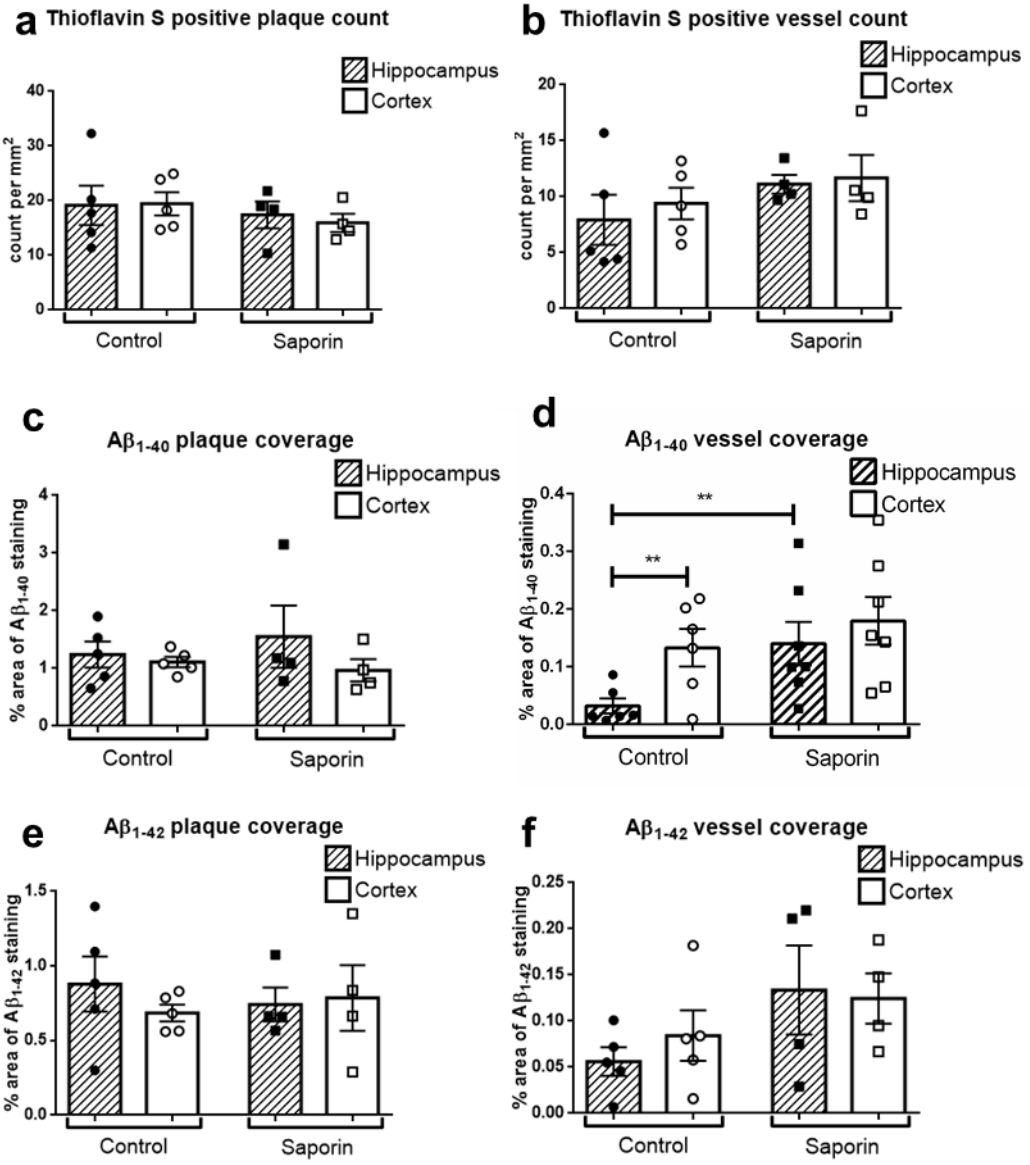

Figure 6.10 Regional comparisons of pathology in control and saporin-treated TetO-APPSweInd mice (a and b) No differences were found in the density of Thioflavin S-labelled plaques (a) or CAA (b) between the hippocampus or cortex in control or saporin-treated mice. (c and d) Regional analysis of $A\beta_{1\text{-}40}$ staining showed no difference in plaque coverage (c), but significantly less vessel staining in the hippocampus compared to the cortex of control mice (p<0.01) (d). (e and f) Regional analysis of $A\beta_{1\text{-}42}$ staining showed no difference in plaque (e) or CAA load (f). (control n=5, saporin n=4), two tailed t-tests, **p<0.01.

In order to identify whether there were any differences in vascular density which may have impacted vascular-mediated clearance of Aβ between the groups, vessel density was

assessed by quantifying the percentage area of laminin staining in the cortex and hippocampus by vessel type. A higher capillary density was noted in the hippocampus of both the control ($p<0.01$) and saporin treated mice compared to the cortex ($p<0.05$) (Fig. 6.11 a-e).

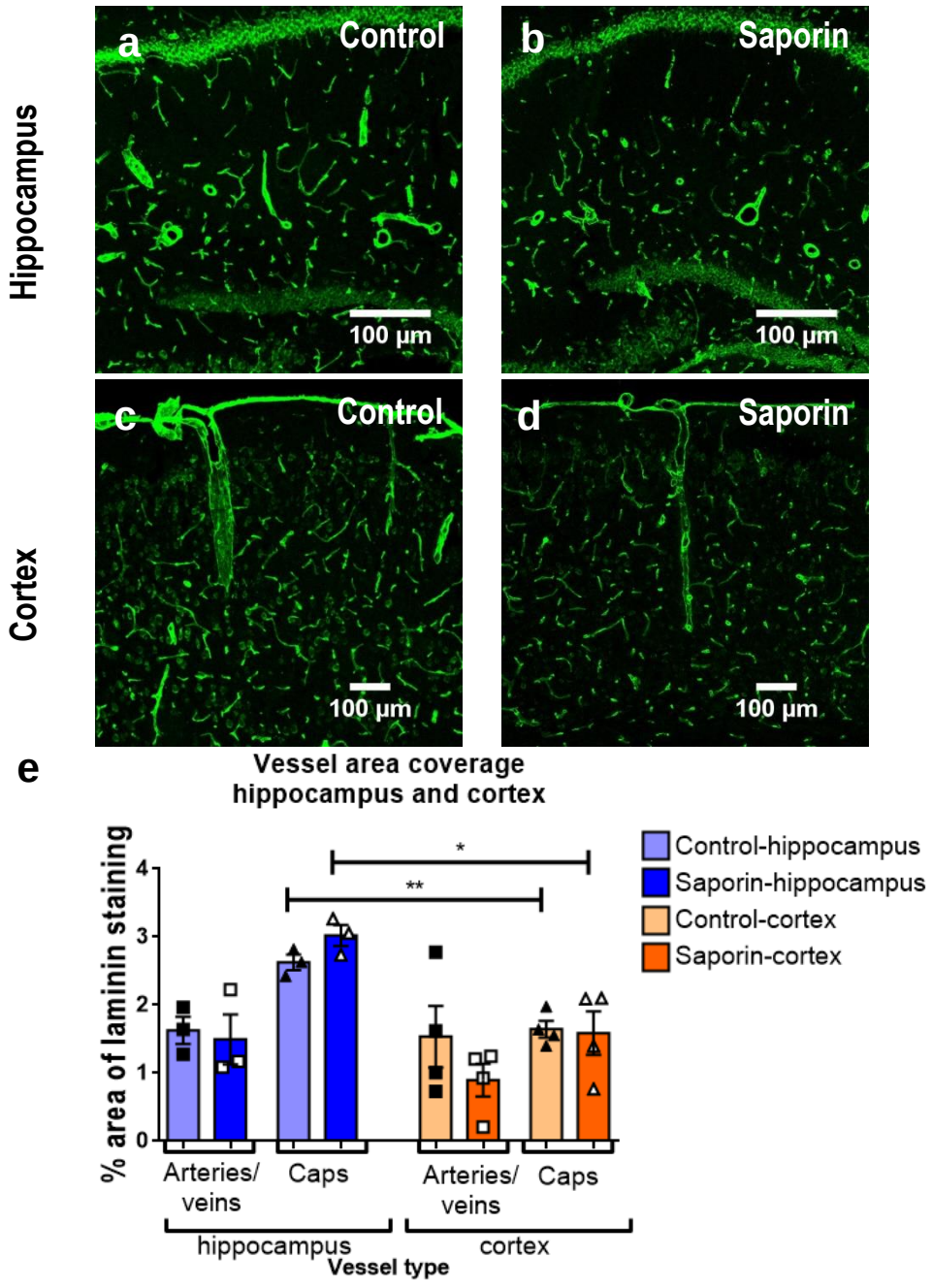

Figure 6.11 Regional variation in vascular density in TetO-APPSweInd mice
(a-d) Photomicrographs of laminin staining in the hippocampus (a and b) and cortex (c and d) of control (a and c) and saporin-treated (b and d) mice. (e) Quantification of laminin staining revealed no difference in the density of capillaries or large diameter vessels between control and saporin mice in either the hippocampus or cortex. However, capillary density was higher in the hippocampus compared to the cortex in both control and saporin-treated mice. (control n=5, saporin n=4), two tailed t-test, *$p<0.05$, **$p<0.01$ Scale bar = 100 µm.

Analysis was also carried out to assess any changes in glial expression induced by saporin treatment. The percentage area of GFAP coverage showed no differences between control and saporin mice in either the hippocampus (Fig. 6.12 a) or cortex (Fig. 6.12 b), but

regional comparisons indicated that significantly more astrocytic coverage was present in the cortex than in the hippocampus in both control (p<0.01) and saporin (p<0.001) groups (Fig. 6.12 c). Iba1 staining for microglia revealed no significant change in percent area covered between treatments but in the saporin treated mice, the hippocampus had significantly more Iba1 staining than the cortex (p<0.05), (Fig. 6.12 d-f).

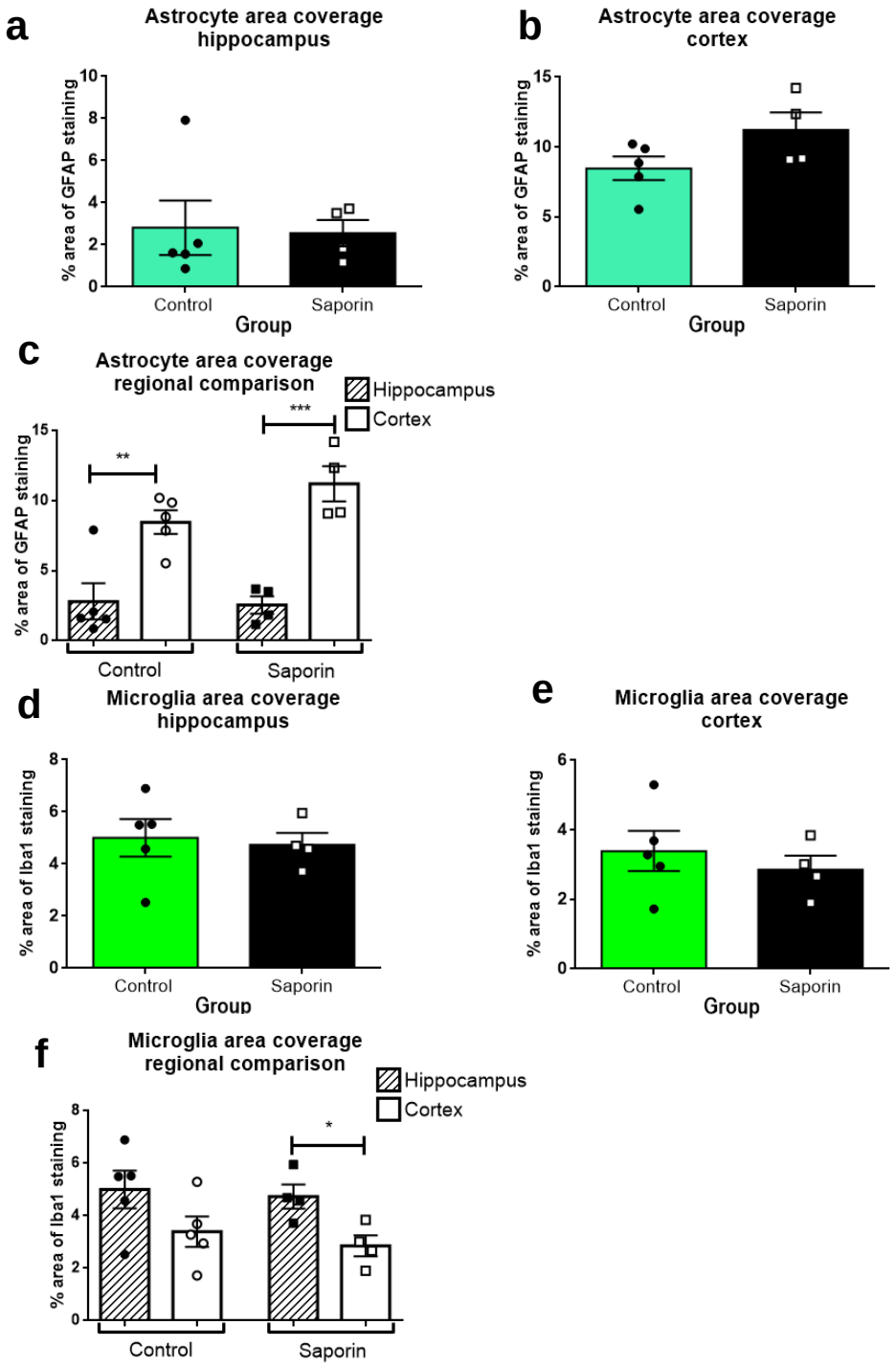

Figure 6.12 Regional variation in astrocytic and microglial staining in TetO-APPSweInd mice
(a-c) Astrocyte coverage was not found to be significantly different with saporin treatment in either the hippocampus (a) or the cortex (b). Regional comparisons revealed significantly more astrocytic coverage in the cortex compared to the hippocampus in both the control and saporin treated mice (c). Microglial coverage was not different between the control and saporin groups in either the hippocampus (d) or cortex (e), but coverage of the cortex was significantly less than the hippocampus in saporin treated mice (f). (control n=5, saporin n=4), two tailed t-test (p<0.05), *p<0.05, **p<0.01, ***p<0.001 scale bar= 100 µm.

Discussion

- Unlike in the C57BL/6 mice, mu-p75-saporin treatment did not induce cholinergic neuronal loss in the MS or nerve fibre loss in the cortex of the TetO-APPSweInd, but did result in fibre loss in the hippocampus.
- No difference in Thioflavin or $A\beta_{1-42}$ -positive plaque density or CAA load was observed between control and mu-p75-saporin treated mice, but a significant increase in $A\beta_{1-40}$-positive vessels was observed in mu-p75-saporin-treated animals.
- $A\beta_{1-40}$-positive vessels were more prevalent in the cortex of control mice compared to the hippocampus.
- In contrast to the C57BL/6 mice, vascular density was higher in the hippocampus compared to the cortex of the TetO-APPSweInd mice, while astrocyte density was higher in the cortex compared to the hippocampus.

Cholinergic loss is known to be an early event in AD, but whether this loss contributes to the initiation and/or progression of CAA remains unknown. The purpose of the experiments carried out in this chapter was to evaluate the effects of cholinergic loss on CAA severity using the TetO-APPSweInd transgenic mouse model.

Unlike with the C57BL/6 mice used in the previous chapters, saporin treatment did not induce cholinergic loss in the medial septum or the cortex, but did significantly reduce fibre density in the hippocampus. The reasons for the discrepancies between the two strains is not clear, but are likely related to inherent differences in ChAT and p75 expression and the effect of Aβ expression on neuronal health. Comparison of ChAT density between wildtype and Tg mice found that the percentage area of coverage by ChAT staining in the MS was higher in the Tg mice, but fibre density was lower in both the cortex and the hippocampus of TetO-APPSweInd mice compared to the C57BL/6 mice. This suggests that the development of Aβ pathology in the Tg mice, which is concentrated in the cortex and hippocampus, may cause degeneration of ChAT fibres, as suggested by their abnormal appearance. This is in keeping with reports from other APP mouse models, where an endogenous decrease in cholinergic nerve fibre density has been described in the cortex of 18 month-old Tg2576 mice (Kuznetsova & Schliebs 2013). In the APP23 model, significant cholinergic fibre loss in the neocortex concurrent with Aβ pathology has been found without significant loss of basal forebrain cholinergic neurons (Boncristiano et al. 2002). Although additional experiments are needed to confirm the expression of the p75 NTR between wildtype and TetO-APPSweInd, it is likely that the lower density in ChAT-positive fibres reduces the surface area for mu-p75-saporin binding and therefore induces

less death than that observed in wildtype mice. The higher density of ChAT-positive fibres in the hippocampus compared to the cortex in the TetO-APPSweInd mice may have also contributed to the observed regional susceptibility to saporin treatment.

Although unexpected, the difference in sensitivity to saporin treatment between the cortex and hippocampus provided somewhat of an internal control to study the effect of cholinergic loss on CAA load. The loss of cholinergic nerve fibres in the hippocampus was associated with significantly increased deposition of $A\beta_{1-40}$ as CAA. By contrast, CAA load was not affected in the cortex where cholinergic fibre density was not affected by saporin treatment. The fact that the CAA-associated $A\beta_{1-40}$ isoform, but not $A\beta_{1-42}$, was altered in the hippocampus leads to further support that these alterations were specific to the vasculature (Suzuki et al. 1994; Hernandez-Guillamon et al. 2012). This is also confirmed by the observation that plaque density did not differ between control and saporin mice in either the cortex or the hippocampus. These findings are similar to a study using the Tg2576 AD mouse model which found that age-related loss of perivascular cholinergic innervation in the cortex did not significantly correlate with increased cortical plaque load (Kuznetsova & Schliebs 2013). However, in the APP/PS1 mouse model, saporin-induced cholinergic loss was found to increase plaque load (Laursen et al. 2013; Ramos-Rodriguez et al. 2013) and a higher plaque load has been associated with decreased cholinergic fibres in aged APP/SweInd mice (Foidl et al. 2016). Many factors may have contributed to these different observations, including the degree of cholinergic degeneration, age of the mice and amount of pre-existing Aβ pathology, ratio of $A\beta_{1-40}$:$A\beta_{1-42}$ and progression of pathology in the different mouse models. Despite these discrepancies, these data support a role for loss of cholinergic innervation on increased Aβ pathology.

In addition to regional differences in ChAT innervation, TetO-APPSweInd mice also showed differences in CAA load and the densities of capillaries and astrocytes between the hippocampus and cortex. The observation that CAA load was higher in the cortex than the hippocampus matches the topography of CAA in humans (Tian et al. 2003; Attems et al. 2011; Vinters et al. 2018) and may relate to the proportionally lower capillary density, and thus reduced surface area for removal of Aβ from the brain, observed in the cortex of TetO-APPSweInd mice. The higher astrocyte density found in the cortex may reflect an astrogliosis associated with higher CAA (Ongali et al. 2010; Kanekiyo et al. 2012), however the fact that this regional difference was maintained after saporin treatment, which did not affect CAA or plaque pathology in the cortex, suggests that other factors contribute to this difference. We also noted that the regional differences in capillary

density and astrocyte coverage seen in the TetO-APPSweInd mice were opposite to those observed in the C57BL/6 mice in previous chapters. As the TetO-APPSweInd mice are bred on a C57BL/6 background, the underlying causes for these discrepancies are not clear. Further characterisation of the effects of APP and TET expression on vascular density, ChAT coverage and astrocyte expression are therefore needed. It would also be of interest to characterise PVD in the TetO-APPSweInd mice as a function of pathology and to determine whether there are inherent age-related changes in cholinergic profile of the basal forebrain.

Chapter 7 : General Discussion

Summary of results

This thesis tested the hypothesis that loss of cholinergic innervation at the NVU contributes to the aetiology of CAA. A summary of the findings in wildtype mice are listed in Tables 7.1 and 7.2. Administration of the immunotoxin mu-saporin induced a loss of cholinergic neurons in the basal forebrain and their nerve fibre projections in both the hippocampus and the cortex. fMRI experiments showed no difference in baseline CBF between control and saporin-treated mice and response to hypercapnia was functional in both groups. However, in saporin-treated animals, cortical CBF did not respond to eNOS disinhibition, while hippocampal CBF was increased in response to administration of fasudil hydrochloride. This was associated with decreased eNOS levels in the cortex, and increased eNOS activity in the hippocampus of denervated mice. PVD of exogenous human $A\beta_{1\text{-}40}$ injected into either the cortex or hippocampus was not affected in this model, although there was significantly increased CAA load in saporin-treated TetO-APPSweInd mice. These results do not support the original hypothesis. However, they suggest that there are differences in the responsiveness of the cortex and hippocampus to the loss of perivascular cholinergic innervation that might have implications for the topographical distribution of CAA, independent of mechanisms related to PVD of Aβ from the brain.

Table 7.1 Endogenous regional differences between the cortex and hippocampus of wildtype mice

Endogenous differences	Hippocampus	Cortex
Cholinergic nerve fibre density	Higher	Lower
Cholinergic perivascular innervation	No difference at basement membrane & smooth muscle cells, but higher at the astrocytic endfeet of the capillary	No difference at basement membrane & smooth muscle cells, but lower at the astrocytic endfeet of the capillary
Basement membrane	Higher volume in veins	Lower volume in veins
Smooth muscle cells volume	No difference	No difference
Astrocyte end feet coverage	Highest at veins	Highest at arteries
Baseline CBF	Higher	Lower
Response to hypercapnia	Increase in CBF	Increase in CBF
Response to Fasudil hydrochloride	Increase in CBF	Increase in CBF
Endogenous NOS activity	Higher	Lower
Vascular density	Lower density of capillaries and arteries/veins	Higher density of capillaries and arteries/veins
Microglial density	Higher	Lower
Astrocytic density	Higher	Lower

Table 7.2 Effect of saporin treatment in cortex and hippocampus of wildtype mice

Response to saporin treatment	Hippocampus	Cortex
Cholinergic nerve fibre density	Significantly decreased	Significantly decreased
Cholinergic perivascular innervation	Significantly decreased at basement membrane & smooth muscle cells	Significantly decreased at basement membrane & smooth muscle cells & astrocyte endfeet
Basement membrane volume	Unaffected	Unaffected
Smooth muscle cells volume	Unaffected	Unaffected
Astrocyte endfeet coverage	Unaffected	Unaffected
Baseline CBF	Unaffected	Unaffected
Response to hypercapnia	Unaffected	Unaffected
Response to Fasudil hydrochloride	Increase in CBF	Unaffected
Endogenous eNOS/nNOS protein levels	eNOS increased, nNOS unchanged	eNOS decreased, nNOS unchanged
Endogenous NOS activity	Higher e/iNOS activity in membrane fraction, more nNOS activity	Lower e/iNOS activity in membrane fraction, overall reduction of eNOS activity
PVD	Unaffected	Unaffected
Vascular density	Unaffected	Unaffected
Microglial density	Unaffected	Unaffected
Astrocytic density	Unaffected	Unaffected

Cholinergic loss in AD

The loss of cholinergic activity as one of the earliest features of AD, gave rise to the cholinergic hypothesis of AD, which suggests that cholinergic denervation plays a significant role in the aetiology of AD and underlying dementia (Francis et al. 1999; Bartus et al. 1982; Van Beek & Claassen 2011; Schliebs & Arendt 2011; Terry & Buccafusco 2003; Perry et al. 1995). Cortical cholinergic nerve fibres, mAChRs and nAChRs are known to be lost in AD (Tong & Hamel 1999; Perry 1980; Perry et al. 1995) and Aβ plaques have been reported in the basal forebrain (Arendt et al. 1988). Binding of Aβ to the p75 NTR leads to apoptosis (Yaar et al. 1997) and application of Aβ reduces ACh synthesis and release (Kar et al. 2004). The importance of the cholinergic system in AD is highlighted by the fact that AChEIs are currently one of only two approved drugs for the treatment of AD (Hampel et al. 2018). Moreover, recent studies have demonstrated that loss of basal forebrain grey matter occurs before the onset of clinical symptoms (Schmitz et al. 2016) and that administration of donepezil during the prodromal stage of AD prevented basal forebrain degeneration (Cavedo et al. 2017). The changes in nesting behaviour as noted in saporin treated mice (Chapter 3) has been associated with

hippocampal pathology (Cunningham et al. 2003) as well as neurovascular dysfunction (Faraco et al. 2018). This highlights the significance of basal forebrain degeneration in AD and the importance of understanding the cholinergic pathway and function.

Regional differences of the NVU and response to loss of cholinergic innervation

In mammalian brains, the cortex in known to receive cholinergic innervation from the nucleus basalis of Meynert and from p75-negative thalamocortical afferents originating from the brainstem, while the hippocampus receives innervation primarily from the diagonal and horizontal bands of Broca and the medial septum (Hallanger et al. 1987; Selden et al. 1998; Mesulam 2013). Some studies have reported no cholinergic neurons are present in the cortex or hippocampus (Mesulam 2013) but Kasashima et al found ChAT-positive neurons are located in the human cortex (Kasashima et al. 1999) and cholinergic cell bodies have been reported in the mouse somatosensory cortex (Consonni et al. 2009). 192IgG and mu-p75-saporin have been used extensively to model the death of p75 positive cholinergic populations and to evaluate the effects on cognitive function and/or AD-like pathology in rats and mice, respectively (Berger-Sweeney et al. 2001; Hunter et al. 2004; Ramos-Rodriguez et al. 2013; Hamlin et al. 2013; Kerbler et al. 2013; Laursen et al. 2013; Perry et al. 2001; Fitz et al. 2008). However, no study has previously examined the effect of loss of perivascular cholinergic input at the NVU across brain regions and vessel types.

In this study, the cortex of wildtype mice was found to have a lower total cholinergic nerve fibre density than the hippocampus, as has been previously reported (Kitt et al. 1994). However, the amount of endogenous perivascular innervation at the basement membrane, smooth muscle cells and astrocytes was similar between the cortex and hippocampus across all vessel types. Saporin treatment resulted in a significant loss of overall cholinergic innervation in both the cortex and hippocampus and the degree of innervation was similar between both regions following treatment. Interestingly, loss of cholinergic innervation at the NVU was only observed at arteries in both brain regions. This may relate to the finding that the arteries showed a trend towards receiving more innervation than the capillaries or veins. A significant decrease in perivascular innervation was observed at all levels of the arterial NVU (basement membrane, SMCs, astrocyte endfeet) in the cortex, but only at the basement membrane and SMCs in the hippocampus. These data suggest that mu-p75-saporin treatment induced a greater loss of cholinergic innervation in the parenchyma of the hippocampus, but that loss of innervation at the NVU was greater in the cortex.

The reason for this variability is unknown. Recent 3D mapping studies have shown that the dendritic arbours of basal forebrain neurons that project to the cortex differ from those that project to the hippocampus in that single cortical dendrites innervate large areas of the neuropil. It is possible that a similar pattern of innervation exists at blood vessels in the cortex such that the loss of one dendritic arbour affects multiple vessels (Li et al. 2017; Wu et al. 2014), and may therefore partly explain the greater loss of innervation in the cortex in comparison to the hippocampus as seen in Chapter 3. In addition, ChAT expression has been found to vary between different layers of the hippocampus and cortex (Cork et al. 1998; Yeo et al. 1997). Thus, it is possible that by analysing randomly chosen vessels, subtle differences in NVU composition between cortical and hippocampal layers may have been overlooked.

Other endogenous differences observed in this study included the presence of a thicker basement membrane and more astrocyte endfeet coverage of veins in the hippocampus compared to those in the cortex. This difference persisted after saporin treatment. A thicker basement membrane, which may be associated with the increased surface area of contact of astrocytic endfeet, is suggestive of decreased flexibility of the vein that may prevent vessel deformation under sheer stress and help to maintain a constant CBF (Thorin-Trescases et al. 2018; Zócalo et al. 2013). Increased collagen content and thicker basement membranes in capillaries and arteries are associated with AD and CAA and may precede the development of CAA (Wyss-Coray et al. 2000; Zarow et al. 1997; Hawkes et al. 2013), but it is unclear whether the thicker basement membranes seen in the veins in this study contributes directly to the aetiology of CAA.

In AD, general loss of parenchymal cholinergic innervation has been found in both the hippocampus and cortex (Mesulam 2013; Van Beek & Claassen 2011; Schliebs & Arendt 2011). Loss of perivascular innervation has been reported in the cortex and hippocampus of AD mouse models (Aucoin et al. 2005; Kuznetsova & Schliebs 2013) and in the cortex of AD brains (Tong & Hamel 1999). However, to our knowledge no studies have been carried out comparing the loss of perivascular cholinergic innervation at the NVU between brain regions during normal ageing or in human or mouse models of AD.

The effect of cholinergic loss on CBF and eNOS

Cholinergic neurons from the basal forebrain are known to play a role in both the maintenance of vascular tone and NVC (Hamel 2006). This action is mediated via activation of mAChRs and nAChRs (Hotta et al. 2011; Van Beek & Claassen 2011) that

are present on endothelial cells (Badaut et al. 1997), smooth muscle cells (Edvinsson et al. 1977), astrocytes (Luiten et al. 1996), and interneurons (Cauli et al. 2004). Binding to ACh triggers an increase in intracellular calcium in endothelial cells (Estrada et al. 1983; Iadecola 2004) that leads to vasodilation via several mechanisms: i) production of arachidonic acid metabolites including epoxyecosatrienoic acid (EET) which hyperpolarises SMCs by stimulating Ca^{2+}-activated potassium channels on their cell membranes, ii) COX1-mediated release of prostacyclin which diffuses across to SMCs, leading to cAMP production and iii) activation of calmodulin and/or PI3K/Akt, which activates eNOS and leads to the production and diffusion of NO into the SMC (Gebremedhin et al. 1992; Zhao et al. 2015; Triggle et al. 2012; Fleming & Busse 2003; Faraci & Heistad 1998; Duchemin et al. 2012; Manicam et al. 2016; Freed & Gutterman 2017).

In the present study, we hypothesized that loss of ACh input at the NVU would result in decreased CBF in the cortex and hippocampus and that this decrease would be more pronounced in the cortex because of the greater loss of perivascular innervation. Saporin treatment had no effect on resting CBF in either brain region and responsiveness to hypercapnia was also similar between control and denervated animals. However, when challenged with the eNOS-mediated vasodilator fasudil hydrochloride, CBF in the cortex of saporin-treated mice was not altered, while blood flow to the hippocampus was increased in both control and saporin-treated animals. Interestingly, endogenous activity of eNOS was found to be significantly higher in the supernatant fractions of the hippocampus compared to the cortex of control mice. Treatment with saporin resulted in a significant decrease in levels of eNOS in the cortex but an increase in eNOS expression and activity in the hippocampus. These findings highlight the importance of ACh-mediated eNOS activity in the regulation of vascular reactivity and also suggest that eNOS regulation in the hippocampus is more sensitive than in the cortex. eNOS is also present in astrocytes (Muñoz et al. 2015), and unlike the cortex, the hippocampus did not lose perivascular innervation at the astrocyte endfeet, which may account for the ability to keep regulation of eNOS activity with cholinergic loss.

Our findings are in contrast to those of Waite et al, who found a global decrease in CBF in the cortex, parietal and temporal cortices in rats treated with 192IgG saporin (Waite et al. 1999). However, another study with the same model found no effect of cholinergic loss on CBF (Sorger et al. 1999) and the same was found in other models with different tracers (Irie et al. 1996; Namba et al. 1991). In another study, where 192IgG saporin induced cholinergic loss but did not affect CBF, administration of the NMDA antagonist MK-801

lead to an increase in CBF in both control and saporin-treated animals (Willis et al. 2006), highlighting a role for ACh in NVC rather than global cerebral autoregulation. This has been recently highlighted in a study by Lecrux et al, who found that although baseline CBF was not affected, there was a decrease in CBF response to NVC stimulated by whisker barrel stimulation in denervated animals compared to control (Lecrux et al. 2017). Additionally, stimulation of the substantia inominata during administration of hypercapnia does not potentiate the increase in CBF (Dauphin et al. 1991), again suggesting ACh-mediated vasodilation is coupled to neuronal activity. Taken together, these studies suggest that, as seen in this thesis, cholinergic neurons do not contribute significantly to resting CBF.

Regionally, NOS activity itself has been found to be similar in both the hippocampus and cortex of the adult human brain (Blum-Degen et al. 1999) and eNOS expression is similar in both regions in normal rat brains (Sessa et al. 1993), suggesting that the changes in eNOS levels seen in this study are directly linked to cholinergic loss. At the SMCs of the NVU, NO-induced vasodilation can be prevented if reactive oxygen species (ROS) are present. Available NO is able to react with ROS to form peroxynitrite, which can prevent further dilation by depleting available NO and also by inhibiting the production of the vasodilator prostacyclin (Iadecola 2004; Zou & Ullrich 1996). NADPH oxidase is a source of ROS and has been demonstrated to be upregulated in AD (Shimohama et al. 2000; Austin et al. 2015). Peroxynitrite has been found in astrocytes, neurons and vessels co-localised with iNOS, nNOS and eNOS in AD cases (Lüth et al. 2002), as well as in glaucoma, where it has been putatively linked to perfusion abnormalities (Feilchenfeld et al. 2008). To our knowledge, no studies have been carried out looking at the direct effect of cholinergic loss on peroxynitrite or oxidative stress. Although peroxynitrite was not investigated in the current study, the loss of perivascular cholinergic fibre contact to astrocytes and the basement membrane concomitant with decreased eNOS levels in the cortex may have led to increased peroxynitrite and contributed to the attenuated response to fasudil hydrochloride treatment in the cortex.

It has been suggested that upregulation of nNOS present in SMCs is able to compensate for decreases in eNOS and maintain vascular tone (Ward et al. 2005). However, in the present study, nNOS levels and activity were not altered by cholinergic loss or as a function of eNOS levels, suggesting that other compensatory mechanisms were at play in this model.

Astrocytes have been found to express mAChRs on their endfeet (Luiten et al. 1996) and as shown in this thesis, receive perivascular contact from cholinergic nerve fibres. Neuron

to astrocyte communication at the NVU has been established (Zonta et al. 2003) and astrocytes are known to buffer glutamate release at the NVU and contribute to the control of NVC (Lind et al. 2013; Stella et al. 1994; Gordon et al. 2008; Petzold et al. 2008; Mishra 2016). Astrocytes have also been demonstrated to regulate vascular tone based on pressure flow feedback from the vasculature, leading to bidirectional feedback with pyramidal neurons in the cortex (Kim et al. 2015; Kim et al. 2016; Filosa et al. 2016). As loss of cholinergic innervation in the cortex was also observed at astrocyte endfeet, it is possible that astrocyte dysfunction may have also contributed to the inability of the cortex to respond to the fasudil hydrochloride.

Activation of mAChRs on interneurons, which is also a potential source of NO (Cauli et al. 2004), has been shown to be involved in the maintenance of vascular tone and NVC. GABA-positive interneurons have been suggested to contribute to the regulation of CBF in the cortex (Lecrux et al. 2011; Cauli et al. 2004). In the cortex, it is estimated that 60% of interneurons received cholinergic innervation, mainly arising from the basal forebrain (Cauli et al. 2004). Thus, loss of cholinergic innervation of interneurons may also have contributed to the lack of CBF responsiveness in the cortex. As a heterogeneous subpopulation of cholinergic interneurons has recently been demonstrated to synapse onto astrocytes at hippocampal arteries (Yi et al. 2015), it would be interesting to investigate the potential role of interneurons on ACh-stimulated vasodilation between different brain regions.

In humans, it has been demonstrated that resting CBF does not differ between people with and without CAA (Dumas et al. 2012). Using blood oxygen level dependent time to peak (BOLD-TTP) fMRI, where visual cues are used to measure NVC, Fotiadis et al showed that the BOLD-TTP was significantly longer in people with both sporadic CAA or HSHWA-D, in association with cortical thinning and higher Aβ load (Fotiadis et al. 2016). Studies in MCI patients have found vascular reactivity to hypercapnia to be impaired in the hippocampus (Glodzik et al. 2011). On the other hand, it has been reported that the hippocampus of AD patients is hyper-perfused and the cortex is hypo-perfused compared to individuals with MCI (Alsop et al. 2008). Other studies have found that basal CBF is higher in the hippocampus than in the cortex of non-demented elderly individuals, but that hypercapnia produced a bigger increase in CBF in the cortex (Rusinek et al. 2011). Taken together, the findings of this thesis and the literature suggest that loss of ACh signalling may contribute to failure of NVC in AD and CAA that is differentially affected in the cortex and hippocampus.

The effect of cholinergic loss on the PVD of Aβ from the brain

In addition to mediating CBF, the cerebrovasculature is also integral to the removal of Aβ from the brain. Three principle vascular-mediated clearance mechanisms have been identified to date; transcytosis of Aβ across the BBB, secretion into the CSF that is removed along para-arterial and -venular spaces (i.e. glymphatic drainage) and drainage of ISF along basement membranes (i.e. PVD) (Agyare et al. 2013; Hladky & Barrand 2018; Iliff et al. 2012; Carare et al. 2008; Weller et al. 2008; Hawkes et al. 2014).

The speed at which clearance of Aβ was observed in the current study suggests that it was too fast to be explained by diffusion alone and that there is a mechanism that drives ISF movement (Schley et al. 2006). However, this driving force remains unknown. Using simulation studies of 3D EM reconstructed images from the hippocampus, Holter et al found that the bulk flow rate generated by hydrostatic pressures was not sufficient to generate solute movement equivalent to speeds reported from experimental data (Holter et al. 2017). They suggest that fluid movement within the brain occurs primarily by diffusion and that the speed of diffusion is mainly driven by interstitial concentration gradients. Other simulation studies have suggested that movement of fluids by convection-mediated bulk flow could not contribute sufficiently to match the observed rate of drainage, and that a pulsatile or oscillating force is more likely to contribute to the rapid diffusion observed (Asgari et al. 2015; Rey & Sarntinoranont 2018). Recent simulations by Diem et al also show that drainage occurring within the periarterial vessel walls occurs at a much faster rate than by diffusion alone (Diem et al. 2016) and highlight the need for a valve-like mechanism as suggested previously (Schley et al. 2006). Recent modelling has determined this valve-like mechanism could be generated by focal arterial contractions during NVC (Diem et al. 2018; Aldea et al. 2018).

We therefore hypothesized that loss of perivascular cholinergic innervation would decrease the force that drives PVD and lead to accumulation of exogenously injected Aβ in the cortex, but not hippocampus, of saporin-treated mice. However, we did not observe any differences in the clearance of Aβ between control and saporin-treated mice in either the cortex or the hippocampus. These results suggest that cholinergic innervation of the vasculature is not essential for PVD to occur. However, the CBF data suggest that disruption of vascular function in denervated mice is only evident when challenged and therefore an additional NVC-specific challenge such as whisker barrel cortical stimulation (Lecrux et al. 2017) or long term fasudil hydrochloride treatment (Rikitake et al. 2005) may be needed to delineate differences in PVD in denervated animals. We and others have previously reported that the efficiency of PVD is decreased with ageing, (Hawkes et al.

2013), in the presence of the ApoE ε4 allele (Hawkes et al. 2012) or after traumatic brain injury (Leclercq et al. 2005). As the current experiments were carried out in young otherwise healthy mice, it is also possible that loss of ACh does not impact on PVD in the absence of other factors that increase the risk of developing AD.

When considering the difference in the regional topography of CAA, such as it being more frequently observed in the cortex than in the hippocampus, it is of note that the cortex was found to have a significantly higher vascular density of large-diameter vessels and capillaries than the hippocampus in wildtype mice. This increased surface area may allow for more clearance of Aβ under normal conditions but equally more opportunity for accumulation if the clearance fails. In the current study, the PVD protocol used for injections into the hippocampus had to be adapted in order to visualise Aβ-positive vessels in the cortex. As discussed in Chapter 5, this may have been due to technical issues related to the proximity of the cortex to the subarachnoid space. However, it is possible that the rate of PVD from the cortex is faster than PVD from the hippocampus. Our lab has previously reported that CAA-vulnerable brain areas are more susceptible than CAA-resistant areas to age-related decreases in the efficiency of Aβ drainage (Hawkes et al. 2013). Thus, it is also possible that different brain areas are differentially affected by an age-related decline in the clearance of Aβ.

Implications of cholinergic loss for CAA

To date, little work has been done to investigate the putative relationship between loss of cholinergic innervation and accumulation of Aβ as CAA. Laursen et al carried out a similar study using saporin to induce cholinergic loss in the TgAPP/PS1 AD mouse model and concluded that cholinergic denervation increased the plaque pathology of AD (Laursen et al. 2013). In the TgAPP23 mouse model, death of cholinergic neurons had no effect on plaque load (Boncristiano et al. 2002). However, Ramos-Rodriguez et al reported increased Aβ deposition in both the hippocampus and cortex with cholinergic denervation in the APP/PS1 mouse model, but with no change in CAA load (Ramos-Rodriguez et al. 2013). A transcriptome analysis of the cholinergic neurons in TgCRND8 model of AD taken at a stage when plaques and CAA were present indicated specific changes in the cholinergic system of the basal forebrain (McKeever et al. 2017), and revealed that there was differential gene expression in different regions of the brain, highlighting regional vulnerabilities which could contribute to the temporal and spatial progression of CAA. Taken together, these studies support a general role for loss of cholinergic innervation in inducing increased Aβ pathology.

Therefore, although saporin treatment did not affect PVD of Aβ, we hypothesized that cholinergic loss could contribute to increased CAA severity. Unexpectedly, we found that treatment of TetO-APPSweInd mice with the same mu-p75-saporin protocol used in the C57BL/6 mice only induced a loss of cholinergic innervation in the hippocampus, while the MS and cortex were unaffected. This may be related to the observation that the cholinergic fibre density in the cortex of TetO-APPSweInd mice was three times lower than that of the C57BL/6 mice, suggesting that there may have been less expression of the p75 NTR to which mu-p75-saporin could bind. It is also likely that there is a higher expression of p75NTR in the hippocampus than in the cortex, as suggested by the higher ChAT fibre density. Interestingly, using APP/PS1 mice with knockout of the p75NTR, Qian et al reported decreased plaque pathology in comparison to the normal APP/PS1 mice and suggested that this may have been due to increased cholinergic nerve fibres and increased vascular drainage (Qian et al. 2018).

Saporin treatment did not affect the density of $A\beta_{1-40}$ or $A\beta_{1-42}$-positive plaques in the hippocampus or cortex. No statistical differences were observed between control and saporin-treated mice in CAA load, apart from significantly increased $A\beta_{1-40}$ positive vessels in the hippocampus of saporin mice. This suggests that loss of cholinergic innervation either does not contribute significantly to the accumulation of CAA or that an additional 'hit', such as ageing or changes to the CVBM (Hawkes et al. 2013), may be required for this loss to contribute to CAA deposition. Using two-photon microscopy, Kress et al found that there was a reduction in the pulsatility of cortical penetrating arteries >50 μm below the brain surface in aged mice which corresponded with reduced CSF-ISF exchange in the subarachnoid space (Kress et al. 2014). Arteriosclerosis, an age-related arterial pathology associated with fibrosis, has been associated with increased risk of developing CAA and has been found to be most prevalent in the occipital lobe, where CAA is most prevalent (Thal et al. 2012; Tian et al. 2004). This suggests that increased age could make cortical vessels vulnerable to CAA deposition due to a reduced capacity to generate the force to clear Aβ contained within the CSF and/or ISF. In the current study, as functional loss of vasoreactivity was only demonstrated in response to a challenge with fasudil hydrochloride, it would be interesting to see whether cholinergic loss could potentiate the deficit in drainage caused by increased age, by inducing loss in middle-aged mice and comparing the effect of cholinergic denervation on drainage and CBF in both the cortex and hippocampus.

Taken together, the findings from this thesis and from the published literature suggest that cholinergic loss may have implications for the development CAA, but that this loss

contributes more strongly to the accumulation of Aβ in the presence of additional risk factors.

Limitations of the current studies and additional experiments

A limitation of using mu-p75-saporin to induce cholinergic loss is that all p75 NTR-positive cells are killed, including a sub-population of astrocytes in the hippocampus (Dougherty & Milner 1999). Therefore, we cannot conclude that the differences that were observed in saporin-treated mice were due solely to loss of cholinergic neurons. It is now possible to selectively target cholinergic populations using techniques such as designer receptor exclusively activated by designer drugs (DREADDs), as in a study where specific mutations on m_4AChRs block receptor activation by ACh so that the channel is only activated by clozapine-*N*-oxide (Nawaratne et al. 2008). This technique has been recently used to specifically target cholinergic neurons in the MS and reduce anxiety in mice *in vivo* (Zhang et al. 2017). This approach may therefore be useful in determining the specific effect on regions of the brain innervated by different parts of the basal forebrain.

Another method to target specific cholinergic neurons is optogenetics, the use of light stimulus in conjunction with genetic modification to turn on or off specific genes, allowing loss or gain of function studies to be carried out (Lin et al. 2015). Recent studies using this technique have highlighted the distinct roles of cholinergic and non-cholinergic neuronal input in mediating behaviours such as attention and responses to reward and punishment conditions (Hangya et al. 2015). However, whether silencing of cholinergic neurons replicates the effect of cell death of neurons in the basal forebrain as seen in AD remains unknown.

As endothelial cells have been suggested to be an important recipient of cholinergic innervation (Manicam et al. 2016), it would be interesting to extend the current 3D analysis to determine if saporin-induced loss of cholinergic innervation also occurs at endothelial cells. A caveat of the 3D modelling system used in this thesis is that it was dependent on fluorescence imaging, which in itself can create artefacts due to the amplification of the signal from the fluorophore needed to be detected, so for specifically validating the perivascular innervation detected in this study, immunolabelling using EM could be used.

Pericytes, which have increasing implications in the control of CBF (Rungta et al. 2018; Attwell et al. 2016), were not evaluated due to the limitation associated with poor antigenicity of pericyte markers in fixed tissue. However, additional studies could be carried out using transgenic mice which express fluorescently-tagged pericyte markers (Fernandez-Klett et al. 2010).

In this thesis, fMRI was used to image regional CBF changes in the cortex and hippocampus. This change was assessed across the whole region and as such small or localised changes to CBF may have been missed. In addition, constraints of imaging anesthetised animals in the MRI machine did not permit us to assess CBF changes in the presence of NVC, which is more sensitive than hypercapnia to loss of ACh signalling. We are also cautious about the interpretation of CBF results in the presence of fasudil hydrochloride, as this is a Rho-kinase inhibitor that is capable of activating eNOS via ACh-independent mechanisms. Finally, CBF was measured using ASL, which is less sensitive to the metabolic state of the tissue than BOLD imaging. Future experiments could therefore be carried out using techniques such as optical coherence tomography with laser Doppler imaging that has recently been shown as a novel way of measuring baseline and evoked CBF in the hippocampus (Park et al. 2018).

This study was limited to specifically looking at the loss of cholinergic neurons in the brains of young adult mice. However, as age is the major risk factor for both sporadic AD and CAA, future studies would aim to investigate the effect of loss of cholinergic innervation in aged animals. In addition, PVD was estimated from *ex vivo* tissues due to the current limitations of visualising deep grey matter tissue *in vivo*.

Lastly, an unavoidable limitation of the study is that the difference between the surface area and white matter content of the human and mouse brain makes it difficult to know if the current conclusions about solute movement and PVD are translational. Additional limitations of the saporin model is that loss of cholinergic innervation may not occur in the same manner as that in the disease, as the mu-p75-saporin model induces retrograde degeneration of cholinergic neurons in the basal forebrain, whereas loss of grey matter in the basal forebrain has been demonstrated as an early indicator of AD (Schmitz et al. 2016). Saporin-induced cholinergic death also occurs much more rapidly than the loss of neurons in AD which may activate a strong acute inflammatory reaction and/or the development of compensatory mechanisms in the animal model that are not present in AD.

Conclusions:

The novel observations generated from work done for this PhD project are that:

1. Treatment with mu-p75-saporin induces loss of cholinergic nerve fibres at the basement membrane and smooth muscle cell at the NVU of arteries in both the hippocampus and cortex, and additional perivascular loss occurs at the astrocytic endfeet in arteries of the cortex.

2. Loss of cholinergic innervation did not affect baseline CBF or response to hypercapnia
3. eNOS-mediated increase in CBF was not observed in the cortex of denervated mice, while the hippocampal response was preserved.
4. Loss of cholinergic innervation was associated with decreased eNOS levels in the cortex, and increased eNOS levels and a trend towards increased activity in the hippocampus.
5. PVD of human Aβ was not affected by saporin treatment in the cortex or hippocampus of wildtype mice.
6. Loss of cholinergic innervation did not significantly potentiate pre-existing CAA severity in the TetO-APPSweInd mouse model of AD.

In conclusion, there is regional heterogeneity between the cortex and hippocampus in terms of the amount of cholinergic innervation that is received from the basal forebrain and the degree to which the NVU is affected by loss of cholinergic innervation. This loss had functional implications for the reactivity of the vasculature, and was dependent on eNOS expression, which was differently and oppositely affected in the hippocampus and the cortex. This loss in function, however, did not impact PVD. The implications of these findings for CAA therefore suggest that cholinergic loss on its own is not sufficient to fully contribute to or account for the pathology of CAA and that other contributing factors may be necessary for a full pathological effect to take place.

References

Abbott, N.J., 2004. Evidence for bulk flow of brain interstitial fluid: significance for physiology and pathology. *Neurochemistry international*, 45(4), pp.545–52.

Abbott, N.J. et al., 2018. The role of brain barriers in fluid movement in the CNS: is there a 'glymphatic' system? *Acta Neuropathologica*, 135(3), pp.387–407.

Adachi, T., Baramidze, D.G. & Sato, A., 1992. Stimulation of the nucleus basalis of Meynert increases cortical cerebral blood flow without influencing diameter of the pial artery in rats. *Neuroscience letters*, 143(1–2), pp.173–6.

Agyare, E.K. et al., 2013. Traffic jam at the blood-brain barrier promotes greater accumulation of Alzheimer's disease amyloid-β proteins in the cerebral vasculature. *Molecular pharmaceutics*, 10(5), pp.1557–65.

Ainslie, P.N. & Brassard, P., 2014. Why is the neural control of cerebral autoregulation so controversial? *F1000prime reports*, 6(March), p.14.

Akoudad, S. et al., 2015. Cerebral Microbleeds Are Associated With an Increased Risk of Stroke: The Rotterdam Study. *Circulation*, 132(6), pp.509–16.

Albargothy, N.J. et al., 2018. Convective influx/glymphatic system: tracers injected into the CSF enter and leave the brain along separate periarterial basement membrane pathways. *Acta neuropathologica*.

Aldea, R. et al., 2018. Cerebrovascular smooth muscle cells as the drivers of periarterial lymphatic drainage of the brain. In *6th ICAA Conference*. Lille, p. 51.

Allen, N. et al., 2014. Patterns of cerebral amyloid angiopathy define histopathological phenotypes in Alzheimer's disease. *Neuropathology and Applied Neurobiology*, 40(2), pp.136–148.

Alsop, D.C. et al., 2008. Hippocampal hyperperfusion in Alzheimer's disease. *NeuroImage*, 42(4), pp.1267–74.

Alzheimer's Disease International (ADI), 2015. *World Alzheimer Report 2015: The Global Impact of Dementia, an analysis of prevalanace, incidence, cost and trends*,

Amenta, F. et al., 1998. Astrocyte changes in aging cerebral cortex and hippocampus: a quantitative immunohistochemical study. *Microscopy research and technique*, 43(1), pp.29–33.

Anenberg, E. et al., 2015. Optogenetic stimulation of GABA neurons can decrease local neuronal activity while increasing cortical blood flow. *Journal of Cerebral Blood Flow and Metabolism*, 35(10), pp.1579–1586.

Antošová, M. et al., 2015. The influence of L-NAME on iNOS expression and markers of oxidative stress in allergen-induced airway hyperreactivity. *Advances in experimental medicine and biology*, 838(1), pp.1–10.

Arai, H., Kosaka, K. & Iizuka, R., 1984. Changes of biogenic amines and their metabolites in postmortem brains from patients with Alzheimer-type dementia. *Journal of neurochemistry*, 43(2), pp.388–93.

Arbel-Ornath, M. et al., 2013. Interstitial fluid drainage is impaired in ischemic stroke and Alzheimer's disease mouse models. *Acta neuropathologica*, 126(3), pp.353–64.

Arendt, T. et al., 1988. Amyloid deposition in the nucleus basalis of Meynert complex: a topographic marker for degenerating cell clusters in Alzheimer's disease. *Acta Neuropathologica*, 75(3), pp.226–232.

Arvanitakis, Z. et al., 2011. Cerebral amyloid angiopathy pathology and cognitive domains in older persons. *Annals of neurology*, 69(2), pp.320–7.

Asgari, M., de Zélicourt, D. & Kurtcuoglu, V., 2015. How astrocyte networks may contribute to cerebral metabolite clearance. *Scientific reports*, 5, p.15024.

Attems, J. et al., 2011. Review: sporadic cerebral amyloid angiopathy. *Neuropathology and applied neurobiology*, 37(1), pp.75–93.

Attems, J., Lintner, F. & Jellinger, K. a, 2004. Amyloid beta peptide 1-42 highly correlates with capillary cerebral amyloid angiopathy and Alzheimer disease pathology. *Acta neuropathologica*, 107(4), pp.283–91.

Attwell, D. et al., 2010. Glial and neuronal control of brain blood flow. *Nature*, 468(7321), pp.232–43.

Attwell, D. et al., 2016. What is a pericyte? *Journal of cerebral blood flow and metabolism : official journal of the International Society of Cerebral Blood Flow and Metabolism*, 36(2), pp.451–5.

Attwell, D. & Iadecola, C., 2002. The neural basis of functional brain imaging signals. *Trends in Neurosciences*, 25(12), pp.621–625.

Aucoin, J.-S. et al., 2005. Selective cholinergic denervation, independent from oxidative stress, in a mouse model of Alzheimer's disease. *Neuroscience*, 132(1), pp.73–86.

Austin, S.A. et al., 2013. Endothelial nitric oxide deficiency promotes Alzheimer's disease pathology. *Journal of neurochemistry*, 127(5), pp.691–700.

Austin, S.A. et al., 2015. Regional heterogeneity of cerebral microvessels and brain susceptibility to oxidative stress. *PLoS ONE*, 10(12), pp.1–12.

Bachstetter, A.D. et al., 2015. Disease-related microglia heterogeneity in the hippocampus of Alzheimer's disease, dementia with Lewy bodies, and hippocampal sclerosis of aging. *Acta neuropathologica communications*, 3(1), p.32.

Badaut, J. et al., 1997. Distribution of muscarinic receptors on the endothelium of cortical vessels in the rat brain. *Brain research*, 778(1), pp.25–33.

Baeres, F.M.M. et al., 2004. Origin of PACAP-immunoreactive nerve fibers innervating the subarachnoidal blood vessels of the rat brain. *Journal of cerebral blood flow and metabolism : official journal of the International Society of Cerebral Blood Flow and Metabolism*, 24(6), pp.628–35.

Ball, K.K. et al., 2010. Trafficking of glucose, lactate, and amyloid-beta from the inferior colliculus through perivascular routes. *Journal of cerebral blood flow and metabolism : official journal of the International Society of Cerebral Blood Flow and Metabolism*, 30(1), pp.162–76.

Bartus, R.T. et al., 1982. The cholinergic hypothesis of geriatric memory dysfunction. *Science (New York, N.Y.)*, 217(4558), pp.408–14.

Bateman, R.J. et al., 2006. Human amyloid-beta synthesis and clearance rates as measured in cerebrospinal fluid in vivo. *Nature medicine*, 12(7), pp.856–61.

Bedussi, B. et al., 2018. Paravascular spaces at the brain surface: Low resistance pathways for cerebrospinal fluid flow. *Journal of Cerebral Blood Flow and Metabolism*, 38(4), pp.719–726.

Van Beek, A.H.E. a & Claassen, J. a H.R., 2011. The cerebrovascular role of the cholinergic neural system in Alzheimer's disease. *Behavioural brain research*, 221(2), pp.537–42.

Bekar, L.K., Wei, H.S. & Nedergaard, M., 2012. The locus coeruleus-norepinephrine network

optimizes coupling of cerebral blood volume with oxygen demand. *Journal of cerebral blood flow and metabolism : official journal of the International Society of Cerebral Blood Flow and Metabolism*, 32(12), pp.2135–45.

Bell, R.D. et al., 2007. Transport pathways for clearance of human Alzheimer's amyloid beta-peptide and apolipoproteins E and J in the mouse central nervous system. *Journal of cerebral blood flow and metabolism : official journal of the International Society of Cerebral Blood Flow and Metabolism*, 27(5), pp.909–18.

Berger-Sweeney, J. et al., 2001. Selective immunolesions of cholinergic neurons in mice: effects on neuroanatomy, neurochemistry, and behavior. *The Journal of neuroscience : the official journal of the Society for Neuroscience*, 21(20), pp.8164–73.

Bertsch, K. et al., 2009. Resting cerebral blood flow, attention, and aging. *Brain Research*, 1267, pp.77–88.

Biesold, D. et al., 1989. Stimulation of the nucleus basalis of Meynert increases cerebral cortical blood flow in rats. *Neuroscience letters*, 98(1), pp.39–44.

Birthelmer, a et al., 2003. Neurotransmitter release and its presynaptic modulation in the rat hippocampus after selective damage to cholinergic or/and serotonergic afferents. *Brain research bulletin*, 59(5), pp.371–81.

Blanco, V.M., Stern, J.E. & Filosa, J.A., 2008. Tone-dependent vascular responses to astrocyte-derived signals. *American journal of physiology. Heart and circulatory physiology*, 294(6), pp.H2855-63.

Bleys, R.L. et al., 1996. Perivascular nerves of the human basal cerebral arteries: I. Topographical distribution. *Journal of cerebral blood flow and metabolism : official journal of the International Society of Cerebral Blood Flow and Metabolism*, 16(5), pp.1034–47.

Bleys, R.L. & Cowen, T., 2001. Innervation of cerebral blood vessels: morphology, plasticity, age-related, and Alzheimer's disease-related neurodegeneration. *Microscopy research and technique*, 53(2), pp.106–18.

Blum-Degen, D. et al., 1999. Characterization and regional distribution of nitric oxide synthase in the human brain during normal ageing. *Brain Res*, 834(1–2), pp.128–135.

Bolte, S. & Cordelieres, F.P., 2006. A guided tour into subcellular colocalisation analysis in light microscopy. *Journal of Microscopy*, 224(3), pp.13–232.

Boncristiano, S. et al., 2002. Cholinergic changes in the APP23 transgenic mouse model of cerebral amyloidosis. *The Journal of neuroscience : the official journal of the Society for Neuroscience*, 22(8), pp.3234–43.

Bonvento, G. et al., 1990. Differential effects of electrical stimulation of the dorsal raphe nucleus and of cervical sympathectomy on serotonin and noradrenaline concentrations in major cerebral arteries and pial vessels in the rat. *Journal of cerebral blood flow and metabolism : official journal of the International Society of Cerebral Blood Flow and Metabolism*, 10(1), pp.123–6.

Boskovic, Z. et al., 2014. The role of p75NTR in cholinergic basal forebrain structure and function. *The Journal of neuroscience : the official journal of the Society for Neuroscience*, 34(39), pp.13033–8.

Bouvier, D.S. et al., 2016. High Resolution Dissection of Reactive Glial Nets in Alzheimer's Disease. *Scientific Reports*, 6(1), p.24544.

Braak, H. & Braak, E., 1991. Neuropathological stageing of Alzheimer-related changes. *Acta neuropathologica*, 82(4), pp.239–59.

Brooks, W.S. et al., 2004. Hemorrhage is uncommon in new Alzheimer family with Flemish amyloid precursor protein mutation. *Neurology*, 63(9), pp.1613–1617.

Brown, D.R.P. et al., 1996. Longitudinal changes in cognitive function and regional cerebral function in Alzheimer's disease: A SPECT blood flow study. *Journal of Psychiatric Research*, 30(2), pp.109–126.

Brown, W.R. et al., 2002. Venous collagenosis and arteriolar tortuosity in leukoaraiosis. *Journal of the neurological sciences*, 203–204, pp.159–63.

Bushong, E. a et al., 2002. Protoplasmic astrocytes in CA1 stratum radiatum occupy separate anatomical domains. *The Journal of neuroscience : the official journal of the Society for Neuroscience*, 22(1), pp.183–192.

Buss, L. et al., 2016. Intracerebral haemorrhage in Down syndrome: protected or predisposed? *F1000Research*, 5, pp.470–476.

Carare, R.O. et al., 2013. Immune complex formation impairs the elimination of solutes from the brain: implications for immunotherapy in Alzheimer's disease. *Acta neuropathologica communications*, 1(1), p.48.

Carare, R.O. et al., 2013. Review: cerebral amyloid angiopathy, prion angiopathy, CADASIL and the spectrum of protein elimination failure angiopathies (PEFA) in neurodegenerative disease with a focus on therapy. *Neuropathology and applied neurobiology*, 39(6), pp.593–611.

Carare, R.O. et al., 2008. Solutes, but not cells, drain from the brain parenchyma along basement membranes of capillaries and arteries: significance for cerebral amyloid angiopathy and neuroimmunology. *Neuropathology and applied neurobiology*, 34(2), pp.131–44.

Cauli, B. et al., 2004. Cortical GABA interneurons in neurovascular coupling: relays for subcortical vasoactive pathways. *The Journal of neuroscience : the official journal of the Society for Neuroscience*, 24(41), pp.8940–9.

Cavedo, E. et al., 2017. Reduced basal forebrain atrophy progression in a randomized Donepezil trial in prodromal Alzheimer's disease. *Scientific Reports*, 7(1), pp.1–10.

Chao, L.L. et al., 2010. ASL perfusion MRI predicts cognitive decline and conversion from MCI to dementia. *Alzheimer disease and associated disorders*, 24(1), pp.19–27.

Chédotal, A. et al., 1994. Distinct choline acetyltransferase (ChAT) and vasoactive intestinal polypeptide (VIP) bipolar neurons project to local blood vessels in the rat cerebral cortex. *Brain Research*, 646(2), pp.181–193.

Chen, B.R. et al., 2014. A critical role for the vascular endothelium in functional neurovascular coupling in the brain. *Journal of the American Heart Association*, 3(3), p.e000787.

Chen, C.P. et al., 2000. Immunocytochemical study of the dorsal and median raphe nuclei in patients with Alzheimer's disease prospectively assessed for behavioural changes. *Neuropathology and applied neurobiology*, 26(4), pp.347–55.

Chen, N. et al., 2012. Nucleus basalis-enabled stimulus-specific plasticity in the visual cortex is mediated by astrocytes. *Proceedings of the National Academy of Sciences of the United States of America*, 109(41), pp.E2832-41.

Cholet, N. et al., 1997. Local uncoupling of the cerebrovascular and metabolic responses to somatosensory stimulation after neuronal nitric oxide synthase inhibition. *Journal of cerebral blood flow and metabolism : official journal of the International Society of Cerebral Blood Flow and Metabolism*, 17(11), pp.1191–201.

Christov, A. et al., 2008. Structural changes in Alzheimer's disease brain microvessels. *Current Alzheimer research*, 5(4), pp.392–5.

Clifford, P.M. et al., 2008. α7 nicotinic acetylcholine receptor expression by vascular smooth muscle cells facilitates the deposition of Aβ peptides and promotes cerebrovascular amyloid angiopathy. *Brain Research*, 1234, pp.158–171.

Cohen, Z. et al., 1992. Cerebrovascular nerve fibers immunoreactive for tryptophan-5-hydroxylase in the rat: distribution, putative origin and comparison with sympathetic noradrenergic nerves. *Brain research*, 598(1–2), pp.203–14.

Consonni, S. et al., 2009. Developmental and neurochemical features of cholinergic neurons in the murine cerebral cortex. *BMC neuroscience*, 10, p.18.

Cork, R.J. et al., 1998. A web-accessible digital atlas of the distribution of nitric oxide synthase in the mouse brain. *Progress in brain research*, 118, pp.37–50.

Court, J. a & Perry, E.K., 2003. Neurotransmitter abnormalities in vascular dementia. *International psychogeriatrics / IPA*, 15 Suppl 1, pp.81–7.

Cragnolini, A.B. & Friedman, W.J., 2008. The function of p75NTR in glia. *Trends in Neurosciences*, 31(2), pp.99–104.

Cunningham, C. et al., 2003. Synaptic changes characterize early behavioural signs in the ME7 model of murine prion disease. *The European journal of neuroscience*, 17(10), pp.2147–55.

Dai, W. et al., 2009. Mild cognitive impairment and alzheimer disease: patterns of altered cerebral blood flow at MR imaging. *Radiology*, 250(3), pp.856–66.

Damasio, A.R. et al., 1985. Amnesia following basal forebrain lesions. *Archives of neurology*, 42(3), pp.263–71.

Dauphin, F. et al., 1991. Hypercapnia and stimulation of the substantia innominata increase rat frontal cortical blood flow by different cholinergic mechanisms. *Brain Research*, 553(1), pp.75–83.

Davis-Salinas, J. et al., 1995. Amyloid beta-protein induces its own production in cultured degenerating cerebrovascular smooth muscle cells. *Journal of neurochemistry*, 65(2), pp.931–4.

Devor, A. et al., 2012. Frontiers in optical imaging of cerebral blood flow and metabolism. *Journal of cerebral blood flow and metabolism : official journal of the International Society of Cerebral Blood Flow and Metabolism*, 32(7), pp.1259–76.

Diem, A.K. et al., 2018. A control mechanism for intra-mural peri-arterial drainage via astrocytes: How neuronal activity could improve waste clearance from the brain. *PloS one*, 13(10), p.e0205276.

Diem, A.K. et al., 2016. A Simulation Model of Periarterial Clearance of Amyloid-β from the Brain. *Frontiers in Aging Neuroscience*, 8(February), pp.1–11.

Diem, A.K. et al., 2017. Arterial Pulsations cannot Drive Intramural Periarterial Drainage: Significance for Aβ Drainage. *Frontiers in neuroscience*, 11(August), p.475.

Dimmeler, S. et al., 1999. Activation of nitric oxide synthase in endothelial cells by Akt-dependent phosphorylation. *Nature*, 399(6736), pp.601–5.

Do, T.M. et al., 2012. ABCG2- and ABCG4-mediated efflux of amyloid-β peptide 1-40 at the mouse blood-brain barrier. *Journal of Alzheimer's disease : JAD*, 30(1), pp.155–66.

Dorheim, M.A. et al., 1994. Nitric oxide synthase activity is elevated in brain microvessels in Alzheimer's disease. *Biochemical and biophysical research communications*, 205(1), pp.659–65.

Dorr, A. et al., 2012. Amyloid-β-dependent compromise of microvascular structure and function in

a model of Alzheimer's disease. *Brain : a journal of neurology*, 135(Pt 10), pp.3039–50.

Dorr, A., Sled, J.G. & Kabani, N., 2007. Three-dimensional cerebral vasculature of the CBA mouse brain: A magnetic resonance imaging and micro computed tomography study. *NeuroImage*, 35(4), pp.1409–1423.

Dougherty, K.D. & Milner, T.A., 1999. p75(NTR) immunoreactivity in the rat dentate gyrus is mostly within presynaptic profiles but is also found in some astrocytic and postsynaptic profiles. *Journal of Comparative Neurology*, 407(1), pp.77–91.

Duchemin, S. et al., 2012. The complex contribution of NOS interneurons in the physiology of cerebrovascular regulation. *Frontiers in neural circuits*, 6(August), p.51.

Dumas, A. et al., 2012. Functional magnetic resonance imaging detection of vascular reactivity in cerebral amyloid angiopathy. *Annals of neurology*, 72(1), pp.76–81.

Duncombe, J. et al., 2017. Ageing causes prominent neurovascular dysfunction associated with loss of astrocytic contacts and gliosis. *Neuropathology and applied neurobiology*, 43(6), pp.477–491.

Edvinsson, L., Falck, B. & Owman, C., 1977. Possibilities for a cholinergic action on smooth musculature and on sympathetic axons in brain vessels mediated by muscarinic and nicotinic receptors. *The Journal of pharmacology and experimental therapeutics*, 200(1), pp.117–26.

Elhusseiny, a & Hamel, E., 2001. Sumatriptan elicits both constriction and dilation in human and bovine brain intracortical arterioles. *British journal of pharmacology*, 132(1), pp.55–62.

Elhusseiny, A. et al., 1999. Functional acetylcholine muscarinic receptor subtypes in human brain microcirculation: identification and cellular localization. *Journal of cerebral blood flow and metabolism : official journal of the International Society of Cerebral Blood Flow and Metabolism*, 19(7), pp.794–802.

Emsley, J.G. & Macklis, J.D., 2006. Astroglial heterogeneity closely reflects the neuronal-defined anatomy of the adult murine CNS. *Neuron glia biology*, 2(3), pp.175–86.

Erickson, M. a & Banks, W. a, 2013. Blood-brain barrier dysfunction as a cause and consequence of Alzheimer's disease. *Journal of cerebral blood flow and metabolism : official journal of the International Society of Cerebral Blood Flow and Metabolism*, 33(10), pp.1500–13.

Estrada, C., Hamel, E. & Krause, D.N., 1983. Biochemical evidence for cholinergic innervation of intracerebral blood vessels. *Brain Research*, 266(2), pp.261–270.

Faraci, F.M. & Heistad, D.D., 1998. Regulation of the cerebral circulation: role of endothelium and potassium channels. *Physiological reviews*, 78(1), pp.53–97.

Faraco, G. et al., 2018. Dietary salt promotes neurovascular and cognitive dysfunction through a gut-initiated TH17 response. *Nature neuroscience*, 21(2), pp.240–249.

Farkas, E. & Luiten, P.G., 2001. Cerebral microvascular pathology in aging and Alzheimer's disease. *Progress in neurobiology*, 64(6), pp.575–611.

Farris, W. et al., 2003. Insulin-degrading enzyme regulates the levels of insulin, amyloid beta-protein, and the beta-amyloid precursor protein intracellular domain in vivo. *Proceedings of the National Academy of Sciences of the United States of America*, 100(7), pp.4162–7.

Farris, W. et al., 2007. Loss of neprilysin function promotes amyloid plaque formation and causes cerebral amyloid angiopathy. *The American journal of pathology*, 171(1), pp.241–51.

Feilchenfeld, Z., Yücel, Y.H. & Gupta, N., 2008. Oxidative injury to blood vessels and glia of the pre-laminar optic nerve head in human glaucoma. *Experimental Eye Research*, 87(5), pp.409–414.

Fernandez-Klett, F. et al., 2010. Pericytes in capillaries are contractile in vivo, but arterioles mediate functional hyperemia in the mouse brain. *Proceedings of the National Academy of Sciences*, 107(51), pp.22290–22295.

Ferreira-Vieira, T.H. et al., 2016. Alzheimer's disease: Targeting the Cholinergic System. *Current neuropharmacology*, 14(1), pp.101–15.

Filosa, J.A. et al., 2016. Beyond neurovascular coupling, role of astrocytes in the regulation of vascular tone. *Neuroscience*, 323, pp.96–109.

Filosa, J.A., 2010. Vascular tone and neurovascular coupling: considerations toward an improved in vitro model. *Frontiers in neuroenergetics*, 2(August), pp.1–8.

Fine, A. et al., 1997. Learning impairments following injection of a selective cholinergic immunotoxin, ME20.4 IgG-saporin, into the basal nucleus of Meynert in monkeys. *Neuroscience*, 81(2), pp.331–43.

Fitz, N.F., Gibbs, R.B. & Johnson, D.A., 2008. Selective lesion of septal cholinergic neurons in rats impairs acquisition of a delayed matching to position T-maze task by delaying the shift from a response to a place strategy. *Brain research bulletin*, 77(6), pp.356–60.

Fleming, I. & Busse, R., 2003. Molecular mechanisms involved in the regulation of the endothelial nitric oxide synthase. *American journal of physiology. Regulatory, integrative and comparative physiology*, 284(1), pp.R1-12.

Foidl, B.M. et al., 2016. Cholinergic neurodegeneration in an Alzheimer mouse model overexpressing amyloid-precursor protein with the Swedish-Dutch-Iowa mutations. *Neurobiology of Learning and Memory*, 136, pp.86–96.

Fotiadis, P. et al., 2016. Cortical atrophy in patients with cerebral amyloid angiopathy: a case-control study. *The Lancet. Neurology*, 15(8), pp.811–819.

Frahm, J. et al., 1996. Dynamic uncoupling and recoupling of perfusion and oxidative metabolism during focal brain activation in man. *Magnetic resonance in medicine*, 35(2), pp.143–8.

Francis, P.T. et al., 1999. The cholinergic hypothesis of Alzheimer's disease: a review of progress. *Journal of neurology, neurosurgery, and psychiatry*, 66(2), pp.137–47.

Freed, J.K. & Gutterman, D.D., 2017. Communication Is Key: Mechanisms of Intercellular Signaling in Vasodilation. *Journal of cardiovascular pharmacology*, 69(5), pp.264–272.

Fulton, D. et al., 2004. Targeting of endothelial nitric-oxide synthase to the cytoplasmic face of the Golgi complex or plasma membrane regulates Akt- versus calcium-dependent mechanisms for nitric oxide release. *The Journal of biological chemistry*, 279(29), pp.30349–57.

Furchgott, R.F. & Zawadzki, J. V., 1980. The obligatory role of endothelial cells in the relaxation of arterial smooth muscle by acetylcholine. *Nature*, 288(5789), pp.373–6.

Gakuba, C. et al., 2018. General anesthesia inhibits the activity of the "glymphatic system." *Theranostics*, 8(3), pp.710–722.

Garcia-Alloza, M. et al., 2011. Cerebrovascular lesions induce transient β-amyloid deposition. *Brain : a journal of neurology*, 134(Pt 12), pp.3697–707.

Garcia-Alloza, M. et al., 2005. Cholinergic-serotonergic imbalance contributes to cognitive and behavioral symptoms in Alzheimer's disease. *Neuropsychologia*, 43(3), pp.442–9.

Gebremedhin, D. et al., 1992. Mechanism of action of cerebral epoxyeicosatrienoic acids on cerebral arterial smooth muscle. *The American journal of physiology*, 263(2 Pt 2), pp.H519–H525.

Geula, C. et al., 2008. Cholinergic neuronal and axonal abnormalities are present early in aging and

in Alzheimer disease. *Journal of neuropathology and experimental neurology*, 67(4), pp.309–18.

Glodzik, L. et al., 2011. Framingham cardiovascular risk profile correlates with impaired hippocampal and cortical vasoreactivity to hypercapnia. *Journal of cerebral blood flow and metabolism : official journal of the International Society of Cerebral Blood Flow and Metabolism*, 31(2), pp.671–679.

Goedert, M., 1987. Neuronal localization of amyloid beta protein precursor mRNA in normal human brain and in Alzheimer's disease. *The EMBO journal*, 6(12), pp.3627–3632.

Gordon, G.R.J. et al., 2008. Brain metabolism dictates the polarity of astrocyte control over arterioles. *Nature*, 456(7223), pp.745–9.

Gotti, S. et al., 2005. Distribution of nitric oxide synthase immunoreactivity in the mouse brain. *Microscopy research and technique*, 68(1), pp.13–35.

Grabowski, T.J. et al., 2001. Novel amyloid precursor protein mutation in an Iowa family with dementia and severe cerebral amyloid angiopathy. *Annals of Neurology*, 49(6), pp.697–705.

Grothe, M.J. et al., 2014. Basal forebrain atrophy and cortical amyloid deposition in nondemented elderly subjects. *Alzheimer's & dementia : the journal of the Alzheimer's Association*, 10(5 Suppl), pp.S344-53.

Grundke-Iqbal, I. et al., 1986. Abnormal phosphorylation of the microtubule-associated protein tau (tau) in Alzheimer cytoskeletal pathology. *Proceedings of the National Academy of Sciences of the United States of America*, 83(13), pp.4913–7.

Hafez, D. et al., 2011. Neprilysin-2 is an important β-amyloid degrading enzyme. *The American journal of pathology*, 178(1), pp.306–12.

Haglund, M. et al., 2006. Differential deposition of amyloid beta peptides in cerebral amyloid angiopathy associated with Alzheimer's disease and vascular dementia. *Acta neuropathologica*, 111(5), pp.430–5.

Hallanger, A.E. et al., 1987. The origins of cholinergic and other subcortical afferents to the thalamus in the rat. *Journal of Comparative Neurology*, 262(1), pp.105–124.

Halliday, M.R. et al., 2016. Accelerated pericyte degeneration and blood-brain barrier breakdown in apolipoprotein E4 carriers with Alzheimer's disease. *Journal of Cerebral Blood Flow and Metabolism*, 36(1), pp.216–227.

Hamel, E., 2006. Perivascular nerves and the regulation of cerebrovascular tone. *Journal of applied physiology (Bethesda, Md. : 1985)*, 100(3), pp.1059–64.

Hamel, E., Edvinsson, L. & MacKenzie, E.T., 1988. Heterogeneous vasomotor responses of anatomically distinct feline cerebral arteries. *British journal of pharmacology*, 94(2), pp.423–36.

Hamilton, N.B., Attwell, D. & Hall, C.N., 2010. Pericyte-mediated regulation of capillary diameter: a component of neurovascular coupling in health and disease. *Frontiers in neuroenergetics*, 2(May), pp.1–14.

Hamlin, A.S. et al., 2013. Lesions of the Basal Forebrain Cholinergic System in Mice Disrupt Idiothetic Navigation. *PLoS ONE*, 8(1).

Hampel, H. et al., 2018. The cholinergic system in the pathophysiology and treatment of Alzheimer's disease. *Brain*, 141(7), pp.1917–1933.

Han, B.H. et al., 2015. Contribution of reactive oxygen species to cerebral amyloid angiopathy, vasomotor dysfunction, and microhemorrhage in aged Tg2576 mice. *Proceedings of the*

National Academy of Sciences, 112(8), pp.E881–E890.

Hangya, B. et al., 2015. Central Cholinergic Neurons Are Rapidly Recruited by Reinforcement Feedback. *Cell*, 162(5), pp.1155–68.

Hannah, R.M. et al., 2011. Endothelial SK(Ca) and IK(Ca) channels regulate brain parenchymal arteriolar diameter and cortical cerebral blood flow. *Journal of cerebral blood flow and metabolism : official journal of the International Society of Cerebral Blood Flow and Metabolism*, 31(5), pp.1175–1186.

Hannocks, M.-J. et al., 2018. Molecular characterization of perivascular drainage pathways in the murine brain. *Journal of cerebral blood flow and metabolism : official journal of the International Society of Cerebral Blood Flow and Metabolism*, 38(4), pp.669–686.

Harada, M., Fuse, A. & Tanaka, Y., 1997. Measurement of nitric oxide in the rat cerebral cortex during hypercapnoea. *Neuroreport*, 8(4), pp.999–1002.

Hardebo, J.E. et al., 1980. Enzymes related to monoamine transmitter metabolism in brain microvessels. *Journal of neurochemistry*, 35(6), pp.1388–93.

Harper, A.M. & MacKenzie, E.T., 1977. Effects of 5-hydroxytryptamine on pial arteriolar calibre in anaesthetized cats. *The Journal of physiology*, 271(3), pp.735–46.

Harrison, I.F. et al., 2018. Non-invasive imaging of CSF-mediated brain clearance pathways via assessment of perivascular fluid movement with DTI MRI. *eLife*, 7, pp.1–14.

Härtig, W. et al., 2014. Immunolesion-induced loss of cholinergic projection neurones promotes β-amyloidosis and tau hyperphosphorylation in the hippocampus of triple-transgenic mice. *Neuropathology and applied neurobiology*, 40(2), pp.106–20.

Hartz, A.M.S., Miller, D.S. & Bauer, B., 2010. Restoring blood-brain barrier P-glycoprotein reduces brain amyloid-beta in a mouse model of Alzheimer's disease. *Molecular pharmacology*, 77(5), pp.715–23.

Hawkes, C., Jhamandas, J.H. & Kar, S., 2005. Selective loss of basal forebrain cholinergic neurons by 192 IgG-saporin is associated with decreased phosphorylation of Ser glycogen synthase kinase-3beta. *Journal of neurochemistry*, 95(1), pp.263–72.

Hawkes, C.A. et al., 2012. Disruption of arterial perivascular drainage of amyloid-β from the brains of mice expressing the human APOE ε4 allele. *PloS one*, 7(7), p.e41636.

Hawkes, C.A. et al., 2014. Failure of perivascular drainage of β-amyloid in cerebral amyloid angiopathy. *Brain pathology (Zurich, Switzerland)*, 24(4), pp.396–403.

Hawkes, C.A. et al., 2011. Perivascular drainage of solutes is impaired in the ageing mouse brain and in the presence of cerebral amyloid angiopathy. *Acta neuropathologica*, 121(4), pp.431–43.

Hawkes, C.A. et al., 2013. Regional differences in the morphological and functional effects of aging on cerebral basement membranes and perivascular drainage of amyloid-β from the mouse brain. *Aging cell*, 12(2), pp.224–36.

Hawkes, C.A. & McLaurin, J., 2009. Selective targeting of perivascular macrophages for clearance of beta-amyloid in cerebral amyloid angiopathy. *Proceedings of the National Academy of Sciences of the United States of America*, 106(4), pp.1261–6.

Heider, M. et al., 1997. Basal forebrain cholinergic immunolesion by 192IgG-saporin: evidence for a presynaptic location of subpopulations of alpha 2- and beta-adrenergic as well as 5-HT2A receptors on cortical cholinergic terminals. *Neurochemical research*, 22(8), pp.957–66.

Hernandez-Guillamon, M. et al., 2012. Plasma β-amyloid levels in cerebral amyloid angiopathy-

associated hemorrhagic stroke. *Neuro-degenerative diseases*, 10(1–4), pp.320–3.

Hill, R.A. et al., 2015. Regional Blood Flow in the Normal and Ischemic Brain Is Controlled by Arteriolar Smooth Muscle Cell Contractility and Not by Capillary Pericytes. *Neuron*, 87(1), pp.95–110.

Hladky, S.B. & Barrand, M.A., 2018. Elimination of substances from the brain parenchyma: efflux via perivascular pathways and via the blood-brain barrier. *Fluids and barriers of the CNS*, 15(1), p.30.

Hladky, S.B. & Barrand, M.A., 2014. Mechanisms of fluid movement into, through and out of the brain: evaluation of the evidence. *Fluids and Barriers of the CNS*, 11(1), p.26.

Högestätt, E.D., Skärby, T. V & Uski, T.K., 1989. Influence of Bay K 8644 on vascular responses mediated by alpha 1- and alpha 2-adrenoceptors. *General pharmacology*, 20(6), pp.799–804.

Holter, K.E. et al., 2017. Interstitial solute transport in 3D reconstructed neuropil occurs by diffusion rather than bulk flow. *Proceedings of the National Academy of Sciences of the United States of America*, 114(37), pp.9894–9899.

Hotta, H. et al., 2011. Control of cerebral cortical blood flow by stimulation of basal forebrain cholinergic areas in mice. *Journal of Physiological Sciences*, 61(3), pp.201–209.

Howarth, C. et al., 2017. A Critical Role for Astrocytes in Hypercapnic Vasodilation in Brain. *The Journal of Neuroscience*, 37(9), pp.2403–2414.

Hu, W.T. et al., 2010. Distinct cerebral perfusion patterns in FTLD and AD. *Neurology*, 75(10), pp.881–8.

Huang, Z. et al., 1994. Effects of cerebral ischemia in mice deficient in neuronal nitric oxide synthase. *Science*, 265(5180), p.1883–5.

Hunter, C.L. et al., 2004. Minocycline protects basal forebrain cholinergic neurons from mu p75-saporin immunotoxic lesioning. *The European journal of neuroscience*, 19(12), pp.3305–16.

Hunter, J.M. et al., 2012. Morphological and pathological evolution of the brain microcirculation in aging and Alzheimer's disease. *PloS one*, 7(5), p.e36893.

Hyman, B.T. et al., 1992. Relative sparing of nitric oxide synthase-containing neurons in the hippocampal formation in Alzheimer's disease. *Annals of neurology*, 32(6), pp.818–20.

Iadecola, C., 2004. Neurovascular regulation in the normal brain and in Alzheimer's disease. *Nature reviews. Neuroscience*, 5(5), pp.347–60.

Iadecola, C. et al., 1994. Nitric oxide synthase inhibition and cerebrovascular regulation. *Journal of cerebral blood flow and metabolism : official journal of the International Society of Cerebral Blood Flow and Metabolism*, 14(2), pp.175–92.

Iadecola, C., 1993. Regulation of the cerebral microcirculation during neural activity: is nitric oxide the missing link? *Trends in neurosciences*, 16(6), pp.206–14.

Iadecola, C. & Xu, X., 1994. Nitro-L-arginine attenuates hypercapnic cerebrovasodilation without affecting cerebral metabolism. *The American journal of physiology*, 266(2 Pt 2), pp.R518-25.

Iadecola, C. & Zhang, F., 1996. Permissive and obligatory roles of NO in cerebrovascular responses to hypercapnia and acetylcholine. *The American journal of physiology*, 271, pp.R990–R1001.

Ichimura, T., Fraser, P.A. & Cserr, H.F., 1991. Distribution of extracellular tracers in perivascular spaces of the rat brain. *Brain Research*, 545(1–2), pp.103–113.

Iliff, J.J. et al., 2012. A paravascular pathway facilitates CSF flow through the brain parenchyma

and the clearance of interstitial solutes, including amyloid β. *Science translational medicine*, 4(147), p.147ra111.

Iliff, J.J. et al., 2013. Cerebral arterial pulsation drives paravascular CSF-interstitial fluid exchange in the murine brain. *The Journal of neuroscience : the official journal of the Society for Neuroscience*, 33(46), pp.18190–9.

Irie, T. et al., 1996. Brain acetylcholinesterase activity: validation of a PET tracer in a rat model of Alzheimer's disease. *Journal of nuclear medicine : official publication, Society of Nuclear Medicine*, 37(4), pp.649–55.

Ishikawa, M., Yamada, S. & Yamamoto, K., 2018. Dilated Perivascular Spaces in the Centrum Semiovale Begin to Develop in Middle Age. *Journal of Alzheimer's Disease*, 61(4), pp.1619–1626.

Itakura, T. et al., 1985. 5-Hydroxytryptamine innervation of vessels in the rat cerebral cortex. Immunohistochemical findings and hydrogen clearance study of rCBF. *Journal of neurosurgery*, 62(1), pp.42–7.

Itakura, T. et al., 1977. Central dual innervation of arterioles and capillaries in the brain. *Stroke; a journal of cerebral circulation*, 8(3), pp.360–5.

Iturria-Medina, Y. et al., 2016. Early role of vascular dysregulation on late-onset Alzheimer's disease based on multifactorial data-driven analysis. *Nature communications*, 7(12), p.11934.

Iwata, N. et al., 2001. Metabolic regulation of brain Abeta by neprilysin. *Science (New York, N.Y.)*, 292(5521), pp.1550–2.

Jack, C.R. et al., 2010. Hypothetical model of dynamic biomarkers of the Alzheimer's pathological cascade. *The Lancet. Neurology*, 9(1), pp.119–28.

Jackowski, A., Crockard, A. & Burnstock, G., 1988. Ultrastructure of serotonin-containing nerve fibres in the middle cerebral artery of the rat and evidence for its localization within catecholamine-containing nerve fibres by immunoelectron microscopy. *Brain research*, 443(1–2), pp.159–65.

Jankowsky, J.L. et al., 2005. Persistent amyloidosis following suppression of Abeta production in a transgenic model of Alzheimer disease. *PLoS medicine*, 2(12), p.e355.

Jankowsky, J.L. & Zheng, H., 2017. Practical considerations for choosing a mouse model of Alzheimer's disease. *Molecular Neurodegeneration*, 12(1), pp.1–22.

Jarrett, J.T., Berger, E.P. & Lansbury, P.T., 1993. The carboxy terminus of the beta amyloid protein is critical for the seeding of amyloid formation: implications for the pathogenesis of Alzheimer's disease. *Biochemistry*, 32(18), pp.4693–7.

Jeffrey, M. & González, L., 2007. Classical sheep transmissible spongiform encephalopathies: Pathogenesis, pathological phenotypes and clinical disease. *Neuropathology and Applied Neurobiology*, 33(4), pp.373–394.

Jellinger, K.A., 2002. Alzheimer disease and cerebrovascular pathology: an update. *Journal of neural transmission (Vienna, Austria : 1996)*, 109(5–6), pp.813–36.

Jessen, N.A. et al., 2015. The Glymphatic System: A Beginner's Guide. *Neurochemical research*, pp.1–17.

Jeynes, B. & Provias, J., 2009. Significant negative correlations between capillary expressed eNOS and Alzheimer lesion burden. *Neuroscience letters*, 463(3), pp.244–8.

Jiang, Z. et al., 2014. Role of nitric oxide synthases in early blood-brain barrier disruption following transient focal cerebral ischemia. *PLoS ONE*, 9(3).

Kacem, K. et al., 1998. Structural organization of the perivascular astrocyte endfeet and their relationship with the endothelial glucose transporter: a confocal microscopy study. *Glia*, 23(1), pp.1–10.

Kalaria, R.N., 2001. Advances in molecular genetics and pathology of cerebrovascular disorders. *Trends in neurosciences*, 24(7), pp.392–400.

Kalaria, R.N., 1999. The blood-brain barrier and cerebrovascular pathology in Alzheimer's disease. *Annals of the New York Academy of Sciences*, 893, pp.113–25.

Kalaria, R.N. & Pax, A.B., 1995. Increased collagen content of cerebral microvessels in Alzheimer's disease. *Brain research*, 705(1–2), pp.349–52.

Kalisch, B.E. et al., 1996. Differential action of 7-nitro indazole on rat brain nitric oxide synthase. *Neuroscience letters*, 219(2), pp.75–8.

Kamp, J. a. et al., 2014. Amyloid β in hereditary cerebral hemorrhage with amyloidosis-Dutch type. *Reviews in the neurosciences*, 25(5), pp.641–51.

Kanekiyo, T. et al., 2012. LRP1 in brain vascular smooth muscle cells mediates local clearance of Alzheimer's amyloid-β. *The Journal of neuroscience : the official journal of the Society for Neuroscience*, 32(46), pp.16458–65.

Kar, S. et al., 2004. Interactions between beta-amyloid and central cholinergic neurons: implications for Alzheimer's disease. *Journal of psychiatry & neuroscience : JPN*, 29(6), pp.427–41.

Kasashima, S. et al., 1999. Neurons with choline acetyltransferase immunoreactivity and mRNA are present in the human cerebral cortex. *Histochemistry and Cell Biology*, 111(3), pp.197–207.

Keable, A. et al., 2015. Deposition of amyloid β in the walls of human leptomeningeal arteries in relation to perivascular drainage pathways in cerebral amyloid angiopathy. *Biochimica et biophysica acta*.

Kelényi, G., 1967. Thioflavin S fluorescent and Congo red anisotropic stainings in the histologic demonstration of amyloid. *Acta neuropathologica*, 7(4), pp.336–48.

Kerbler, G.M. et al., 2013. Diffusion-weighted magnetic resonance imaging detection of basal forebrain cholinergic degeneration in a mouse model. *NeuroImage*, 66, pp.133–41.

Khan, U.A. et al., 2014. Molecular drivers and cortical spread of lateral entorhinal cortex dysfunction in preclinical Alzheimer's disease. *Nature neuroscience*, 17(2), pp.304–11.

Kim, K.J. et al., 2015. Astrocyte contributions to flow/pressure-evoked parenchymal arteriole vasoconstriction. *The Journal of neuroscience : the official journal of the Society for Neuroscience*, 35(21), pp.8245–57.

Kim, K.J. et al., 2016. Vasculo-Neuronal Coupling: Retrograde Vascular Communication to Brain Neurons. *The Journal of neuroscience : the official journal of the Society for Neuroscience*, 36(50), pp.12624–12639.

Kimelberg, H.K., 2004. The problem of astrocyte identity. *Neurochemistry international*, 45(2–3), pp.191–202.

Kitt, C.A. et al., 1994. Cholinergic innervation of mouse forebrain structures. *The Journal of comparative neurology*, 341(1), pp.117–29.

Klohs, J. et al., 2014. Imaging of cerebrovascular pathology in animal models of Alzheimer's disease. *Frontiers in aging neuroscience*, 6(March), p.32.

Knudsen, K. a. et al., 2001. Clinical diagnosis of cerebral amyloid angiopathy: validation of the

Boston criteria. *Neurology*, 56(4), pp.537–9.

Könnecke, H. & Bechmann, I., 2013. The role of microglia and matrix metalloproteinases involvement in neuroinflammation and gliomas. *Clinical & developmental immunology*, 2013, p.914104.

Kress, B.T. et al., 2014. Impairment of paravascular clearance pathways in the aging brain. *Annals of neurology*, 76(6), pp.845–61.

Kuga, N. et al., 2009. Rapid and local autoregulation of cerebrovascular blood flow: a deep-brain imaging study in the mouse. *The Journal of physiology*, 587(Pt 4), pp.745–752.

Kuznetsova, E. & Schliebs, R., 2013. β-Amyloid, cholinergic transmission, and cerebrovascular system -- a developmental study in a mouse model of Alzheimer's disease. *Current pharmaceutical design*, 19(38), pp.6749–65.

de la Torre, J.C., 2000. Critically attained threshold of cerebral hypoperfusion: can it cause Alzheimer's disease? *Annals of the New York Academy of Sciences*, 903, pp.424–436.

Lacalle-Aurioles, M. et al., 2014. Cerebral Blood Flow is an Earlier Indicator of Perfusion Abnormalities than Cerebral Blood Volume in Alzheimer's Disease. *Journal of Cerebral Blood Flow & Metabolism*, 34(4), pp.654–659.

Laursen, B. et al., 2013. Cholinergic degeneration is associated with increased plaque deposition and cognitive impairment in APPswe/PS1dE9 mice. *Behavioural brain research*, 240(1), pp.146–52.

Leanza, G., 1998. Chronic elevation of amyloid precursor protein expression in the neocortex and hippocampus of rats with selective cholinergic lesions. *Neuroscience letters*, 257(1), pp.53–6.

Leclercq, P.D. et al., 2005. Cerebral amyloid angiopathy in traumatic brain injury: association with apolipoprotein E genotype. *Journal of neurology, neurosurgery, and psychiatry*, 76(2), pp.229–33.

Lecrux, C. et al., 2017. Impact of altered cholinergic tones on the neurovascular coupling response to whisker stimulation. *The Journal of Neuroscience*, 37(6), pp.1784–16.

Lecrux, C. et al., 2011. Pyramidal neurons are "neurogenic hubs" in the neurovascular coupling response to whisker stimulation. *The Journal of neuroscience : the official journal of the Society for Neuroscience*, 31(27), pp.9836–47.

Lecrux, C. & Hamel, E., 2011. The neurovascular unit in brain function and disease. *Acta Physiologica*, 203(1), pp.47–59.

Lehmann, O. et al., 2002. 5,7-DHT-induced hippocampal 5-HT depletion attenuates behavioural deficits produced by 192 IgG-saporin lesions of septal cholinergic neurons in the rat. *The European journal of neuroscience*, 15(12), pp.1991–2006.

Li, W. et al., 2012. Changes in regional cerebral blood flow and functional connectivity in the cholinergic pathway associated with cognitive performance in subjects with mild Alzheimer's disease after 12-week donepezil treatment. *NeuroImage*, 60(2), pp.1083–91.

Li, X. et al., 2017. Generation of a whole-brain atlas for the cholinergic system and mesoscopic projectome analysis of basal forebrain cholinergic neurons. *Proceedings of the National Academy of Sciences*, 115(2), p.201703601.

Librizzi, L., Folco, G. & de Curtis, M., 2000. Nitric oxide synthase inhibitors unmask acetylcholine-mediated constriction of cerebral vessels in the in vitro isolated guinea-pig brain. *Neuroscience*, 101(2), pp.283–7.

Van Lieshout, J.J. et al., 2003. Syncope, cerebral perfusion, and oxygenation. *Journal of applied*

physiology (Bethesda, Md. : 1985), 94(3), pp.833–48.

Lin, L. et al., 1999. Cognitive changes and modified processing of amyloid precursor protein in the cortical and hippocampal system after cholinergic synapse loss and muscarinic receptor activation. *Proceedings of the National Academy of Sciences of the United States of America*, 96(21), pp.12108–13.

Lin, S.-C. et al., 2015. Optogenetic Dissection of the Basal Forebrain Neuromodulatory Control of Cortical Activation, Plasticity, and Cognition. *Journal of Neuroscience*, 35(41), pp.13896–13903.

Lincoln, J., 1995. Innervation of cerebral arteries by nerves containing 5-hydroxytryptamine and noradrenaline. *Pharmacology & therapeutics*, 68(3), pp.473–501.

Lind, B.L. et al., 2013. Rapid stimulus-evoked astrocyte Ca2+ elevations and hemodynamic responses in mouse somatosensory cortex in vivo. *Proceedings of the National Academy of Sciences of the United States of America*, 110(48), pp.E4678-87.

Liu, T.T. & Brown, G.G., 2007. Measurement of cerebral perfusion with arterial spin labeling: Part 1. Methods. *Journal of the International Neuropsychological Society : JINS*, 13(3), pp.517–25.

Liu, X. et al., 2012. Relative contribution of cyclooxygenases, epoxyeicosatrienoic acids, and pH to the cerebral blood flow response to vibrissal stimulation. *American journal of physiology. Heart and circulatory physiology*, 302(5), pp.H1075-85.

López, O.L. & DeKosky, S.T., 2008. Clinical symptoms in Alzheimer's disease. In *Handbook of clinical neurology*. pp. 207–216.

Lou, N. et al., 2016. Purinergic receptor P2RY12-dependent microglial closure of the injured blood–brain barrier. *Proceedings of the National Academy of Sciences*, 113(4), pp.1074–1079.

Lourenço, C.F. et al., 2018. Age-dependent impairment of neurovascular and neurometabolic coupling in the hippocampus. *Frontiers in Physiology*, 9(JUL), pp.1–11.

Lourenço, C.F. et al., 2017. Neurovascular-neuroenergetic coupling axis in the brain: master regulation by nitric oxide and consequences in aging and neurodegeneration. *Free radical biology & medicine*, 108(July 2016), pp.668–682.

Lourenço, C.F. et al., 2014. Neurovascular coupling in hippocampus is mediated via diffusion by neuronal-derived nitric oxide. *Free radical biology & medicine*, 73, pp.421–9.

Louveau, A. et al., 2015. Structural and functional features of central nervous system lymphatic vessels. *Nature*, 523(7560), pp.337–41.

Lovick, T.A., Brown, L.A. & Key, B.J., 1999. Neurovascular relationships in hippocampal slices: Physiological and anatomical studies of mechanisms underlying flow-metabolism coupling in intraparenchymal microvessels. *Neuroscience*, 92(1), pp.47–60.

Luff, S.E., 1996. Ultrastructure of sympathetic axons and their structural relationship with vascular smooth muscle. *Anatomy and embryology*, 193(6), pp.515–31.

Luiten, P.G. et al., 1996. Ultrastructural localization of cholinergic muscarinic receptors in rat brain cortical capillaries. *Brain research*, 720(1–2), pp.225–229.

Lüth, H.J., Münch, G. & Arendt, T., 2002. Aberrant expression of NOS isoforms in Alzheimer's disease is structurally related to nitrotyrosine formation. *Brain Research*, 953(1–2), pp.135–143.

Ma, Q. et al., 2018. Rapid lymphatic efflux limits cerebrospinal fluid flow to the brain. *Acta*

neuropathologica, (0123456789).

Mackic, J.B. et al., 1998. Human blood-brain barrier receptors for Alzheimer's amyloid-beta 1- 40. Asymmetrical binding, endocytosis, and transcytosis at the apical side of brain microvascular endothelial cell monolayer. *The Journal of clinical investigation*, 102(4), pp.734–43.

Magaki, S. et al., 2018. The effects of cerebral amyloid angiopathy on integrity of the blood-brain barrier. *Neurobiology of aging*, 70(7387), pp.70–77.

Maggio, P. et al., 2013. Does hypercapnia-induced impairment of cerebral autoregulation affect neurovascular coupling? A functional TCD study. *Journal of applied physiology (Bethesda, Md. : 1985)*, 115(0), pp.491–7.

Maki, T. et al., 2014. Phosphodiesterase III inhibitor promotes drainage of cerebrovascular β-amyloid. *Annals of clinical and translational neurology*, 1(8), pp.519–33.

Manicam, C. et al., 2016. The Gatekeepers in the Mouse Ophthalmic Artery: Endothelium-Dependent Mechanisms of Cholinergic Vasodilation. *Scientific reports*, 6(October 2015), p.20322.

Mann, D.M., Yates, P.O. & Marcyniuk, B., 1984. A comparison of changes in the nucleus basalis and locus caeruleus in Alzheimer's disease. *Journal of neurology, neurosurgery, and psychiatry*, 47(2), pp.201–3.

Mann, D.M.A. et al., 2018. Patterns and severity of vascular amyloid in Alzheimer's disease associated with duplications and missense mutations in APP gene, Down syndrome and sporadic Alzheimer's disease. *Acta neuropathologica*, pp.1–19.

Di Marco, L.Y. et al., 2015. Is vasomotion in cerebral arteries impaired in Alzheimer's disease? *Journal of Alzheimer's Disease*, 46(1), pp.35–53.

Mateo, C. et al., 2017. Entrainment of Arteriole Vasomotor Fluctuations by Neural Activity Is a Basis of Blood-Oxygenation-Level-Dependent "Resting-State" Connectivity. *Neuron*, 96(4), p.936–948.e3.

McConnell, H.L. et al., 2017. The Translational Significance of the Neurovascular Unit. *The Journal of biological chemistry*, 292(3), pp.762–770.

McGinty, J.F., Milner, T. a & Loy, R., 1982. Association of sympathetic axons in denervated hippocampus to intracerebral vasculature. I. Fluorescence histochemistry combining glyoxylic acid and pontamine sky blue. *Anatomy and embryology*, 164(1), pp.95–100.

McKeever, P.M. et al., 2017. Cholinergic neuron gene expression differences captured by translational profiling in a mouse model of Alzheimer's disease. *Neurobiology of aging*, 57(2017), pp.104–119.

McNeely, A.A. et al., 2015. Cholinergic subcortical hyperintensities in Alzheimer's disease patients from the Sunnybrook Dementia Study: relationships with cognitive dysfunction and hippocampal atrophy. *Journal of Alzheimer's disease : JAD*, 43(3), pp.785–96.

Melnikova, T. et al., 2013. Reversible pathologic and cognitive phenotypes in an inducible model of Alzheimer-amyloidosis. *The Journal of neuroscience : the official journal of the Society for Neuroscience*, 33(9), pp.3765–79.

Meretoja, A. et al., 2012. SMASH-U: a proposal for etiologic classification of intracerebral hemorrhage. *Stroke; a journal of cerebral circulation*, 43(10), pp.2592–7.

Merlini, M., Wanner, D. & Nitsch, R.M., 2016. Tau pathology-dependent remodelling of cerebral arteries precedes Alzheimer's disease-related microvascular cerebral amyloid angiopathy. *Acta neuropathologica*, 131(5), pp.737–52.

Mesulam, M.., 2013. Cholinergic circuitry of the human nucleus basalis and its fate in Alzheimer's disease. *The Journal of comparative neurology*, 521(18), pp.4124–44.

Mesulam, M.. & Geula, C., 1988. Nucleus basalis (Ch4) and cortical cholinergic innervation in the human brain: Observations based on the distribution of acetylcholinesterase and choline acetyltransferase. *Journal of Comparative Neurology*, 275(2), pp.216–240.

Mesulam, M.M., Mufson, E.J., et al., 1983. Central cholinergic pathways in the rat: An overview based on an alternative nomenclature (Ch1-Ch6). *Neuroscience*, 10(4), pp.1185–1201.

Mesulam, M.M., Mufson, E.J., et al., 1983. Cholinergic innervation of cortex by the basal forebrain: Cytochemistry and cortical connections of the septal area, diagonal band nuclei, nucleus basalis (Substantia innominata), and hypothalamus in the rhesus monkey. *The Journal of Comparative Neurology*, 214(2), pp.170–197.

Metherate, R. & Ashe, J.H., 1993. Nucleus basalis stimulation facilitates thalamocortical synaptic transmission in the rat auditory cortex. *Synapse (New York, N.Y.)*, 14(2), pp.132–43.

Michalski, D. et al., 2017. Neurovascular Specifications in the Alzheimer-Like Brain of Mice Affected by Focal Cerebral Ischemia: Implications for Future Therapies. *Journal of Alzheimer's Disease*, 59(2), pp.655–674.

Miners, J.S. et al., 2008. Angiotensin-converting enzyme (ACE) levels and activity in Alzheimer's disease, and relationship of perivascular ACE-1 to cerebral amyloid angiopathy. *Neuropathology and Applied Neurobiology*, 34(2), pp.181–193.

Miners, J.S. et al., 2014. Aβ degradation or cerebral perfusion? Divergent effects of multifunctional enzymes. *Frontiers in aging neuroscience*, 6(September), p.238.

Miners, J.S., Palmer, J.C. & Love, S., 2015. Pathophysiology of hypoperfusion of the precuneus in early Alzheimer's disease. *Brain pathology (Zurich, Switzerland)*, p.n/a-n/a.

Miravalle, L. et al., 2000. Substitutions at codon 22 of Alzheimer's Aβ peptide induce diverse conformational changes and apoptotic effects human cerebral endothelial cells. *Journal of Biological Chemistry*, 275(35), pp.27110–27116.

Mishra, A. et al., 2016. Astrocytes mediate neurovascular signaling to capillary pericytes but not to arterioles. *Nature neuroscience*, 19(12), pp.1619–1627.

Mishra, A., 2016. Binaural blood flow control by astrocytes: listening to synapses and the vasculature. *The Journal of physiology*, 58(12), pp.7250–7.

Moore, P.K. et al., 1993. Characterization of the novel nitric oxide synthase inhibitor 7- nitro indazole and related indazoles: antinociceptive and cardiovascular effects. *British Journal of Pharmacology*, 110(1), pp.219–224.

Morris, A.W.J. et al., 2014. The Cerebrovascular Basement Membrane: Role in the Clearance of β-amyloid and Cerebral Amyloid Angiopathy. *Frontiers in aging neuroscience*, 6(September), p.251.

Morris, A.W.J. et al., 2016. Vascular basement membranes as pathways for the passage of fluid into and out of the brain. *Acta neuropathologica*, 131(5), pp.725–36.

Mulligan, S.J. & MacVicar, B. a, 2004. Calcium transients in astrocyte endfeet cause cerebrovascular constrictions. *Nature*, 431(7005), pp.195–9.

Muñoz, M.F., Puebla, M. & Figueroa, X.F., 2015. Control of the neurovascular coupling by nitric oxide-dependent regulation of astrocytic Ca2+ signaling. *Frontiers in Cellular Neuroscience*, 9(March), pp.1–9.

Murray, M.E. et al., 2011. Neuropathologically defined subtypes of Alzheimer's disease with

distinct clinical characteristics: a retrospective study. *The Lancet. Neurology*, 10(9), pp.785–96.

Namba, H. et al., 1991. Lesion of the nucleus basalis magnocellularis does not affect cerebral cortical blood flow in rats. *Neuroscience Research*, 12(3), pp.463–467.

Nawaratne, V. et al., 2008. New insights into the function of M4 muscarinic acetylcholine receptors gained using a novel allosteric modulator and a DREADD (designer receptor exclusively activated by a designer drug). *Molecular pharmacology*, 74(4), pp.1119–31.

Nelson, A.R., Kolasa, K. & McMahon, L.L., 2014. Noradrenergic sympathetic sprouting and cholinergic reinnervation maintains non-amyloidogenic processing of AβPP. *Journal of Alzheimer's disease : JAD*, 38(4), pp.867–79.

Nimmerjahn, A., Kirchhoff, F. & Helmchen, F., 2005. Resting microglial cells are highly dynamic surveillants of brain parenchyma in vivo. *Science (New York, N.Y.)*, 308(5726), pp.1314–8.

Nizari, S., Romero, I.A. & Hawkes, C.A., 2017. The role of perivascular innervation and neurally mediated vasoreactivity in the pathophysiology of Alzheimer's disease. *Clinical science (London, England : 1979)*, 131(12), pp.1207–1214.

Obici, L. et al., 2005. A novel AβPP mutation exclusively associated with cerebral amyloid angiopathy. *Annals of Neurology*, 58(4), pp.639–644.

Ogawa, S. et al., 1990. Brain magnetic resonance imaging with contrast dependent on blood oxygenation. *Proceedings of the National Academy of Sciences of the United States of America*, 87(24), pp.9868–72.

Oishi, K., Kamiyashiki, T. & Ito, Y., 2007. Isometric contraction of microvascular pericytes from mouse brain parenchyma. *Microvascular Research*, 73(1), pp.20–28.

Ongali, B. et al., 2010. Transgenic mice overexpressing APP and transforming growth factor-beta1 feature cognitive and vascular hallmarks of Alzheimer's disease. *The American journal of pathology*, 177(6), pp.3071–80.

Oomen, C.A. et al., 2009. Resveratrol preserves cerebrovascular density and cognitive function in aging mice. *Frontiers in Aging Neuroscience*, 1(DEC), pp.1–9.

van Opstal, A.M. et al., 2016. Cerebrovascular function in presymptomatic and symptomatic individuals with hereditary cerebral amyloid angiopathy: a case-control study. *Lancet Neurology*, 4422(16), pp.1–8.

Palmer, a M. et al., 1987. Presynaptic serotonergic dysfunction in patients with Alzheimer's disease. *Journal of neurochemistry*, 48(1), pp.8–15.

Palmer, J.C., Kehoe, P.G. & Love, S., 2010. Endothelin-converting enzyme-1 in Alzheimer's disease and vascular dementia. *Neuropathology and applied neurobiology*, 36(6), pp.487–97.

Park, K.S. et al., 2018. Deep brain optical coherence tomography angiography in mice: in vivo, noninvasive imaging of hippocampal formation. *Scientific Reports*, 8(1), pp.1–7.

Park, L. et al., 2014. Age-dependent neurovascular dysfunction and damage in a mouse model of cerebral amyloid angiopathy. *Stroke*, 45(6), pp.1815–21.

Partyka, P.P. et al., 2017. Mechanical stress regulates transport in a compliant 3D model of the blood-brain barrier. *Biomaterials*, 115, pp.30–39.

Peng, W. et al., 2016. Suppression of glymphatic fluid transport in a mouse model of Alzheimer's disease. *Neurobiology of disease*, 93, pp.215–25.

Perez, S.E. et al., 2007. Cholinergic forebrain degeneration in the APPswe/PS1DeltaE9 transgenic mouse. *Neurobiology of disease*, 28(1), pp.3–15.

Perry, E.K. et al., 1995. Alteration in nicotine binding sites in Parkinson's disease, Lewy body dementia and Alzheimer's disease: Possible index of early neuropathology. *Neuroscience*, 64(2), pp.385–395.

Perry, E.K., 1980. The cholinergic system in old age and Alzheimer's disease. *Age and ageing*, 9(1), pp.1–8.

Perry, T.A., Hodges, H. & Gray, J.A., 2001. Behavioural, histological and immunocytochemical consequences following 192 IgG-saporin immunolesions of the basal forebrain cholinergic system. *Brain Research Bulletin*, 54(1), pp.29–48.

Petzold, G.C. et al., 2008. Coupling of neural activity to blood flow in olfactory glomeruli is mediated by astrocytic pathways. *Neuron*, 58(6), pp.897–910.

Pey, P. et al., 2014. Phenotypic profile of alternative activation marker CD163 is different in Alzheimer's and Parkinson's disease. *Acta neuropathologica communications*, 2(1), p.21.

Pezzini, A. et al., 2009. Cerebral Amyloid Angiopathy: A Common Cause of Cerebral Hemorrhage. *Current Medicinal Chemistry*, 16(20), pp.2498–2513.

Pfeifer, L. a et al., 2002. Cerebral amyloid angiopathy and cognitive function: the HAAS autopsy study. *Neurology*, 58(11), pp.1629–34.

Poulakis, K. et al., 2018. Heterogeneous patterns of brain atrophy in Alzheimer's disease. *Neurobiology of aging*, 65(2018), pp.98–108.

Pradhan, R.K. & Chakravarthy, V.S., 2011. Informational dynamics of vasomotion in microvascular networks: A review. *Acta Physiologica*, 201(2), pp.193–218.

Preston, S.D. et al., 2003. Capillary and arterial cerebral amyloid angiopathy in Alzheimer's disease: defining the perivascular route for the elimination of amyloid beta from the human brain. *Neuropathology and applied neurobiology*, 29(2), pp.106–17.

Prince, M. et al., 2014. *Dementia UK: Update*,

Puzzo, D. et al., 2015. The keystone of Alzheimer pathogenesis might be sought in Aβ physiology. *Neuroscience*, 307, pp.26–36.

Qian, J. et al., 2010. Role of local production of endothelium-derived nitric oxide on cGMP signaling and S-nitrosylation. *American journal of physiology. Heart and circulatory physiology*, 298(1), pp.H112-8.

Qian, L. et al., 2018. Removal of p75 Neurotrophin Receptor Expression from Cholinergic Basal Forebrain Neurons Reduces Amyloid-β Plaque Deposition and Cognitive Impairment in Aged APP/PS1 Mice. *Molecular neurobiology*, pp.36–41.

Qosa, H. et al., 2014. Differences in amyloid-β clearance across mouse and human blood-brain barrier models: kinetic analysis and mechanistic modeling. *Neuropharmacology*, 79, pp.668–78.

Raignault, A. et al., 2017. Pulse pressure-dependent cerebrovascular eNOS regulation in mice. *Journal of cerebral blood flow and metabolism : official journal of the International Society of Cerebral Blood Flow and Metabolism*, 37(2), pp.413–424.

Ramirez, J. et al., 2015. Visible virchow-robin spaces on magnetic resonance imaging of Alzheimer's disease patients and normal elderly from the sunnybrook dementia study. *Journal of Alzheimer's disease : JAD*, 43(2), pp.415–24.

Ramos-Rodriguez, J.J. et al., 2013. Rapid β-amyloid deposition and cognitive impairment after cholinergic denervation in APP/PS1 mice. *Journal of neuropathology and experimental neurology*, 72(4), pp.272–85.

Reinikainen, K.J., Soininen, H. & Riekkinen, P.J., 1990. Neurotransmitter changes in Alzheimer's disease: implications to diagnostics and therapy. *Journal of neuroscience research*, 27(4), pp.576–86.

Rennels, M.L. et al., 1985. Evidence for a "Paravascular" fluid circulation in the mammalian central nervous system, provided by the rapid distribution of tracer protein throughout the brain from the subarachnoid space. *Brain Research*, 326(1), pp.47–63.

Rey, J. & Sarntinoranont, M., 2018. Pulsatile flow drivers in brain parenchyma and perivascular spaces: A resistance network model study. *Fluids and Barriers of the CNS*, 15(1), pp.1–11.

Rhodin, J.A.G., 1968. Ultrastructure of mammalian venous capillaries, venules, and small collecting veins. *Journal of Ultrastructure Research*, 25(5–6), pp.452–500.

Rikitake, Y. et al., 2005. Inhibition of Rho kinase (ROCK) leads to increased cerebral blood flow and stroke protection. *Stroke*, 36(10), pp.2251–7.

Rivadulla, C. et al., 2011. Vasomotion and neurovascular coupling in the visual thalamus in vivo. *PLoS ONE*, 6(12).

Rivera-Rivera, L.A. et al., 2016. 4D flow MRI for intracranial hemodynamics assessment in Alzheimer's disease. *Journal of cerebral blood flow and metabolism : official journal of the International Society of Cerebral Blood Flow and Metabolism*, 36(10), pp.1718–1730.

Roher, A.E. et al., 2003. Cortical and leptomeningeal cerebrovascular amyloid and white matter pathology in Alzheimer's disease. *Molecular medicine (Cambridge, Mass.)*, 9(3–4), pp.112–22.

Roher, A.E. et al., 2000. Cortical cholinergic denervation elicits vascular A beta deposition. *Annals of the New York Academy of Sciences*, 903(602), pp.366–73.

Román, G.C. & Kalaria, R.N., 2006. Vascular determinants of cholinergic deficits in Alzheimer disease and vascular dementia. *Neurobiology of aging*, 27(12), pp.1769–85.

Rosengarten, B. et al., 2006. Acetylcholine esterase inhibitor donepezil improves dynamic cerebrovascular regulation in Alzheimer patients. *Journal of neurology*, 253(1), pp.58–64.

Rosengarten, B. et al., 2009. Neurovascular coupling in Alzheimer patients: effect of acetylcholine-esterase inhibitors. *Neurobiology of aging*, 30(12), pp.1918–23.

Rouach, N. et al., 2008. Astroglial metabolic networks sustain hippocampal synaptic transmission. *Science (New York, N.Y.)*, 322(5907), pp.1551–5.

Rungta, R.L. et al., 2018. Vascular Compartmentalization of Functional Hyperemia from the Synapse to the Pia. *Neuron*, pp.362–375.

Rusinek, H. et al., 2011. Hippocampal blood flow in normal aging measured with arterial spin labeling at 3T. *Magnetic Resonance in Medicine*, 65(1), pp.128–137.

Rye, D.B. et al., 1984. Cortical projections arising from the basal forebrain: a study of cholinergic and noncholinergic components employing combined retrograde tracing and immunohistochemical localization of choline acetyltransferase. *Neuroscience*, 13(3), pp.627–43.

Sato, A. & Sato, Y., 1995. Cholinergic neural regulation of regional cerebral blood flow. *Alzheimer disease and associated disorders*, 9(1), pp.28–38.

Sato, A., Sato, Y. & Uchida, S., 2004. Activation of the intracerebral cholinergic nerve fibers originating in the basal forebrain increases regional cerebral blood flow in the rat's cortex and hippocampus. *Neuroscience letters*, 361(1–3), pp.90–3.

Sato, A., Sato, Y. & Uchida, S., 2002. Regulation of cerebral cortical blood flow by the basal

forebrain cholinergic fibers and aging. *Autonomic neuroscience : basic & clinical*, 96(1), pp.13–9.

Scheiderer, C.L. et al., 2006. Sympathetic sprouting drives hippocampal cholinergic reinnervation that prevents loss of a muscarinic receptor-dependent long-term depression at CA3-CA1 synapses. *The Journal of neuroscience : the official journal of the Society for Neuroscience*, 26(14), pp.3745–56.

Schley, D. et al., 2006. Mechanisms to explain the reverse perivascular transport of solutes out of the brain. *Journal of theoretical biology*, 238(4), pp.962–74.

Schliebs, R. & Arendt, T., 2011. The cholinergic system in aging and neuronal degeneration. *Behavioural brain research*, 221(2), pp.555–63.

Schmitz, T.W., Nathan Spreng, R. & Alzheimer's Disease Neuroimaging Initiative, 2016. Basal forebrain degeneration precedes and predicts the cortical spread of Alzheimer's pathology. *Nature communications*, 7(Pt 2), p.13249.

Sehba, F.A. et al., 2000. Acute decrease in cerebral nitric oxide levels after subarachnoid hemorrhage. *Journal of cerebral blood flow and metabolism : official journal of the International Society of Cerebral Blood Flow and Metabolism*, 20(3), pp.604–11.

Selden, N.R. et al., 1998. Trajectories of cholinergic pathways within the cerebral hemispheres of the human brain. *Brain : a journal of neurology*, 121 (Pt 1, pp.2249–57.

Sercombe, R. et al., 1990. Amine-induced responses of pial and penetrating cerebral arteries: evidence for heterogeneous responses. *Journal of cerebral blood flow and metabolism : official journal of the International Society of Cerebral Blood Flow and Metabolism*, 10(6), pp.808–18.

Serrano-Pozo, A. et al., 2011. Neuropathological alterations in Alzheimer disease. *Cold Spring Harbor perspectives in medicine*, 1(1), p.a006189.

Sessa, W.C. et al., 1993. Genomic analysis and expression patterns reveal distinct genes for endothelial and brain nitric oxide synthase. *Hypertension*, 21(6), pp.934–938.

Sharp, M.K. et al., 2016. Peristalsis with Oscillating Flow Resistance: A Mechanism for Periarterial Clearance of Amyloid Beta from the Brain. *Annals of biomedical engineering*, 44(5), pp.1553–65.

Shibata, M. et al., 2000. Clearance of Alzheimer's amyloid-ss(1-40) peptide from brain by LDL receptor-related protein-1 at the blood-brain barrier. *The Journal of clinical investigation*, 106(12), pp.1489–99.

Shimohama, S. et al., 2000. Activation of NADPH oxidase in Alzheimer's disease brains. *Biochemical and Biophysical Research Communications*, 273(1), pp.5–9.

Shin, H.K. et al., 2007. Rho-kinase inhibition acutely augments blood flow in focal cerebral ischemia via endothelial mechanisms. *Journal of cerebral blood flow and metabolism : official journal of the International Society of Cerebral Blood Flow and Metabolism*, 27(5), pp.998–1009.

Shu, X. et al., 2015. Endothelial nitric oxide synthase in the microcirculation. *Cellular and molecular life sciences : CMLS*, 72(23), pp.4561–75.

Simic, G. et al., 2014. Early failure of the default-mode network and the pathogenesis of Alzheimer's disease. *CNS neuroscience & therapeutics*, 20(7), pp.692–8.

Sinha, S. & Lieberburg, I., 1999. Cellular mechanisms of beta-amyloid production and secretion. *Proceedings of the National Academy of Sciences of the United States of America*, 96(20), pp.11049–53.

Smith, A.J. et al., 2017. Test of the 'glymphatic' hypothesis demonstrates diffusive and aquaporin-4-independent solute transport in rodent brain parenchyma. *eLife*, 6, pp.1–16.

Smith, A.J. & Verkman, A.S., 2018. The "glymphatic" mechanism for solute clearance in Alzheimer's disease: Game changer or unproven speculation? *FASEB Journal*, 32(2), pp.543–551.

Sobreviela, T. et al., 1994. TrkA-immunoreactive profiles in the central nervous system: colocalization with neurons containing p75 nerve growth factor receptor, choline acetyltransferase, and serotonin. *The Journal of comparative neurology*, 350(4), pp.587–611.

Sobreviela, T. & Mufson, E.J., 1995. Reduced nicotinamide adenine dinucleotide phosphate-diaphorase/nitric oxide synthase profiles in the human hippocampal formation and perirhinal cortex. *Journal Of Comparative Neurology*, 358(3), pp.440–464.

Sorger, D. et al., 1999. Iodo-QNB cortical binding and brain perfusion: Effects of a cholinergic basal forebrain lesion in the rat. *Nuclear Medicine and Biology*, 26(1), pp.9–16.

van der Staay, F.J. et al., 1989. Selective fimbria lesions impair acquisition of working and reference memory of rats in a complex spatial discrimination task. *Behavioural brain research*, 32(2), pp.151–61.

Steininger, T.L. et al., 1993. High-affinity nerve growth factor receptor (Trk) immunoreactivity is localized in cholinergic neurons of the basal forebrain and striatum in the adult rat brain. *Brain Research*, 612(1–2), pp.330–335.

Stella, N. et al., 1994. Glutamate-evoked release of arachidonic acid from mouse brain astrocytes. *The Journal of neuroscience : the official journal of the Society for Neuroscience*, 14(2), pp.568–75.

Stobart, J.L.L. et al., 2013. Astrocyte-induced cortical vasodilation is mediated by D-serine and endothelial nitric oxide synthase. *Proceedings of the National Academy of Sciences*, 110(8), pp.3149–3154.

Streit, W.J. et al., 2004. Dystrophic microglia in the aging human brain. *Glia*, 45(2), pp.208–12.

Streit, W.J., 2004. Microglia and Alzheimer's disease pathogenesis. *Journal of neuroscience research*, 77(1), pp.1–8.

Suzuki, N. et al., 1994. High tissue content of soluble beta 1-40 is linked to cerebral amyloid angiopathy. *The American journal of pathology*, 145(2), pp.452–60.

Svensson, A.L., Alafuzoff, I. & Nordberg, A., 1992. Characterization of muscarinic receptor subtypes in Alzheimer and control brain cortices by selective muscarinic antagonists. *Brain research*, 596(1–2), pp.142–8.

Szot, P. et al., 2006. Compensatory changes in the noradrenergic nervous system in the locus ceruleus and hippocampus of postmortem subjects with Alzheimer's disease and dementia with Lewy bodies. *The Journal of neuroscience : the official journal of the Society for Neuroscience*, 26(2), pp.467–78.

Tajima, Y. et al., 2014. Changes in cortical microvasculature during misery perfusion measured by two-photon laser scanning microscopy. *Journal of Cerebral Blood Flow & Metabolism*, 34(8), pp.1363–1372.

Tan, X.-L. et al., 2015. Partial eNOS deficiency causes spontaneous thrombotic cerebral infarction, amyloid angiopathy and cognitive impairment. *Molecular Neurodegeneration*, 10(1), p.24.

Tanzi, R.E. & Bertram, L., 2005. Twenty years of the Alzheimer's disease amyloid hypothesis: a genetic perspective. *Cell*, 120(4), pp.545–55.

Tarasoff-Conway, J.M. et al., 2015. Clearance systems in the brain-implications for Alzheimer disease. *Nature reviews. Neurology*, 11(8), pp.457–70.

Teipel, S. et al., 2014. Cholinergic basal forebrain atrophy predicts amyloid burden in Alzheimer's disease. *Neurobiology of aging*, 35(3), pp.482–91.

Terry, A. V & Buccafusco, J.J., 2003. The cholinergic hypothesis of age and Alzheimer's disease-related cognitive deficits: recent challenges and their implications for novel drug development. *The Journal of pharmacology and experimental therapeutics*, 306(3), pp.821–7.

Thal, D.R., Grinberg, L.T. & Attems, J., 2012. Vascular dementia: different forms of vessel disorders contribute to the development of dementia in the elderly brain. *Experimental gerontology*, 47(11), pp.816–24.

Thorin-Trescases, N. et al., 2018. The impact of pulse pressure on cerebrovascular events leading to age-related cognitive decline. *American Journal of Physiology-Heart and Circulatory Physiology*, (69), p.ajpheart.00637.2017.

Thorin, E., 2001. Influence of nitric oxide synthase inhibition and endothelin-1 receptor blockade on acetylcholine-induced coronary artery contraction in vitro in dilated and ischemic cardiomyopathies. *Journal of cardiovascular pharmacology*, 38(1), pp.90–8.

Thorns, V., Hansen, L. & Masliah, E., 1998. nNOS expressing neurons in the entorhinal cortex and hippocampus are affected in patients with Alzheimer's disease. *Experimental neurology*, 150(1), pp.14–20.

Tian, J. et al., 2003. Negative association between amyloid plaques and cerebral amyloid angiopathy in Alzheimer's disease. *Neuroscience letters*, 352(2), pp.137–40.

Tian, J. et al., 2004. Relationships between arteriosclerosis, cerebral amyloid angiopathy and myelin loss from cerebral cortical white matter in Alzheimer's disease. *Neuropathology and applied neurobiology*, 30(1), pp.46–56.

Tikka, S. et al., 2009. Congruence between NOTCH3 mutations and GOM in 131 CADASIL patients. *Brain*, 132(4), pp.933–939.

Toda, N., Ayajiki, K. & Okamura, T., 1996. Hypercapnia relaxes cerebral arteries and potentiates neurally-induced relaxation. *Journal of cerebral blood flow and metabolism : official journal of the International Society of Cerebral Blood Flow and Metabolism*, 16(5), pp.1068–74.

Tong, X.K. & Hamel, E., 1999. Regional cholinergic denervation of cortical microvessels and nitric oxide synthase-containing neurons in Alzheimer's disease. *Neuroscience*, 92(1), pp.163–75.

Toribatake, Y. et al., 1997. Regulation of vasomotion of arterioles and capillaries in the cat spinal cord: role of alpha actin and endothelin-1. *Spinal cord*, 35(1), pp.26–32.

Triggle, C.R. et al., 2012. The endothelium: influencing vascular smooth muscle in many ways. *Canadian Journal of Physiology and Pharmacology*, 90(6), pp.713–738.

Vaucher, E. & Hamel, E., 1995. Cholinergic basal forebrain neurons project to cortical microvessels in the rat: electron microscopic study with anterogradely transported Phaseolus vulgaris leucoagglutinin and choline acetyltransferase immunocytochemistry. *The Journal of neuroscience : the official journal of the Society for Neuroscience*, 15(11), pp.7427–41.

Vaucher, E., Linville, D. & Hamel, E., 1997. Cholinergic basal forebrain projections to nitric oxide synthase-containing neurons in the rat cerebral cortex. *Neuroscience*, 79(3), pp.827–36.

Verbeek, M.M. et al., 2009. Cerebrospinal fluid amyloid beta(40) is decreased in cerebral amyloid angiopathy. *Annals of neurology*, 66(2), pp.245–9.

Vinters, H. V. et al., 2018. Review: Vascular dementia: clinicopathologic and genetic considerations. *Neuropathology and Applied Neurobiology*, 44(3), pp.247–266.

Vinters, H. V, 1987. Cerebral amyloid angiopathy. A critical review. *Stroke; a journal of cerebral circulation*, 18(2), pp.311–24.

Wainer, B.H. et al., 1993. Chapter 2: Ascending cholinergic pathways: functional organization and implications for disease models. In *Progress in Brain Research*. pp. 9–30.

Waite, J.J., Holschneider, D.P. & Scremin, O.U., 1999. Selective immunotoxin-induced cholinergic deafferentation alters blood flow distribution in the cerebral cortex. *Brain research*, 818(1), pp.1–11.

Wang, W. et al., 2013. Simvastatin Ameliorates Liver Fibrosis via Mediating Nitric Oxide Synthase in Rats with Non-Alcoholic Steatohepatitis-Related Liver Fibrosis. *PLoS ONE*, 8(10), pp.1–11.

Ward, M.E. et al., 2005. Hypoxia induces a functionally significant and translationally efficient neuronal NO synthase mRNA variant. *Journal of Clinical Investigation*, 115(11), pp.3128–3139.

Weller, R.O., Preston, S.D., et al., 2009. Cerebral amyloid angiopathy in the aetiology and immunotherapy of Alzheimer disease. *Alzheimer's research & therapy*, 1(2), p.6.

Weller, R.O., Djuanda, E., et al., 2009. Lymphatic drainage of the brain and the pathophysiology of neurological disease. *Acta neuropathologica*, 117(1), pp.1–14.

Weller, R.O. et al., 2008. Perivascular drainage of amyloid-beta peptides from the brain and its failure in cerebral amyloid angiopathy and Alzheimer's disease. *Brain pathology (Zurich, Switzerland)*, 18(2), pp.253–66.

Weller, R.O., Boche, D. & Nicoll, J. a R., 2009. Microvasculature changes and cerebral amyloid angiopathy in Alzheimer's disease and their potential impact on therapy. *Acta neuropathologica*, 118(1), pp.87–102.

Wells, J. a et al., 2015. Increased cerebral vascular reactivity in the tau expressing rTg4510 mouse: evidence against the role of tau pathology to impair vascular health in Alzheimer's disease. *Journal of cerebral blood flow and metabolism : official journal of the International Society of Cerebral Blood Flow and Metabolism*, 35(3), pp.359–62.

Whitehouse, P.J. et al., 1982. Alzheimer's disease and senile dementia: loss of neurons in the basal forebrain. *Science (New York, N.Y.)*, 215(4537), pp.1237–9.

Whitwell, J.L. et al., 2012. Neuroimaging correlates of pathologically defined subtypes of Alzheimer's disease: a case-control study. *The Lancet. Neurology*, 11(10), pp.868–77.

Wierenga, C.E., Hays, C.C. & Zlatar, Z.Z., 2014. Cerebral blood flow measured by arterial spin labeling MRI as a preclinical marker of Alzheimer's disease. *Journal of Alzheimer's disease : JAD*, 42 Suppl 4, pp.S411-9.

Wilcock, D.M. et al., 2004. Passive amyloid immunotherapy clears amyloid and transiently activates microglia in a transgenic mouse model of amyloid deposition. *The Journal of neuroscience : the official journal of the Society for Neuroscience*, 24(27), pp.6144–51.

Wilcock, D.M., Vitek, M.P. & Colton, C.A., 2009. Vascular amyloid alters astrocytic water and potassium channels in mouse models and humans with Alzheimer's disease. *Neuroscience*, 159(3), pp.1055–69.

Williams, R.J. et al., 2017. Identification of neurovascular changes associated with cerebral amyloid angiopathy from subject-specific hemodynamic response functions. *Journal of cerebral blood flow and metabolism : official journal of the International Society of Cerebral*

Blood Flow and Metabolism, 37(10), pp.3433–3445.

Willis, C.L. et al., 2006. Basal forebrain cholinergic lesions reduce heat shock protein 72 response but not pathology induced by the NMDA antagonist MK-801 in the rat cingulate cortex. *Neuroscience Letters*, 407(2), pp.112–117.

Wirth, M. et al., 2017. Divergent regional patterns of cerebral hypoperfusion and gray matter atrophy in mild cognitive impairment patients. *Journal of cerebral blood flow and metabolism : official journal of the International Society of Cerebral Blood Flow and Metabolism*, 37(3), pp.814–824.

Woolf, N.J. & Butcher, L.L., 2011. Cholinergic systems mediate action from movement to higher consciousness. *Behavioural Brain Research*, 221(2), pp.488–498.

World Health Organisation, 2011. *ICD-10 International Statistical Classification of Diseases and Related Health Problems*,

Wu, D.M. et al., 2003. Cholinergic regulation of pericyte-containing retinal microvessels. *American Journal of Physiology - Heart and Circulatory Physiology*, 284(6), pp.H2083–H2090.

Wu, H., Williams, J. & Nathans, J., 2014. Complete morphologies of basal forebrain cholinergic neurons in the mouse. *eLife*, 3(3), p.e02444.

Wyss-Coray, T. et al., 2000. Chronic overproduction of transforming growth factor-beta1 by astrocytes promotes Alzheimer's disease-like microvascular degeneration in transgenic mice. *The American journal of pathology*, 156(1), pp.139–50.

Xie, L. et al., 2013. Sleep drives metabolite clearance from the adult brain. *Science (New York, N.Y.)*, 342(6156), pp.373–7.

Xu, G. et al., 2007. Perfusion fMRI detects deficits in regional CBF during memory-encoding tasks in MCI subjects. *Neurology*, 69(17), pp.1650–6.

Xu, H.L. et al., 2004. Influence of the glia limitans on pial arteriolar relaxation in the rat. *American journal of physiology. Heart and circulatory physiology*, 287(1), pp.H331–H339.

Yaar, M. et al., 1997. Binding of beta-amyloid to the p75 neurotrophin receptor induces apoptosis. A possible mechanism for Alzheimer's disease. *The Journal of clinical investigation*, 100(9), pp.2333–40.

Yeo, T.T. et al., 1997. Absence of p75NTR causes increased basal forebrain cholinergic neuron size, choline acetyltransferase activity, and target innervation. *The Journal of neuroscience : the official journal of the Society for Neuroscience*, 17(20), pp.7594–605.

Yi, F. et al., 2015. Hippocampal "cholinergic interneurons" visualized with the choline acetyltransferase promoter: Anatomical distribution, intrinsic membrane properties, neurochemical characteristics, and capacity for cholinergic modulation. *Frontiers in Synaptic Neuroscience*, 7(MAR), pp.1–18.

Yoon, S., Zuccarello, M. & Rapoport, R.M., 2012. pCO2 and pH regulation of cerebral blood flow. *Frontiers in Physiology*, 3(September), pp.1–8.

Yuan, Z. et al., 2004. Evidence of nuclear localization of neuronal nitric oxide synthase in cultured astrocytes of rats. *Life Sciences*, 74(26), pp.3199–3209.

Zarow, C. et al., 1997. Vascular basement membrane pathology and Alzheimer's disease. *Annals of the New York Academy of Sciences*, 826, pp.147–60.

Zhang, E.T., Inman, C.B. & Weller, R.O., 1990. Interrelationships of the pia mater and the perivascular (Virchow-Robin) spaces in the human cerebrum. *Journal of anatomy*, 170(1),

pp.111–23.

Zhang, F., Xu, S. & Iadecola, C., 1995. Role of nitric oxide and acetylcholine in neocortical hyperemia elicited by basal forebrain stimulation: evidence for an involvement of endothelial nitric oxide. *Neuroscience*, 69(4), pp.1195–204.

Zhang, Y. et al., 2017. Inhibiting medial septal cholinergic neurons with DREADD alleviated anxiety-like behaviors in mice. *Neuroscience Letters*, 638, pp.139–144.

Zhao, Y., Vanhoutte, P.M. & Leung, S.W.S., 2015. Vascular nitric oxide: Beyond eNOS. *Journal of Pharmacological Sciences*, 129(2), pp.83–94.

Zlokovic, B. V., 2005. Neurovascular mechanisms of Alzheimer's neurodegeneration. *Trends in neurosciences*, 28(4), pp.202–8.

Zócalo, Y. et al., 2013. Structural and Functional Properties of Venous Wall: Relationship between Elastin, Collagen, and Smooth Muscle Components and Viscoelastic Properties. *ISRN Physiology*, 2013, pp.1–9.

Zonta, M. et al., 2003. Neuron-to-astrocyte signaling is central to the dynamic control of brain microcirculation. *Nature neuroscience*, 6(1), pp.43–50.

Zou, M.H. & Ullrich, V., 1996. Peroxynitrite formed by simultaneous generation of nitric oxide and superoxide selectively inhibits bovine aortic prostacyclin synthase. *FEBS letters*, 382(1–2), pp.101–4.